## *Synthesis, photophysical characterisation and testing of a new type of photobleaching agent*

MANICI, VALENTINA

Durham University

Department of Chemistry

# Synthesis, photophysical characterisation and testing of a new type of photobleaching agent

**Valentina Manici**

A thesis submitted for the degree of Doctor of Philosophy

**2016**

## Declaration

The work described herein was undertaken at the Department of Chemistry, Durham University between January 2012 and September 2015. All of the work in my own, except where specifically stated otherwise. No part has previously been submitted for a degree at this or any other university.

## Statement of Copyright

*Nel mezzo del cammin di nostra vita*
*mi ritrovai per una selva oscura,*
*ché la diritta via era smarrita.*

*Ahi quanto a dir qual era è cosa dura*
*esta selva selvaggia e aspra e forte*
*che nel pensier rinova la paura!*

*Dante Alighieri*

*Divina Commedia, Canto I*

# Abstract

The purpose of this work, funded by Procter and Gamble (P&G), was the synthesis, photophysical characterization and testing of thioxanthone (TX) derivatives as photobleaching agents (PBA) for use in laundry products (Figure 1).

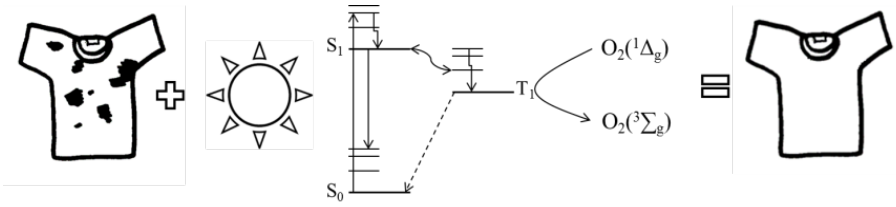


***Figure 1*** *Photobleaching agent process: sunlight can promote the activation of PBA adsorbed on a not clean cloth, thanks to an efficient intersystem crossing and high rate of oxygen quenching it is possible to create singlet oxygen and continue the cleaning process during the drying*

Procter and Gamble selected thioxanthone for its photophysical characteristics and high potential to be the next PBA generation. Firstly the main electronic absorption transition occurs in the near ultraviolet region; the solid compound is pale yellow and solution colourless, a distinct advantage compared to the PBA currently in use. Another important property is the efficient formation by photosensitisation of singlet oxygen. Thioxanthone is a good photosensitiser and has been used for almost a century in photodynamic therapy. Finally, the overall cost for TX production and storage is drastically lower compared to the available commercial PBA.

Unfortunately, TX has a poor solubility in water which limits the concentration in solution. In this work, ten new thioxanthone derivatives have been synthesised with the intent to maintain TX photophysical properties and increase water solubility. The synthetic pathways

proposed in this work aim to be cheap, simple and highly reproducible, an advantage compared to current PBA.

P&G started a collaboration with Durham University aiming to overcome these disadvantages and to have a full understanding of the photophysical behaviour of the potential new PBA.

The achievement of this project is articulated and explained in this manuscripts as follow:

1. **Introduction**: historical role and evolution of detergents, state of the art on available commercial PBA, literature review on thioxanthone (TX)
2. **Experimental**: overview of equipment used for the photophysical characterization of derivatives (Chapter 4) and during tests performed at P&G (Chapter 5)
3. **Synthesis**: description of the synthetic route used to produce thioxanthone derivatives
4. **Photophysical characterization of thioxanthone derivatives:** a full analysis of photophysical behaviour of thioxanthone derivatives, interaction with crocin as stain simulator and detergents
5. **Thioxanthone derivatives as Photobleaching Agents:** a series of tests which simulate, in a small scale, the washing and drying process in the presence of current PBA and a selection of thioxanthone derivatives
6. **The behaviour of thioxanthone upon acidification:** an extensive analysis on the photophysical property on thioxanthone in the presence of $H_2SO_4$ and TFA
7. **Conclusions and future steps**

**Contents**

# Symbols and acronyms

| | |
|---|---|
| P&G | Procter and Gamble |
| PBA | Photobleaching Agents |
| TX | Thioxanthone |
| PDT | Photodynamic Therapy |
| TPS | Tetra Propylene benzene Sulfonate |
| LAS | Linear Alkyl benzene Sulfonic Acid |
| ROS | Reactive Oxygen Species |
| A | Acceptor |
| PC | Phthalocyanines |
| MPC | Metal Phthalocyanine |
| HOMO | Highest Occupied Molecular Orbital |
| LUMO | Lowest Unoccupied Molecular Orbital |
| PP | Porphyrins |
| UV | Ultra Violet |
| MeP | Metallo Porphyrin |
| $\Phi_{\Delta}$ | Quantum yields of singlet oxygen |
| $\Phi_{T}$ | Quantum yields of triplet state |
| OB | Optical Brighteners |
| ISC | Inter-System Crossing |
| OLED | Organic Light-Emitting Diode |
| $k_f$ | Unimolecular rate constant for fluorescence |
| $k_{ISC}$ | Unimolecular rate constant for intersystem crossing |
| $\Phi_f$ | Fluorescence quantum yield |

| | |
|---|---|
| LASER | Linear solvation energy relationship |
| TL | Thermal Lens |
| PL | Population Lens |
| IC | Internal Conversion |
| CI | Conical Intersection |
| VR | Vibrational Relaxation |
| ε | Molar absorption coefficient( l $mol^{-1}$ $cm^{-1}$) |
| EPA | Ethanol, 2-methylbutane and diethylether 2:5:5 v/v/v |
| TCSPC | Time-Correlated Single Photon Counting |
| TAC | Time to Amplitude Converter |
| PHA | Pulse Height Analyser |
| PMT | Photomultiplier Tube |

# Acknowledgments

I would like to thank Prof. Andy Beeby for the opportunity to work in his group, for the supervision and inspiration during the entire PhD.

Thanks to P&G Newcastle team for the financial support and help during the tests.

Special thanks to my friend Dr Kate Nicholson, for all the times she cheers me up and helps me, especially in the hospital. Special thanks to my dear friend Dr Marco Milioli, for all the phone calls, time and effort; without his support this thesis would not be here. I would like to thanks, Dr Robert Pal for our crazy coffee breaks. Thanks to Prof. John Evans and Tony Parker for the help and support with my thesis.

Thanks to all members of Beebs groups of these four years. In particular to Ducky, Gerry and Bob for their support, laughs and friendship.

Thanks to my friends Alessandro, Elena, Valentina, Cecilia, Gabriele, Simona, Anastasia which have been there for me since day one of undergraduate. Thanks to Martina, Mick and Alex for the great friendship and help along the years in Durham, I will always miss our pint at the Vic on Wednesday evening. Thanks to Sons of Durham for all the crazy nights out, to Brunella for our inappropriate voice message, to all my housemates for their patience. Thanks to Francesco, Valentina, Anna, Michela, Salim, Roberto, Bansri, Paolo, Marie and all the people I met at The New Inn on Friday evening. I will never forget our Italian food and fun together.

At last, I need to thanks my family and my cat. In particular my parents, I will never be grateful enough for all your support along these years away. I will always be your special Bruno.

# Chapter 1

# Introduction

## 1.1 Historical overview of laundry products

Ever since the ancient civilisations, laundry has always been part of everyday life. Egyptians and Romans had specific symbols and words to describe it[1]. At that time washing clothes consisted of mechanical friction on and with an abrasive or hard surface. Despite the limited scientific knowledge even at that time, the population realised certain conditions could affect the cleaning process performance. Egyptians were used to adding soda ash to decrease the hardness of the water. This simple, but effective, additive mixed with sodium silicate were the main two ingredients for the first water softener developed by Henkel in 1878. Another parameter which always played a fundamental role is the temperature of the washing process. Through laundry history, there have been several turning points, little discoveries in technology and chemistry which had a crucial impact on modern society. One of the main changes was the introduction of the first modern detergent known as tetra propylene benzene sulfonate (TPS) (Figure 1).

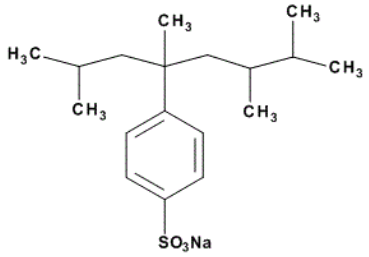


***Figure 1*** *TPS structure*

TPS was introduced in the 1940's by Procter and Gamble (P&G). Before TPS, there were only 'natural' soaps based on different combinations of long-chain fatty acids derived from

animal or vegetable oils mixed with sodium carbonate, sodium silicate, and sodium perborate. In only one decade TPS revolutionised the chemistry beyond laundry detergents. Since the beginning surfactants had a tremendous impact on research, manufacturing processes and everyday life. The schematic formula for a surfactant is shown in Figure 2. As shown, there are two parts, a hydrophilic head, which is completely water soluble, and a hydrophobic tail. Thus, surfactants can interact with stains and fabrics during the washing process to achieve the removal of the stain.

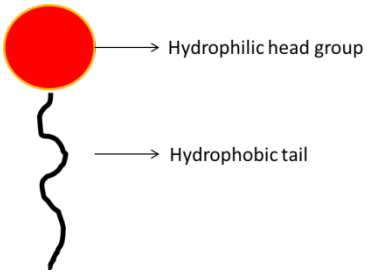


***Figure 2*** *General structure of surfactant*

In the past 70 years, a wide range of surfactants has been developed, with a current worldwide production estimated around 15 Mton/yr. The majority of surfactants produced, across the globe, are used as domestic and industrial detergents, but they have a crucial role in several other manufacturing areas, such as petroleum, food and pharmaceutical production.

Usually, surfactants can be classified as anionic (i.e. TPS), cationic, zwitterionic and non-ionic.

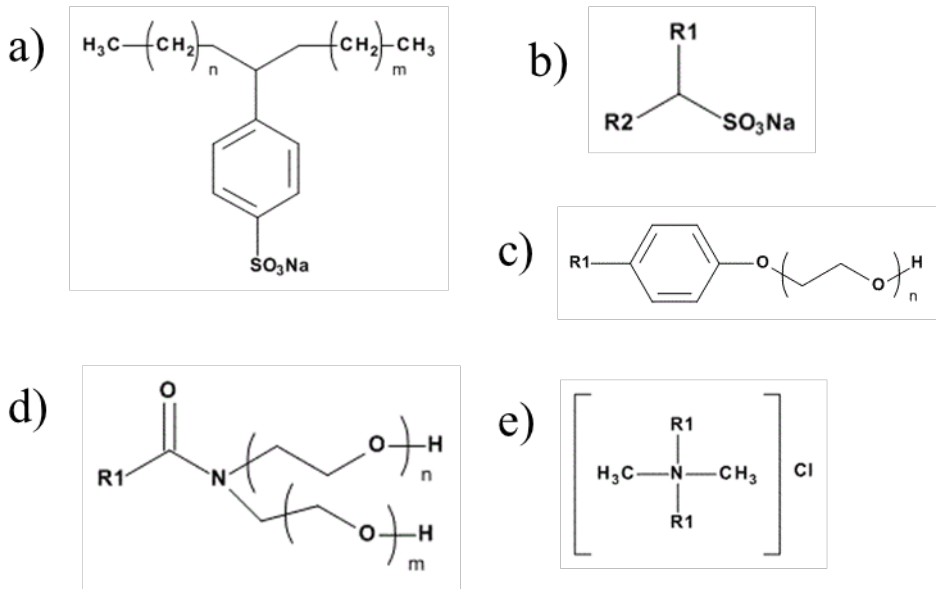


***Figure 3*** *a)LAS general structure n+m=7-10 b) Secondary Alkanesulfonates (SAS)R1and R2 $C_{11-17}$ c)Alkylphenol Ethoxylates (APE)R1 $C_{8-12}$ n 5-10 d) Fatty Acid Alkanolamides (FAA)R $C_{11-17}$ n 1,2m 0,1e) Dialkyldimethylammonium Chlorides R $C_{16-18}$*

In this work a linear alkyl benzene sulfonic acid (LAS) has been used as the surfactant, to investigate the behaviour of PBA in the presence of surfactants. LAS is one of the most widely used mixtures of anionic surfactants for laundry detergents. It was first introduced in the late 70s as a more biodegradable replacement of TPS. The main difference between TPS and LAS is the alkyl chain which in the TPS case present methyl ramifications and in the latest type, only a linear, variable length, chain.

As mentioned above, LAS is a mix of different surfactants due to the difficulty of controlling the length of the final alkyl chain during production. The commercially available LAS presents a combination of chain length between 7 and 10 for each branch. Unfortunately, LAS decreases cleaning performance with increasing water hardness. In the last 40 years, this problem has been avoided with the use of zeolites or any others chemicals which increase ion exchange and, consequently, decrease hardness.

Another important turning point for laundry was the introduction of automatic washing machines in the late 1940s[1]. Previously clothes were immersed for a long time in a mixture of water and natural soap, then rubbed until the stain was completely removed. The combination of fast spinning and temperature control of the washing process and the drastic reduction of time for the cleaning were the main reasons why washing machines became one of the most wanted electronic items in the early 50s. The introduction of this new and highly-used item increased the world production and consumption of TPS based detergents. After only one-decade surfactants manufacturers faced a new challenge: product biodegradability. In fact, the first environment act was legislated in the 1960s in Germany after one of the first reported water pollutions in the world. The environmental legislation affected not only the production of detergents but even washing machine manufacturing. With the introduction of different programs with set temperature and duration, it was possible to minimise electricity and water consumption. This significant achievement was not possible without strong engineering development. The new legislation also caused the synthesis of LAS based detergents.

When a new type of fabric, polyester based, was introduced the detergent manufacturers faced another challenge. Due to the different chemical and physical composition of the material all the surfactant producers were forced to innovate the formula. With the introduction of a variety of cationic and zwitterionic surfactants and others ingredients, it was possible to achieve an excellent washing performance across all the type of fabrics.

In the past decades, one of the main research areas for laundry manufacturers focused on the possibility of deep cleaning even at low temperature. This goal was achieved by the introduction of several ingredients such as zeolites, enzymes, fluorescent whitening agents such as optical brighter and bleach activators. This achievement represents another turning point for our modern society. In fact, the majority of the population could now decrease electricity consumption due to the reduction in the ideal washing temperature using these

more efficient and environmentally friendly detergents. One of the biggest obstacles to the full achievement of this significant result are the consumers who do not believe in the performance of the detergent at low temperature and continue to wash at a high temperature out of habit. It is important that consumers receive adequate education on detergents and electro domestics to create a more aware population and reduce our impact on nature.

Another waste of electrical energy, water and detergents occurs when an item has not been thoroughly cleaned in the washing machine. In the attempt to stem this waste most of the detergents companies introduced, in the late 80s, a new type of additive called photobleaching agents (PBA)[2]. These molecules do not play any role during the conventional washing process and deposit on the surface of the fabrics. Only when the items are hung in the sunlight, these materials can activate and quench the atmospheric oxygen creating highly oxidising species and continue the cleaning process during the drying. Unfortunately, commercially available PBA does not have sufficient efficiency to achieve an overall positive impact. This project has as its primary goal the development and photophysical characterization of new types of photobleaching agents.

## 1.2 Photochemistry

Different spectroscopic techniques will be employ to accomplish the main goal of this projects. In this section an overview on photochemistry principals and application will be given.

When light irradiates a molecule, a variety of phenomena can arise. It is well known that the energy of each photon is associated with the vibration of the light wave or particle that is given by Planck's law $E = h\nu = hc/\lambda$, where $h$ is the Planck constant ($6.63*10^{-34}$ $Js^{-1}$), $c$ is the speed of light (m $s^{-1}$), $\nu$ and $\lambda$ are the frequency (Hz) and the wavelength (m) associated with the electromagnetic wave, replevin. If the energy carried by a photon matches the energy gap

between the ground and excited state of the molecule, then subject to other selection rules, then the absorption process may occur, and the molecule is promoted to this excited electronic state. The excited state is characterised by it having a different electronic configuration to the ground state and a different equilibrium nuclear geometry. An important selection rule is that $\Delta S = 0$, thus, the usual singlet ground state can only undergo absorption to an excited singlet state. Higher singlet excited states usually undergo rapid Internal Conversion (IC), to create a vibrationally excited level of a lower electronic state and consequently, decay by fast vibrational relaxation (VR). Typically the $S_1$-$S_0$ energy gap is much larger than the $S_n$-$S_{n-1(n>1)}$ gaps, and hence internal conversion from higher excited singlet states to the first excited singlet state is rapid, while that from the first excited singlet state to the ground state is relatively slow. Decay from the first excited singlet state to the ground state can occur via two pathways; a radiative process where the molecule loses the energy in the form of a single quantum of emitted light known as fluorescence, and non-radiative processes including internal conversion and intersystem crossing.

Intersystem Crossing (ISC) leads to the population of the triplet excited state, $T_1$. This state can also decay by a radiative process, phosphorescence, or by back-intersystem crossing and vibrational relaxation to the ground state. Since the triple to single conversion is spin forbidden the lifetime of the triplet state can be long (μs – s), allowing quenching by impurities or oxygen. The combination of a low constant for phosphorescence and moderately high quenching rate constants means that triplet-state emission is absent at room temperature. It is still possible to observe it at the cryogenic temperature where quenching induced by external agents can be stopped by incorporation of the molecule in a solvent glass. For some organometallic complexes, it is possible to observe the phosphorescence by simply degassing the sample. All these processes are summarised in the Jablonski diagram (Figure 4); moreover, it is crucial to investigate the timescale of every process especially the fluorescence and the phosphorescence lifetime and the efficiency of these processes.

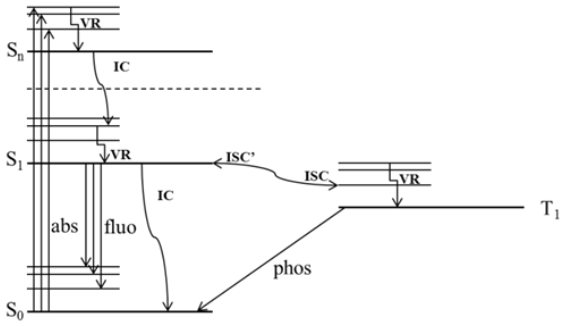


| Process | Timescale (s) |
|---|---|
| VR | $10^{-13}$-$10^{-9}$ |
| IC | $10^{-9}$-$10^{-7}$ |
| ISC | $10^{-11}$-$10^{-8}$ |
| Fluorescence | $10^{-12}$-$10^{-6}$ |
| Phosphorescence | $10^{-3}$-$10^{2}$ |

***Figure 4*** *Jablonski diagram*

Standard absorption experiments involve a light source with a particular intensity ($I_{in}$) that irradiates a solution of a sample contained in a cuvette with a well-defined path length (l cm) and known concentration (c, mol $l^{-1}$). The intensity of the emerging light after the absorption ($I_{out}$) can be related to c and l through the follow equation

$$\log (I_{in}/ I_{out}) = \varepsilon\, c\, l$$

where ε stands for the molar absorption coefficient( l $mol^{-1}$ $cm^{-1}$); the quantity on the left side of the equation is the absorbance, A, this provides a linear relationship between absorbance, path length and concentration expressed by the Beer-Lambert law

$$A= \varepsilon\, c\, l$$

Another two critical parameters are the fluorescence quantum yield ($\Phi_F$) which expresses the efficiency of photons emission from the first excited stated to the ground state. In fact, $\Phi_F$ is defined as the fraction of molecules that decay by fluorescence, determined from the ratio of the number of photons emitted as fluorescence to the number of photons absorbed. This can be expressed regarding decay processes assuming steady state conditions, i.e., the rate of formation of singlet state equals the rate of decay.

| Process | Rate |
|---|---|
| $S_0 + hv \rightarrow S_1$ | $I_a$ |
| $S_1 \rightarrow S_0 + hv$ | $k_{f0}[S_1]$ |
| $S_1 \rightarrow S_0 + \text{heat}$ | $k_{ic}[S_1]$ |
| $S_1 \rightarrow T_1$ | $k_{isc}[S_1]$ |

Using the steady state approximation:

$$I_a = k_f [S_1] + k_{ic} [S_1] + k_{isc} [S_1]$$

$$\Phi_F = \frac{k_f}{k_f + k_{ic} + k_{isc}}$$

It is possible to understand through the fluorescence emission if the singlet excited state is quenched by external agents. Stern and Volmer developed a theory to rationalised this interaction, a central part of this approach is the following equation

$$I_0/I = \tau_0/\tau = 1+k_q\tau_0[Q] = 1+ K_D[Q]$$

Where $I_0$ is the fluorescence in the absence of quencher, $I$ is the fluorescence in the presence of quencher, $k_q$ is the bimolecular quenching constant, $\tau_0$ is the lifetime of the fluorophore in the absence of quencher, [Q] is the concentration of the quencher, $K_D$ is the dynamic Stern-Volmer constant. Quenching data are usually presented as plots of $I_0/I$ or $\tau_0/\tau$ versus [Q], from which a straight line plot with a gradient of $k_q[Q]$ indicates dynamic quenching.

### 1.2.1 Flash photolysis

"One of the principal activities of man as scientist and technologist has been the extension of the very limited sense with which he is endowed so as to enable him to observe phenomena with dimensions very different from those he can normally experience […] In dimension of

time, without the aid of special techniques, he is limited in his perception of time between about one twentieth of second (the response time of the eye) and about $10^9$ seconds (his lifetime). Most of the fundamental processes and events, particularly those in the molecular world which we call chemistry, occur in milliseconds or less, and it is, therefore, natural that the chemist should seek methods for the study of events in micro time." With those words, Lord Porter started his Noble Prize lecture in 1967 for the development of the flash photolysis technique[3].

During Porter's PhD, under the supervision of Norrish, he realised that if a short and intense pulse of light irradiated a solution containing a photoactive reagent, there would be an instantaneous production of an intermediate species[4]. If the concentration of the transient species is high enough, it can be monitored by conventional spectroscopic techniques. Until the introduction of lasers in ca. 1970 the light impulses were created by a combination of shutters and flash-lamps. The advent of Q-switched lasers made possible the study of nanosecond events and later on, with the development of mode-locking, the picosecond range and eventually the femtosecond regime. Moreover, this technique is not limited to the solution state because, during the 80's, Wilkinson et al. introduce the method of diffuse reflectance flash-photolysis for the investigation of scattering samples. In this project, flash photolysis has been using to investigate the triplet excited state of different PBAs. A ns laser pulse is used to populate the $S_1$ excited state, which by efficient ISC, also populates the $T_1$ state.

Using a broadband light source allows the triplet-triplet absorption process to be investigated (Figure 5).

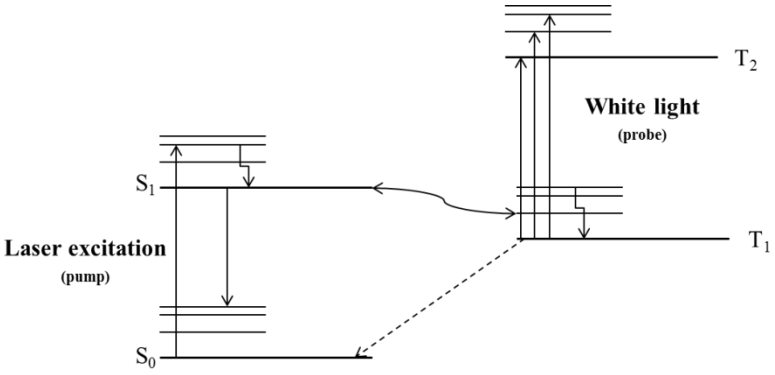


***Figure 5*** *Jablonski diagram outlining the process involved in flash photolysis*

By monitoring the changing in the optical density of the species (ΔOD(λ,t)), it is possible to follow the evolution of the concentration of the triplet excited state created at the different wavelengths.

$$\Delta OD(\lambda,t) = OD(\lambda,t) - OD(\lambda,t<0)$$

It is necessary to define t=0, the time at which the pulse is irradiats the sample. In this way OD(t<0) results from the sample absorbance before the excitation pulse and OD(λ,t) the evolution of it after the excitation pulse. It is also possible to define OD(λ,t) with the follow equation

$$\Delta OD(\lambda,t) = log_{10}\left(\frac{I_0}{I_t(t)}\right) - log_{10}\left(\frac{I_0}{I_t(t<0)}\right)$$

Where $I_0$ is the incident probe beam, and $I_t$ is the time-dependent transmitted light intensity changing in time. Due to the dependence of ΔOD on two parameters, it is to possible to run two different types of experiments: wavelength dependent and time dependent. The first one provides the ΔOD value at the different wavelengths and creates the triplet-triplet absorption spectrum of the sample; in this way, it is possible to understand at which wavelength is the maximum of the triplet-triplet absorption (Figure 6).

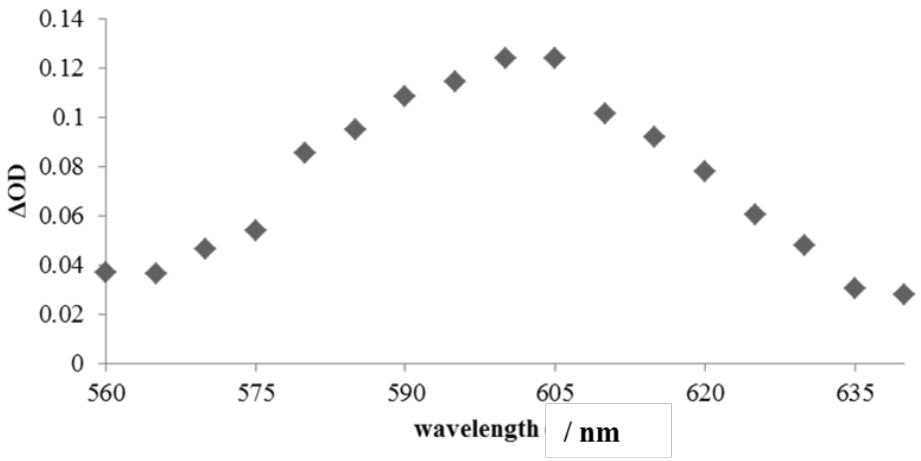


***Figure 6*** *Example of T-T absorption recorded with flash photolysis equipment*

The time dependence experiment provides kinetic information, which is possible to be extrapolated from the exponential decay of the transient species. In this way, it is possible to determine the lifetime of the metastable species (Figure 7).

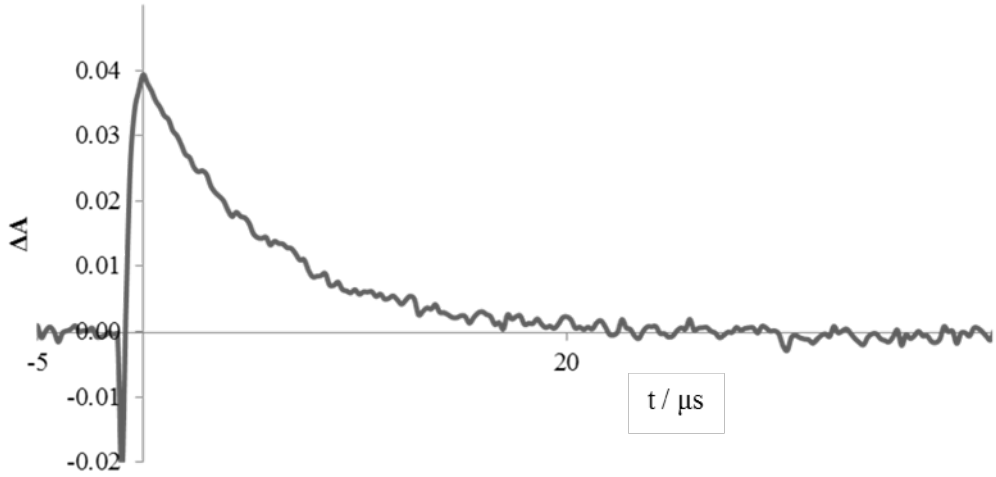


***Figure 7*** *Example of transient absorption signal recorded with flash photolysis equipment*

### 1.2.2 Singlet oxygen generation

Singlet oxygen $O_2(^1\Delta_g)$ is generated from PBA exclusively through triplet state quenching by $O_2(^3\sum_g)$. The $^1\Delta_g$ state lies approximately 96 kJ $mol^{-1}$ above the ground state, and in gaseous media may have a lifetime of minutes due to the spin forbade nature of the transition ($^1\Delta_g$ -> $^3\sum_g$). The quantum yield of singlet oxygen formation ($\Phi_\Delta$) can be expressed by the follow equation

$$\Phi_\Delta = \Phi_T \frac{k_{\Delta O_2}[O_2]}{(k_{\Delta O_2} + k_{\sum O_2})[O_2] + k_{nr} + k_r}$$

where $\Phi_T$ is the quantum yield of the triplet state formation, $k_{\Delta O_2}$ is the rate constant for quenching by $O_2$ to from $O_2(^1\Delta_g)$, $k_{\sum O_2}$ is the rate constant for quenching by $O_2$ to from $O_2(^3\sum_g)$ and $k_{nr}$, $k_r$ represent rate constant for non-radiative and radiative deactivation pathways of $T_1$ respectively. In most systems quenching by oxygen is very rapid and $(k_{\Delta O_2} + k_{\sum O_2}) \gg k_{nr} + k_r$, so the equation can be simplified to yield

$$\Phi_\Delta = \Phi_T \frac{k_{\Delta O_2}}{k_{\Delta O_2} + k_{\sum O_2}}$$

The rate terms in the fraction represent the proportion of triplet state molecules quenched by ground state oxygen to yield singlet oxygen.

Deactivation of singlet oxygen in solution occurs via two pathways: non-irradiative by transfer of vibrational energy to solvent molecules, and radiative decay as phosphorescence emission at 1270 nm.

Non-radiative decay pathways are controlled by the ability to surround solvent molecules to act as energy sinks by accepting electronic energy from excited oxygen molecules as vibrational energy. Hence, the lifetime of singlet oxygen, $\tau_\Delta$, is vastly different in different

solvents. The reciprocal of lifetime of emission, $\tau_\Delta$, can be calculated by the sum of molecular quenching rates, $k_{nr}, k_r$, and molecular quenching rates, $k_Q$,

$$\frac{1}{\tau_\Delta} = k_{nr} + k_r + \sum k_Q[Q]$$

In this work the term $k_Q$[Q] has been found negligible, mainly due to the low concentrations of quenching species employed, and the upper limit for $k_Q$ dictated by the diffusion limit. Consequently the lifetime can be founded directly by fitting a single exponential decay to the data.

## 1.3 Photobleaching process and classical PBA

Photobleaching agents are molecules which continue the washing process during the drying phase[2]. During the washing, the photobleacher can be adsorbed on the surface of the clothes, but it is only during the dry process the agent starts to react. Sunlight promotes the PBA from the molecular ground state to singlet excited states. Due to an efficient intersystem crossing, it is possible to start to populate the triplet excited state.

If this state has a sufficiently long lifetime and the right energy, it can be quenched by the atmospheric molecular oxygen, $^3O_2$, and generate singlet oxygen, $^1O_2$. Following further reactions, singlet oxygen can create reactive oxygen species (ROS). Singlet oxygen and ROS are powerful oxidising agents and can easily degrade residual stains on the fabric. If this additive has an excellent efficiency, it can help to save a considerable amount of energy and natural resources (Figure 8).

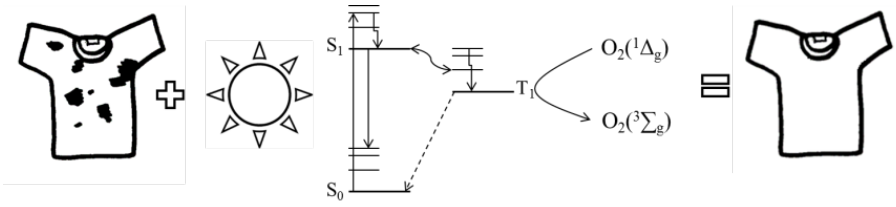


***Figure 8*** *Photobleaching agent process: sunlight can promote the activation of PBA adsorbed on an unclean cloth. By an efficient intersystem crossing and high rate of oxygen quenching singlet oxygen is formed and continues the cleaning process during the drying*

PBA can be considered as a photosensitizer, and the efficiency of quenching with oxygen is a critical parameter in the choice of the possible PBA candidate[2]. Ideally, PBA should absorb strongly at longer wavelengths compared to those at which the acceptor (A) absorbs, which, in this case, it is represented by molecular oxygen. The standard pathway for an excellent photosensitizer can be described as following

$$S \xrightarrow{h\nu} {}^1S^*$$

$${}^1S^* \xrightarrow[\text{crossing}]{\text{Intersystem}} {}^3S^*$$

$${}^3S^* + A \xrightarrow[\text{transfer}]{\text{Energy}} S + {}^3A^*$$

In general, there are two ways by which a triplet state can interact with a molecule or a biomolecule; these are known as the type I and II reactions. In the type I the photosensitizers upon irradiation undergoes a direct reaction with the substrate, via hydrogen abstraction or electron transfer:

$${}^3S^* + RH \longrightarrow SH^{\bullet} + R^{\bullet}$$

or

$${}^3S^* + D/A \longrightarrow S^{\pm\bullet} \pm D^{+\bullet}/A^{-\bullet}$$

The type II mechanism involves singlet oxygen formation as a result of electron exchange energy transfer from the excited synthesiser to molecular oxygen.

$$^{3}S^{*} + {}^{3}O_{2} \longrightarrow S + {}^{1}O_{2}$$

The reactive oxygen species either undergoes decay to regenerate ground state molecular oxygen or reactions with a substrate. All the PBA examples studied in this thesis are type II synthesisers.

Since the 1980s P&G has been keen to develop and commercialise a highly efficient PBA. Harriman et al. collaborate closely with P&G and have investigated the proprieties of porphyrin and phthalocyanines to be used as PBAs.

## 1.4 Phthalocyanine and porphyrin

Phthalocyanines (PC) are planar aromatic macrocycles consisting of four isoindole units presenting π–aromatic electrons which are delocalized over an arrangement of alternant carbon and nitrogen atoms (Figure 9).

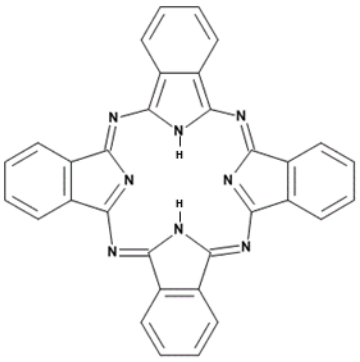

***Figure 9*** *General structure of phthalocyanine*

Thanks to this property PC and their derivatives have been used as important functional materials in a variety of fields. Due to their intense blue/green colour the primary use of these materials, since first discovery in 1907, has been in textile dye industries as a pigment. The central cavity has the capability to accommodate ions of up to 50 different elements[5–8]. A phthalocyanine containing one or two metal ions is called metal phthalocyanine (MPC). PC and MPC have been used in many types of research and commercial fields such as electronics, solar cells, catalysis, photonics, etc[9–14]. Particularly nontoxic derivatives with a higher water solubility have been developed for use in photodynamic therapy (PDT)[15–18]. Due to an intense absorption in the far-red light, where it is possible to have greater tissue penetration and excellent efficiency in singlet oxygen generation, PC and MPC show good characteristics for PDT.

In general, the strongest absorption maxima for MPC are in the visible region, the so-called Q-band which it can be attributed to the allowed HOMO-LUMO ($\pi$-$\pi^*$) transition. The Q-band of MPC's can undergo a bathochromic shift through an extension of the $\pi$ conjugation system[13].

Another class of macrocycles used as PBAs are porphyrins (PP) which have similar chemistry and photophysical behaviour to PCs[9,17–22]. In general, a porphyrin is composed of four modified pyrrole subunits interconnected at their $\alpha$ carbon atoms via methine bridges (=CH−) (Figure 10).

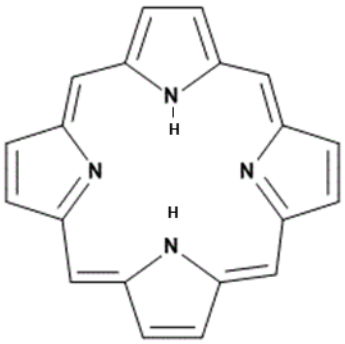


***Figure 10*** *General structure of porphyrin*

The porphyrin macrocycle has 26 (delocalized) π electrons in total. Like PCs, porphyrin macrocycles are highly conjugated systems, and consequently, they typically have very intense absorption bands in the visible region and may be intensely coloured. In fact, the name "porphyrin" comes from the Greek word *porphyra*, meaning *purple*. Like PCs, porphyrins can include a metal ion in the central cavity. Some iron-containing porphyrins are called haems, which form one of the cofactors in haemoglobin protein. Haemoglobin and myoglobin are two $O_2$-binding proteins that contain iron porphyrins. Various cytochromes are also haemoproteins. Due to the crucial role in human biology porphyrins have been studied extensively, and they have been used in different fields. Like PC porphyrins are employed in PDT to treat various cancers. Moreover, porphyrins and metal porphyrins have been used in biomimetic catalysis, molecular electronics, and supermolecular chemistry.

## 1.5 Phthalocyanine and porphyrin as PBA

Harriman et al. have investigated porphyrins and phthalocyanines as PBA compounds[2]. All their measurements were carried out in methanol or water, at pH 9, to mimic washing conditions. Due to the nature of the macrocycle, PC and PP can aggregate easily in solution and affect the photophysical properties of the compounds. This problem put a concentration

limit down to $10^{-6}$ M across all the measurements. Later in his reports, Harriman, investigated the interaction of few selected compounds with surfactants and optical brighteners to study how PC and PP behave in a more realistic washing environment.

Conjugation of the macrocycle and the type of metal ion in the central cavity, have a significant impact on the photophysical behaviour of this class of compounds (*v.s.)*. In general metal PCs and PPs present two absorptions named as Q- and B- bands. The Q-band position is in the far red region between 600-800 nm while the B-band has the maximum peak located in the near UV region of the spectrum. Both transitions have been associated with redistribution of electrons within the $\pi$ orbitals. Electrons residing on the metal cations and the molecular orbitals of ring N atoms are situated at too high energy to contribute to the photophysical properties of the molecules. Excited state behaviour is dominated by ($\pi$,$\pi$*) transitions and the excited singlet state manifold possesses two highly allowed absorption transitions. The lower energy transition, Q-band, relates to the first excited singlet state and its position on an energy scale depends upon the nature of the porphyrin ring. The second allowed absorption transition, B-band, relates to the population of the second excited singlet state. Changing the conjugation of the macrocycle may cause shifts in the position and the intensity of these bands.

The metal ions in the central cavity of a PP or PC can play a fundamental role in the efficiency of singlet oxygen generation. Due to spin-coupling effects, different cations can lead to highly efficient but short-lived triplet states, or, on the other hand, to longer lived but with a lower yield triplet states.

Harriman has investigated several substituted macrocycles such as sulfonated-, tetraphenyl-, and meso-tetraphenyl- porphyrins, which differ from the PC family by the meso bridge being methylene groups or aza atoms. The effect of these two variables was evaluated in the compounds shown in Figure 7.

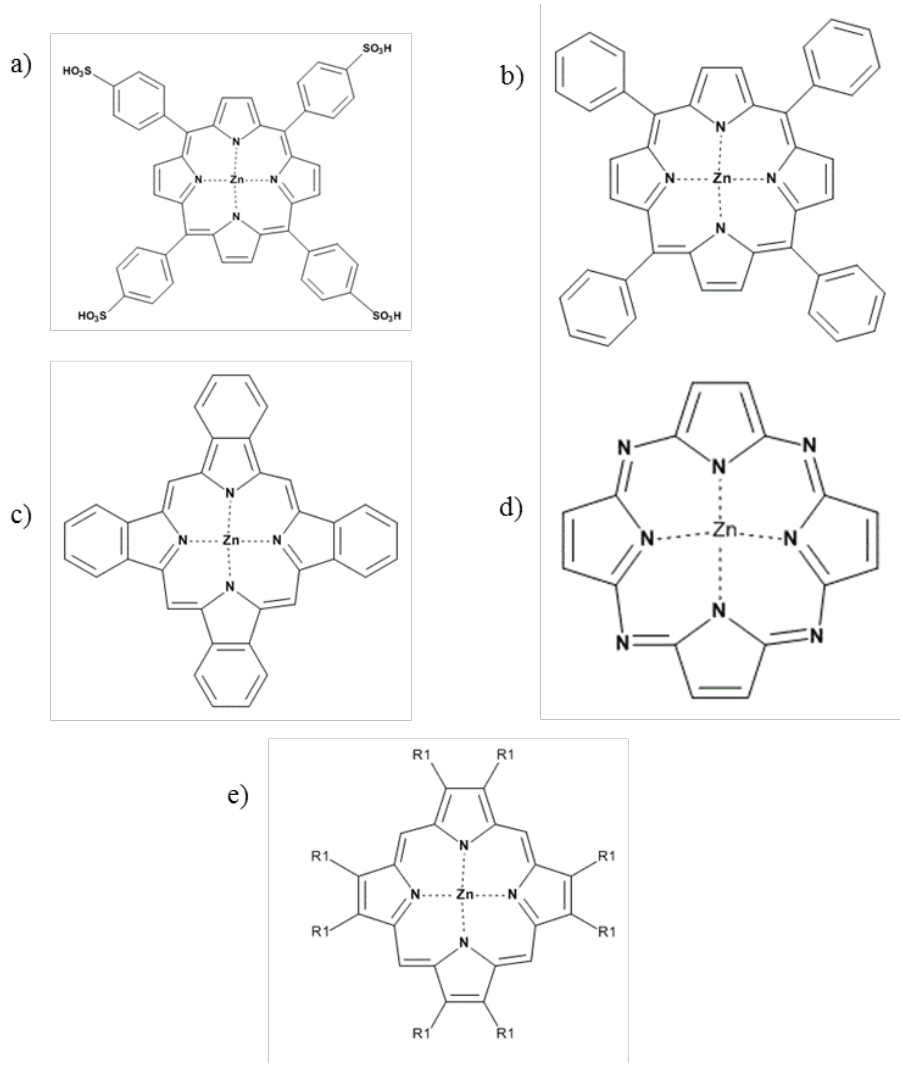


***Figure 11*** *Structure of zinc phthalocyanines and porphyrins studied by Harriman: a) sulphonated tetraphenylporphyrin b) tetraphenylporphyrin (ZnTPP) c) tetrabenzporphyne (ZnTBP) d) meso – tetraazaporphyne (ZnTAP) e) octaethylporphyne (ZnOEP)*

This study has included expansion of the pyrrole using a zinc naphthalocyanine (Figure 12).

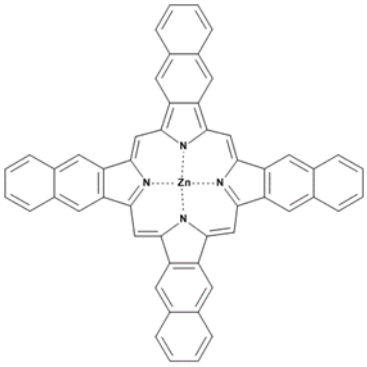


***Figure 12*** *Zinc naphthalocyanine*

The conjugation around the porphyrin macrocycle was varied by partial reduction of the ring forming chlorine and bacteriochlorins. Even if further reduction in conjugation gives colourless products, which is an advantage from a PBA perspective, these porphyrins have a high sensitivity to air and are difficult to synthesise, which are a significant disadvantage for commercial use and general characterisation. For consistency, Harriman used only zinc as a metal cation, although, in few cases, aluminium was also studied (Figure 13).

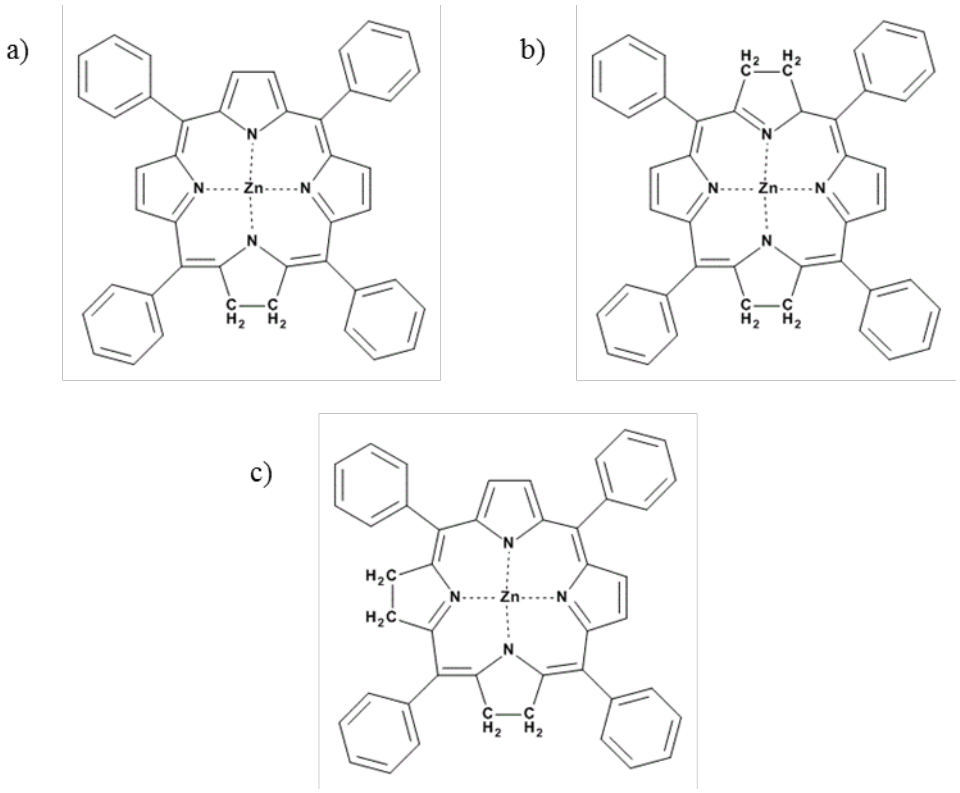


***Figure 13*** *Various reduced conjugation zinc porphyrins: a) chlorine (ZnCH) b) isobacteriochlorin (ZnIBC) c) bacteriochlorin*

Increasing the level of conjugation around the pyrrole units has the effect of lowering the energy of the Q-band, raising the energy of the B-band, and enhance the absorptivity of the Q-band. Replacing the methine bridge with a nitrogen also causes a substantial change in the absorption spectrum, with the Q-bands shifting towards lower energy. Moreover, Harriman observed an increase B- and Q- bands in the reduced-conjugation porphyrins, depending upon the level of reduction. In his report, Harriman recorded fluorescence quantum yields and lifetimes, and the quantum yields for the formation of the triplet state and triplet lifetime of all complexes. It was found that increasing the degree of conjugation around the pyrrole groups increased the fluorescence quantum yield but decreased both the triplet yield and lifetime. The increase in fluorescence yield is associated with the increasing absorptivity of the lowest energy Q-band.

The excited singlet state lifetime has been found to be practically insensitive to the degree of conjugation around the pyrrole units; on the other hand, the triplet yield progressively decreased with increasing level of conjugation. As the Q-band moves towards lower energy**,** the triplet energy decreases also and, since the triplet state lifetime is directly related to the triplet energy, decreases with increasing level of conjugation.

For the reduced-conjugation porphyrins, the fluorescence quantum yield increases with increasing level of reduction along the series ZnTPP<ZnCH<ZnIBC. It is evident there is a marked increase in the singlet excited state lifetime and a substantial decrease in the triplet yield. Such changes appear to be connected with changes in symmetry around the porphyrin ring. Again, as the Q-band moves towards lower energy there is a decrease in the triplet state lifetime, and the biggest problem concerns the reduction in triplet yield. The decrease in triplet lifetime is not a cause for concern: in the presence of oxygen the rate of quenching of the excited state, and hence sensitisation of singlet oxygen, will remain the dominate deactivation pathway.

The crucial process, which Harriman was keen to understand in his reports, is the oxygen quenching with the metal complex.

There are three different pathways that can be followed (MeP = metallo porphyrin):

$$^{3}MeP^{*} + {}^{3}O_2 = MeP + {}^{1}O_2 \quad (1)$$

$$^{3}MeP^{*} + {}^{3}O_2 = MeP + {}^{3}O_2^{*} \quad (2)$$

$$^{3}MeP^{*} + {}^{3}O_2 = MeP^{+} + {}^{3}O_2^{-} \quad (3)$$

Reactions 1 and 2 involve a transfer of excitation energy from the porphyrin triplet excited state to a molecule of oxygen in its ground state. Reaction (1) forms excited singlet oxygen $^1\Delta_g$, and reaction 2 produces oxygen in a vibrationally excited ground state, $^3\Sigma_g^-$. Reaction 3 differs from the others in that it involves a transfer of an electron from the triplet excited state of the porphyrin to an oxygen molecule, forming superoxide and the radical cation of the porphyrin. Despite the formation of singlet oxygen in reaction 1, the formation of radical porphyrin leads to the degradation of the dye. The desired reaction product is singlet oxygen formed by reaction 1. To maximise such reaction, it is necessary to ensure that electron transfer (reaction 3) does not occur and, also, that the yield of vibrationally excited ground state oxygen (reaction 2) is kept to a minimum. This can be achieved by the triplet energy of the phthalocyanines and porphyrin by changing the central cation and the conjugation, as explained above.

For the different complexes studied by Harriman, the quantum yields of singlet oxygen $\Phi_\Delta$, paralleled the triplet state yields, $\Phi_T$ with an overall quenching efficiency around 80%. The variation of triplet lifetime has been found to be irrelevant for the singlet oxygen formation, on the other hand, the variation of triplet quantum yield has a greater effect on the oxygen quench. Complex with the same triplet lifetime will be a better singlet oxygen synthesiser if they will present a higher triplet quantum yield. On the other hand compounds with the same triplet quantum yield but with longer lifetime will not be a greater synthesiser. Moreover, it appears that the combination of a conjugated macrocycle and a heavy atom central metal cation lead to a porphyrin macrocycles with optimum efficiency for generation of singlet oxygen.

It is well known under normal circumstances that the lowest energy singlet excited state of a phthalocyanine can fluoresce, undergo non-radiative deactivation to form the ground state or undergo intersystem crossing to form the corresponding triplet excited state. This last process is forbidden by spin restrictions. It occurs only because there is some mixing

between the excited singlet and triplet states that overcome the formal spin conservation requirements. The extent of state mixing determines the efficiency with which the singlet state undergoes intersystem crossing. This mixing of states, in phthalocyanines and porphyrins, is termed "spin-orbit coupling" and promoted by the presence of the heavy metal ion in the metallo-complex. For a system where there is very little spin-orbit coupling, the triplet manifold will not be populated to any significant degree, but any triplet state that is formed will have a very long lifetime. Alternatively, metal PCs and porphyrins with a higher spin-orbit-coupling effect have short lifetimes, often less than 1 ns. Paramagnetic metal ions, present a significant spin-orbit-coupling effect. Other diamagnetic transition metals have also been shown to display very short triplet lifetimes. This situation is due to the cation perturbing the phthalocyanine π-system to such a degree that the lowest energy excited states are no longer of π,π* but contain the appreciable charge-transfer character.

The same photophysical properties have also been measured in the presence of optical brighteners (OB) (e.g. Figure 14). This class of compound are widely used in laundry detergents. Also, the effect of adsorption onto a cotton surface on the performance of the PBA was also investigated.

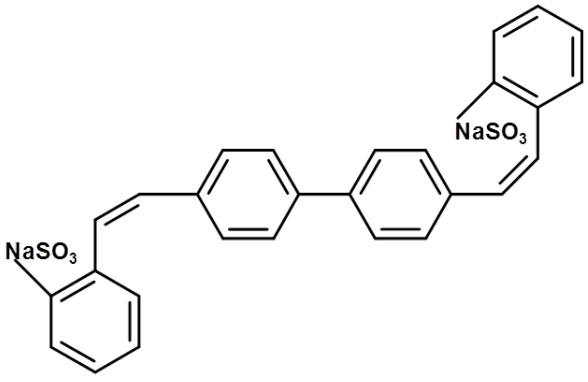


***Figure 14*** *Optical brighteners 49*

It was found that the singlet oxygen lifetime decrees upon increasing concentration of brightener in the mixture, indicating either a chemical reaction or quenching of the singlet oxygen occurs. The products from this reaction were not identified, but the presence of such brighteners do restrict the amount of singlet oxygen available to attack the stain. An additional possible quenching mechanism was taken into account between the macrocycles and OB. By monitoring the triplet, the excited state of the dye is observed an energy transfer from the porphyrin triplet state to the brightener is observed to produce the corresponding triplet state of the brightener.

$$^{3}\text{ZnTSPP}^{*} + \text{OB} = \text{ZnTSPP} + {}^{3}\text{OB}^{*}$$

Long-term irradiation of the solution under an $N_2$ atmosphere does not result in any apparent degradation of the porphyrin, but the high concentrations of brightener needed for these experiments prevented any meaningful quantitative estimates on the brighteners themselves.

In the last experiment, Harriman used cotton fabric that was soaked in aqueous solutions of ZnPCS to dye them and dried in warm air. Reflectance spectra recorded for the dry cloth showed that the adsorbed dye was present in an aggregated state, regardless of the extent of loading.

This suggests that the dye preferentially adsorbs onto surface bound dye rather than onto clean surface. Adsorbed dye is not easily removed by soaking in cold water, but it dissolves in hot water or water containing 1% w/w liquid “Tide” which contains surfactants capable of disaggregating the PBA. Dye adsorbed onto the cotton fabric fluoresces weakly and forms the triplet state upon excitation with a laser pulse.

Diffuse reflectance flash photolysis studies of moistened cotton dyed with ZnPCS showed the transient formation of the ZnPCS radical anion. This species must be generated by electron abstraction from the cotton, but it is formed only in low yield. The radical anion

decays by transferring its extra electron to oxygen, forming reactive superoxide anions. The fate of this species remains unknown.

$$ZnPCS^- + O_2 = ZnPCS + O_2^-$$

Despite the aggregation, the strong blue/green colour, the low purity and the difficult synthesis, PBAs based on phthalocyanines have been used as a laundry additive since 1990. With the intent of improving the PBA impact on laundry products, P&G started a collaboration with Durham University. The main aim of this project is to investigate thioxanthone derivatives as a replacement or additional additives of PBAs.

## 1.6 Aromatic ketones and thioxanthone

### 1.6.1 Aromatic ketones

The objective of this project is the synthesis and photo characterization of new photobleaching agents based on thioxanthone. In general aromatic ketones have a low $S_1$ state and $T_1$ closer in energy, which promotes the ISC efficiency and increases the population of the triplet excited state[23].

Several factors can be influenced the energy level of the excited states and the ISC, the two most important being the nature of the substituent on the aromatic rings and the solvent used. An electron-accepting substituent can stabilise the (n,π*) triplet state more than the (π,π*) triplet state. On the other hand, the (π,π*) triplet state can be stabilised more by an electron-donating substituent compared to the (n,π*) triplet state. The solvent polarity has a strong effect on the energies of the singlet and triplet excited states: this can be observed by a shift to longer wavelengths of the absorption spectra with increased in solvent polarity, and consequently in the emission wavelength and lifetime. Solvent and substituent effect not only spectroscopic properties but also the principal reaction of the ketone excited states which are:

- Norrish type 1 reaction or α-cleavage

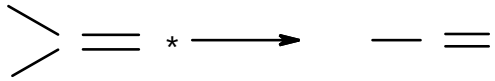

- Intermolecular hydrogen abstraction or Norrish type 2 reaction

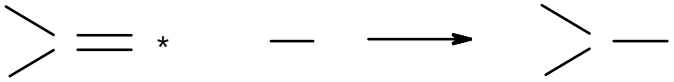

- Addition to a C=C bond

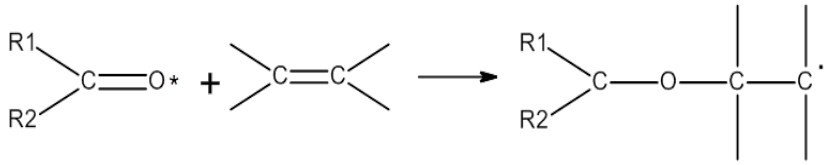


The last reaction has a significant role, especially in polymer science. Ketones such as thioxanthone play an important part in different areas, like photochemical formation and degradation of polymers, photodynamic therapy, nanoparticle, and OLEDs[24–32].

### 1.6.2 Thioxanthone: use and photophysical properties

Since the beginning of last century, thioxanthone (TX) has been used in medical science as a powerful chemotherapy agent. Several drugs based on TXs derivatives have been developed and used to treat a variety of tumours. More recently TX derivatives have been used as an anti-tumour agent and anti-schizophrenia drugs[26,33–37].

In the chemical industry, TXs have been used for more than 50 years as a photoinitiator for polymerisation[24,25,27,28,38–50]. This class of compounds have been using to initiate a radical photo-induced polymerization reaction upon exposure to UV light. Furthermore, those compounds can reach high conversions of the monomer compare to another photoinitiator. Photoinitiated radical polymerization may be initiated by both α-cleavage (Type I) and H-abstraction (Type II) initiators. Type II photoinitiators are a second class of photoinitiators and are based on compounds whose triplet excited states are reached with donors, often amines, thereby producing the initiating ketyl radical.

Because the initiation relies on bimolecular reactions, the Type II reaction is slower than Type I. On the other hand; the Type II process has better optical absorption properties in the near-UV spectral region. The most used Type II photoinitiators are based on benzophenone and thioxanthone due to their long-lived triplet excited states and the efficient charge transfer. Many TX derivatives have been synthesised and characterised with the intent of improving tertiary amine quenching or TX water solubility. One of the main changes in free radical polymerization has been introduced with macro photoinitiators[28,41,5127,52].

Thioxanthone disilycatylene derivatives have been recently published by Lalevee and co-workers[53]. Those molecules exhibit a red-shift in adsorption which facilitates not only free radical polymerization but also cationic polymerization. Recently Malval and co-workers used TX-anthracene derivatives as a new generation of two-photon initiated polymerization agents (TPIP)[29,54]. This material could be considered as the future for the production of complex three-dimensional microstructures that cannot be obtained otherwise. One of the main advantages of TPIP is that it offers excellent spatial control due to confinement of the photo-induced reaction to the focal volume where both excitation and a two-photon absorption process occur. The use of long wavelengths as excitation source allows a greater depth penetration. This variety of publications shown how flexible and tunable are TX properties as photoinitiatos[46].

Due to the high efficiency of hydrogen abstraction, TX and a few derivatives have been used for photo-induced size-controlled generation of silver nanoparticles[30]. As already established, the morphological change constitutes the key for optical, electronic, magnetic, and catalytic properties. In their work Maval et al. concentrated on a photoactivated reaction in which the silver cations are reduced in the presence of α-aminoalkyl radicals produced by the hydrogen abstraction process between TX triplet excited states and aliphatic amines[55]. Such a system has been demonstrated as able to control the growth rate and size regulation of the silver nanoparticles. TX and its derivatives have been used in many other research areas such as stabilisers against electrical breakdown for high voltage cable application or as organic ligands for OLEDs application[56].

Since the 1960s aromatic ketones have been investigated for their unusual energy transfer concentration dependency from the T($\pi$,$\pi$*) state to the aceptor[57]. Excimer formation and self-quenching were the two most important routes of explanations for these observations. In the early papers, how those two phenomena contributed to the energy transfer was not thoroughly investigated and interpreted[58]. Yip et al. monitored quenching and self-quenching measurements on TX as a function of solvent factors, evaluating the $k_q$ values in acetonitrile, benzene, and tertiary-butanol with several quenchers[59]. The results showed a strong solvent dependency for the reaction, with a difference in the rate of self-quenching of one order of magnitude and an even higher difference in the rates of intermolecular quenching. In the following publication, Abdullah and co-workers reinvestigated $^3$TX quenching with inorganic anions[60]. They performed more accurate analysis with nanosecond laser flash photolysis equipment. Thanks to those results they were able to confirm that electron-transfer is the major route for the quenching of both singlet and triplet states. The triplet state quenching mechanism proposed followed the mechanism developed by Rehm and Weller [61] and modified for triplet state quenching (Figure 15).

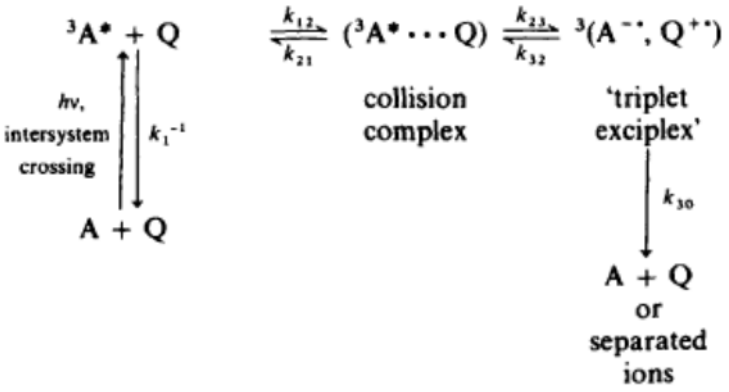


***Figure 15*** *Triplet excited state quenching mechanism of TX, image was taken from*[60]

Quenching experiments have shown that TX has unusual solvatochromic behaviour; this has been investigated for over half a century and is still not fully understood. An early publication on solvent effects was carried out by Dalton and Montgomery in 1974 who reported the fluorescence emission, quantum yields and lifetimes across aprotic and protic solvents[62]. The fluorescence quantum yield was found to be particularly weak in an aprotic solvent (0.01% in cyclohexane) and increases with increasing solvent polarity. The largest yield was determined in methanol (23.4%) and trifluoroethanol (90.2%). Solvent polarity has an effect on fluorescence emission wavelength and lifetime too. The authors connected the fluorescence lifetime and quantum yield with the radiative and non-radiative decay rates through the following equations

$$\Phi_f = \frac{k_f}{k_f + k_{ISC}} = k_f \tau_f$$

$$\tau_f = \frac{1}{k_f + k_{ISC}}$$

where $k_f$ is the unimolecular rate constant for fluorescence and $k_{ISC}$ is the unimolecular rate constant for intersystem crossing to the $T_1$ state. Dalton and Montgomery omitted completely the internal conversion rate under the assumption its contribution would be negligible. Under

such conditions, an increase in $\Phi_f$ can be due to an increase in $k_f$ and/or a decrease in $k_{ISC}$. To evaluate which rate constant is influencing the change in emission behaviour Dalton and Montgomery calculated the values of $k_f$ from the absorption spectra. This showed only a minimal change in different solvents. This suggested that it was the rate of intersystem crossing ($k_{ISC}$) that was the source of the observed solvent effects. This theory was supported by measurements of the lifetime in protic solvents, the value increasing with polarity and with hydrogen bond formation. Dalton and Montgomery suggested the reason for such a large solvent effect on $k_{ISC}$ could be found in a change in the states involved in ISC. They proposed that in TX ISC occurs predominantly from $^1\pi,\pi^*$ ($S_1$) to $^3n,\pi^*$ ($T_2$) in non-polar, weak hydrogen bonding solvents and is therefore fast. With the increase of the polarity or a higher H-bounding formation, the energy of the $^3n,\pi^*$ ($T_2$) become greater and creates an energy gap. Hence the ISC required a larger activation energy (Figure 16).

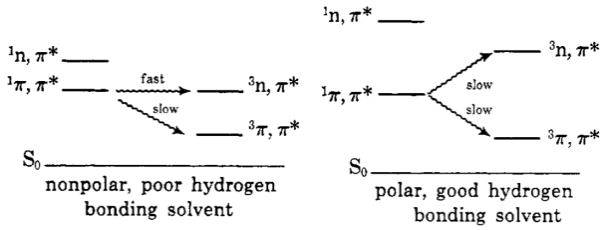


***Figure 16*** *Differences in intersystem crossing of TX in nonpolar and polar solvents, figure taken from*[62]

Moreover, for the solvent with intermediate polarity and H-bounding ability, the observed ISC has been interpreted as a mix of ISC to $T_2$ and $T_1$. Lai and Lim gave a new interpretation for ISC and fluorescence in a later publication [63]. They consider the relative energy gap between the $S_1(\pi\pi^*)$ and $S_2(n\pi^*)$ states and how those states can vibronically couple and increase the radiationless decay rate from the lowest excited state. This phenomenon, termed the proximity effect, was first studied in heterocyclic nitrogen compounds where their observed luminescence behaviour changed by modifying solvent, substitution, and temperature. The proximity effect leads to the potential energy distortion (frequency shift) and displacement (geometry change) along the vibronically active out-of-plane bending

modes. Lai and Lim believed the proximity effect needed to be considered even for the close-lying nπ* and ππ* states of aromatic compounds, and published the first investigation on thioxanthone in 1980. They investigated solvent, temperature, and viscosity dependence of fluorescence and triplet formation of TX on the proximity effect. As reported previously, a shift in $\lambda_{max}$ has been observed, and the fluorescence quantum yield ($\Phi_f$) shows an increase with solvent polarity. As the same time, the quantum yields of triplet formation ($\Phi_T$) were unaffected by solvent polarity and remain constant. Moreover, they investigated the temperature effect of these parameters in EPA (Figure 17).

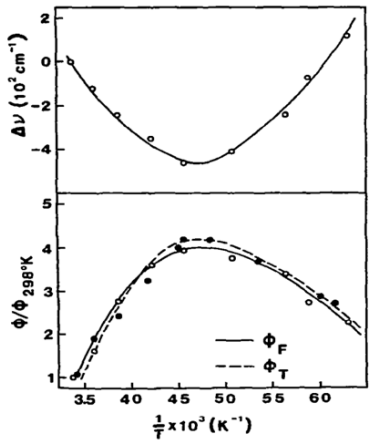


***Figure 17*** *Temperature dependence of fluorescence maximum, yield, and triplet formation yield of TX in EPA (5:5:2 by volume of ether, isopentane and ethanol), measured by the values of 298 K, figure taken from*[63]

Because the temperature at which $\lambda_{max}$ presents the maxima in red-shift coincides with the temperature at which $\Phi_f$ and $\Phi_T$ are the largest, this indicates that the non-radiative decay strongly depends on internal conversion from $S_1$ to the ground state and the energy of $S_1$. The authors viewed this behaviour as a direct consequence of the proximity effect. Lai and Lim concluded that polar, but not strongly hydrogen bonding solvents increase the $S_1$ (ππ*)-$S_2$ (nπ*) energy gap by stabilising the singlet ππ* state, while strongly hydrogen bonding solvents increase the energy gap by destabilising the nπ* state. The former has been seen as primarily a consequence of the solvent relaxation around the electronically excited solute

molecule, while the latter is largely a result of ground state hydrogen bonding. They also took into account how viscosity changes with temperature. At low temperatures, solvent molecules would not have sufficient time to reorient themselves in the reaction field of the electronically excited solute molecule. On the other hand, at high temperatures, where the relaxation time is very short, the solvent stabilisation of the ππ* state would be small since thermal motion disrupts the favoured orientation of the solvent molecules. The $S_1$ (ππ*)-$S_2$(nπ*) energy gap is expected to be larger at the inversion temperature. The observation of a maximum fluorescence and triplet quantum yields at the inversion temperature is a strong indication that the rate of $S_1$ -> $S_0$ IC varies strongly with the separation of the ππ* and nπ* excited singlet states, consistent with the proximity effect. In non-polar solvents, where the solvent relaxation is not necessary, the $S_1$ -> $S_0$ IC, resulting from the proximity effect, should be greatly enhanced by thermal excitation of the vibronically active out-of-plane bending modes, which are of low frequencies in $S_1$. Later, the same authors performed time-resolved fluorescence experiments on thioxanthone in ethanol, trying to clarify the role of solvent relaxation in the proximity effect[64]. Lai and Lim considered the dipole moment of $S_1$(ππ*) to be much larger than for the $S_2$(nπ*) and ground states, consequently they expect the solvent relaxation to decrease in the energy of this excited states. This leads to an increase of the $S_1$ (ππ*) - $S_2$(nπ*) energy gap and a drop in the relative importance of the vibronic coupling.

The solvent relaxation has been investigated via changing the viscosity of ethanol with increasing and decreasing temperature. At lower temperature, the solvent will not have the time to relax and interact with $S_1$(ππ*) state and the emission will be dominated by the proximity effect. Consequently the vibronic coupling between the $S_1$(ππ*) - $S_2$(nπ*) states will be the major influence on the fluorescence emission. By raising the temperature where the solvent relaxation becomes comparable to the $S_1$(ππ*) lifetime it is possible to observe two different lifetimes and a shift to a longer wavelength. The rise time of the longer-

wavelength fluorescence has been interpreted as a reflection of the time scale of the solvent reorientation which competes with the decay process of the $S_1(\pi\pi^*)$ state. A third case has been taken into consideration when relaxation time is much shorter than the lifetime of $S_1(\pi\pi^*)$. Under this circumstance, the emission will be stronger in intensity and red-shifted. The work of Lai and Lim has been fundamental for numerous later publications, which investigated the photophysical behaviour of TX and substituted TX with more advanced equipment[65–67].

In a subsequent publication, Ley and Morlet-Savary re-investigated the solvent dependence of TX but focused only on the measurement of intersystem crossing kinetics[68]. They evaluated ISC in several solvents by employing picosecond pump-probe spectroscopy. The interpretation of ISC rate constants resulted in difficulties due to the overlap of the $T_1$-$T_n$ and $S_1$-$S_n$ transitions and to the solvatochromism of the triplet-triplet absorption (Figure 18).

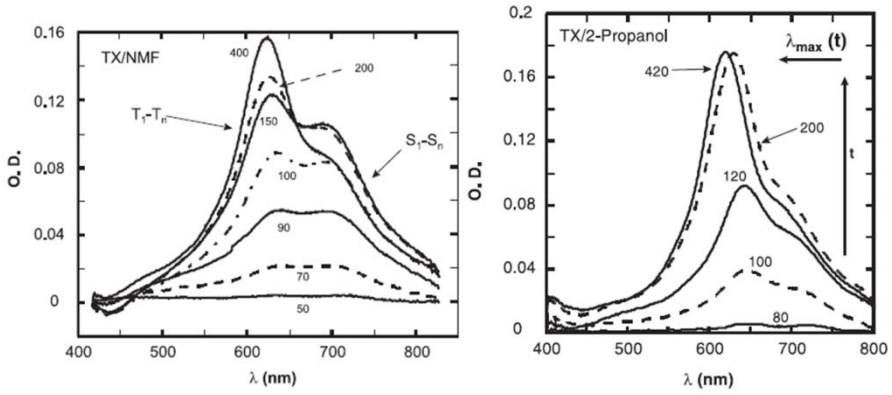


***Figure 18*** *Picosecond transient absorption spectra of TX in N-methylformamide (left) showing the $T_1$-$T_n$ and $S_1$-$S_n$ overlap, on the right solvatochromic shift of the $T_1$-$T_n$ in 2-propanol (time in ps), figure took*[68]

The authors confirmed once again the unusual photophysical behaviour of TX and tried to interpret it by taking into account not only $S_1$, $S_2$, and $T_1$ energy but even $T_2$. Using a four-state model introduced previously by Cavalieri[69], they were hoping to clarify the ISC process in TX (Figure 19).

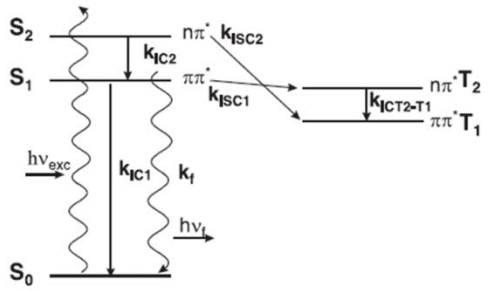


***Figure 19*** *Four excited states diagram of TX, $k_{IC2}$ and $k_{ICT2\text{-}T1}$ rate constant of internal conversion, respectively, from $S_2$ to $S_1$ and $T_2$ to $T_1$, $k_{ISC2}$ and $k_{ISC1}$ rate constant of intersystem crossing respectively from $S_2$ to $T_1$ and $S_1$ to $T_2$, $k_f$ and $k_{IC1}$ rate constant of deactivation of $S_1$ back to the ground state $S_0$ by fluorescence and internal conversion, figure taken from*[70]

Unfortunately, the exact energy of the $T_2$ state remains unknown, and it has been assumed to be close to the $S_1$ state. The key point of this model is to evaluate by which pathways $T_1$ state is populated. The authors suggested the combination of two distinct routes of formation

$$S_2^{n\pi*} \xrightarrow{k_{ISC2}} T_1^{\pi\pi*} \quad \text{very fast direct mechanism}$$

$$S_1^{\pi\pi*} \xrightarrow{k_{ISC1}} T_2^{n\pi*} \xrightarrow{k_{ISCT2\text{-}T1}} T_1^{\pi\pi*} \quad \text{slow indirect mechanism}$$

Lay and co-workers could not extrapolate the $k_{ISC1}$ value, the slower rate of intersystem crossing, even if $k_f$ is constant and independent of the solvent polarity. $k_{ISC1}$ could be an activated process, especially in polar and hydroxylic solvents, where the $T_2$ ($n\pi^*$) state is supposed to be higher in energy than the $S_1(\pi\pi^*)$ state: as the energy gap between these two states increases with the polarity, the rate of intersystem crossing $k_{ISC1}$ decreases. With the intent of giving a proper evaluation of $k_{ISC1}$, the authors tried to estimate the energy of the $T_2$ ($n\pi^*$) state. It has been possible to calculate the first triplet and singlet energy from the steady-state phosphorescence and fluorescence spectra. It is not impossible that the second excited triplet state, $T_2(n\pi^*)$, lies below the $S_1(\pi\pi^*)$ state even in strongly polar and hydroxylic solvents. In this case, an increase of $k_{ISC1}$ is, expected when the polarity of the solvent is enhanced: the $T_2(n\pi^*)$ state is destabilised by solute-solvent interactions and

becomes closer in energy to the stabilised $S_1(\pi\pi^*)$ state. This phenomenon (the standard gap effect) would lead to a decrease of the singlet state lifetime with the polarity in contradiction with their experimental observations. However, for such a small singlet-triplet energy gap, the rate of intersystem crossing, $k_{ISC1}$, could decrease due to the inverse gap effect: the density of vibronic triplet states which is nearly isoenergetic with the singlet state decreases as the energy gap decreases leading to lower intersystem crossing rates. In fact, these three approaches (proximity effect, inverse gap effect, activated intersystem crossing rate) predict an increase of the fluorescence lifetime and quantum yield of TX when the polarity of the solvent is enhanced.

To evaluate the two pathways population mechanism Lay et al. collected the fluorescence emission at different wavelengths (340-420 nm) (Figure 20).

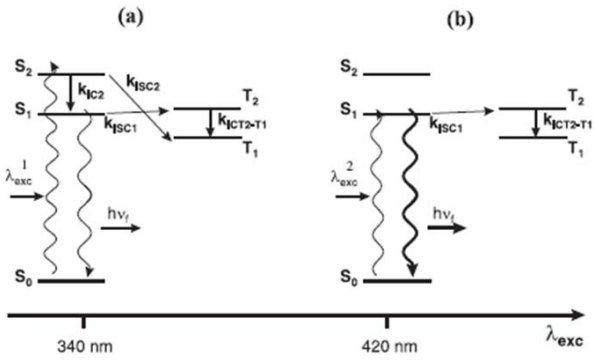


***Figure 20*** *Effect of tuning the excitation wavelength $\lambda_{exc}$ on the excited state population of TX in methanol: (a) using 340 nm wavelength populate the $S_2$ state, (b) using 420 nm excitation wavelength populate the $S_1$ state, figure took from*[70]

The relative fluorescence intensity was found to increase significantly as the excitation wavelength increased. On the one hand, when the system has been excited at 400 nm, only the $S_1$ state is populated, the triplet is no longer populated from the $S_2$ state and, consequently, the fluorescence intensity was higher. Alternatively, exciting at 355 nm results

in only the $S_2$ state being populated, and this creates a competition between the population by internal conversion to generate the $S_1$ states and the direct population of $T_1$ by ISC.

Abdullah et al. proposed an alternative interpretation of the solvatochromic effect in the fluorescence and triplet-triplet absorption[71]. The authors used well-established methods to correlate the different photophysical parameters in a polarisation function. According to various treatment[72,73], the Stokes shift depends linearly on the solvent polarisation function, the dielectric constant ε and the reflective index *n* of the solvent medium. The authors proceeded with the interpolation despite the already observed incapacity of those methods with hydroxylic solvents. Abdullah and Kemp applied the method of Bilot and Kwaski to estimate the value of the excited singlet dipole moment ($\mu_{S1}$) for TX. As already predicted, protic solvents present a strong deviation from the linear regression (Figure 21).

$$\Delta\nu_{SS} = \frac{(\mu_{s1}-\mu_{s0})^2}{hca^3}\,\mathrm{BK} + \text{constant}$$

Where

$$\mathrm{BK} = \frac{\frac{(\varepsilon-1)}{(2\varepsilon+1)} - \frac{n^2-1}{2n^2+1}}{\frac{(\varepsilon-1)}{(2\varepsilon+1)} * \frac{n^2-1}{2n^2+1}}$$

| *Solvent* | BK[a] |
|---|---|
| (1) *n*-Hexane | 0.002 |
| (2) Benzene | 0.008 |
| (3) Carbon tetrachloride | 0.023 |
| (4) Diethyl ether | 0.365 |
| (5) Dichloromethane | 0.586 |
| (6) Acetone | 0.793 |
| (7) Acetonitrile | 0.864 |
| (8) 2-Methyl-2-propanol | 0.673 |
| (9) 2-Propanol | 0.766 |
| (10) Ethanol | 0.812 |
| (11) Methanol | 0.858 |

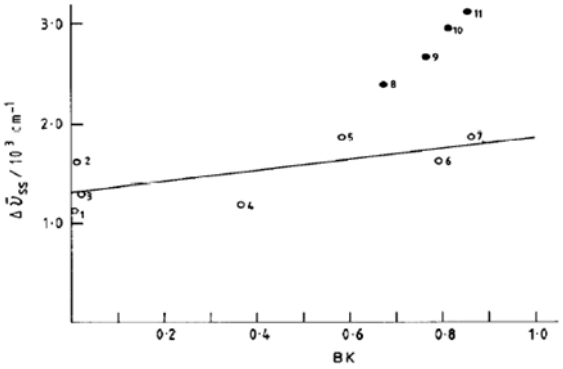


***Figure 21*** *Correlation of the Stokes shifts $\Delta\nu_{SS}$ for TX with the value of the function BK: filled circle alcoholic solvents ( excluded from the regression analysis), circles non-polar solvents. The numbering of the solvents is as in the left table. Figure is taken from*[71]

Using triplet-triplet absorption spectroscopy, the authors noticed a marked solvatochromic effect on the $T_1$-$T_n$ absorption. The spectra showed an unusual feature of a strong blue shift on increasing the solvent polarity (Figure 22). The change $\Delta\mu(T_1 \rightarrow T_n)$ in dipole moment accompanying the transition $T_1 \rightarrow T_n$ has been calculated according to Suppan's method. The authors explained the observed blue shift in the $T_1 \rightarrow T_n$ transition maxima by a decrease in the dipole moment of $T_n$ compared to that of $T_1$.

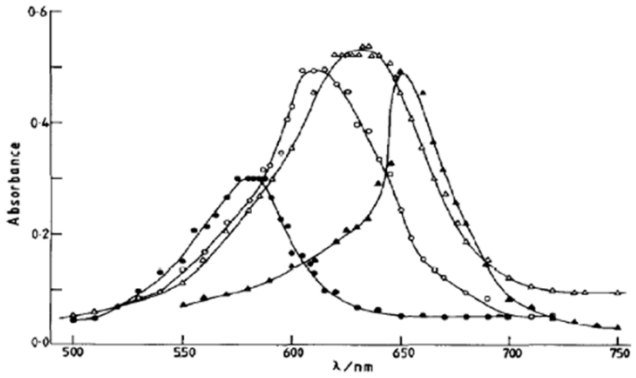


***Figure 22*** *Triplet-triplet absorption spectra of TX obtained on laser flash photolysis of deaerated solution: triangle in acetonitrile measured 5μs after the end of the excimer laser pulse; circle in ethanol measured 2μs after the end of the ruby laser pulse; full circle in 2,2,2-trifluoroethanol measured 2μs after the end of the ruby laser pulse; full triangle in cyclohexane measured 500 ns after the end of the excimer laser pulse. Figure is taken from*[71]

A decade later Morlet-Savary et al. further developed the work of Abdullah with a picosecond investigation of the solvent dependence of the $T_1$-$T_n$ absorption spectra[74]. The faster detection of the T-T absorption made it possible to observe the evolution of the triplet absorption over the time (Figure 23).

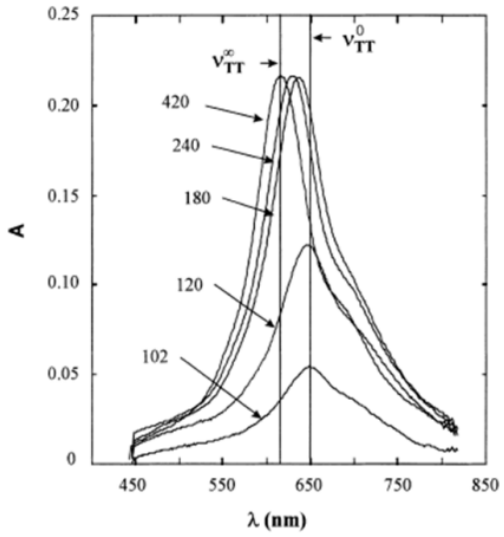


***Figure 23*** *Blue shift (Δν=775 cm-1) of the T-T absorption in 1-butanol $\nu^{0}_{TT}$ corresponds to the extrapolated minimum at time t=0 which is evaluated to be $\lambda_{max}$=648 nm. $\nu^{\infty}_{TT}$ corresponds to the maximum ($\lambda_{max}$=617 nm) observed after relaxation of the solvent and total influence of the hydrogen bond specific interaction (t=∞). Intermediate times in ps. Figure is taken from*[74]

The authors found it convenient to define two distinct maximum absorptions (Figure 19) positions for the $T_1$-$T_n$, one corresponding to the growing of the triplet state immediately after light excitation ($\nu^{0}_{TT}$), the second one ($\nu^{\infty}_{TT}$) corresponding to transition of the $T_1$-$T_n$ spectrum observed after the solute/solvents interactions. The simplest model of these observations is to consider the solvent as an environment with a static dielectric constant with an appropriate refractive index. A complete description of the solvatochromic effects would need the introduction of a term related to the transition dipole moment. This term tries to take into account the motion of electrical charges during the transition. Unfortunately, the method mentioned above does not consider any of the specific interactions such as the hydrogen bonds. In order to evaluate the greater role of those bonds in the excited states of TX the authors consider two other approaches: (1) the totally empirical method which describes all the solvent/solute interactions using one parameter $E_T(30)$, a parameter based on the UV transition energy of a betadine dye, and (2) a semi-empirical method called solvatochromic comparison method (SCM), which is in fact a multilinear approach. The

SCM method aims to unravel, quantify, correlate and rationalise all the solvent/solute interactions. This method was intended for use in linear solvation energy relationship (LASERs):

$$XYZ = XYZ_0 + \mathbf{s\pi^*} + a\boldsymbol{\alpha} + b\boldsymbol{\beta}$$

where XYZ and $XYX_0$ are the investigated proprieties in the solvent and gas phases, respectively, $\boldsymbol{\pi}^*$ is an index of solvent polarity/polarizability which measures the ability of the solvent to stabilize a charge or a dipole by virtue of its dielectric effect, $\boldsymbol{\alpha}$ describes the ability of the solvent to give a proton in a solute hydrogen bond. $\boldsymbol{\beta}$ provides the ability of the solvent to accept a proton in a solute hydrogen bond. Morlet-Savary et al. applied those three methods to the two components $\nu_{TT}^{0}$ and $\nu_{TT}^{\infty}$. For relaxed the triplet TX state solvatochromic $\nu_{TT}^{\infty}$is already been study with steady state methods in protic and H-donor solvents where $E_T(30)$ and LASER can fit perfectly all the solvents considered in the work.

Due to the nature of $\nu_{TT}^{0}$ the authors classified the solvents used based on their relaxation time as :

1.1 Nonpolar solvents

2.1 Polar but non-hydroxylic solvents

3.1 Polar and hydroxylic solvents:

$III_s$ Containing the ‘slow hydroxylic solvents', for which relaxation times are longer than 10 ps.

$III_f$ Containing the ‘fast hydroxylic solvents’, for which relaxation times are shorter than 10 ps.

With this differentiation, the authors could extrapolate the $\nu_{TT}^{0}$ dependence on the electronic polarizabilities of the solvents. From the simpler static model based on Onsager polarity

function, it can be seen that ‘fast' hydroxylic solvents fit well to the linear regression. This is a clear indication of how in these solvents, classical dipolar interactions are effective. However, the $\nu_{TT}^{\infty}$ of slow hydroxylic solvents do not correlate with the other solvents, and, moreover, are lower than expected, indicating that in these ‘slow' solvents classical dipolar interactions are not effective. Thus, in the solvents of the Classes, II and $III_f$ an equilibrium state between TX and solvent molecules has been observed, where all classical dipolar and polarizability interactions are effective (but not the specific interactions). On the other hand, in the non-polar solvents of Class I, only the electronic polarisability of the solvent can play a role in the solvation of TX. A similar case is found in the solvents of the Class $III_s$, in which dipolar interactions are not fast enough to relax before the measurement of $\nu_{TT}^{\infty}$. The authors conclude that the solvatochromism of TX should depend only on the electronic polarizability of the solvents.

It is evident the triplet excited states and quantum yield have a pivotal role. Allonas and co-workers measured and investigated the triplet quantum yield of TX with time-resolved thermal lens spectroscopy in different solvents[75]. One of the primary reasons for the lack of reliable $\Phi_T$ values is that its determination requires the knowledge of molar absorption coefficients of the transient states, an experimental parameter that is not readily determined experimentally.

For this reason, Allonas et al. used time-resolved thermal lens spectroscopy which provides a compelling alternative to transient absorption spectroscopy. Based on a change in refractive index of the solution resulting from deactivation or photoreaction of excited states and the release of the energy of excited states as heat into the solvent bath, photothermal, and the closely related photoacoustic methods have become widely used techniques for the study of photochemical processes. Moreover, the contribution of the so-called population lens (PL) to the thermal lens (TL) signal has been evidenced. This effect, arising from a change in the solute refractive index, can be one of the major artefacts that can distort the signal.

In their work, the PL due to the TX triplet state was evidenced. It was found that its effect on the TL signal depended on the wavelength of the probe beam. Accurate measurement of the triplet absorption spectrum allowed calculation of the relative change in refractive index associated with the triplet state as a function of the wavelength. Therefore, choosing a suitable probe beam wavelength made it possible to avoid perturbations caused by the PL in the TL signal, thus, enabling the measurement of $\Phi_T$ in a range of solvents.

| **Solvent** | **$\Phi_T$** |
|---|---|
| Methanol | 0.56 ± 0.08 |
| Acetonitrile | 0.66 ± 0.05 |
| Butyl acetate | 0.80 ± 0.05 |
| Benzene | 0.84 ± 0.05 |
| n- Hexane | 0.85 ± 0.05 |

Recently, Krystkowaik and co-workers have proposed an explanation for the large bathochromic shift of fluorescence emission and the increase in fluorescence lifetime and quantum yield of TX in protic solvents[76]. Using steady-state and time-resolved experiments, they confirmed the peculiar solvatochromic behaviour of TX. The spectral and photophysical results obtained in nonpolar solvents revealed a very fast deactivation of the first excited singlet state of TX through the intermolecular radiationless process of internal conversion and intersystem crossing. The rate constant of these processes strongly depended on the energy gaps between the excited singlet and triplet states $\Delta E(S_2\text{-}S_1)$(proximity effect) and $\Delta E(S_1\text{-}T_2)$. The solvatochromic data reported by Krystkowaik show that the primary pathway for $S_1$ deactivation in a protic solvent is strongly dependent on the formation of a complex between the $S_1$ state and the solvent.

$$S_1^{rel} \xrightarrow{h\nu'} S_0 \quad k_F$$
$$S_1^{rel} \rightarrow S_0 \quad k_{S_1S_0}$$
$$S_1^{rel} \rightarrow T_2(n,\pi^*) \quad \sum k_{S_1T_n} \quad n = 1, 2$$
$$S_1^{rel} \rightarrow T_1(\pi,\pi^*)$$
$$S_1^{rel} + (H-O-R)_n \xrightarrow{k_S} S_1\text{-complex}$$
$$\text{where } R = H, D, CH(CF_3)_2;\ n = 1, 2$$

This $S_1$-solvent complex can undergo deactivation by radiative and radiationless pathways

$$S_1\text{-complex} \xrightarrow{h\nu'} S_0\text{-complex} \quad k_F'$$
$$S_1\text{-complex} \rightarrow T_1\text{-complex} \quad k_{S_1T_1}'$$
$$S_1\text{-complex} \rightarrow S_0\text{-complex} \quad k_{S_1S_0}'$$

It was shown that the radiative deactivation has a higher quantum yield in most of the protic solvents and a longer lifetime in aprotic solvents.

In recent years, quantum calculations have been given greater support in the interpretation and explanations of many photophysical measurements.

In 2005 Rubio-Pons and co-workers performed a theoretical, quantum-chemical study on TX using MP2 and CASPT2 levels theory[77]. Geometry, transition energies, and excited state properties have been investigated. The authors found the existence of two different conformers with planar and non-planar structures that are close in energy. The latter has been characterised by a dihedral angle θ= 173.3° representing the bend of the outer benzene rings and an out-of-plane angle of the C=O bond (Figure 24). As a consequence of the analysis of the TX absorption spectrum, it was suggested that TX should be viewed as a dynamically changing its conformation between the planar and non-planar conformation (Figure 25). Rubio-Pons and co-workers named such behaviour as a butterfly-like motion. This dynamic view of TX could be one of the many factors which influence TX photophysical property.

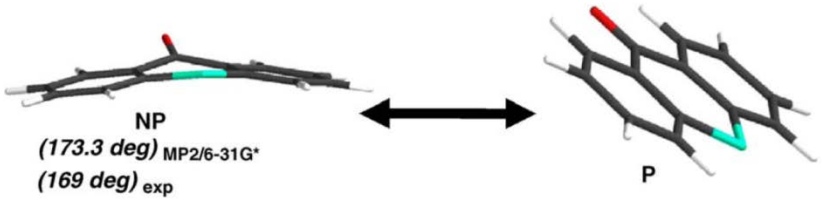


***Figure 24*** *Planar (P) and non-planar (NP) structure of TX, figure taken from*[77]

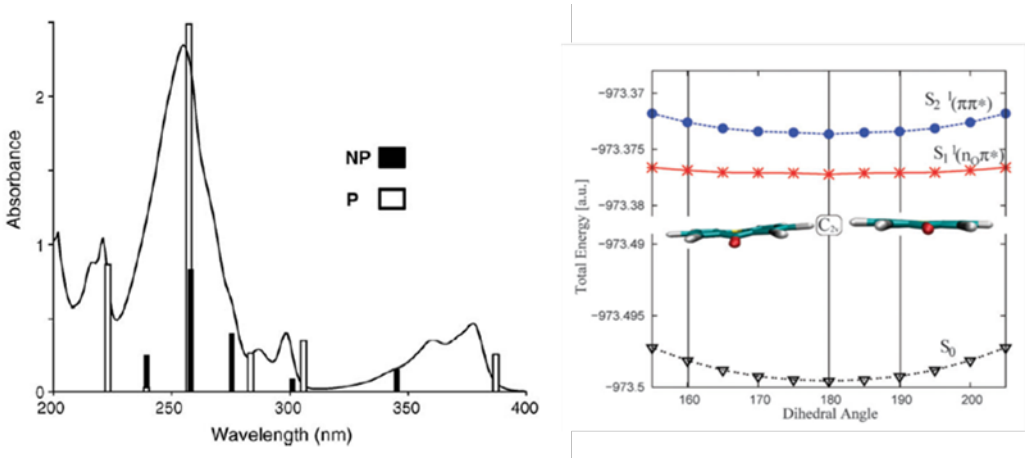


**Figure 25** *On the left TX adsorption spectra in cyclohexane. CASPT2 transitions for the planar(P) and non-planar (NP) conformation. On the right total DFT/MRC1 energies of ground electronic state ($S_0$), optically dark ($S_1$) and the optically bright state ($S_2$) along the butterfly motion reaction coordinate. Figure is taken from*[77]

A few years later Rai-Canstapel repeated the same kind of calculation but had an entire interpretation of the calculation results[78]. By optimising the ground state and the lowest-lying singlet (ππ*) geometry they found no evidence of a non–planar conformer. The first absorption band of TX has been analysed and, by comparing the results of the calculation with the measured properties, they interpreted those as various in-plane vibrational modes of the $S_0$ -> $S_2$ transition. The exact nature of the ground state of TX is still unclear and a controversial topic. In the following year, Rai-Canstapel performed further analysis with TX in the vacuum and simulated solution[79]. Using the DFT method they optimised the various electronic states, and a continuum solvent model was employed to describe the solvent environment. From their calculation, they deduced that the major structural variation is seen in the bond length of the carbonyl bond, which surprisingly has been found to have the same

lengths in water and vacuum. Even for quantum calculations polarity and hydrogen bonding play a decisive role in the energetics and the vertical excitation spectrum.

In recent work, Angulo et al. explored the ultrafast decay of the singlet excited states in several aprotic solvents again and tried to match those results with CASPT2 calculations[80]. Using ultrafast photophysical measurements Angulo et al. showed how the behaviour of TX is governed by the IC and ISC processes from the spectroscopic $S_1(\pi\pi^*)$ state toward the ground state and the lowest triplet $T_1(\pi\pi^*)$ state, respectively, which take place through intermediate $n\pi^*$-type states, $S_2(n\pi^*)$ (IC) and $T_2(n\pi^*)$ (ISC). The role of the $n\pi^*$ state in the decay dynamics was earlier emphasised by suggesting TX as a paradigm for the occurrence of the proximity effect model. Large vibronic coupling between near-degenerate $\pi\pi^*$ and $n\pi^*$ states was supposed to lead to efficient decay to the ground state via high-lying vibrational states of the latter. The photophysical behaviour of TX has been rationalised regarding conical intersection (CI) and singlet–triplet crossings connecting the different states (*v. s.*). In this respect, two CIs, readily available in the gas phase, connect the $S_1(\pi\pi^*)$ and $S_2(n\pi^*)$ states and the last state with the ground state.

Such a decay path is found to be less accessible in polar solvents, hence explaining the measured decrease in the IC rate and thus the observed increase in the quantum yield of fluorescence. This behaviour could be understood if it will be taken into consideration the role of the $S_2(n\pi^*)$ state as an intermediate, which is widely destabilised to higher energies in polar and protic solvents, and the firm stabilisation of the $S_1(\pi\pi^*)$ state, leading in both cases to the same outcome: the energy barriers to access the CIs increase and the IC is hindered. On the other hand, the ISC takes place closer to the FC configuration in polar solvents giving the system less time to evolve to the triplet state. Similar behaviour to the IC is expected for these processes because in this case, a $n\pi^*$-type state acts as an intermediate between the initial, $S_1(\pi\pi^*)$, and final $T_1(\pi\pi^*)$ states.

Another variable which can affect TX properties is the presence of substituents on the two aromatic rings, particularly those that significantly affect the electronic structure of the molecule. Particularly relevant to this work is the study of Neuman et al. who wanted to prepare TX derivatives that maintained the same photophysical properties of TX but had improved water solubility[67]. They developed and studied a variety of substituted thioxanthones, their photophysical properties and the interaction of the excited states (Figure 26).

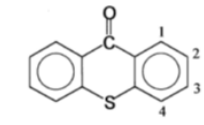


substituents

| | |
|---|---|
| TX | ----- |
| TX1 | 1-$CH_3$ + 4-$OCH_2CH_2CH_3$ |
| TX2 | 2-$OCH_2CH_2CH_3$ |
| TX3 | 1-$CH_3$ + 4-$O(CH_2)_3OCOCH{=}CH_2$ |
| TX4 | 2-$O(CH_2)_3OCOCH{=}CH_2$ |
| TXC | 2-$OCOCH_3$ |
| TX6 | 2-$OCOCH{=}CH_2$ |
| TX7 | 4-$OCH_2CH_2CH_3$ |
| TX8 | 1-OH |
| TX10 | 2-$OCH_2Ph$ |
| TXMe | 2-$CH_3$ |
| TXOH | 2-OH |

| xanthone | $\lambda_{max}$ (ACN)/nm | Singlet lifetimes/ns τ (MeOH) | τ (ACN) | Φ (ACN) |
|---|---|---|---|---|
| TX | 407 | 2.59 | 0.13 | 0.006 |
| TX1 | 438 | 8.22 | 1.01 | 0.012 |
| TX3 | 432 | 7.60 | 0.68 | 0.009 |
| TX2 | 438 | 1.02 (3%)<br>11.06 (97%) | 1.74 (10%)<br>5.09 (90%) | 0.22 |
| TX7 | | 7.80 | 1.01 | |
| TX4 | 437 | 1.87 (3%)<br>11.21 (97%) | 1.94 (10%)<br>5.81 (90%) | 0.20 |
| TXC | 415 | | 0.40 | 0.013 |
| TX6 | 415 | 3.52 | 0.46 | 0.013 |
| TX10 | | 2.37 (3%),<br>11.41 (97%) | 1.89 (14%)<br>4.52 (86%) | |
| TXMe | | 4.20 | 0.43 | 0.023 |
| TXOH | | | | 0.21 |

***Figure 26*** *Structure of TX and its substituted derivatives (left). Fluorescence lifetime and quantum yields in methanol and acetonitrile at 25 C. Figures taken from*[67]

The measurements showed that electron donor groups in position 2 lead to higher fluorescence quantum yields, a red-shift in the emission spectra and long singlet lifetimes (Figure 23). The authors explained such behaviour with an increase $S_1(\pi\pi^*)$ and $S_2(n\pi^*)$gap due to a higher electron density in the aromatic system. On the other hand, electron attractor groups on the TX ring, always in position 2, had an opposite behaviour. Moreover, the incorporation of double bonds on the side chains of the compounds did not affect the lifetime and reactivity of the TXs. Compounds substituted in position 1 with methyl or hydroxyl groups have much shorter triplet lifetimes due to the formation of an intramolecular

hydrogen bond to the carbonyl group. This type of behaviour is well known in benzophenone derivatives.

## 1.7 Photoreactivity of carotenoids

Carotenoids have an important role in the food industries and are used in most of the commercial sauces and pastes. For example, the main two carotenoids in tomato paste are lycopene and β-carotene (Figure 27 and 28 respectively). Like the vast majority of carotenoids, these compounds are not water soluble.

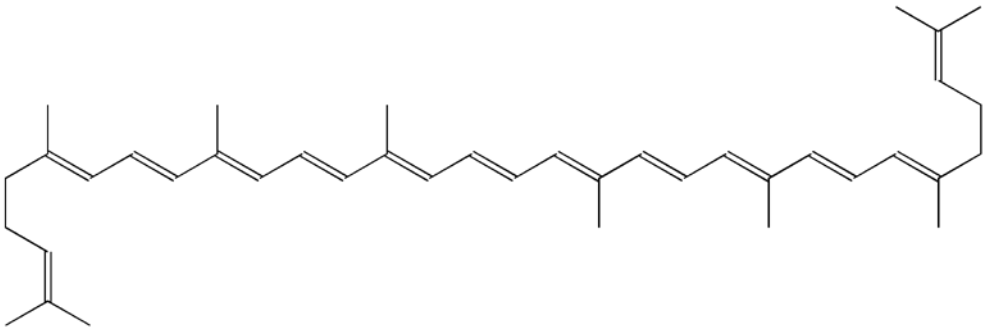

***Figure 27*** *Lycopene structure*

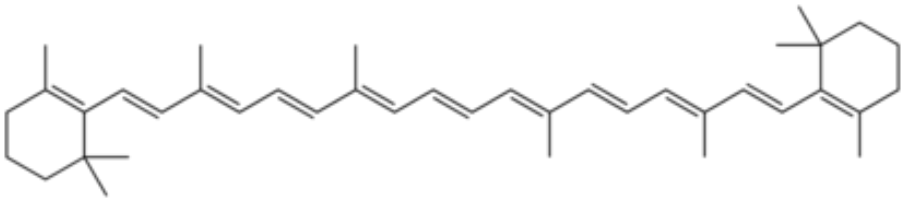

***Figure 28*** *β-carotene structure*

Even the common red spices present non-water soluble carotenoids. For example, paprika has a predominant presence of four different components β-carotene, xanthophyll, capsanthin, and capsorubin (Figure 29, 30 and 31 respectively).

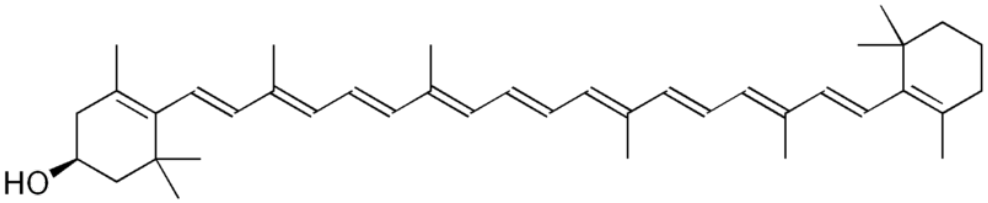


***Figure 29*** *Xanthophyll structure*

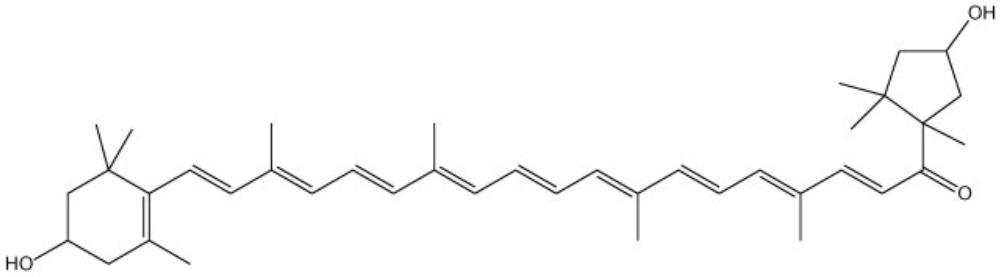


*Figure 30 Capsanthin structure*

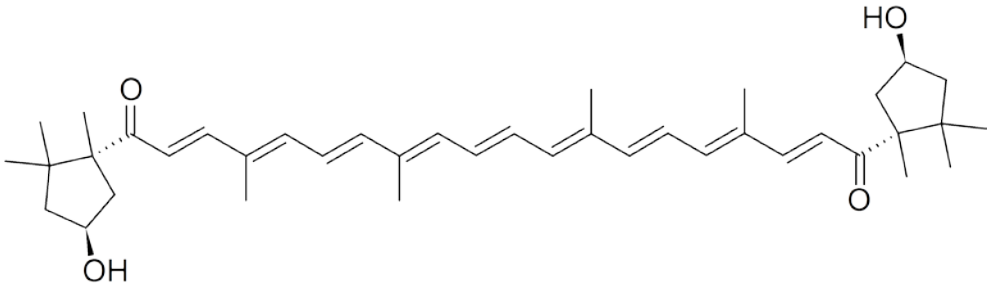


***Figure 31*** *Capsorubin structure*

Due to their wide use and poor water solubility this class of compound from stains that are amongst the most highly coloured and hardest to remove from clothes. By using efficient PBA, it will be possible remove remaining carotenoids stain during the drying process.

In this work, crocin is used to mimic the presence of a carotenoid-based stain in solution. Crocin is chosen for its unusual water solubility (Figure 32).

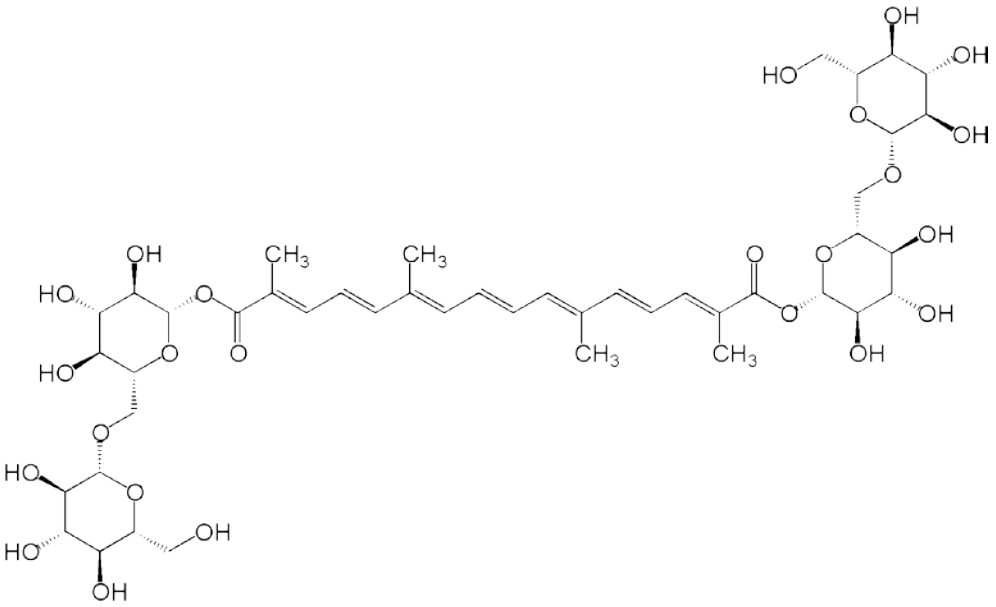

***Figure 32*** *Crocin structure*

In General, carotenoids play an important role in the photosynthetic membranes of plants and bacteria[81]. Most of the photobiological properties of carotenoids are related to their peculiar photophysical behaviour and the characteristics of their excited states which are strongly determined by their one-dimensional π-electron conjugated system. The characteristic intense absorption band in the visible region (400-500 nm) is an allowed transition from the ground state ($S_0$) to the second excited singlet state $S_2$. In general, the $S_2$ lifetime is very short (< 200 fs) and fluorescence yield extremely low. However, carotenoids show photochemical activity either by inter- or intramolecular population of their singlet and triplet excited states. Under irradiation by UV or visible light, this class of compounds undergoes a bleaching of the absorption peak. The extent of the photodegradation can be measured by the photodegradation quantum yield, $\phi_{pd}$, which is defined as the fraction of molecules degraded by the number of photons that were absorbed. In general, shorter irradiation wavelengths, higher solvent polarity and higher oxygen concentration increase $\phi_{pd}$.

In the presence of photosensitizers such as TX and derivatives, and ground state oxygen, $^3O_2$, two pathways lead to the population of $^3$Car* which can lead to *cis-trans* isomerization of the carotenoid and its possible degradation.

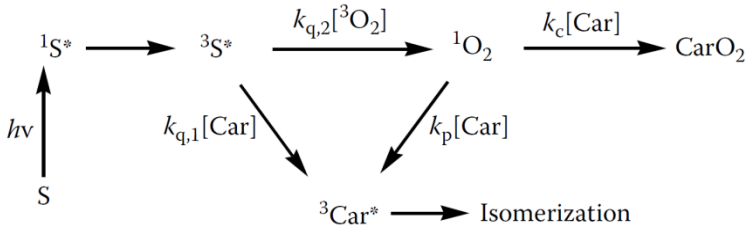


Under aerobic conditions, $^3O_2$ competes with the carotenoid molecules for the deactivation of the triplet state of the sensitizer, and in a dilute aerated solution, it is usual for $k_{q.2}[^3O_2]$ to be much greater than $k_{q.1}$[Car]. The degradation of carotenoid with singlet oxygen has been found to be dependent upon the length of the carotenoid chain. Carotenoids with more than nine conjugated double bonds have $k_{q,1}$ and $k_{q,2}$ in the diffusional range, but carotenoids with shorter chain have rate constants approximately an order of magnitude lower than the diffusion limit. Crocin is having fewer than nine conjugated double bonds, it should present a quenching rate constant below the diffusion limit.

# Chapter 2
# Experimental techniques and Synthesis

## 2.1 UV-visible spectroscopy

Absorption spectra in this work have been recorded using an ATI Unicam UV-2 spectrometer. This employs two light sources, a deuterium and a tungsten lamp. The first lamp has the maximum emission in the UV range, and the tungsten lamp mainly emits in the visible spectrum. The spectrometer automatically alternates between the two lamps at a wavelength chosen by the user. Baseline correction was carrying out by subtracting the solvent spectra.

## 2.2 Fluorescence spectroscopy

Fluorescence emission and excitation spectra have been recorded using a Fluorolog-3-22 tau from Jobin-Yvon Horiba. The applied light source in the Fluorolog is a xenon lamp, which has a broad emission spectrum and high power. The excitation wavelength is selected by a double monochromator which provides variable bandwidth (0.1 – 10 nm) and low stray light. It is possible to collect the fluorescence signal in two different ways: the typical 90° geometry and the front face which can be used for thin films or solids such as fabric samples or to study concentrated solutions. The last double monochromator before the detector scans the emission wavelengths and again offers variable bandwidth and low stray light. The emission intensity is detected by a single photon counting PMT, and the spectrum recorded on the computer using the Datamax software package.

### 2.2.1 Fluorescence quantum yields

Fluorescence quantum yields determined in this work were obtained using the comparative method of Williams et al. in which the quantum yield is expressed as[82]

$$\Phi_x = \Phi_{std} \frac{A_{std}}{A_x} \frac{I_x}{I_{std}} \frac{\eta_x^2}{\eta_{std}^2}$$

Where $\Phi_x$ and $\Phi_{std}$ are the quantum yields of the unknown and the standards respectively. A is the absorbance of the solution at the excitation wavelength, *I* is the integrated area of fluorescence emission, and $\eta$ is the refractive index of the solvent. Stock solutions of the unknown and standards were prepared with absorbance below 0.1 to minimise excitation and emission inner-filter effects. Measurements were performed using several dilutions of each sample to ensure that concentration had no effect on the fluorescence yield. In this work anthracene in ethanol is used as standard ($\Phi_{std}$ = 0.27).

### 2.2.2 Low temperature fluorescence measurements

With the same spectrometer, it is possible to record the emission and excited fluorescence at low temperature (77K) using an optical cryostat, Oxford Instruments DN1704. The solvent used to carry out this experiment is EPA, a mixture of ethanol, 2-methylbutane and diethylether 2:5:5 v/v/v. This forms a clear glass without cracks at low temperature. Samples were held in low-temperature cuvettes made from Spectrosil B. With this experiment has been possible to observe the phosphorescence of PBA.

## 2.3 Time Correlated Singlet Photon Counting

The technique of time-correlated single photon counting (TCSPC) has been used to obtain all fluorescence lifetimes of the PBA synthesised in this work (Figure 33)[83,84].

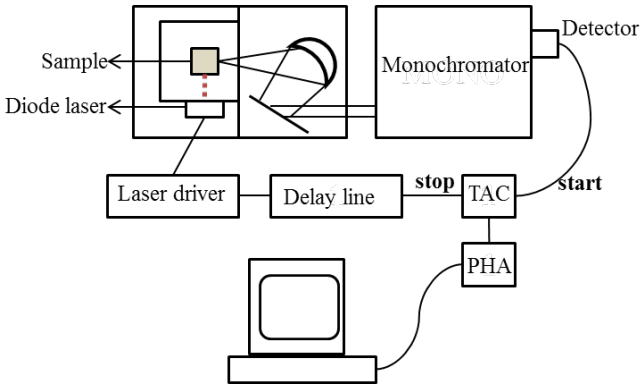


***Figure 33*** *TCSPC equipment*

Decays are obtained using a sub-nanosecond pulsed excitation source to excite the sample repeatedly, (IBH Nanoled operating at 371 or 395 nm). For each excitation pulse, the system is so arranged that only a single randomly select photon is detected following the pulse, and the time taken between pulse and photon arrival is recorded for each event. This time, an interval is measured using the voltage ramp of a time to amplitude converter (TAC). A histogram of the number of photons arriving versus time interval is built up by a pulse height analyser (PHA). At a short time interval after excitation, the probability of photon emission is greater than at a large time interval when the fluorescence has decayed, and hence, the resulting histogram represents the variation of fluorescence intensity directly with time.

The TAC works by charging a capacitor during the time interval between the start and stop pulses. In general, the TAC is the rate-limiting component in the photon counting experiment. The capacitor discharge and TAC reset take several microseconds, and so with a high repetition laser source, the TAC will be overloaded by start pulses. This problem is circumvented by operating the TAC in reverse mode, in which the detected photon triggers the start pulse, and the signal from the subsequent excitation pulse the stop signal. Hence, the TAC is only activated if an emitted photon is detected, rather than for every excitation pulse. The resulting histogram appears reversed, but correction by software is trivial.

The general and reliable method used for the analysis of the convolved data is that of non-linear least-squares analysis, which involves iterative reconvolution of the instrument response function with a chosen function and non-linear least-squares fitting[84–86]. The fitting procedure is carried out using the Solver function in Microsoft Excel, and yields values for the amplitude (A) and lifetime (τ) of the fluorescence decay. The first singlet excited state of a fluorophore usually decays via a first order process. However, in case where there are more than one emitting species the decay may be described by a sum of exponential terms,

$$I(t) = A_1\exp(-t/\tau_1)+A_2\exp(-t/\tau_2)+ \ldots$$

where A represents the fluorescence intensity at time t = 0 for the $n^{th}$ component, $\tau_n$ the lifetime for the $n^{th}$ component and I(t) the total intensity of fluorescence at time t. The contribution of each component to the overall fluorescence intensity is represented by the yield.

$$\text{Yield of } n^{th} \text{ component} = \frac{A_n\tau_n}{\sum_i A_i\tau_i} \times 100$$

The quality of fits obtained for this work was based according to two parameters:

$\chi_R^2$ (Reduced chi-squared) if only random errors contribute to $\chi_R^2$ the value is expected to be near unity.

DW (Durbin-Watson parameter), this parameter tests for correlation between deviations, returning a discrete number. A good fit will yield DW values greater than 1.7 and 1.75 for single and double exponential functions respectively.

## 2.4 Flash Photolysis

The equipment used for the flash photolysis experiment consisted of a Q switched Nd: YAG (Spectra Physics, Quanta Ray GCR-150-10) producing a 10 Hz train of pulses at 355 nm. This laser has been used to excite the sample in solution. The transient signal was probed at 90’ using a tungsten-halogen lamp (~100 W) (Figure 34).

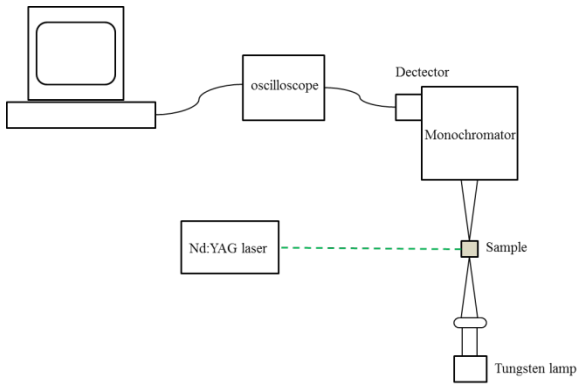


***Figure 34*** *Flash photolysis equipment*

The resulting probe beam was focused onto the entrance slit of a monochromator (Jobin Yvon Triax 320) and detected by a photomultiplier tube. Decays were averaged over 256 laser pulses, displayed in a digital oscilloscope (Tektronix TDS-340) and saved on a computer with a program developed in LabVIEW.

## 2.5 Singlet oxygen detection

The quantum yield and kinetics of singlet oxygen can be determined using the following setup (Figure 35 and 36). A pulsed nitrogen laser (337.1 nm and 357.6 nm) or the third harmonic of a Nd: YAG laser (355 nm) provides a train of short (< 5 ns) pulses which are used to excite the sample.

The singlet oxygen phosphorescence at 1270 nm is collected via an interference filter and detected by a liquid nitrogen cooled semiconductor germanium photodiode (North Coast E0-817P) or a cooled PMT (HamamatsuH1033B-45).

The signal is acquired using a digital oscilloscope which is combined with a power meter that monitors the intensity of the beam before and after the sample was used. Finally, the oscilloscope is connected to the computer and employs a program developed in LabVIEW to record the decay of the singlet oxygen emission.

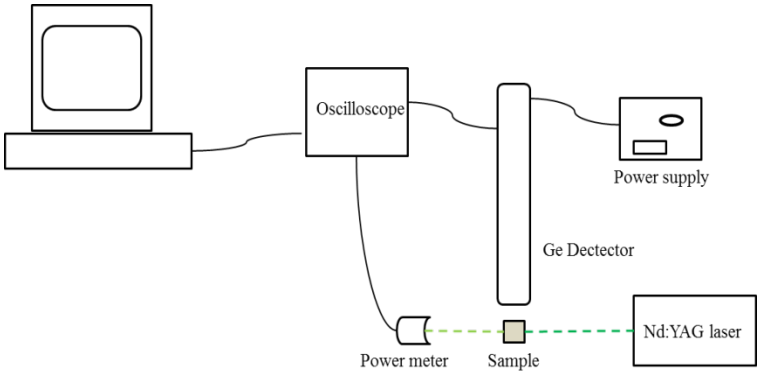


***Figure 35*** *Singlet oxygen generation equipment with Ge detector*

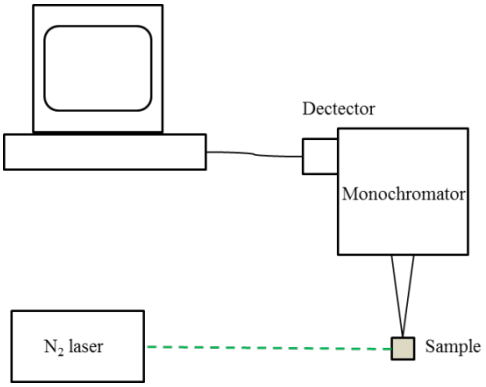


***Figure 36*** *Singlet oxygen generation equipment with PMT*

Quantum yields were determined by comparison with reference compounds. In this work, Rose Bengal in EtOH or MeOH ($\Phi_\Delta$ = 0.85) was used as a standard. The intensity of the emission was measured as a function of laser power for the unknown and the standard, and the gradients, I, compared

$$\Phi_{\Delta_x} = \Phi_{\Delta_{std}} \frac{A_{std}}{A_x} \frac{I_x}{I_{std}}$$

A is the absorbance of the solution of the standard and the unknown (x)at the excitation wavelength.

## 2.6 Colour measurement

Several tests have been carried out in P&G's research laboratories to determine the behaviour of PBAs under real-life wash conditions. These tests were made using squares of cotton cloth with a specified stain applied on it.

More details on the swatches will be given in the 5th chapter where methodology and results will be discussed. The aim of those tests is to evaluate the cleanness performance of detergent and PBAs on the swatches. To establish their action, all the swatches were marked with a unique alphanumeric code and analysed before and after the washing and drying processes. The analysis was carried out with DigiEye[87] equipment in use in P&G Newcastle innovation centre (Figure 37).

***Figure 37*** *DigiEye equipment in use in P&G Newcastle, imagine taken from manufactures website*[87]

DigiEye full system is VeriVide equipment for textile and apparel and records data with a sensitivity matching a human eye. The equipment consists of a case within an extractable tray with A4 dimension. The user can place samples on the plate and introduce these into the cube where it will be illuminated with diffuse CIE D65 white light to give the most realistic appearance of the items. An aperture is located perpendicular to the tray centre where a high definition camera is placed.

Before the first measurement, the system needs to be calibrated by taking a picture of a dedicated grid where all different colours are placed in a precise position. By loading the photograph into the software, the system recognises the colours in the different position and calibrates itself automatically. The software will alert the user every time a calibration is needed (Figure 38).

***Figure 38*** *Example of calibration procedure with DigiEye, imagine taken from manufactureswebsite*[87]

Users can easily analyse the sample by taking pictures of them and extrapolating the point-by-point colour values thanks to dedicated software (Figure 39). Firstly the user needs to create a circle with a chosen diameter and by clicking on the area want to be analysed. With this software, it is possible to create templates with different fixed positions from which the circle will automatically extrapolate the colour value. This option reduces the analysis time drastically. Once the software extrapolates the colour value, the user can pass this information into an excel file for further analysis

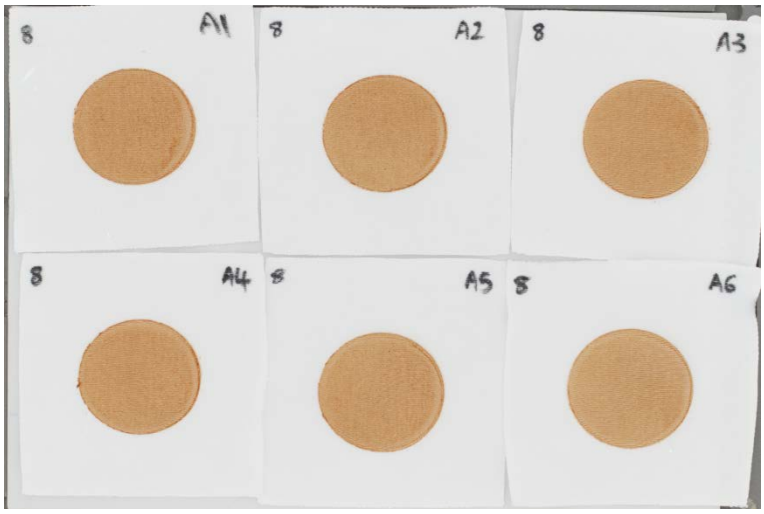


***Figure 39*** *Example of picture taken with DigiEye equipment of swatchers before washing*

As already mentioned the software employed can determine the colour value from a highlighted area. The colour is classified by **L, a,b** values which identify every colour uniquely with a particular combination of those parameters. **L, a,b** can be represented as Cartesian axes and create a colour space[88] (Figure 40).

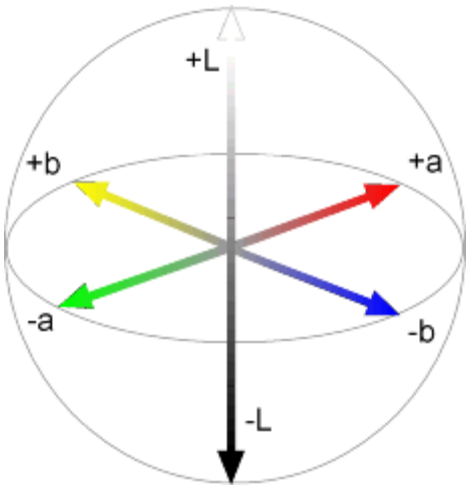


***Figure 40*** *L,a,b colour space*

As shown in the picture **L** represents the brightness of the sample, with the darkest black at **L** = 0, and the brightest white at **L** = 100. The colour channels, **a** and **b**, will represent true neutral grey values at **a** = 0 and **b** = 0. The red/green opponent colours are represented along the **an** axis, with green at negative values and red at positive a values. The yellow/blue opponent colours are represented along the **b** axis, with blue at negative **b** values and yellow at positive **b** values. Another key point of the **L, a,b** model is that it is device independent. This means the colour value extrapolated with DigiEye will be consistent with any other device using the same **L, a,b** method.

## 2.7 General synthetic procedures

All reagents were used as received from their respective suppliers. Solvents were laboratory grade. Air sensitive reactions were carried out under an atmosphere of nitrogen using Schlenk-line techniques.

Electrospray mass spectra were obtained on a TQD mass spectrometer equipped with an Acquity UPLC, an electrospray ion source and an Acquity photodiode array detector ( Waters Ltd, UK). Methanol was used as the carrier solvent.

Accurate masses were recorded on a QTOF Premier mass spectrometer equipped with an Acquity UPLC, a lock-mass electrospray ion source and an Acquity photodiode array detector (Wasters Ltd, UK). Methanol was used as the carrier solvent.

$^{1}H$,$^{13}C$ NMR spectra were obtained at 295 K on Varian spectrometers operating at 4.7, 9.4, 11.7, 14.1 16.5 Tesla, specifically on a Mercury 200 ($^{1}H$ at 200.06 MHz, $^{13}C$ at 50.30 MHz), a Mercury 400 spectrometer ($^{1}H$ at 399.97 MHz, $^{13}C$ at 100.61 MHz), a Varian Inova-500 spectrometer ($^{1}H$ at 499.78 MHz, $^{13}C$ at 155.69), a Varian VNMRS-600 spectrometer ($^{1}H$ at 599.94 MHz, $^{13}C$ at 150.86 MHz) and a Varian VNMRS-700 spectrometer ($^{1}H$ at 700.00 MHz, $^{13}C$ at 175.95 MHz). Commercially available deuterated solvents were used. All chemical shifts are given in ppm with coupling constants in Hz.

**1 9-oxothioxanthene-2-carboxylic acid - TXCOOH**

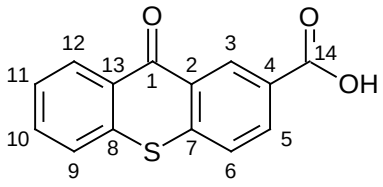


Under nitrogen 4-bromoisophthalic acid (1 g, 4 mmol), thiophenol (0.44 g, 4 mmol), Cu-bronze (12 mg, 0.2 mmol), and $K_2CO_3$ (1.75 g, 12.67 mmol) were refluxed overnight in DMF (50 mL). After cooling, the mixture was filtered, and the residue was dissolved in

water (minimum amount). The solution was carefully acidified with concentrated HCl to pH<1. The product was precipitated and collected. Under nitrogen, the intermediate (1g, 3.65 mmol) was refluxed in dichloroethane (50 mL) and $SOCl_2$ (10 mL) until the evolution of HCl gas had ceased. The mixture was concentrated in vacuo; the residue was washed twice with dichloroethane (10 mL each time). The residue was dissolved in dichloroethane (20 mL) and cooled at -5°C after which $AlCl_3$ (2 g, 14 mmol) was added. The resulting black mixture was stirred for 90 minutes at -5°C. The reaction was quenched by careful addition of water (100 mL). The product was extracted with DCM (twice 20 mL). The combined organic layers were washed with water, dried, and concentrated in vacuo[89]. Yield 95%. This molecule was used as a precursor for most of the derivatives synthesised later. $^1$H NMR (600 MHz, Chloroform-*d*) $\delta_H$ 9.37 (d, *J* = 2.1 Hz, 1H, $H^3$), 8.64 (dd, *J* = 8.2, 1.5 Hz, 1H, $H^{12}$), 8.24 (dd, *J* = 8.5, 2.1 Hz, 1H, $H^5$), 7.72 – 7.68 (m, 2H, $H^{6,11}$), 7.62 (d, *J* = 7.7 Hz, 1H, $H^9$), 7.57 (ddd, *J* = 8.1, 7.0, 1.1 Hz, 1H, $H^{10}$).$^{13}$C NMR (600 MHz, Chloroform-*d*) $\delta_C$ 178.57 ($C^1$), 128.98 ($C^2$), 130.34 ($C^3$), 141.93 ($C^4$), 132.38 ($C^5$), 127.20 ($C^6$),126.33 ($C^7$),128.27 ($C^8$),127.20 ($C^9$),127.33 ($C^{10}$),133.42 ($C^{11}$),129.19 ($C^{12}$),136.11 ($C^{13}$),166.46 ($C^{14}$). *m/z* (ESI) 257.0 $[M + H]^+$

**7-tert-butyl-9-oxo-thioxanthene-2-carboxylic acid - TERTTX**

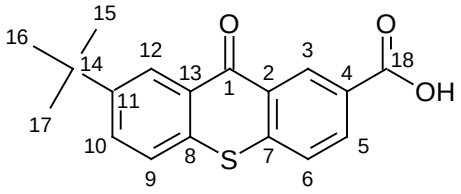


Under nitrogen 4-bromoisophthalic acid (1 g, 4 mmol), 4-tert-butylbenzenethiol (0.64 g, 4 mmol), Cu-bronze (12 mg, 0.2 mmol), and $K_2CO_3$ (1.75 g, 12.67 mmol) were refluxed overnight in DMF (50 mL). After cooling, the mixture was filtered, and the residue was dissolved in water (minimum amount). The solution was carefully acidified with concentrated HCl to pH<1. The product was precipitated and collected. Under nitrogen, the

intermediate (1g, 3.65 mmol) was refluxed in dichloroethane (50 mL) and $SOCl_2$ (10 mL) until the evolution of HCl gas had ceased. The mixture was concentrated in vacuo; the residue was washed twice with dichloroethane (10 mL each time). The residue was dissolved in dichloroethane (20 mL) and cooled at -5°C after which $AlCl_3$ (2 g, 14 mmol) was added. The resulting black mixture was stirred for 90 minutes at -5°C. The reaction was quenched by careful addition of water (100 mL). The product was extracted with DCM (twice 20 mL). The combined organic layers were washed with water, dried, and concentrated in vacuo. Final yield 93%. $^1$H NMR (600 MHz, DMSO-$d_6$) δ 8.98 (d, $J$ = 1.9 Hz, 1H, $H^3$), 8.46 (d, $J$ = 2.2 Hz, 1H, $H^{12}$), 8.19 (dd, $J$ = 8.4, 2.0 Hz, 1H, $H^5$), 7.95 (d, $J$ = 8.4 Hz, 1H, $H^6$), 7.91 (dd, $J$ = 8.5, 2.3 Hz, 1H, $H^9$), 7.82 (d, $J$ = 8.4 Hz, 1H, $H^{10}$), 1.36 (s, 9H, $H^{15\text{-}17}$).$^{13}$C NMR (151 MHz, DMSO-$d_6$) δ 179.06 ($C^1$), 166.81 ($C^{18}$), 150.50 ($C^{11}$), 141.79 ($C^4$), 133.72 ($C^{13}$), 132.67 ($C^5$), 131.90 ($C^9$), 130.73 ($C^3$), 129.30 ($C^2$), 128.62($C^7$), 128.28($C^8$), 127.66($C^6$), 127.14($C^{10}$), 125.17 ($C^{12}$), 35.15 ($C^{15\text{-}17}$), 31.26 ($C^{14}$). *m/z* (ESI) 313.1 $[M + H]^+$

**N-(1-ethylpropyl)-9-oxo-thioxanthene-2-carboxamide - TXCONET$_2$**

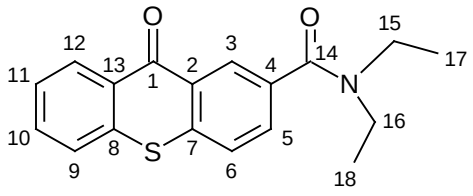


Under nitrogen 9-oxothioxanthene-2-carboxylic acid (100 mg, 0.39 mmol), pentan-3-amine (53.34 mg, 0.59 mmol), DCC (1.1 equivalent), and DMAP (3-10 mol %) were dissolved in DCM (50 mL) in a -5°C bath for 5 hours. The reaction was quenched by addition of water (25 mL). The product was extracted with DCM (twice 20 mL). The combined organic layers were washed with water, dried , and concentrated in vacuo. The crude of mixture was purified by flash column chromatography (silica, DMC: ethil acetate 30 – 60 %). Final yield 80%. $^1$H NMR (700 MHz, Chloroform-*d*) δ 8.62 – 8.61 (m, 2H, $H^{3,12}$), 7.69 (dd, $J$ = 8.2, 1.9 Hz, 1H,

$H^{5}$), 7.66 – 7.62 (m, 2H, $H^{6,11}$), 7.59 (ddd, *J* = 8.0, 1.2, 0.6 Hz, 1H, $H^{9}$), 7.51 (ddd, *J* = 8.2, 7.0, 1.3 Hz, 1H, $H^{10}$), 3.45 (d, *J* = 186.5 Hz, 4H, $H^{14,16}$), 1.22 (d, *J* = 76.4 Hz, 6H, $H^{15,17}$). $^{13}$C NMR (176 MHz, Chloroform-*d*) δ 179.47 ($C^{1}$), 169.74 ($C^{14}$), 138.27 ($C^{4}$), 136.91 ($C^{13}$), 135.10 ($C^{11}$), 132.53 ($C^{5}$), 130.70 ($C^{3}$), 129.93 ($C^{2}$), 129.09 ($C^{12}$), 128.70 ($C^{8}$), 127.44 ($C^{6}$), 126.62 ($C^{9}$), 126.50 ($C^{10}$), 126.05 ($C^{7}$), 43.65 ($C^{15}$), 39.58 ($C^{17}$), 14.44 ($C^{7}$),12.88 ($C^{15,18}$). *m/z* (ESI) 312.1 $[M + H]^{+}$

**N-heptyl-9-oxo-thioxanthene-2-carboxamide - TXCONC$_7$**

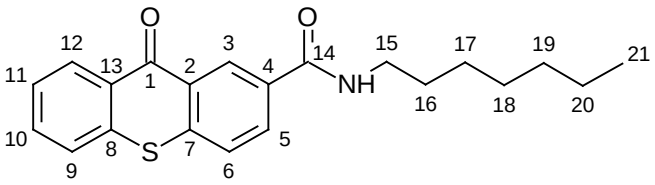


Under nitrogen 9-oxothioxanthene-2-carboxylic acid (100 mg, 0.39 mmol), heptan-1-amine (67.46 mg, 0.59 mmol), DCC (1.1 equivalent), and DMAP (3-10 mol %) were dissolved in DCM (50 mL) in a -5°C bath for 5 hours. The reaction was quenched by addition of water (25 mL). The product was extracted with DCM (twice 20 mL). The combined organic layers were washed with water, dried , and concentrated in vacuo. The crude of mixture was purified by flash column chromatography (silica, DMC: ethil acetate 30 – 60 %). Final yield 83%. $^{1}$H NMR (600 MHz, Chloroform-*d*) δ 8.84 (d, *J* = 2.1 Hz, 1H, $H^{3}$), 8.64 (dd, *J* = 8.1, 1.5 Hz, 1H, $H^{12}$), 8.22 (dd, *J* = 8.4, 2.1 Hz, 1H, $H^{5}$), 7.69 – 7.65 (m, 2H, $H^{6,11}$), 7.63 – 7.60 (m, 1H, $H^{9}$), 7.54 (ddd, *J* = 8.2, 7.0, 1.3 Hz, 1H, $H^{10}$), 3.54 – 3.49 (m, 2H, $H^{15}$), 1.66 (p, *J* = 7.4 Hz, 2H, $H^{16}$), 1.45 – 1.16 (m, 8H, $H^{17-20}$), 0.93 – 0.84 (m, 3H, $H^{21}$). $^{13}$C NMR (151 MHz, Chloroform-*d*) δ 179.65 ($C^{1}$), 165.84 ($C^{14}$), 140.59 ($C^{4}$), 136.85 ($C^{13}$), 132.73 ($C^{11}$), 132.64 ($C^{2}$), 131.63 ($C^{5}$), 129.96 ($C^{12}$), 128.98 ($C^{7}$), 128.50 ($C^{8}$), 126.80 ($C^{10}$), 126.75 ($C^{6}$), 126.64 ($C^{3}$), 126.14 ($C^{9}$), 40.31 ($C^{15}$), 31.73( $C^{17}$), 29.64 ($C^{16}$), 28.98 ($C^{20}$), 26.98 ($C^{19}$), 22.59 ($C^{18}$), 14.05 ($C^{21}$). *m/z* (ESI) 354.2 $[M + H]^{+}$

**N-(2-hydroxyethyl)-9-oxo-thioxanthene-2-carboxamide - TXCONCO$_2$OH**

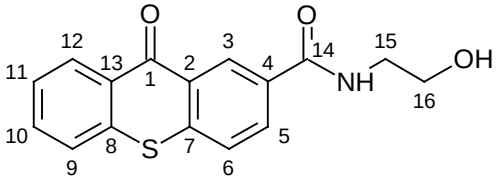


Under nitrogen 9-oxothioxanthene-2-carboxylic acid (100 mg, 0.39 mmol), 2-aminoethanol (35.76 mg, 0.59 mmol), DCC (1.1 equivalent), and DMAP (3-10 mol %) were dissolved in DCM (50 mL) in a -5°C bath for 5 hours. The reaction was quenched by addition of water (25 mL). The product was extracted with DCM (twice 20 mL). The combined organic layers were washed with water, dried , and concentrated in vacuo. The crude of mixture was purified by flash column chromatography (silica, DMC: ethil acetate 30 – 60 %). Final yield 79%.

$^1$H NMR (600 MHz, Chloroform-*d*) δ 8.90 (d, *J* = 2.1 Hz, 1H, H$^3$), 8.45 (dd, *J* = 8.1, 1.5 Hz, 1H, H$^{12}$), 8.08 (dd, *J* = 8.4, 2.1 Hz, 1H, H$^5$), 7.54 – 7.51 (m, 2H, H$^{6,11}$), 7.49 – 7.46 (m, 1H, H$^9$), 7.37 (ddd, *J* = 8.2, 6.9, 1.3 Hz, 1H, H$^{10}$), 3.66 – 3.63 (m, 2H, H$^{15}$), 3.47 (q, *J* = 5.1 Hz, 2H, H$^{16}$). $^{13}$C NMR (151 MHz, Chloroform-*d*) δ 179.38 (C$^1$), 166.32 (C$^{14}$), 140.20 (C$^4$), 136.65 (C$^{13}$), 132.57 (C$^{11}$), 132.56 (C$^5$), 131.48 (C$^2$), 129.66 (C$^{12}$), 128.92 (C$^7$), 128.46 (C$^8$), 127.74 (C$^{10}$) , 126.60 (C$^6$), 126.31 (C$^3$), 126.07 (C$^9$), 61.41 (C$^{15}$), 43.22 (C$^{16}$). *m/z* (ESI) 300.1 [M + H]$^+$

**N-(3-hydroxypropyl)-9-oxo-thioxanthene-2-carboxamide - TXCONCO$_3$OH**

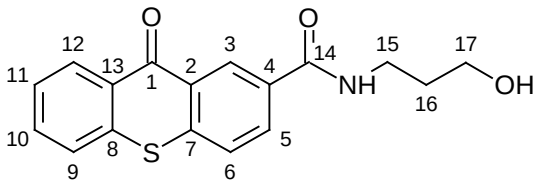

Under nitrogen 9-oxothioxanthene-2-carboxylic acid (100 mg, 0.39 mmol), 3-aminopropan-1-ol (43.96 mg, 0.59 mmol), DCC (1.1 equivalent), and DMAP (3-10 mol %) were dissolved in DCM (50 mL) in a -5°C bath for 5 hours. The reaction was quenched by addition of water (25 mL). The product was extracted with DCM (twice 20 mL). The combined organic layers were washed with water, dried , and concentrated in vacuo. The crude of mixture was purified by flash column chromatography (silica, DMC: ethil acetate 30 – 60 %). Final yield 81%. $^{1}$H NMR (600 MHz, Chloroform-*d*) δ 8.81 (d, *J* = 2.1 Hz, 1H, $H^{3}$), 8.41 – 8.38 (m, 1H, $H^{12}$), 8.00 (dd, *J* = 8.4, 2.1 Hz, 1H, $H^{5}$), 7.50 – 7.45 (m, 2H, $H^{6,11}$), 7.43 (dd, *J* = 8.1, 1.2 Hz, 1H, $H^{9}$), 7.32 (ddd, *J* = 8.2, 7.0, 1.3 Hz, 1H, $H^{10}$), 3.49 (t, *J* = 5.7 Hz, 2H, $H^{15}$), 3.40 (q, *J* = 6.0 Hz, 2H, $H^{16}$), 1.63 (p, *J* = 5.9 Hz, 2H, $H^{17}$). $^{13}$C NMR (151 MHz, Chloroform-*d*) δ 179.26 ($C^{1}$), 166.27 ($C^{14}$), 140.08 ($C^{4}$), 136.59 ($C^{13}$) , 132.56 ($C^{5}$), 132.55 ($C^{11}$),131.27 ($C^{2}$), 129.58 ($C^{7}$), 128.85 ($C^{8}$), 128.43 ($C^{10}$), 127.66 ($C^{6}$), 126.57 ($C^{3}$), 126.27 ($C^{9}$), 126.04 ($C^{12}$), 59.27 ($C^{15}$), 36.94 ($C^{16}$), 31.78 ($C^{17}$). *m/z* (ESI) 314.1 $[M + H]^{+}$

**Methyl 2-[(7-tert-butyl-9-oxo-thioxanthene-2-carbonyl)amino]acetate - TERTTXGLY**

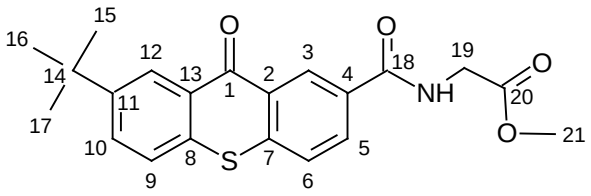


Under nitrogen 7-tert-butyl-9-oxo-thioxanthene-2-carboxylic acid (117 mg, 0.39 mmol), methyl 2-aminoacetate (52.16 mg, 0.59 mmol), DCC (1.1 equivalent), and DMAP (3-10 mol %) were dissolved in DCM (50 mL) in a -5°C bath for 5 hours. The reaction was quenched by addition of water (25 mL). The product was extracted with DCM (twice 20 mL). The combined organic layers were washed with water, dried , and concentrated in vacuo. The crude of mixture was purified by flash column chromatography (silica, DMC: ethil acetate 30 – 60 %). Final yield 80%. $^{1}$H NMR (700 MHz, Chloroform-*d*) δ 8.95 (d, *J* = 2.1 Hz, 1H, $H^{3}$),

8.64 (d, *J* = 2.2 Hz, 1H, $H^{12}$), 8.16 (dd, *J* = 8.4, 2.1 Hz, 1H, $H^{5}$), 7.73 (dd, *J* = 8.4, 2.3 Hz, 1H, $H^{6}$), 7.68 – 7.66 (m, 1H, $H^{9}$), 7.56 – 7.54 (m, 1H, $H^{10}$), 4.30 (d, *J* = 5.1 Hz, 2H, $H^{19}$), 3.82 (s, 3H, $H^{21}$), 1.41 (s, 9H, $H^{15\text{-}17}$). $^{13}$C NMR (176 MHz, Chloroform-*d*) δ 179.44 ($C^{1}$), 170.18 ($C^{20}$), 166.04 ($C^{18}$), 141.10 ($C^{11}$), 136.68 ($C^{13}$), 132.73 ($C^{7}$), 131.52 ($C^{9}$), 131.31 ($C^{3}$), 129.98 ($C^{2}$), 128.98 ($C^{5}$), 128.64 ($C^{8}$),127.47 ($C^{4}$), 126.84 ($C^{6}$) , 126.74 ($C^{10}$), 126.11 ($C^{12}$), 52.52 ($C^{21}$), 41.82 ($C^{19}$), 34.99 ($C^{14}$), 31.06 ($C^{15\text{-}17}$). *m/z* (ESI) 384.1 $[M + H]^{+}$

**Methyl 2-[(9-oxothioxanthene-2-carbonyl)amino]acetate - TXCOGLY**

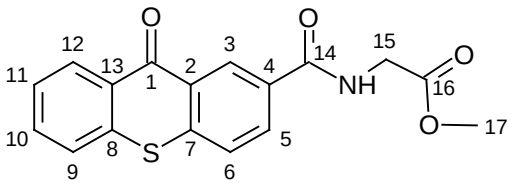


Under nitrogen 9-oxothioxanthene-2-carboxylic acid (100 mg, 0.39 mmol), methyl 2-aminoacetate (52.16 mg, 0.59 mmol), DCC (1.1 equivalent), and DMAP (3-10 mol %) were dissolved in DCM (50 mL) in a -5°C bath for 5 hours. The reaction was quenched by addition of water (25 mL). The product was extracted with DCM (twice 20 mL). The combined organic layers were washed with water, dried , and concentrated in vacuo. The crude of mixture was purified by flash column chromatography (silica, DMC: ethil acetate 30 – 60 %). Final yield 84%. $^{1}$H NMR (600 MHz, Chloroform-*d*) δ 8.95 (dd, *J* = 2.1, 0.6 Hz, 1H, $H^{3}$), 8.65 – 8.62 (m, 1H, $H^{12}$), 8.19 (dd, *J* = 8.4, 2.1 Hz, 1H, $H^{5}$), 7.69 – 7.65 (m, 2H, $H^{6,11}$), 7.62 – 7.60 (m, 1H, $H^{9}$), 7.53 (ddd, *J* = 8.2, 7.0, 1.3 Hz, 1H, $H^{10}$), 4.30 (s, 2H, $H^{15}$), 3.82 (s, 3H, $H^{17}$). $^{13}$C NMR (151 MHz, Chloroform-*d*) δ 179.43 ($C^{1}$), 170.13 ($C^{14}$), 165.96 ($C^{16}$), 141.11 ($C^{13}$), 136.67 ($C^{11}$), 132.74 ($C^{5}$), 131.51 ($C^{3}$), 131.30 ($C^{4}$), 130.00 ($C^{2}$), 129.01 ($C^{12}$), 128.69 ($C^{8}$), 127.45 ($C^{6}$), 126.86 ($C^{9}$), 126.76 ($C^{7}$), 126.12 ($C^{10}$), 52.53 ($C^{17}$), 41.72 ($C^{15}$). *m/z* (ESI) 328.1 $[M + H]^{+}$

**7-tert-butyl-N-(2-morpholinoethyl)-9-oxo-thioxanthene-2-carboxamide- TERTTXMORPHO**

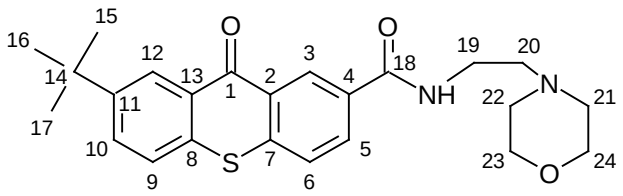


Under nitrogen 7-tert-butyl-9-oxo-thioxanthene-2-carboxylic acid (117 mg, 0.39 mmol), 2-morpholinoethanamine (76.22 mg, 0.59 mmol), DCC (1.1 equivalent), and DMAP ( 3-10 mol %) were dissolved in DCM (50 mL) in a -5°C bath for 5 hours. The reaction was quenched by addition of water (25 mL). The product was extracted with DCM (twice 20 mL). The combined organic layers were washed with water, dried , and concentrated in vacuo. The crude of mixture was purified by flash column chromatography (silica, DMC: ethil acetate 30 – 60 %). Final yield 85%. $^{1}$H NMR (600 MHz, Chloroform-*d*) δ 8.94 (s, 1H, $H^{3}$), 8.62 (dd, *J* = 8.1, 1.5 Hz, 1H, $H^{12}$), 8.22 (dd, *J* = 8.4, 2.0 Hz, 1H, $H^{5}$), 7.68 – 7.64 (m, 2H, $H^{6,11}$), 7.60 (dd, *J* = 7.9, 1.1 Hz, 1H, $H^{9}$ ), 7.53 (ddd, *J* = 8.2, 7.1, 1.3 Hz, 1H, $H^{10}$), 1.95 – 1.91 (m, 2H, $H^{23}$), 1.69 (dt, *J* = 13.6, 4.0 Hz, 2H, $H^{20}$), 1.63 – 1.56 (m, 2H, $H^{19}$), 1.36 (s, 9H, $H^{15-17}$), 1.34 – 1.30 (m, 2H, $H^{18}$), 1.19 – 1.05 (m, 4H, $H^{19,22}$). $^{13}$C NMR (151 MHz, Chloroform-*d*) δ 179.54 ($C^{1}$), 166.12 ($C^{14}$), 156.66 ($C^{11}$), 140.69 ($C^{4}$), 136.75 ($C^{13}$), 135.25 ($C^{5}$), 132.68 ($C^{9}$), 131.28 ($C^{3}$), 129.95 ($C^{2}$), 129.02 ($C^{7}$), 128.66 ($C^{8}$), 126.80($C^{6}$), 126.66 ($C^{10}$), 126.11 ($C^{12}$), 35.15 ($C^{18-19}$), 33.94($C^{15,16}$), 31.26 ($C^{14}$), 25.60 ($C^{20,22}$), 24.92 ($C^{21,23}$). *m/z* (ESI) 425.2 $[M + H]^{+}$

**N-(2-morpholinoethyl)-9-oxo-thioxanthene-2-carboxamide - TXCOMORPHO**

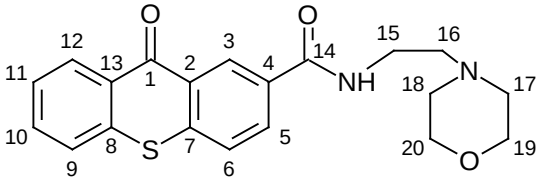

Under nitrogen 9-oxothioxanthene-2-carboxylic acid (100 mg, 0.39 mmol 2-morpholinoethanamine (76.22 mg, 0.59 mmol), DCC ( 1.1 equivalent), and DMAP ( 3-10 mol %) were dissolved in DCM (50 mL) in a -5°C bath for 5 hours. The reaction was quenched by addition of water ( 25 mL). The product was extracted with DCM (twice 20 mL). The combined organic layers were washed with water, dried , and concentrated in vacuo. The crude of mixture was purified by flash column chromatography ( silica, DMC: ethil acetate 30 – 60 %). Final yield 86%. $^{1}$H NMR (600 MHz, Chloroform-*d*) δ 8.94 (s, 1H, $H^{3}$), 8.62 (dd, *J* = 8.1, 1.5 Hz, 1H, $H^{12}$), 8.22 (dd, *J* = 8.4, 2.0 Hz, 1H, $H^{5}$), 7.68 – 7.64 (m, 2H, $H^{6,11}$), 7.60 (dd, *J* = 7.9, 1.1 Hz, 1H, $H^{9}$ ), 7.53 (ddd, *J* = 8.2, 7.1, 1.3 Hz, 1H, $H^{10}$), 1.95 – 1.91 (m, 2H, $H^{15}$), 1.69 (dt, *J* = 13.6, 4.0 Hz, 2H, $H^{20}$), 1.63 – 1.56 (m, 2H, $H^{19}$), 1.38 – 1.30 (m, 2H, $H^{18}$), 1.19 – 1.05 (m, 4H, $H^{16,17}$). $^{13}$C NMR (151 MHz, Chloroform-*d*) δ 179.54 ($C^{1}$), 166.12 ($C^{14}$), 156.66 ($C^{11}$), 140.69 ($C^{4}$), 136.75 ($C^{13}$), 135.25 ($C^{5}$), 132.68 ($C^{9}$), 131.28 ($C^{3}$), 129.95 ($C^{2}$), 129.02 ($C^{7}$), 128.66 ($C^{8}$), 126.80($C^{6}$), 126.66 ($C^{10}$), 126.11 ($C^{12}$), 33.94($C^{15,16}$), 25.60 ($C^{20,17}$), 24.92 ($C^{19,18}$). *m/z* (ESI) 396.1 $[M + H]^{+}$

# Chapter 3
# Photophysical characterization of thioxanthone derivatives

In this chapter, a full analysis of the photophysical properties of thioxanthone and derivatives is reported.

The primary goal of this project is the synthesis of new TX derivatives that conserve the unique ability of TX to act as a photosensitizer. The new compounds need to maintain the UV absorption transition and ideally have an equal or higher quantum yield of singlet oxygen formation.

Another important aspect to be taken into account is the interaction of these new compounds, with other laundry components such as detergent and stains, particularly those containing carotenoids. To have a full comprehension of the behaviour in a simulated consumer situation, all the compounds have been dissolved in LAS soap provided by P&G. The use of this surfactant could help to solubilise the derivatives of TX in the wash liquor. These derivatives do not need to be completely water soluble as this might mean that are more likely to be washed out during the washing process.

Crocin, a well-known water-soluble carotenoid, has been used to mimic a carotenoid stain in solution. By measuring derivatives fluorescence lifetime measurements in the presence of increasing concentration of crocin it has been possible to measure the rate of quenching between the two species. Furthermore, it has been possible to measure the singlet oxygen quantum yield in the presence of increasing amount of quencher.

## 3.1 UV-visible spectroscopy

The first step into the photophysical characterisation of the derivatives of TX was to record the absorption spectrum of the derivatives.

It is crucial, for the full achievement of the project, all the derivatives present a maximum absorption peak in the near ultra-violet region and have no, or little, absorption in the visible spectrum. Consequently, all the compounds can be considered virtually colourless in solution, like TX.

The solvent used to investigate the absorption is a 1:1 v/v mixture of methanol: water. The presence of methanol improves the solubility of TX.

The maximum absorption peak of all the derivatives has been found approximately at the same wavelength of TX ($\lambda_{abs}$= 388 nm) (Table 1). These results show that the new groups do not significantly affect the electronic structure of the dyes or the energy gap between the ground and excited state (Figure 41,43,45). The molar extinction coefficients were obtained via the well-known Beer-Lambert low (see Introduction)( Figure 42,44,46).

| | $\lambda_{abs}$ | $\varepsilon$ / $M^{-1}cm^{-1}$ | $R^2$ |
|---|---|---|---|
| TX | 388 | 2990 | 1.00 |
| TXCOOH | 385 | 1870 | 0.99 |
| TERTTX | 385 | 2200 | 0.99 |
| $TXCONC_2OH$ | 387 | 1800 | 1.00 |
| $TXCONC_3OH$ | 387 | 1970 | 0.92 |
| $TXCONC_7$ | 386 | 1300 | 0.99 |
| $TXCONET_2$ | 388 | 3100 | 0.93 |
| TXCOGLY | 385 | 2570 | 0.99 |
| TXCOMORPHO | 385 | 3270 | 0.98 |
| TERTTXGLY | 380 | 2240 | 0.98 |
| TERTTXMORPHO | 388 | 2100 | 0.99 |

***Table 1*** *Maximum absorption wavelength, molar extinction coefficient, and associated error calculated at maximum of all TX's derivatives*

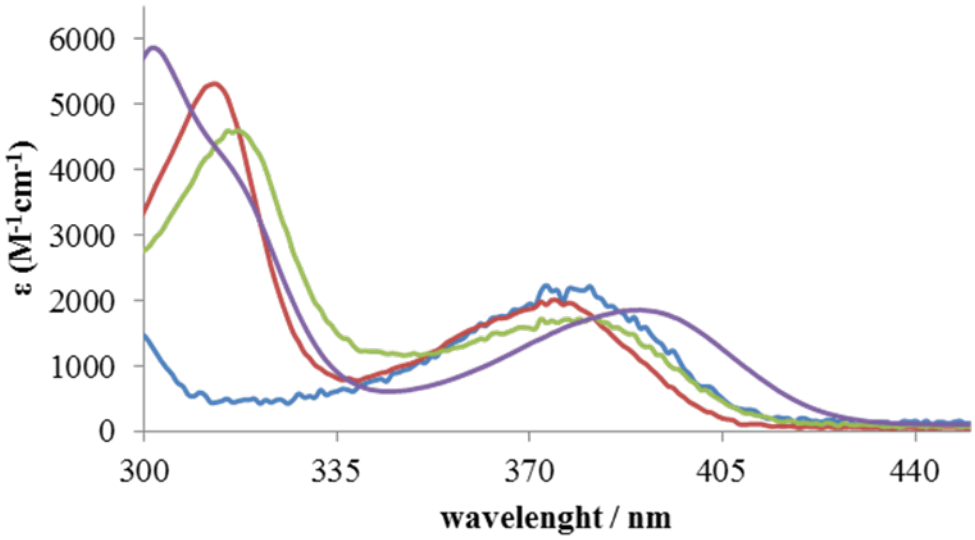


***Figure 41*** *Absorption spectra in equal MeOH:$H_2O$ of TX (blue), TXCOOH (red), TERTTX (green), TXCONC$O_2$OH (purple)*

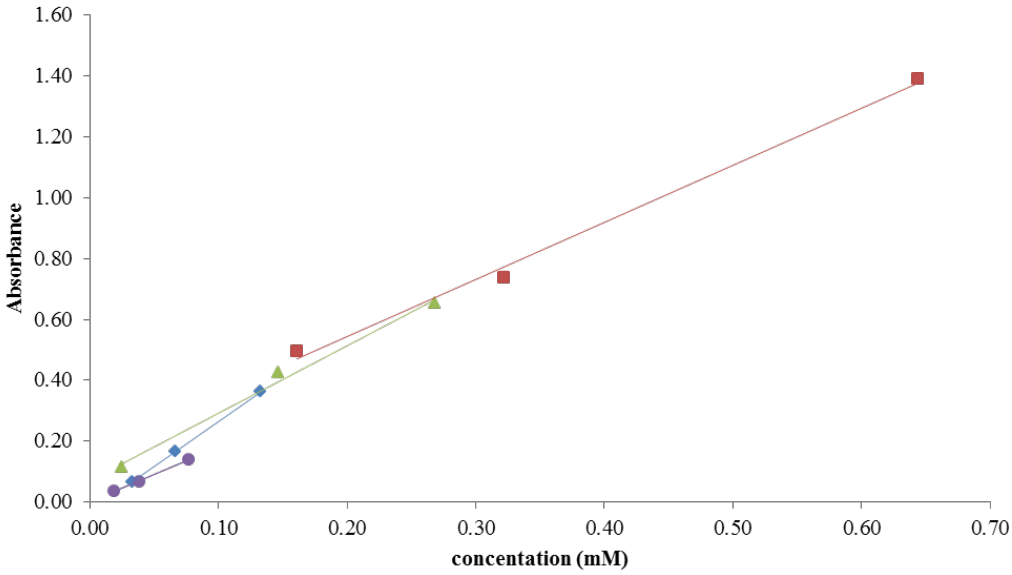


***Figure 42*** *Beer-Lambert data in equal MeOH:$H_2O$ of TX (blue), TXCOOH (red), TERTTX (green), TXCONC$O_2$OH (purple)*

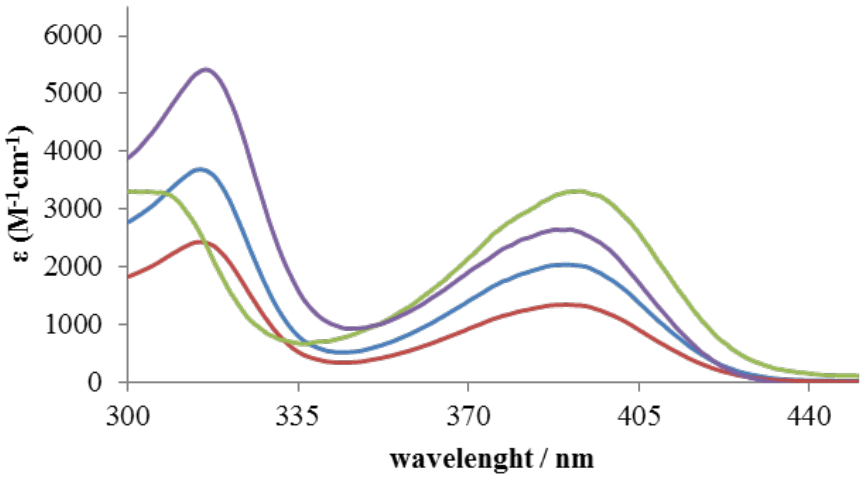


***Figure 43*** *Absorption spectra in equal MeOH:$H_2O$ of TXCONCO$_3$OH (blue), TXCONC$_7$ (red), TXCONET$_2$ (green), TXCOGLY (purple)*

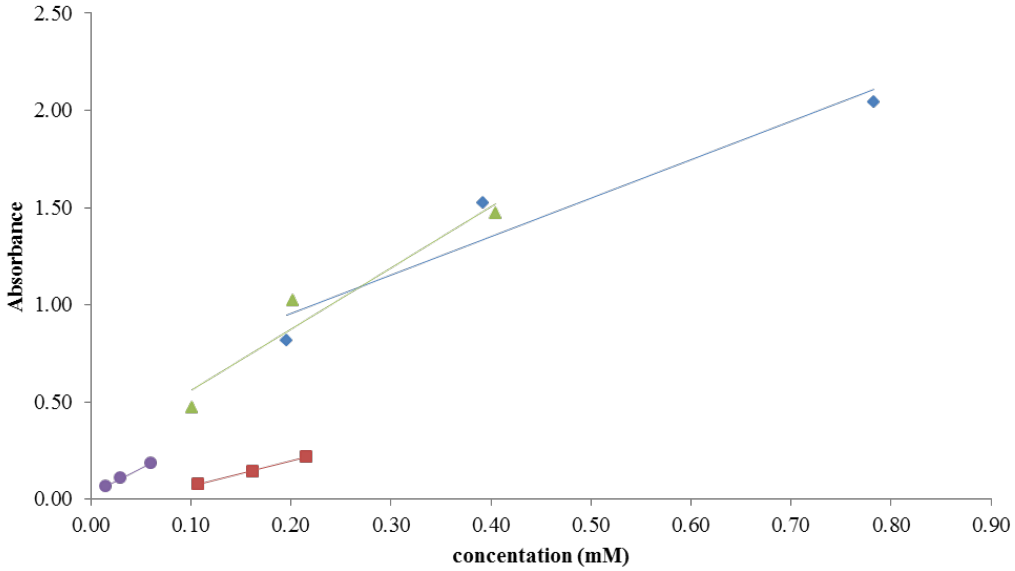


***Figure 44*** *Beer-Lambert data in equal MeOH:$H_2O$ of TXCONCO$_3$OH (blue), TXCONC$_7$ (red), TXCONET$_2$ (green), TXCOGLY (purple)*

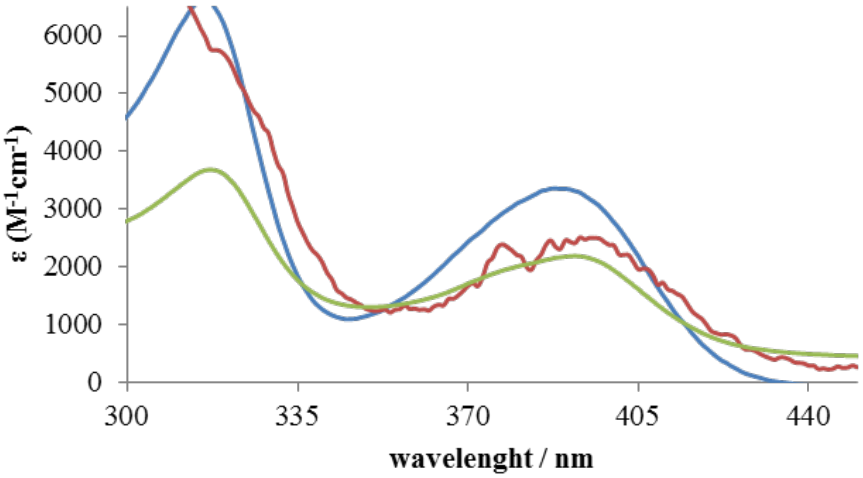


***Figure 45*** *Absorption spectra in equal MeOH:$H_2O$ of TXCOMORPHO (blue), TERTMORPHO (red), TERTTXGLY (green)*

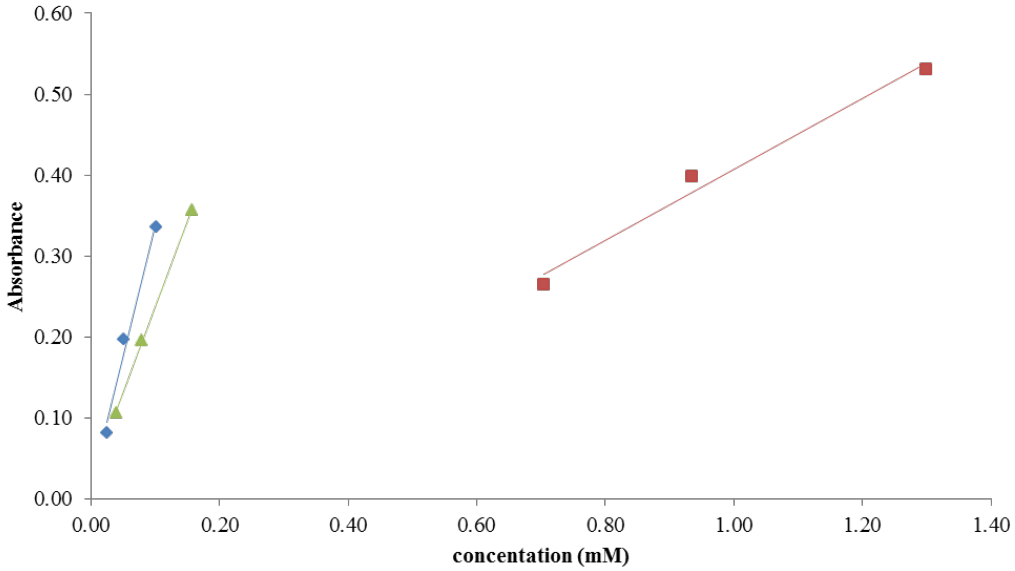


***Figure 46*** *Beer-Lambert data in equal MeOH:$H_2O$ of TXCOMORPHO (blue), TERTMORPHO (red), TERTTXGLY (green)*

The absorption spectra of all derivatives are dominated by bands that can be assigned to $S_0$ (nπ) -> $S_1$ (ππ*) transitions, as for TX in polar solvents.

More importantly, all the derivatives present a similar molar extinction.

In general ε(λ) expresses the ability of TX and derivatives to absorb light at the maximum absorption peak in MeOH:$H_2O$.

However, a more suitable parameter, connected to ε(λ), is the oscillator strength. Typically a high molar absorption coefficient implies a more probable transition. However, because absorption bands are not infinitely narrow, a more rigorous way to define the strength of a transition involves the integration of the absorption coefficient over a range of wavelengths associated with the transition (375-385 nm). In classical theory, the molecular light absorption can be described by considering the transition as an oscillating dipole. Which allows the introduction of a dimensionless quantity called the oscillation strength, directly related to the integral of the absorption band as following

$$f = \frac{4ln10m\varepsilon_0 c^2}{N_a e^2} \int \varepsilon(\nu)d\nu$$

Where *m* and *e* are the mass and the charge of an electron, respectively, $\varepsilon_0$ is the vacuum permittivity, *c* is the speed of light, ν is the frequency. For *n* -> π* transitions, the values of ε are in order of a few thousand, like in this work, and *f* values are no greater than $10^{-2}$. In the quantum mechanical approach, the transition moment is introduced to characterise the transition between an initial state and a final state. The transition moment represents the transient dipole resulting from the displacement of charges during the transition; therefore, it is not a strictly a dipole moment.

$$f = \frac{8\pi^2 mc}{3he^2\lambda_{av}} |M_{12}|^2$$

Where $M_{12}$= $\langle\psi_g|M|\psi_e\rangle$, $\psi_g$ and $\psi_e$ being the wave functions of ground and excited state. From the equation, it is evident that the value of *f* is influenced by the geometry of states involved and their spatial overlap. In this case, *f* can reveal more information regarding the last parameter.

The molecular overlap between ground and excited states of derivatives can be modified by the presence of the new group compared to TX.

From the absorption spectra, it is evident the introduction of the groups employed in this work does not interfere significantly with $S_0$-$S_1$ energy gap or the oscillator strength (Table 2).

| | $\varepsilon$ / $M^{-1}cm^{-1}$ | $f$ $(10^{-2})$ |
|---|---|---|
| TX | 2990 | 4.13 |
| TXCOOH | 1870 | 2.78 |
| TERTTX | 2200 | 2.78 |
| $TXCONC_2OH$ | 1800 | 2.76 |
| $TXCONC_3OH$ | 1970 | 2.76 |
| $TXCONC_7$ | 1300 | 1.39 |
| $TXCONET_2$ | 3100 | 4.13 |
| TXCOGLY | 2570 | 4.17 |
| TXCOMORPHO | 3270 | 4.17 |
| TERTTXGLY | 2240 | 1.13 |
| TERTTXMORPHO | 2100 | 2.76 |

***Table 2*** *Molar extinction coefficient and oscillation strength of TX's derivatives in MeOH:$H_2O$*

Overall the derivatives present a similar oscillator strength, showing a similar behaviour of thioxanthone.

## 3.2 Fluorescence emission, quantum yield and lifetime

Another fundamental property is the fluorescence emission, which for TX in MeOH:$H_2O$ has a maximum at 441 nm when excited at 380 nm.

The fluorescence of derivatives prepared in this study shows a similar maximum when excited at 380 nm. As for the absorption, the energy gap between the states involved has been preserved (Table 3) (Figure 47,48).

| | $\lambda_{em}$ / nm |
|---|---|
| TX | 441 |
| TXCOOH | 440 |
| TERTTX | 439 |
| $TXCONC_2OH$ | 441 |
| $TXCONC_3OH$ | 440 |
| $TXCONC_7$ | 440 |
| $TXCONET_2$ | 443 |
| TXCOGLY | 440 |
| TXCOMORPHO | 441 |
| TERTTXGLY | 441 |
| TERTTXMORPHO | 443 |

***Table 3*** *Maximum fluorescence emission wavelength of TX's derivatives ($\lambda_{ex}$ 380 nm)*

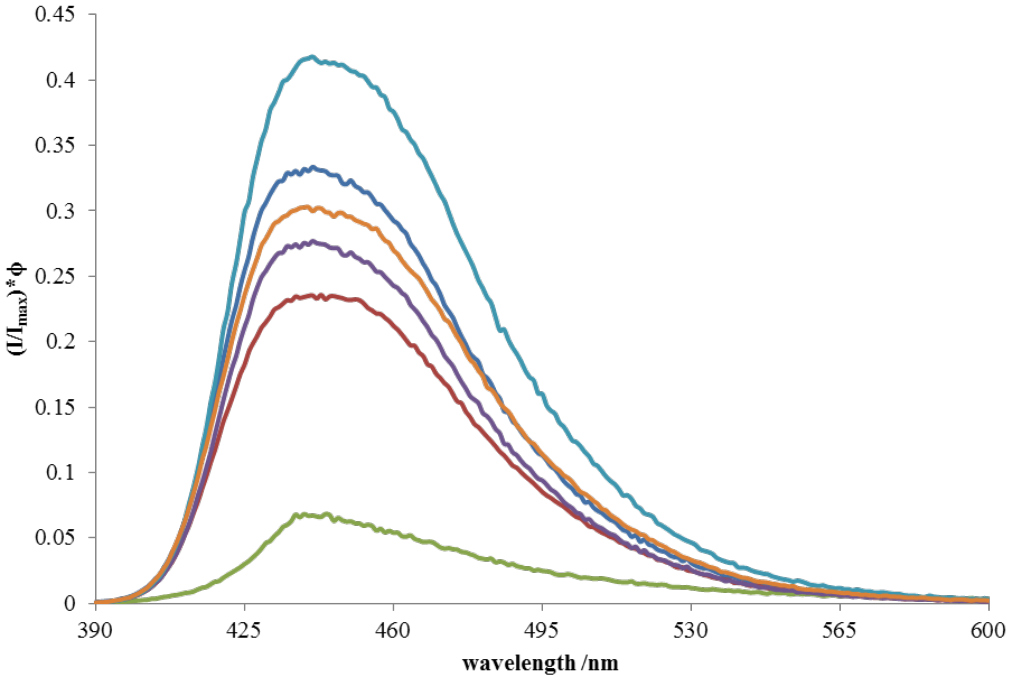


***Figure 47*** *Fluorescence emission in equal MeOH:$H_2O$ $\lambda_{ex}$ 380 nm of TX (light blue), $TXCONCO_2OH$ (blue), $TXCONCO_3OH$ (orange), TERTMORPHO (purple), TERTTXGLY (orange), TERTTX (green)*

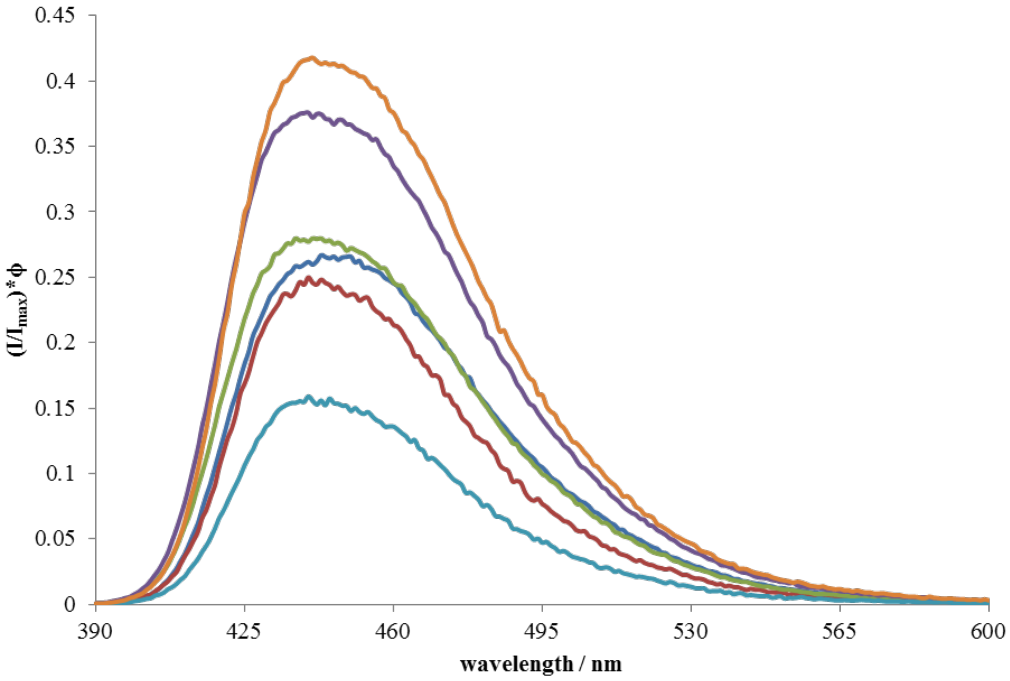


***Figure 48*** *Fluorescence emission in equal MeOH:$H_2O$ $\lambda_{ex}$ 380 nm of TX (orange), TXCONC$_7$ (purple), TXCOGLY (green), TXCONET$_2$ (blue), TXCOOH (red), TXCOMORPHO (light blue)*

More evident differences have observed within the fluorescence quantum yields and lifetimes values.

The fluorescence lifetimes of all the derivatives, except TERTTX and TERTMORPHO, are shorter than that observed for TX by ca. 18%. TXCONCO$_2$OH, TXCONCO$_3$OH, TXCONC$_7$, TXCOMORPHO, TXCOGLY, and TERTTXGLY present an average lifetime of 6.6 ns. Furthermore, all of the TX derivatives have lower fluorescence quantum yields (Table 4).

| | $\Phi_f$ | τ / ns | $\tau_0$ / ns |
|---|---|---|---|
| TX | 0.42 | 7.8 | 19 |
| TXCOOH | 0.25 | 7.1 | 29 |
| TERTTX | 0.28 | 8.2 | 30 |
| $TXCONC_2OH$ | 0.33 | 6.9 | 21 |
| $TXCONC_3OH$ | 0.30 | 6.7 | 22 |
| $TXCONC_7$ | 0.38 | 6.7 | 18 |
| $TXCONET_2$ | 0.27 | 7.7 | 29 |
| TXCOGLY | 0.16 | 6.7 | 42 |
| TXCOMORPHO | 0.28 | 6.4 | 23 |
| TERTTXGLY | 0.28 | 8.5 | 31 |
| TERTTXMORPHO | 0.24 | 6.4 | 27 |

***Table 4*** *Fluorescence lifetime (τ, ns), quantum yield (ϕ), and natural lifetime ($\tau_0$, ns) of all derivatives in MeOH:$H_2O$*

It is possible to calculate the natural lifetime, $\tau_0$, from the lifetime and quantum yield of a compound.

$$\frac{\phi}{\tau} = \tau_0$$

An increasing of oscillator strength leads to a faster rate of radiative decay and a shorter pure radiative lifetime. Typically, this results in a higher emission quantum yields.

The fluorescence quantum yield and lifetime can be correlated with the rate constant for radiative ($k_r$)($s^{-1}$) and non-radiative ($k_{nr}$)($s^{-1}$) deactivation $S_1$->$S_0$

$$\Phi_f = \frac{k_r}{k_r + k_{nr}} = k_r\tau$$

$$\tau = \frac{1}{k_r + k_{nr}}$$

The non-radiative decay constant can be divided into two different components $k_{nr}$= $k_{IC}$ + $k_{ISC}$, where $k_{IC}$ is the rate constant for internal conversion and $k_{ISC}$ is the rate constant for intersystem crossing (Table 5). In the present work, those two contributions are not calculated separately.

| | $10^7 k_r$ / $s^{-1}$ | $10^7 k_{nr}$ / $s^{-1}$ | $\tau_0$ / ns | *f* ($10^{-2}$) |
|---|---|---|---|---|
| TX | 5.33 | 7.42 | 19 | 4.13 |
| TXCOOH | 3.5 | 10.5 | 29 | 2.78 |
| TERTTX | 3.35 | 8.79 | 30 | 2.78 |
| $TXCONC_2OH$ | 4.86 | 9.71 | 21 | 2.76 |
| $TXCONC_3OH$ | 4.51 | 10.4 | 22 | 2.76 |
| $TXCONC_7$ | 5.61 | 9.31 | 18 | 1.39 |
| $TXCONET_2$ | 3.49 | 9.58 | 29 | 4.13 |
| TXCOGLY | 2.53 | 12.6 | 42 | 4.17 |
| TXCOMORPHO | 4.39 | 11.3 | 23 | 4.17 |
| TERTTXGLY | 3.24 | 8.47 | 31 | 1.13 |
| TERTTXMORPHO | 3.7 | 12 | 27 | 2.76 |

***Table 5*** *Radiative ($k_r$)($s^{-1}$) , non-radiative ($k_{nr}$)($s^{-1}$) deactivation $S_1$->$S_0$ , oscillation strength and natural lifetime($\tau_0$, ns) of TX's derivatives in MeOH:$H_2O$*

All derivatives have lower radiative rate constants compared to TX and higher, non-radiative rate constants.

These results are encouraging on the main goal of this project, in fact, a higher $k_{nr}$ is likely to be a sign of a greater rate of intersystem crossing and hence higher triplet yield.

## 3.3 Phosphorescence emission and transient absorption

Phosphorescence emission has been recorded from the TX derivatives in EPA glass at 77K, following excitation at 380 nm (see Chapter 2). This solvent is chosen for its good glass forming properties, and although it is not the same as that used for absorption and fluorescence experiments.

The triplet emission of TX shows a band with some fine vibrational structure, with two vibrational components, a primary transition at 458 nm with an additional shoulder around 480 nm.

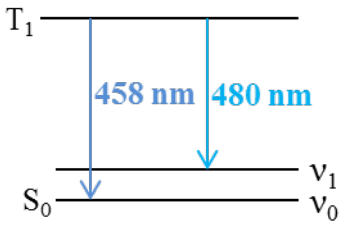


In the majority of TX derivatives reported here, the maximum intensity is at 480 nm, Table 6.

| | $\lambda_{pho}$ / nm |
|---|---|
| TX | 458 |
| TXCOOH | 476 |
| TERTTX | 481 |
| $TXCONC_2OH$ | 481 |
| $TXCONC_3OH$ | 481 |
| $TXCONC_7$ | 458/478 |
| $TXCONET_2$ | 488 |
| TXCOGLY | 480 |
| TXCOMORPHO | 483 |
| TERTTXGLY | 458 |
| TERTTXMORPHO | 480 |

***Table 6*** *Phosphorescence emission of TX's derivatives in EPA at 77K $\lambda_{ex}$ 380 nm*

The shift in phosphorescence emission it can be interpreted as changing the transition strength between the lowest vibrational state of the $T_1$ state and the different vibrational levels of the electronic ground states (Figures 49,50,51). Such interpretation can be made assuming the energy gap between $T_1$ and $S_0$ remains the same as thioxanthone, the chance is . an indication of the geometry change between the excited state and the ground state.

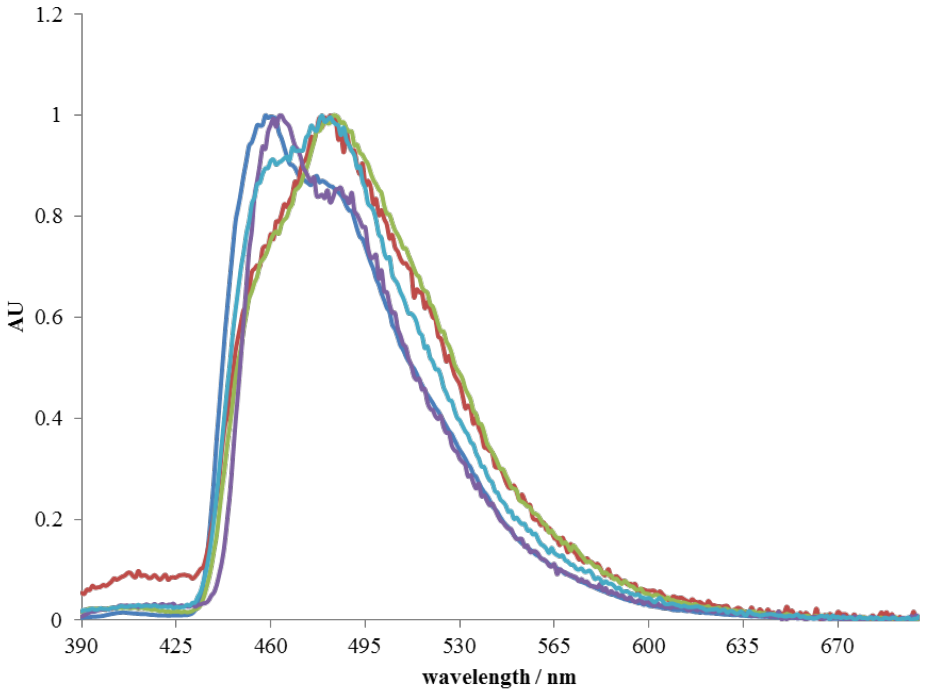


***Figure 49*** *Normalised phosphorescence emission in EPA at 77K $\lambda_{ex}$ 380 nm of TX (blue), TXCOMORPHO(red), TXCOGLY (green), TERTTXMORPHO (purple), TERTTXGLY (light blue)*

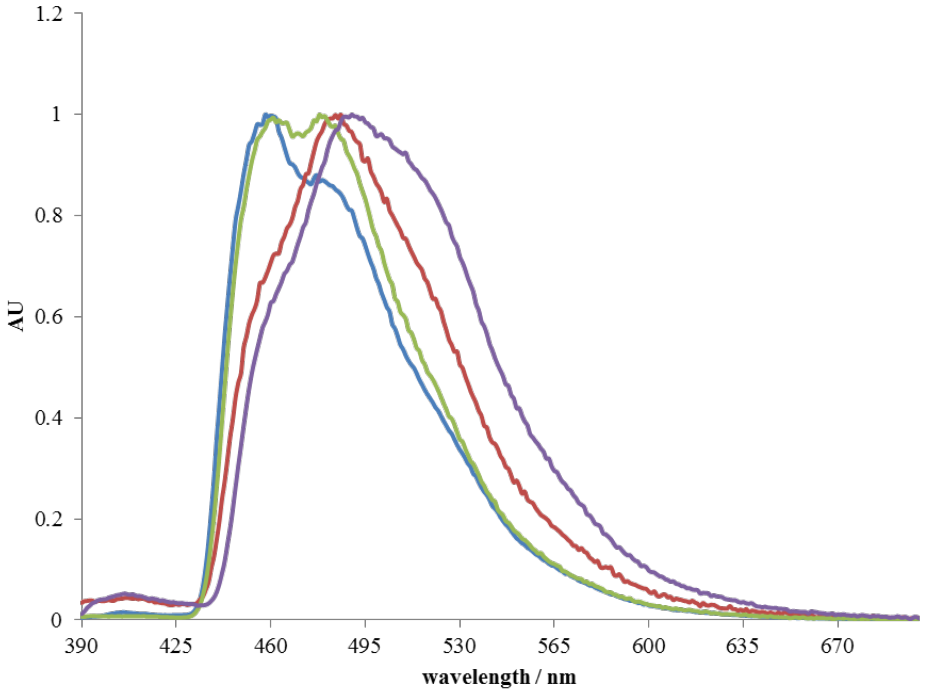


***Figure 50*** *Normalised phosphorescence emission in EPA at 77K $\lambda_{ex}$ 380 nm of TX (blue), TXCONCO$_3$OH (red), TXCONC$_7$ (green), TXCONET$_2$ (purple)*

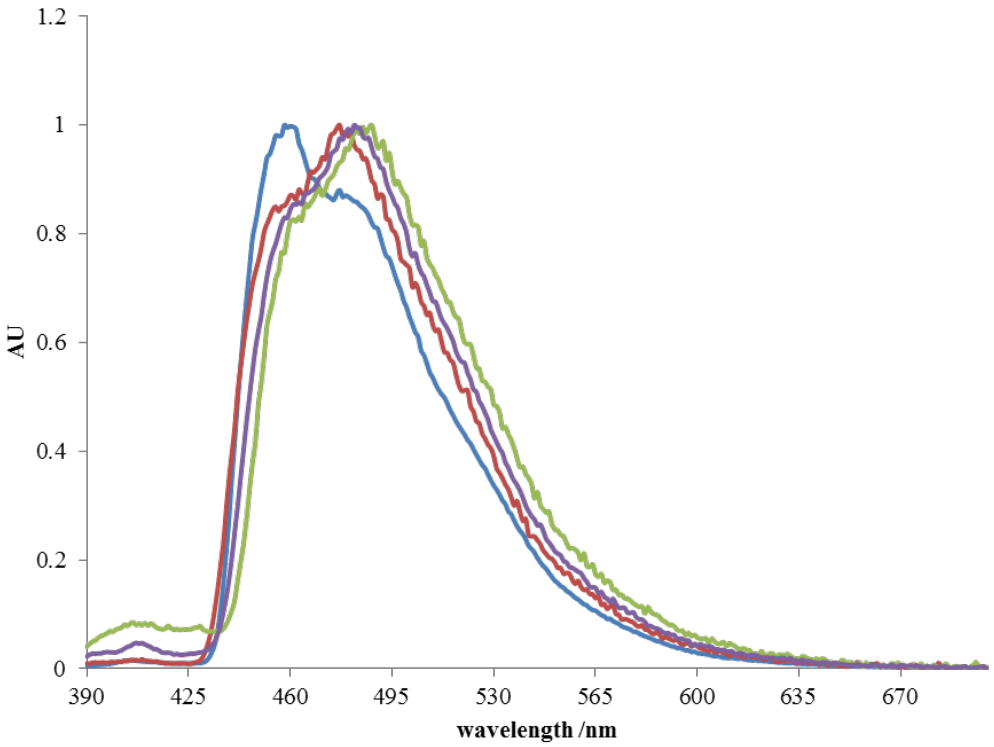


***Figure 51*** *Normalised phosphorescence emission in EPA at 77K $\lambda_{ex}$ 380 nm of TX (blue), TXCOOH (red), TERTTX (green), TXCONCO$_2$OH (purple)*

Although the derivatives prepared in this work show a maximum emission occurs at 480 nm, the majority of phosphorescence spectra of TX derivatives display a shoulder around 460 nm. This is unlike that of TX which shows the main band at 460 nm, with a shoulder at ca 480 nm. Moreover, TXCONC$_7$ spectra present the two peaks (458 nm and 478 nm) with equal intensity. In the case of TXCOMORPHO, the emission is entirely overlapping with TX spectra. The phosphorescence quantum yields were not measured in this work. Consequently a comparison in relative intensity cannot be made.

From the data collected, regarding the phosphorescence emission, it is possible to conclude the presence of a new group attached does not significantly affect the $T_1$-$S_0$ energy gap, but the change in the fine vibrational structure of the emission spectra suggests a small difference in the structure of the excited states.

The unchanged energy gap is a significant result for this project, a change in the triplet excited state energy can lead to a lower probability of quenching by $^3O_2$ and a less efficient PBA.

Flash photolysis has been used to measure triplet-triplet ($T_1$-$T_n$) absorption spectra and the triplet lifetimes in solution. Assuming the triplet states involved in the transient absorption remain the same for TX and derivatives, this technique can reveal the energy gap between these states. The solvent used, for this experiment was pure methanol, all of the solutions used had the same absorption across all compounds (1.2), and a beam power of 100 mJ across all the experiments.

Thioxanthone T-T absorption has its maximum at 610 nm and the triplet state possess a lifetime of 7.4 μs (Table 7).

| | $\lambda_{T\text{-}T}$ / nm | $\tau_{T\text{-}T}$ / μs |
|---|---|---|
| TX | 610 | 7.4 |
| TXCOOH | 620 | 3.9 |
| TERTTX | 610 | 7.4 |
| $TXCONC_2OH$ | 600 | 5.5 |
| $TXCONC_3OH$ | 600 | 14.0 |
| $TXCONC_7$ | 620 | 20.4 |
| $TXCONET_2$ | 620 | 18.8 |
| TXCOGLY | 620 | 14.1 |
| TXCOMORPHO | 620 | 18.6 |
| TERTTXGLY | 610 | 23.3 |
| TERTTXMORPHO | 630 | 14.3 |

***Table 7*** *Triplet-Triplet maximum absorption and decay of TX's derivatives in degassed methanol*

The data collected showed a shift in the maximum T-T absorption at longer wavelengths, compared to TX, of the majority of derivatives. Furthermore, the compounds studied present an overall longer decay. The transient absorption of all derivatives presents a lower intensity

compared to TX (Figures 52,53,54). A lower ΔOD can be due to a smaller molar extinction coefficient of the triplet- triplet transition.

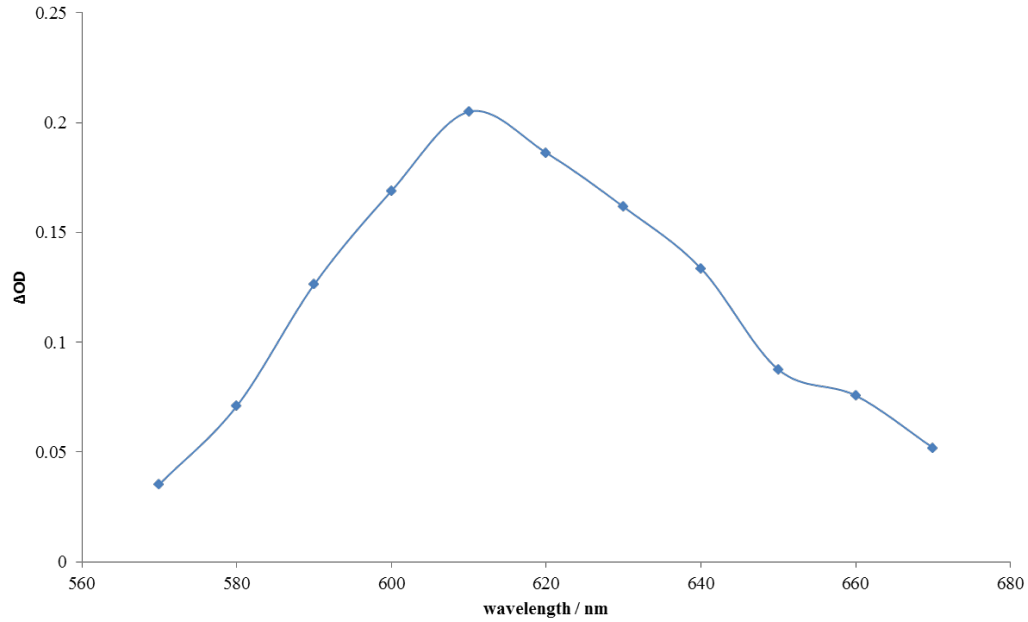


***Figure 52*** *Triplet-Triplet absorption spectra of TX in methanol ($\lambda_{exc}$= 355 nm)*

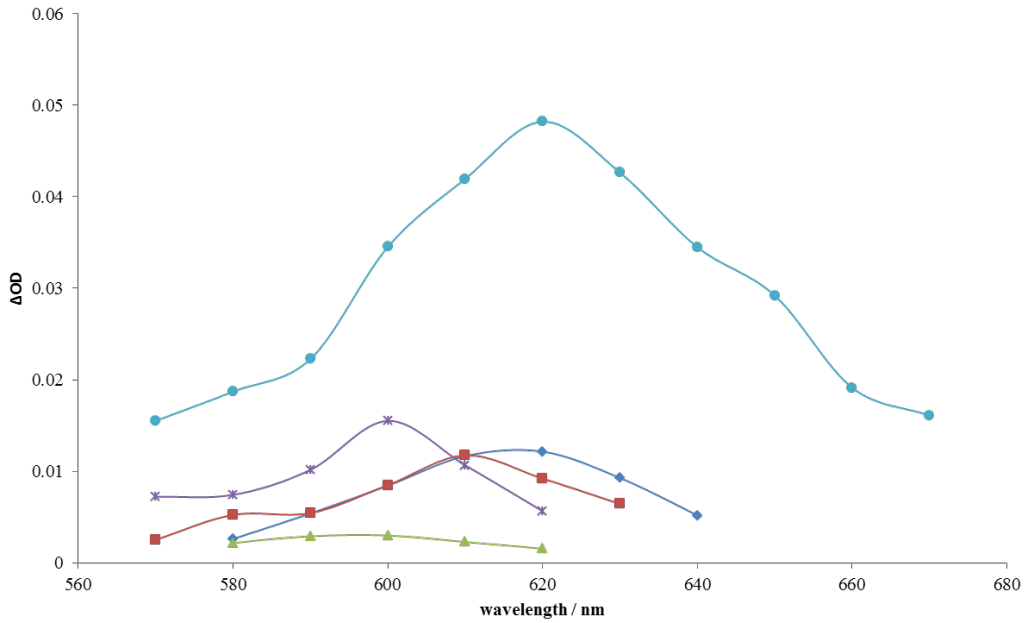


***Figure 53*** *Triplet-Triplet absorption spectra in methanol of TXCONC$_7$ (light blue), TERTTX (red), TXCONCO$_2$OH (green), TXCONCO$_3$OH (purple), TXCOOH (blue) ($\lambda_{exc}$= 355 nm)*

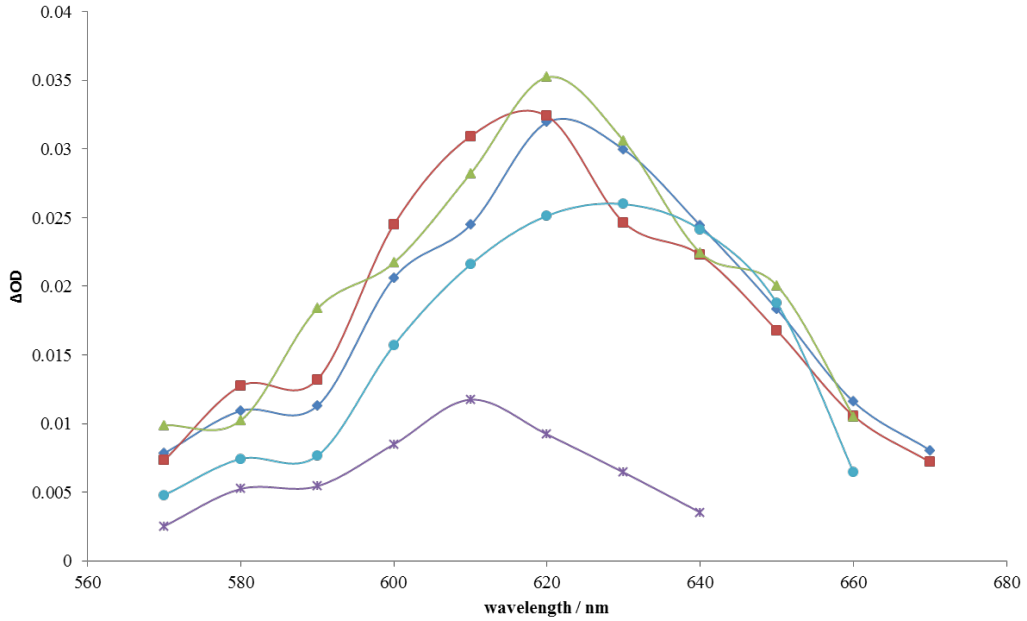


***Figure 54*** *Triplet-Triplet absorption spectra in methanol of TXCONET$_2$ (blue), TXCOMORPHO (red), TXCOGLY (green), TERTTXMORPHO (purple), TERTTXGLY (light blue) ($\lambda_{exc}$= 355 nm)*

## 3.4 Singlet oxygen generation

An important property of these photobleaching agents is their ability to sensitise the formation of singlet oxygen. The singlet oxygen quantum yield and lifetime were recorded using the method of Nonell et al., by monitoring the singlet oxygen phosphorescence at 1270 nm following pulsed laser excitation[90]. Using low concentrations of sensitisers, where self-quenching of singlet oxygen is unlikely to occur, the lifetime of $^1O_2$ is constant but does change with the solvent. To reach a reliable and reproducible result TX and its derivatives were dissolved in methanol at a constant absorbance of 0.3. In this solvent $^1O_2$ phosphorescence decay is known to occur in a lifetime of 14 μs.

Ideally, all the derivatives should present the same lifetime as reported in the literature.

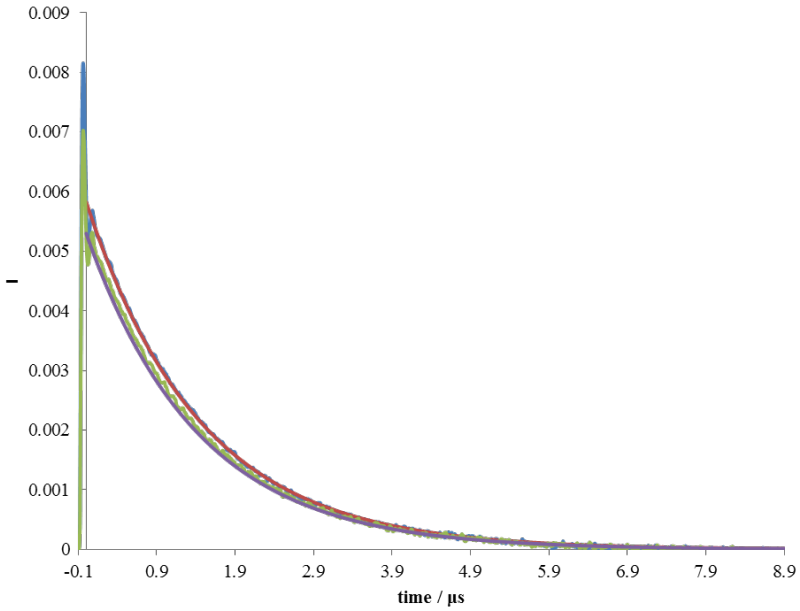


***Figure 55*** *Phosphorescence decay of* $^1O_2$ *in methanol of TX (blue), TX fitting (red), TXCOOH ( green), TXCOOH fitting (purple)*

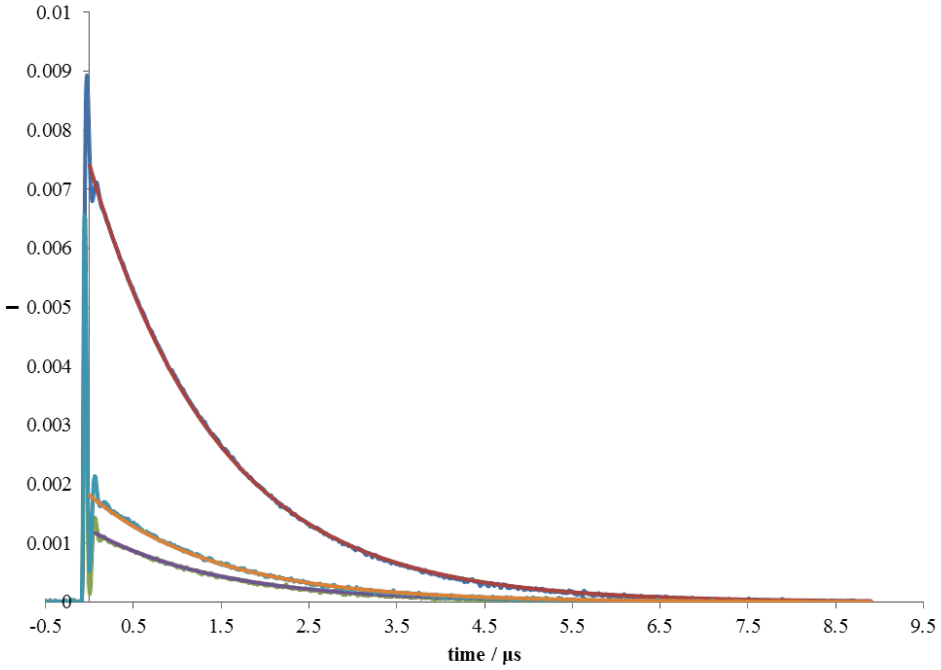


***Figure 56*** *Phosphorescence decay of* $^1O_2$ *in methanol of TXCONC*$_7$ *(blue), TXCONC*$_7$ *fitting (red), TERTTX ( green), TERTTX fitting (purple), TXCOMORPHO ( light blue), TXCOMORPHO fitting (orange)*

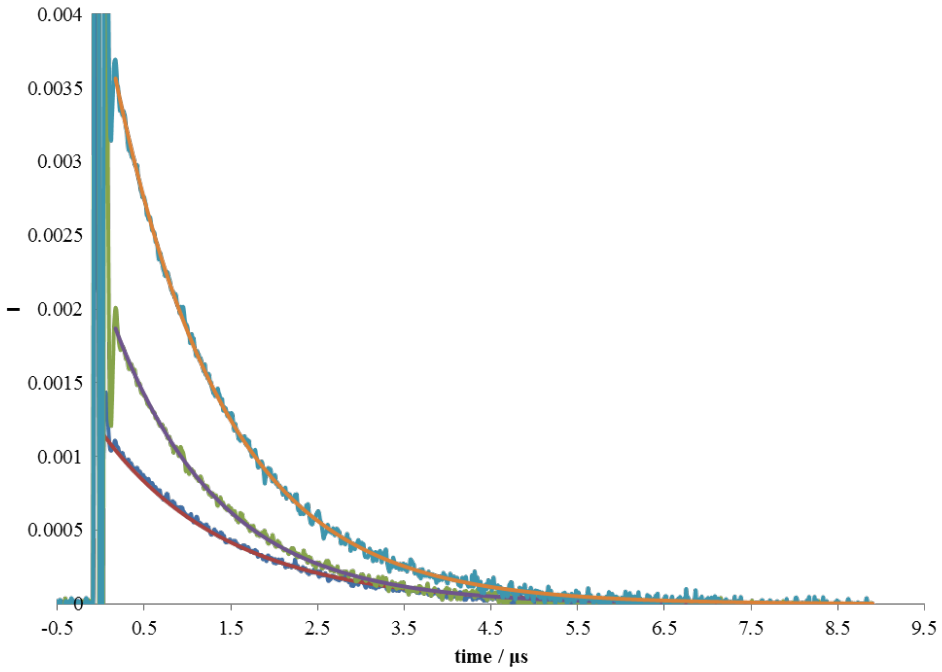


***Figure 57*** *Phosphorescence decay of $^1O_2$ in methanol of TERTTXMORPHO (blue), TERTTXMORPHO fitting (red), TERTTXGLY ( green), TERTTXGLY fitting (purple), TXCONET$_2$ ( light blue), TXCONET$_2$ fitting (orange)*

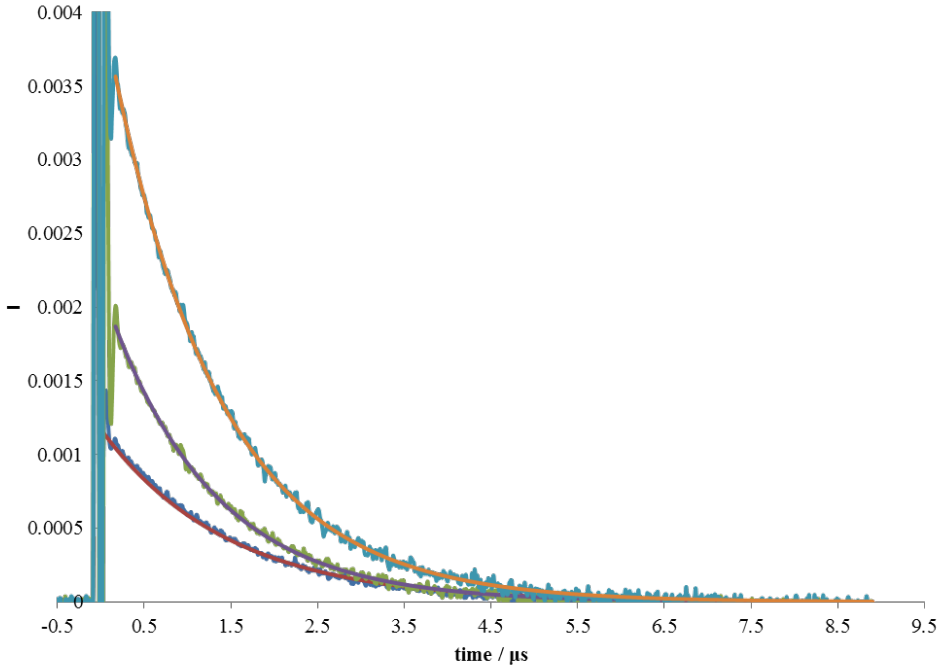


***Figure 58*** *Phosphorescence decay of $^1O_2$ in methanol of TXCONCO$_3$OH (blue), TXCONCO$_3$OH fitting (red), TXCONCO$_2$OH ( green), TXCONCO$_2$OH fitting (purple), TXCOGLY ( light blue), TXCOGLY fitting (orange)*

In all of the samples the measured singlet oxygen decays followed a single exponential decay and in each case, the lifetime was 14.0 ± 0.5 μs. From the concentration of TX derivatives used, 7.2 x $10^{-5}$ $M^{-1}$, and the assumption that a lifetime change of 1 μs would be detectable with our instrumentation it can be shown that the rate constant for the quenching of singlet oxygen with the TX derivatives is < $10^{9}$ $s^{-1}$. Thus, the presence of the new functional groups does not interfere with the singlet oxygen produced

The singlet oxygen quantum yield reveals the efficiency of production of the reactive species produced by the sensitizer. As shown in Table 8, all of the derivatives show slightly higher yields of singlet oxygen formation than the parent TX, itself a good sensitizer. This result suggests the potential of those molecules as PBA

| | $\phi_{^1O_2}$ |
|---|---|
| TX | 0.31 |
| TXCOOH | 0.37 |
| TERTTX | 0.76 |
| $TXCONC_2OH$ | 0.57 |
| $TXCONC_3OH$ | 0.43 |
| $TXCONC_7$ | 0.31 |
| $TXCONET_2$ | 0.3 |
| TXCOGLY | 0.52 |
| TXCOMORPHO | 0.64 |
| TERTTXGLY | 0.73 |
| TERTTXMORPHO | 0.59 |

***Table 8*** *Singlet oxygen quantum yield of TX's derivatives in methanol*

## 3.5 Reactivity with crocin and degradation

From the photophysical results, it is evident TX and derivatives proposed in this work can be considered for the next generation of PBA. It is important to have a good understanding of how those molecules interact with a potentially stained material. It was suggested that crocin would be a good model compound for monitoring the interaction of the PBA with a carotenoid type material in solution: this carotenoid has been chosen for its water solubility.

Crocin can interact at various stages of the photosensitisation process, quenching the excited singlet or triplet states of the TX derivatives. Furthermore, the carotenoid can quench singlet oxygen produced by the series of compounds studied.

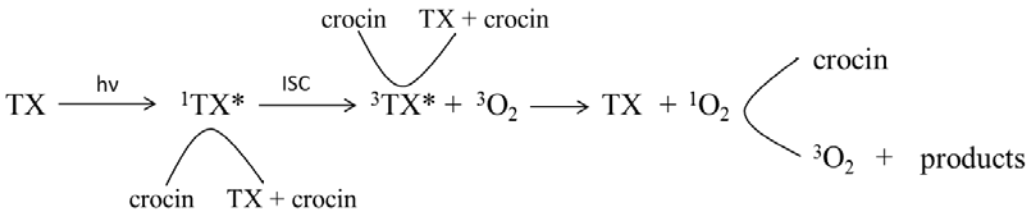


The interaction with the excited singlet state can be monitored by fluorescence quenching studies, in which the fluorescence lifetime of the TX derivatives is monitored as a function of added quencher concentration. Consequently, the rate quenching constant could have been calculate via the Stern-Volmer treatment (Figures 59, 60, 61).

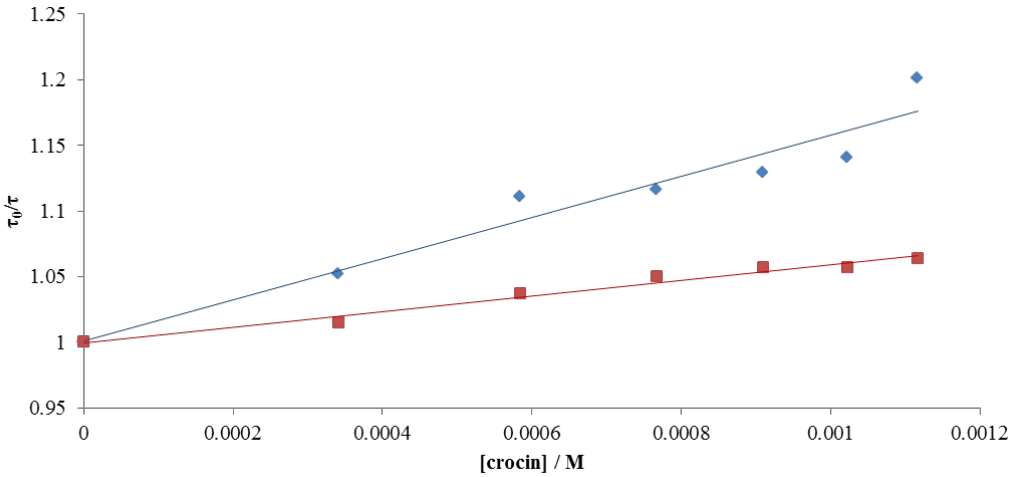


***Figure 59*** *$\tau_0/\tau$ vs. crocin (M) in methanol:water: TXCONCO$_2$OH (blue), TXCONCO$_3$OH (red)*

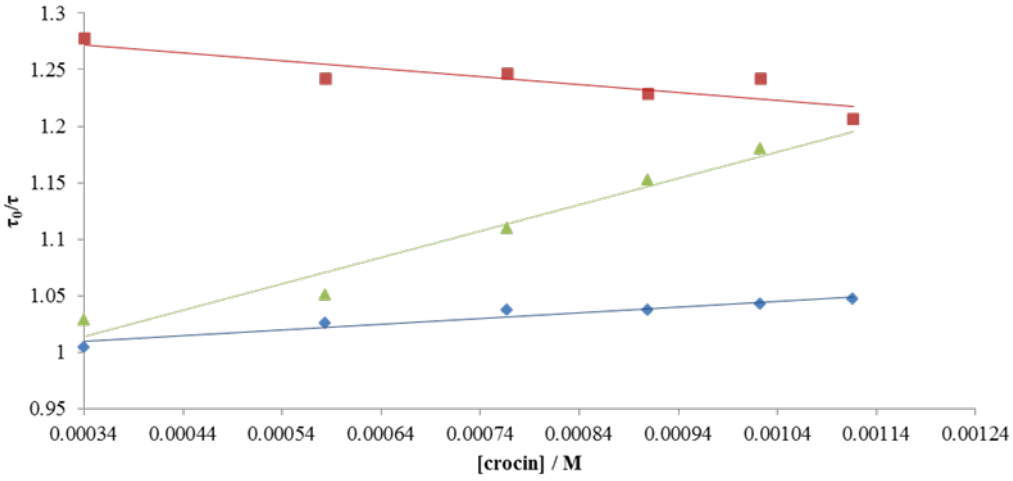


***Figure 60*** *$\tau_0/\tau$ vs. crocin (M) in methanol:water: TERTTXGLY (blue), TERTTXMORPHO (red), TX (green)*

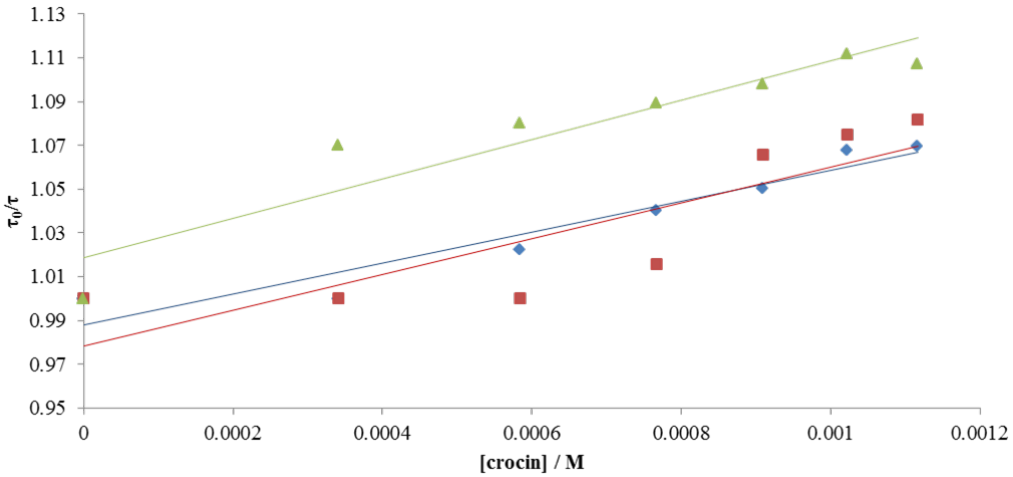


***Figure 61*** *$\tau_0/\tau$ vs. crocin (M) in methanol:water: $TXCONC_7$ (blue), TXCOOH (red), $TXCONET_2$ (green)*

| | $10^{10}\ k_q$ / $M^{-1}s^{-1}$ |
|---|---|
| TX | 1.1 |
| TXCOOH | 0.9 |
| TERTTX | 2.2 |
| $TXCONC_2OH$ | 2.3 |
| $TXCONC_3OH$ | 0.9 |
| $TXCONC_7$ | 2.7 |
| $TXCONET_2$ | 0.7 |
| TXCOGLY | 2.1 |
| TXCOMORPHO | 0.7 |
| TERTTXGLY | 1.0 |
| TERTTXMORPHO | 1.1 |

***Table 9*** *Florescence quenching rate constant of TX's derivative in methanol:water*

In each case, there is evidence that the crocin does quench the excited singlet states and that the $k_q$ of all compounds occurs at the diffusion limit (Table 9). Due to the limited solubility of the crocin and its high absorption in the UV spectral region, it was not possible to extend the study over a wider concentration range.

The quenching of $^1O_2$ by crocin was carried out by monitoring the phosphorescence lifetime of the singlet oxygen in methanol as a function of crocin concentration (Figures 62,63,64).

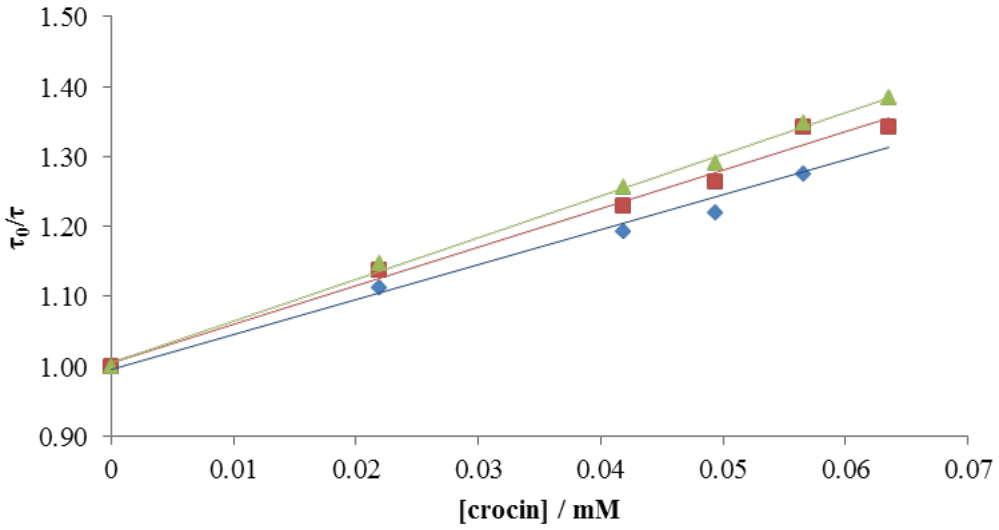


***Figure 62*** *Kinetics of phosphorescence $^1O_2$ lifetime in methanol of TX (blue), TXCOOH (red), $TXCONET_2$ (green)*

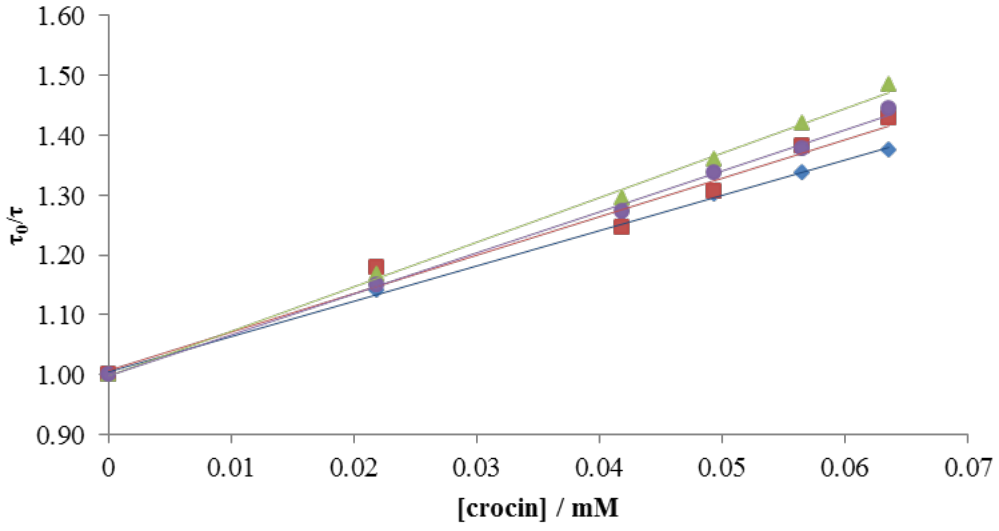


***Figure 63*** *Kinetics of phosphorescence $^1O_2$ lifetime in methanol of $TXCONCO_3OH$ (blue), TXCOGLY (red), $TXCONCO_2OH$ (green), $TXCONC_7$(purple)*

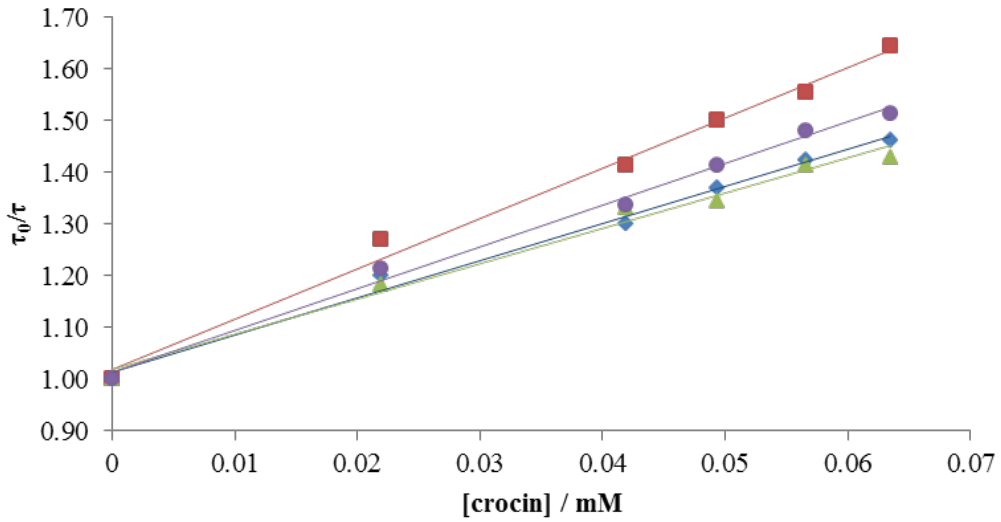


***Figure 64*** *Kinetics of phosphorescence $^1O_2$ lifetime in methanol of TXCOMORPHO (blue), TERTTX (red), TERTTXGLY (green), TERTTXMORPHO (purple)*

In summary, this work has shown that thioxanthone and its derivatives act as a type II photosynthesiser and do not themselves interact with the singlet oxygen in solution. However, $^1O_2$ is quenched by crocin in solution (Table 10). The results confirm the already well-established interaction between singlet oxygen and other carotenoids.

| | $10^8\ k_q$ / $M^{-1}s^{-1}$ |
|---|---|
| TX | 3.4 |
| TXCOOH | 3.9 |
| TERTTX | 6.7 |
| $TXCONC_2OH$ | 5.1 |
| $TXCONC_3OH$ | 4.1 |
| $TXCONC_7$ | 4.7 |
| $TXCONET_2$ | 4.2 |
| TXCOGLY | 5.1 |
| TXCOMORPHO | 4.5 |
| TERTTXGLY | 5.7 |
| TERTTXMORPHO | 5.0 |

***Table 10*** *Singlet oxygen quenching rate constant for quenchers by crocin in MeOH:$H_2O$*

The quenching rate constants are below the diffusion limits. Such result is expected due to the carotenoid chain length dependence of $k_q$. In fact, carotenoids with a reduced number of double bonds, such as crocin, are known to present a quenching rate constant approximately an order of magnitude lower than the diffusion range (see introduction).

One of the consequences of the interaction of $^1O_2$ with crocin is the oxidation of the conjugated chain and degradation of the carotenoid. To study these processes two experiments were set-up. In the first a solutions containing firstly only crocin in order to observe the natural photon-degradation of the carotenoid. Later a mixtures of crocin, with a constant concentration, and TX derivatives were exposed to white light to investigate the degradation of the carotenoid in presence of singlet oxygen synthesiser. The set-up consist in a tungsten lamp illuminated an aerated solution of crocin and derivatives. The solution was stirred for all the duration of the experiment. Absorption spectra were taken every 5 minutes to follow changes in absorption of crocin over time (Figures 65,66,67,68,69,70,71).

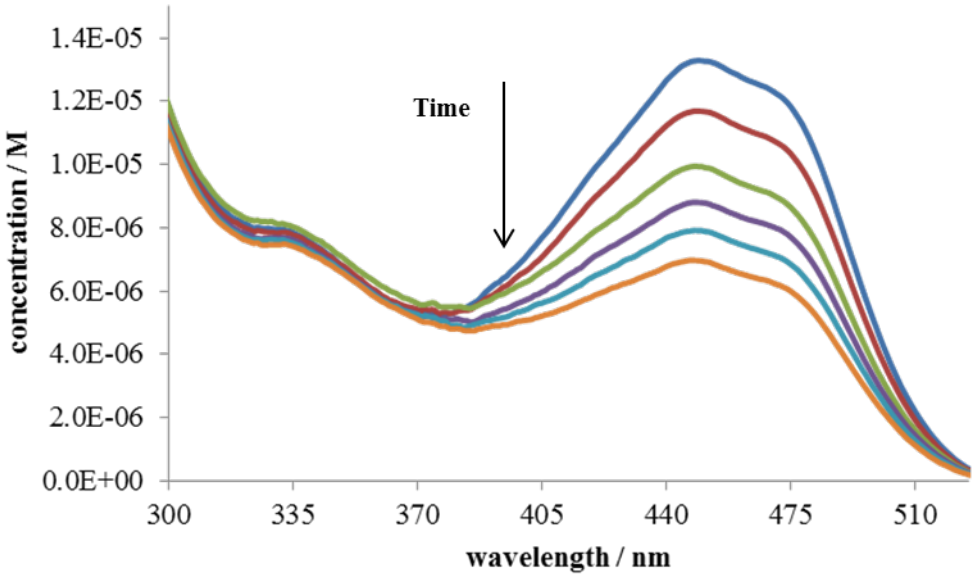


***Figure 65*** *Absorption spectra of crocin degradation in methanol:water*

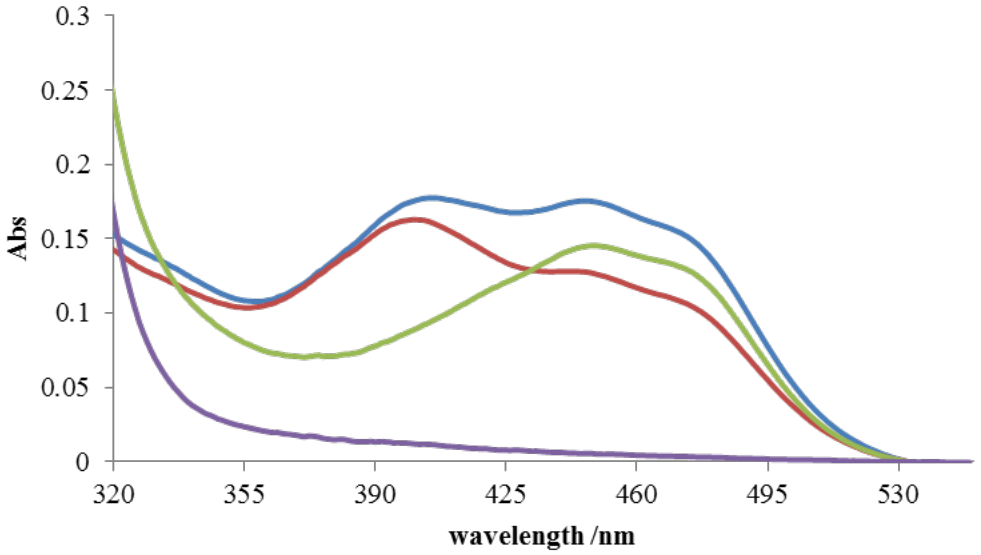


***Figure 66*** *Absorption spectra of crocin degradation in methanol:water in presence of TX (0 min, blue), TX (25 min, red), TERTTX (0 min, green), TERTTX (25 min, purple)*

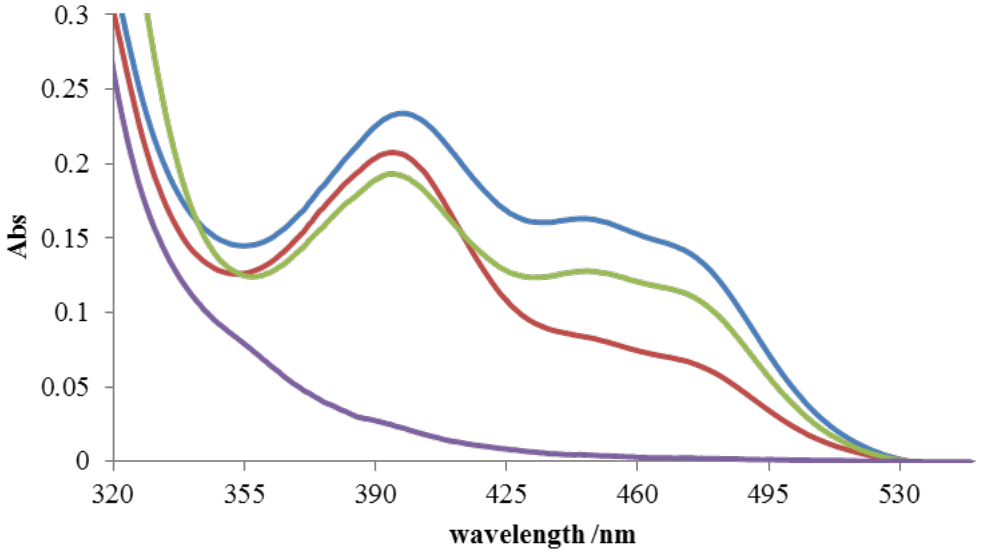


***Figure 67*** *Absorption spectra of crocin degradation in methanol:water in presence of TXCOOH (0 min, blue), TXCOOH (25 min, red) TXCOGLY (0 min, green), TXCOGLY (25 min, purple)*

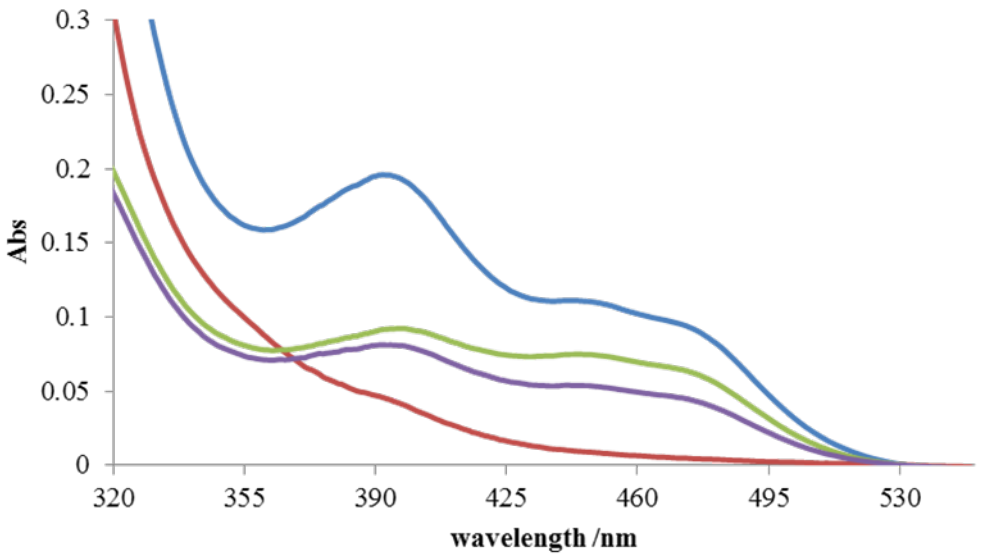


***Figure 68*** *Absorption spectra of crocin degradation in methanol:water in presence of TXCOMORPHO (0 min, blue), TXCOMORPHO (25 min, red), TXCONCO$_2$OH (0 min, green), TXCONCO$_2$OH (25 min, purple)*

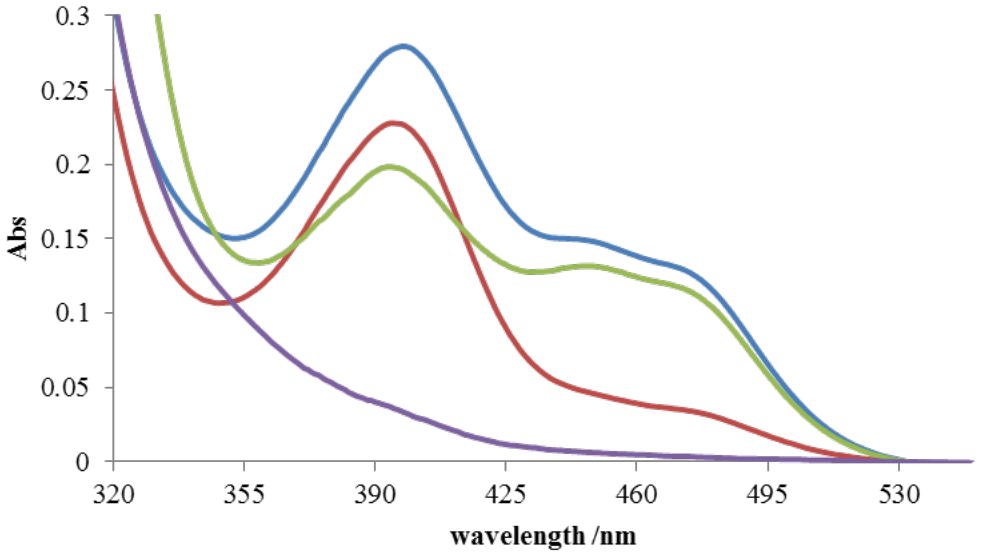


***Figure 69*** *Absorption spectra of crocin degradation in methanol:water in the presence of TXCONET$_2$ (0 min, blue), TXCONET$_2$ (25 min, red), TERTTXGLY (0 min, green), TERTTXGLY (25 min, purple)*

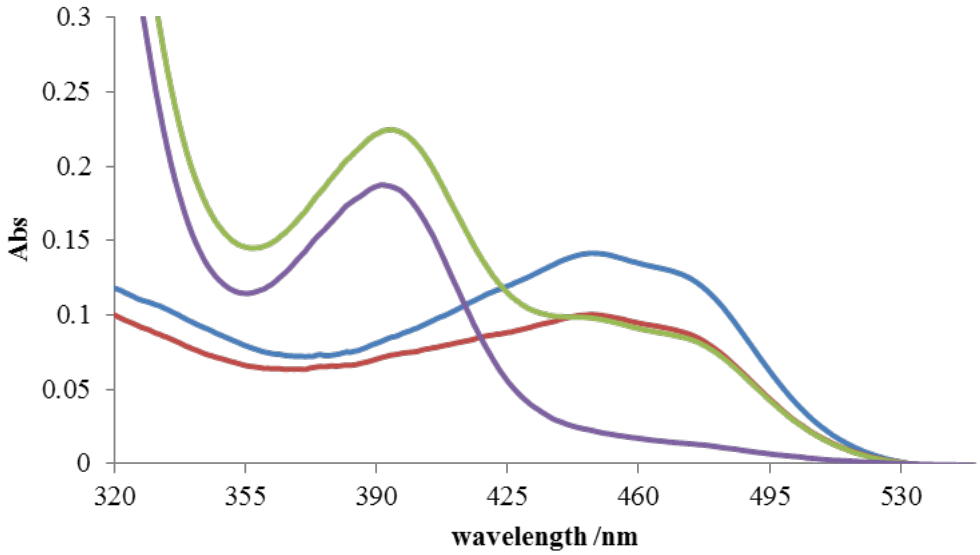


***Figure 70*** *Absorption spectra of crocin degradation in methanol:water in the presence of TXCONC$_7$ (0 min, blue), TXCONC$_7$ (25 min, red)TXCONCO$_3$OH (0 min, green), TXCONCO$_3$OH (25 min, purple)*

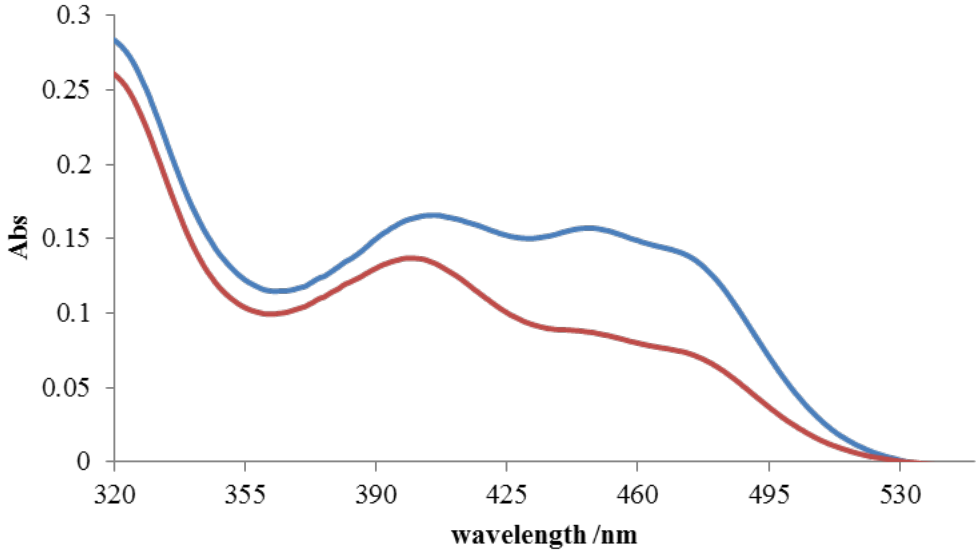


***Figure 71*** *Absorption spectra of crocin degradation in methanol:water in the presence of TERTTXMORPHO (0 min, blue), TERTTXMORPHO (25 min, red)*

It is evident that the crocin concentration slowly decreases with irradiation in all of the experiments performed. By monitoring crocin absorption maximum (442 nm, ε = 10710 $M^{-1}$ $cm^{-1}$), it is possible to calculate the decrease in concentration and the overall loss over the 25 minutes (Table 11).

| | [crocin] / M | | | | | | |
|---|---|---|---|---|---|---|---|
| | **0 min** | **5 min** | **10 min** | **15 min** | **20 min** | **25 min** | **difference** |
| TX | 1.7E-05 | 1.6E-05 | 1.5E-05 | 1.5E-05 | 1.3E-05 | 1.2E-05 | 4.8E-06 |
| TXCOOH | 1.5E-05 | 1.4E-05 | 1.1E-05 | 1.0E-05 | 8.9E-06 | 7.6E-06 | 1.4E-05 |
| TERTTX | 1.4E-05 | 7.4E-06 | 2.2E-06 | 4.9E-07 | 4.7E-07 | 3.5E-07 | 7.9E-06 |
| $TXCONC_2OH$ | 1.3E-05 | 6.8E-06 | 6.3E-06 | 5.8E-06 | 5.5E-06 | 5.0E-06 | 1.2E-05 |
| $TXCONC_3OH$ | 1.3E-05 | 5.1E-06 | 3.5E-06 | 2.4E-06 | 2.0E-06 | 1.7E-06 | 9.6E-06 |
| $TXCONC_7$ | 1.4E-05 | 1.3E-05 | 1.2E-05 | 1.1E-05 | 1.0E-05 | 9.7E-06 | 4.1E-06 |
| $TXCONET_2$ | 1.4E-05 | 1.1E-05 | 9.4E-06 | 6.7E-06 | 5.6E-06 | 3.9E-06 | 7.9E-06 |
| TXCOGLY | 1.2E-05 | 8.0E-06 | 3.6E-06 | 4.2E-07 | 4.5E-07 | 5.0E-07 | 1.2E-05 |
| TXCOMORPHO | 1.0E-05 | 7.8E-06 | 4.2E-06 | 1.4E-06 | 5.7E-07 | 8.0E-07 | 1.0E-05 |
| TERTTXGLY | 1.3E-05 | 7.5E-06 | 2.9E-06 | 1.1E-06 | 4.2E-07 | 6.0E-07 | 6.9E-06 |
| TERTTXMORPHO | 1.5E-05 | 1.3E-05 | 1.2E-05 | 1.1E-05 | 9.4E-06 | 8.2E-06 | 1.2E-05 |
| CROCIN | 1.4E-05 | 1.2E-05 | 1.0E-05 | 9.1E-06 | 8.0E-06 | 7.3E-06 | 6.6E-06 |

***Table 11*** *Absorbance decreasing of crocin in the presence of TX's derivatives in methanol:water ($\lambda_{obs}$= 442 nm)*

Even though crocin present a rate of concentration loss of 6.6 x $10^{-6}$ (M) over the 25 minutes, the carotenoid loss is higher in the presence of the majority of thioxanthone derivatives. Furthermore, crocin loss is greater in most of the derivatives compare to TX. Such a scenario could be explained considering all the derivatives are better singlet oxygen sensitizers. Consequently, crocin degrades faster due to the presence of higher concentration of $^1O_2$ in solution. This result shows the potential of those compound as a new type of PBA.

From the absorption spectra presented it is evident not only crocin degrades but the absorption at 380 nm of TX's derivatives also decreases, suggesting that the TX derivatives themselves are also degrading during the irradiation (Figures 72,73,74).

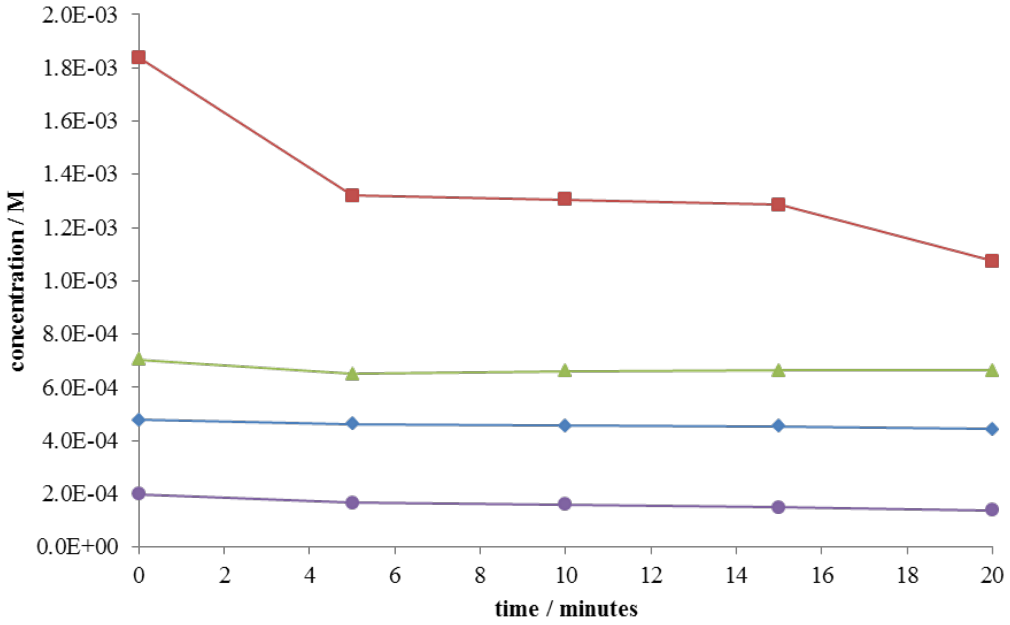


***Figure 72*** *Degradation of crocin of TERTTXMORPHO (blue), TERTTX (red), TXCOOH (green), TX (purple) in methanol:water in the absence*

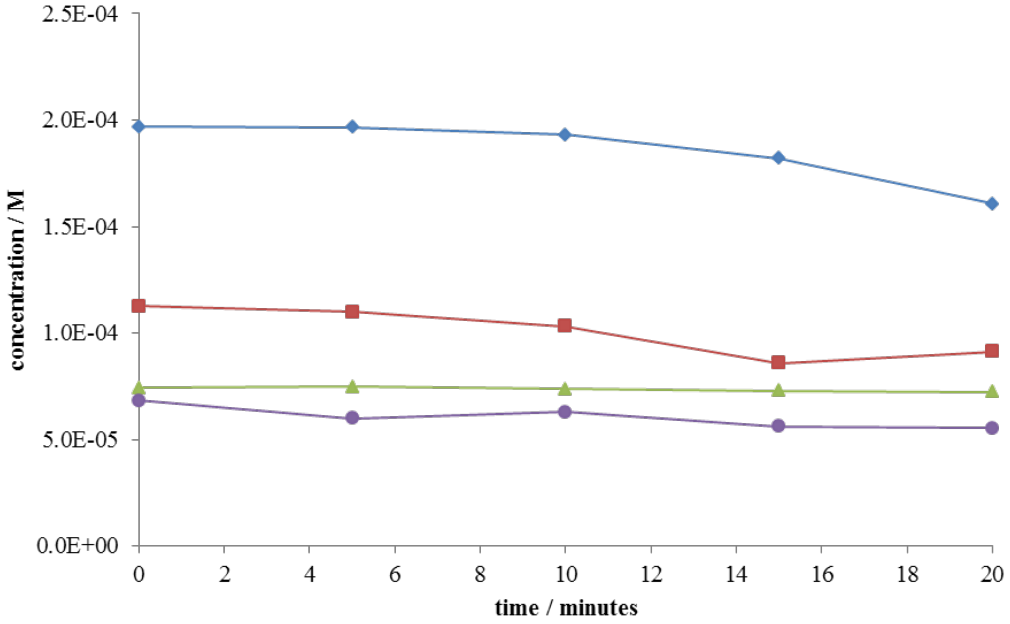


***Figure 73*** *Degradation of TXCONCO$_3$OH (blue), TXCONET$_2$ (red), TXCONCO$_2$OH (green), TXCONC$_7$ (purple) in methanol:water in the absence of crocin*

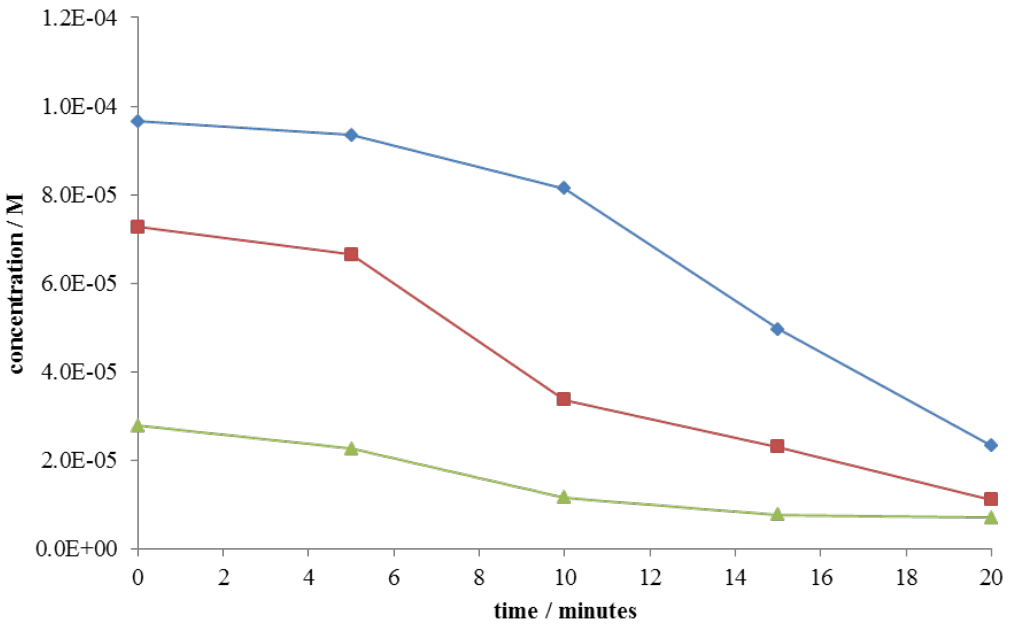


***Figure 74*** *Degradation crocin of TXCOGLY (blue), TXCOMORPHO (red), TERTTXGLY (green) in methanol:water in the absence of*

| | [derivative] / M | | | | | |
|---|---|---|---|---|---|---|
| | **0 min** | **5 min** | **10 min** | **15 min** | **20 min** | **difference** |
| TX | 2.0E-04 | 1.7E-04 | 1.6E-04 | 1.5E-04 | 1.4E-04 | 6.0E-05 |
| TXCOOH | 7.0E-04 | 6.5E-04 | 6.6E-04 | 6.6E-04 | 6.6E-04 | 4.1E-05 |
| TERTTX | 1.8E-03 | 1.3E-03 | 1.3E-03 | 1.3E-03 | 1.1E-03 | 7.6E-04 |
| $TXCONC_2OH$ | 7.4E-05 | 7.5E-05 | 7.4E-05 | 7.3E-05 | 7.2E-05 | 1.9E-06 |
| $TXCONC_3OH$ | 2.0E-04 | 2.0E-04 | 1.9E-04 | 1.8E-04 | 1.6E-04 | 3.6E-05 |
| $TXCONC_7$ | 6.8E-05 | 6.0E-05 | 6.3E-05 | 5.6E-05 | 5.5E-05 | 1.3E-05 |
| $TXCONET_2$ | 1.1E-04 | 1.1E-04 | 1.0E-04 | 8.6E-05 | 9.1E-05 | 2.1E-05 |
| TXCOGLY | 9.7E-05 | 9.4E-05 | 8.1E-05 | 5.0E-05 | 2.3E-05 | 7.3E-05 |
| TXCOMORPHO | 7.3E-05 | 6.6E-05 | 3.4E-05 | 2.3E-05 | 1.1E-05 | 6.1E-05 |
| TERTTXGLY | 2.8E-05 | 2.3E-05 | 1.2E-05 | 7.8E-06 | 7.2E-06 | 2.1E-05 |
| TERTTXMORPHO | 4.8E-04 | 4.6E-04 | 4.6E-04 | 4.5E-04 | 4.4E-04 | 3.3E-05 |

***Table 12*** *Decreasing concentration of TX's derivatives in methanol:water at the $\lambda_{abs}$ maximum*

It is evident that all derivatives are subjected to a photodeterioration process over the 20 minutes of light exposure (Table 12). The most stable compound is $TXCONCO_2OH$ with a

loss of just 1.9 x $10^{-6}$ M, on the contrary, TERTTX is the most unstable with a difference of 7.6 x $10^{-4}$ M over 20 minutes.

## 3.6 Derivatives in LES

The final experiment of this chapter aims to explore the absorption spectra of TX's derivatives in the presence of LES. The surfactant can improve the solubility of the derivatives by interacting with the chromophore or incorporating the molecule into a micelle. By monitoring the absorption spectra of a constant concentration of derivatives and increasing concentrations of LES, it is possible to monitor the effect of surfactant on the chromophore, although it is not feasible distinguishing the type of the interaction occurring (Figure 75,76,77,78,79).

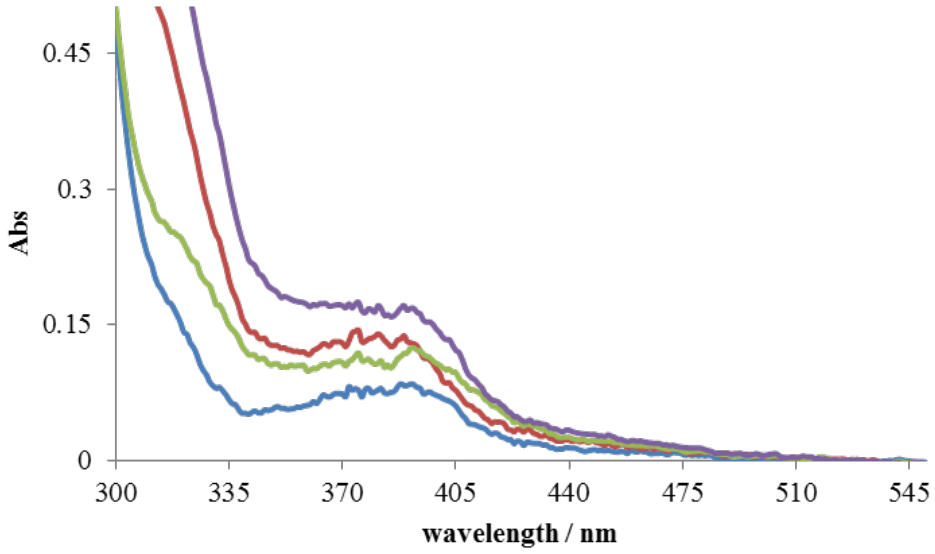


***Figure 75*** *Absorption spectra of derivatives degradation in methanol:water of TX ([LES]=0 M, blue), TX ([LES]=3.6 M, red), TERTTX ([LES]=0 M, green), TERTTX ([LES]=3.6 M, purple)*

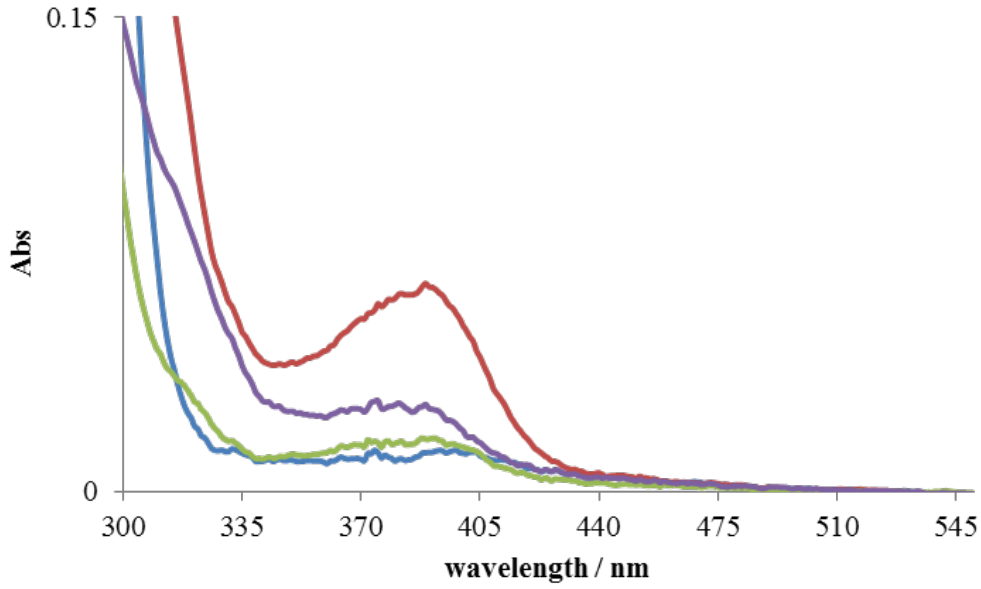


***Figure 76*** *Absorption spectra of derivatives degradation in methanol:water of TXCOOH ([LES]=0 M, blue), TXCOOH (25 min, red) TXCOGLY ([LES]=0 M, green), TXCOGLY (25 min, purple)*

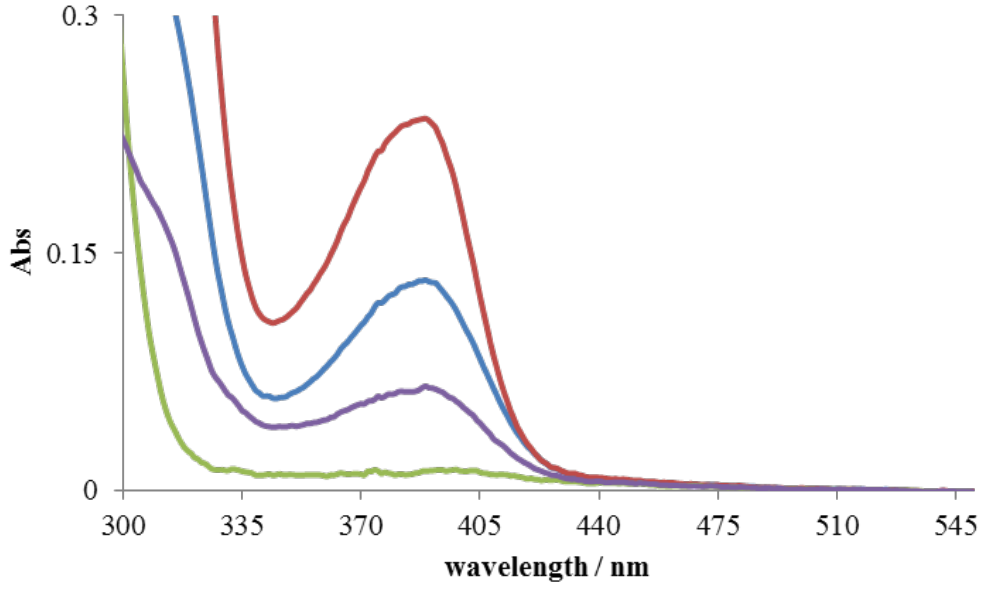


***Figure 77*** *Absorption spectra of derivatives degradation in methanol:water of TXCOMORPHO ([LES]=0 M, blue), TXCOMORPHO ([LES]=3.6 M, red), TXCONCO₂OH ([LES]=0 M, green), TXCONCO₂OH ([LES]=3.6 M, purple)*

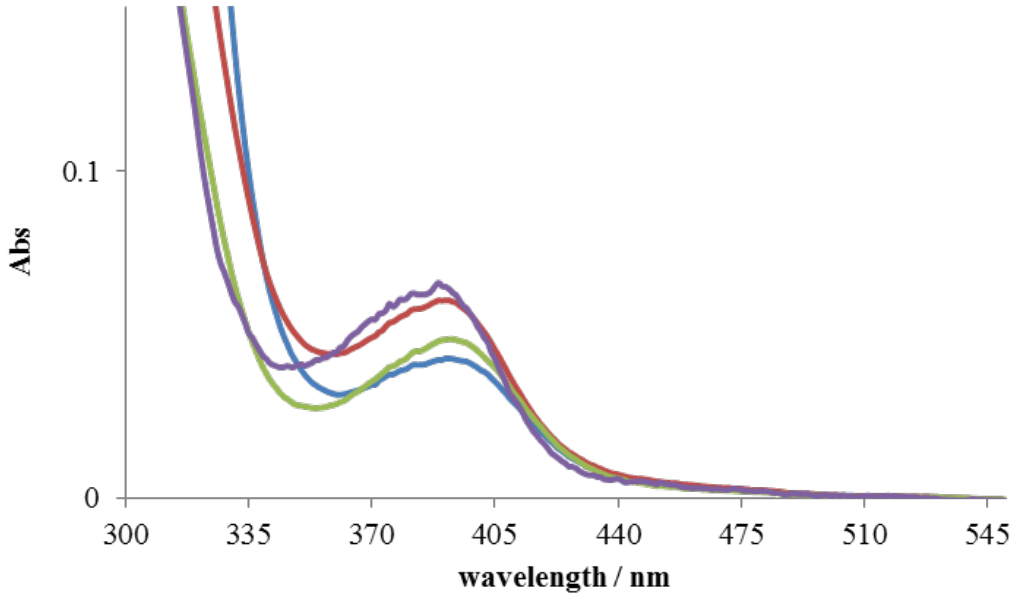


***Figure 78*** *Absorption spectra of derivatives degradation in methanol:water of $TXCONET_2$ ([LES]=0 M, blue), $TXCONET_2$ ([LES]=3.6 M, red), TERTTXGLY ([LES]=0 M, green), TERTTXGLY ([LES]=3.6 M, purple)*

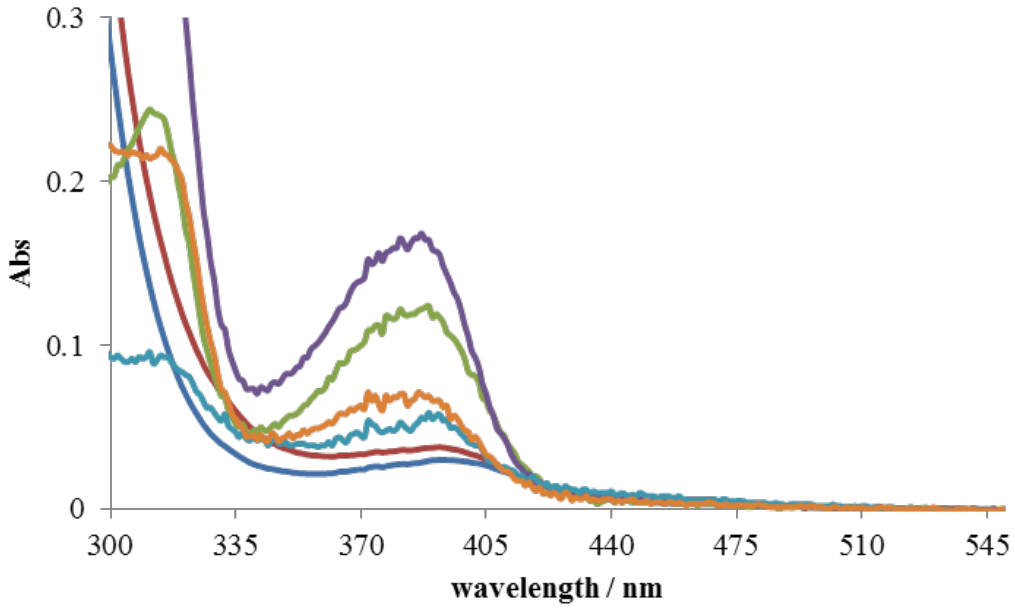


***Figure 79*** *Absorption spectra of derivatives degradation in methanol:water of $TXCONC_7$ ([LES]=0 M, blue), $TXCONC_7$ ([LES]=3.6 M, red)$TXCONCO_3OH$ ([LES]=0 M, green), $TXCONCO_3OH$ ([LES]=3.6 M, purple), TERTTXMORPHO ([LES]=0 M, blue), TERTTXMORPHO ([LES]=3.6 M, red)*

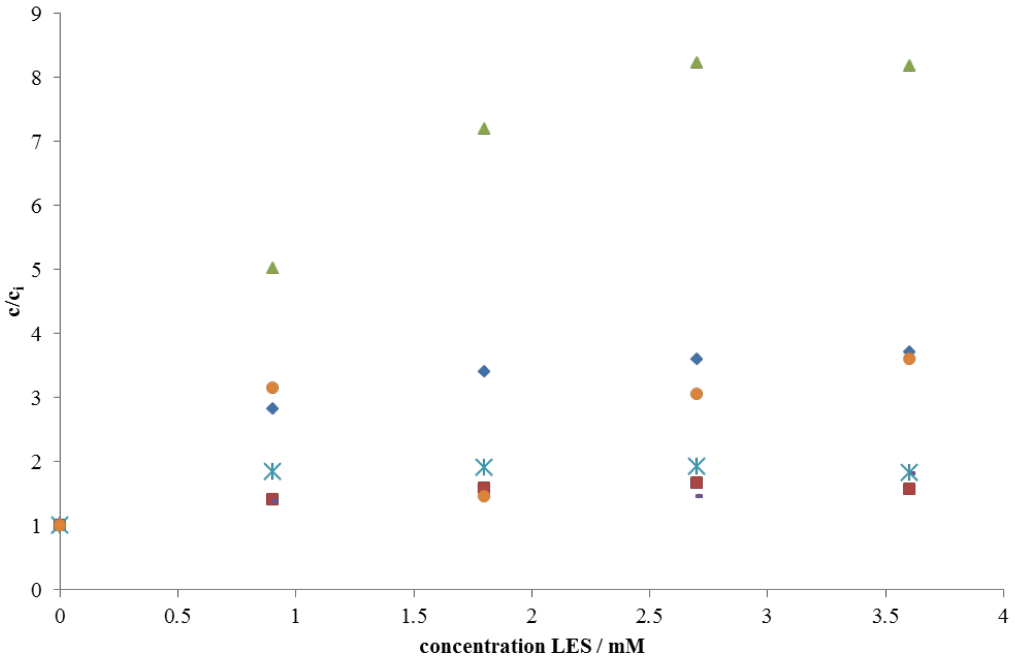


***Figure 80*** *Concentration changing of TX (blue), TERTTX (red), TXCOOH (green), TXCOGLY (purple), TXCOMORPHO (light blue), TXCONC$_7$ (orange) upon concentration of LES*

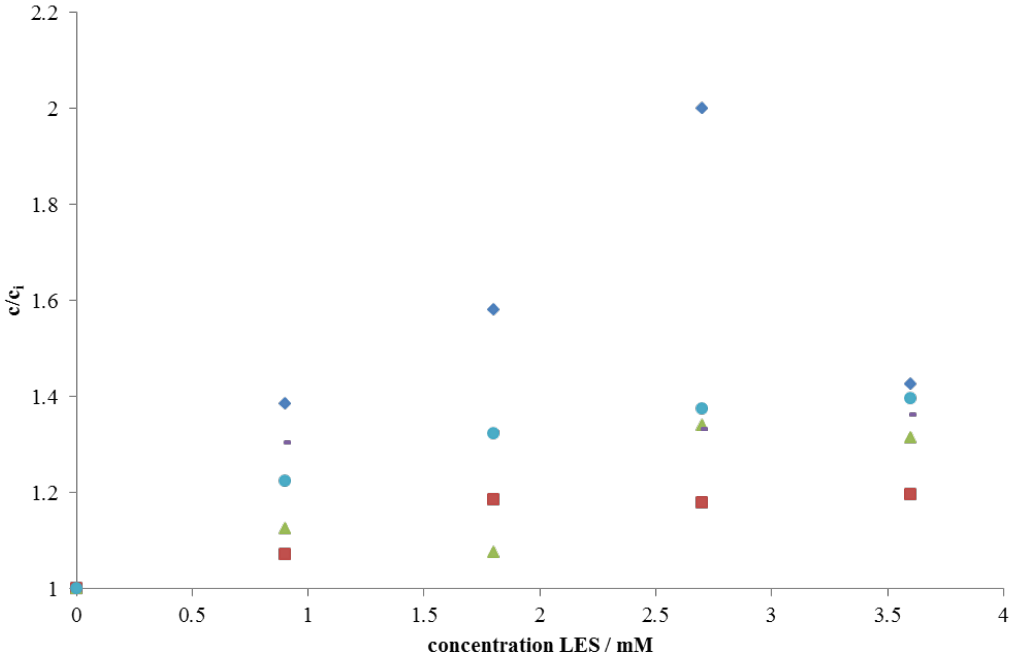


***Figure 81*** *Concentration changing of TXCONCO$_2$OH (blue), TXCONCO$_3$OH (red), TXCONET$_2$ (green), TERTTXMORPHO (purple), TERTTXGLY (light blue) upon concentration of LES*

Assuming the molar extinction coefficient does not change in the presence of LES, it is evident all derivatives increase the concentration in solution upon LES addition (Figures 80,81). TXCOOH displays the greatest improvement with a final concentration almost nine times higher compared to the initial. Even TX, $TXCONCO_2OH$ and $TXCONC_7$ increase three times the solubility in LES solution.

This positive interaction with detergent could help the adsorption of the derivatives onto clothes surface creating an efficient PBA for real applications.

## 3.7 Conclusions

The photophysical properties of thioxanthone derivatives are studied in this chapter. The primary goal of this project is the creation of novel TX derivatives with similar photophysical behaviour compared to thioxanthone to replace the current used PBA in laundry detergent.

From the absorption spectra, it is evident the principal transitions remain in near UV region (380 nm), and all the solutions are colourless. This result confirms the presence of a new fragment does not have any significant effect on the energy of the electronic transition. Furthermore, all compounds present a similar extinction coefficient and a similar solubility in water. Even the fluorescence emission occurs at the same wavelength (440 nm) confirming the unchanged energy gap between the ground and excited states of all compounds again.

The main differences appear in fluorescence lifetimes and quantum yields. All derivatives present a lower fluorescence quantum yield, and a shorter lifetime compared to TX.

The triplet excited state has been investigated using phosphorescence and flash photolysis. The first experiment presents a shift in the emission at 77K which can be interpreted has an involvement of vibronic states in ground and triplet state.

The flash photolysis experiment reveals similar maximum in the triplet-triplet absorption spectra but a different relative intensity between derivatives and thioxanthone.

All the derivatives behave as type II singlet oxygen synthesiser and present a higher yield compared to TX. The creation of singlet oxygen can lead to the degradation of crocin which is used as a stain simulator in solution.

The quenching of singlet oxygen by crocin occurs at the diffusion limit, this unusual result is expected due to carotenoids quenching chain dependency (see Chapter 1 Introduction).

Crocin degradation, in the absence and presence of TX derivatives, was performed by illumination of the different solution with a tungsten lamp and monitored via UV-Vis absorption spectra over 25 minutes. In the presence of TX's derivatives, the concentration loss rate is faster than the natural crocin disappearance.

The last experiment with LES and TX's derivatives intended to explore the interaction between detergents and the derivatives. Upon LES addition all TX's derivatives increase the concentration in aqueous solution.

Overall all derivatives present the similar photophysical properties to thioxanthone and therefore have a potential as new photobleaching agent.

# Chapter 4
# Thioxanthone derivatives as Photobleaching Agents

This section details several tests personally performed during a secondment to the P&G Newcastle innovation centre. These experiments aimed to explore and apply the properties of a selection of newly synthesised thioxanthone derivatives, in 'real' consumer situations. From these results, it will be possible to compare the performance of the TX derivative against PBA currently in use, specifically phthalocyanine and porphyrin PBAs. Furthermore, the detergent–PBA interaction has been investigated in all of the experiments. To obtain good and reproducible results, an *ad hoc* method has been developed for sample loading, and several repetitions of each set have been carried out. The washing system used is unique equipment developed by P&G and Peerless Systems detailed below. Because of the positive results collected during these tests, it will be possible to think of a new PBA additive based on TX and expand the investigation, which can lead to a future replacement.

## 4.1 Introduction

PBAs were introduced in the late 80s as additives with the eco-friendly goals to reduce water, energy, and detergent use using a post-washing photo-activation[2]. A mixture of different phthalocyanine and porphyrin compounds has been adopted by P&G as the PBA for their overall positive impact on stain removal and singlet oxygen generation.

During the drying process in sunlight, PBAs become active, absorbing light and react with atmospheric oxygen to degrade the remaining stains (Figure 82).

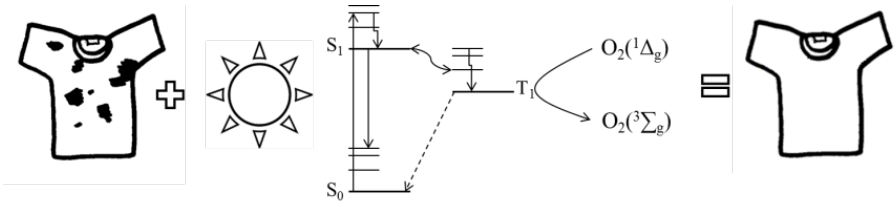


***Figure 82*** *Photobleaching agent process: sunlight can promote the activation of PBA adsorbed on an unclean cloth. Thanks to an efficient intersystem crossing and high rate of oxygen quenching it is possible to create singlet oxygen and continue the cleaning process during the drying*

Unfortunately, these highly conjugated metal complexes which have an intense blue/purple coloration are often not easy to synthesise, have a relatively high cost and are not stable for prolonged storage. Those limitations restrict the concentration used in the conventional detergents to < 0.5 mg/L. By using a small amount of material, the PBA can be adsorbed on the clothes' surfaces and not change the apparent colour of the item. However, the PBAs employed by P&G have limitations regarding stain removal efficiency. In fact, the currently used PBA show a real improvement in the removal of beverage (coffee, tea, etc.) or soil stains but a low efficiency for carotenoid-based stains. The deposition of blue material onto yellow/red stain can worsen the appearance of spills or spots on clothes. For these reasons, there is a drive in the industry to find suitable chemicals to replace the materials currently used. There are a few important parameters that the new PBAs should have. First, they should be colourless in solution or virtually transparent particles ($\lambda_{abs}$<400 nm) at the concentrations at which they are deployed, and should be good a photosensitizer. Secondly, they should be relatively cheap to obtain and stable in long storage conditions.

Thioxanthone has been identified as a potential new PBA, and several TX derivatives have been created in this work to improve water solubility. A selection of seven derivatives was chosen for these tests. The choice of chemicals has been made on availability, and for comparison purposes, TX has been used in all of the experiments.

Because of the known lower performance of existing PBA's with carotenoids, all of the stains chosen were based on this class of chemical. To reproduce a realistic consumer situation, consumer product stains like baby food, curry paste, and various sauces based on tomato were selected. Using this type of dye helps to mimic the action of detergent and PBA in real-world consumer using, on the other, it must be recognised that these present complicated chemical environments. All of the stains contain not only the important carotenoid but also a series of other ingredients, like oil, spices, herbs, and other additives typical of food stuff. It will be hard to give a definite conclusion on the chemical behaviour of the chosen PBA in solution and when adsorbed onto clothes' surface. However, it will be possible to measure the overall impact of PBAs through cleanness parameters. Tests have been designed to have a control where no PBA was added and can be used as a reference; the difference in cleanness can be taken as a sign of good or bad performance of the PBA.

In the past, these types of tests were carried out in a conventional washing machine with a total load of 8 kg. Such a system gave limited control of washing variables such as duration, temperature, and spinning and are limited by the cost of running multiple experiments under different conditions. A smaller-scale equipment was used for initial trials and minor tests. Despite the more controlled environment regarding length and temperature of the cycle, with a maximum load of 0.5 kg, this system has an obvious limitation in the variety of stains washed under the same conditions. In recent years, P&G started a collaboration with Peerless Systems to manufacture medium-size washing equipment for experimental purposes. This system is composed of a series of 10 pots with 1 L capacity each that can perform simultaneous washing under the same conditions (Figure 83).

***Figure 83*** *Overview pictures of the washing system used in the P&G Newcastle innovation centre, system customised from Peerless Systems*

A variety of parameters can be chosen, such as temperature, duration of the washing, rinsing, and spinning. Furthermore, with an ion-exchange column directly attached to the system water supply, options of soft, hard, and city water are available.

| **Description** | **Hardness in mg/L as Calcium** | **Hardness in mg/L as Calcium Carbonate** |
|---|---|---|
| Soft | 0–30 | 0–75 |
| City | 30–60 | 75–150 |
| Hard | 60–100 | 150–225 |

The detergent used during the tests was specially formulated by P&G so as not to contain any bleach or optical brighteners, which would interfere with PBA performance. The PBA was added to the detergent separately. Due to the lack of absorption bands in the visible spectrum tests with TX-based PBA could be performed with concentrations five and ten times higher than the current PBA without any significant colour changes in the fabric, an essential outcome for laundry use.

The carotenoid-based target stains were provided by an external specialist supplier. To mimic clothes-washing conditions, squared cotton swatches with a dimension of 10 cm by 10 cm were used. In the centre of each fabric, a circular stain of 5 cm diameter was applied (Figure 84).

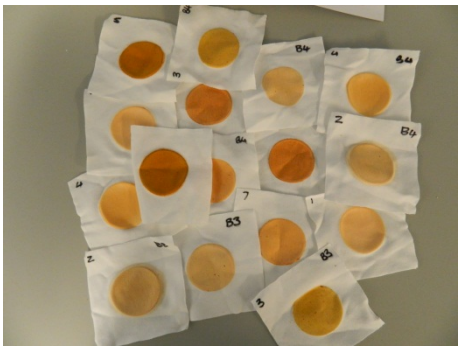

***Figure 84*** *Example of stained swatches used*

The stains created were clearly over-concentrated compared with regular consumers' experience. In general, consumers have small splashes or spots of 'dirt', whereas in this model system a significant amount of material has been pressed into the cloth. Using swatches can be useful for two reasons; firstly, it will be easier to measure any changes between the pre- and post-wash, which is detected by optical equipment based on **L**, **a**,**b** measurements. Secondly, a good performance of detergents and PBA on this thick and over-concentrated stain can lead to an astounding performance in real situations.

The crucial part of these tests was the drying process where, under a light, the PBAs are activated. To mimic the sun exposure, swatches were hung in a special room where several high-power lamps irradiated them. The light source used covered two different regions, visible (400–700 nm) and ultraviolet (300–400 nm). The power in the two regions is different and depends on the duration of the exposure; in general, visible light can generate 185 $W/m^2$ when cold, to 308 $W/m^2$ when the lamps are warmed up. In the UV region the power generated is between 18 and 30 $W/m^2$, for the experiments' duration it was possible to reach the maximum intensity at the end of one hour of exposure. The room has been created to mimic the light of a typical Mexican day. After a one-hour exposure, swatches were left in the dark until dry (Figure 85).

***Figure 85*** *Example of swatches hanging in the solar room*

## 4.2 Sample Preparation, Analysis, and Equipment

Ten washing processes were performed simultaneously: 9 of them had a single PBA added, and the tenth control experiment was detergent-only. Each pot was filled with 1 L of city water with a constant temperature of 30 °C. A conventional washing machine has a full capacity of 8 kg using 16 g of detergent. Consequently, detergent and PBA amounts were adjusted to mimic the use on a smaller scale. Across all of the experiments 2 g/L of non-bleached detergent and 0.5 mg/L, 2.5 mg/L, and 5 mg/L of PBAs were used. Phthalocyanine and porphyrin-based PBAs has been named BH in this work and were provided by P&G. Because BH is a commercially used material, it has already been encapsulated to give better stability for storage and is only 10% efficient. This factor has been considered when BH samples were weighed out.

The TX-based PBAs used during the tests were the following with the acronyms used. The TX-based PBAs used during the tests were the following with the abbreviations used (Figure 86).

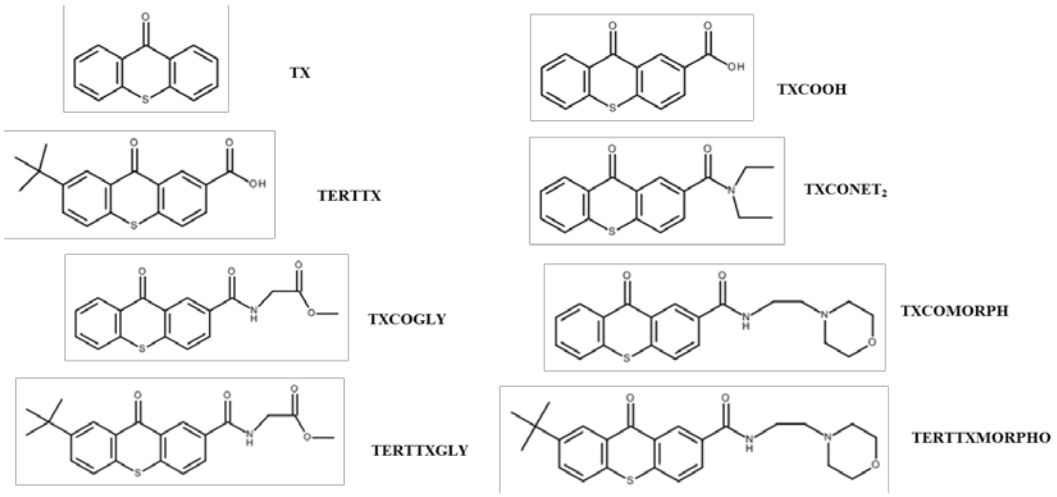


***Figure 86*** *Thioxanthone derivatives and acronyms used in P&G tests*

The eight target stains were all carotenoid-based: carrot & potato baby food, bolognese, vindaloo, hot pepper sauce, paprika, ragu, sundried tomato, and tomato puree. They were chosen because of their extensive domestic use and, for most of them, difficulty in removal. To reproduce an average clothes weight and better statistics in each pot, two swatches of each stain were used. All of them have been uniquely marked labelled to track which stain and PBA combination was used.

## 4.3 Sample loading

The water was warmed until it reached the chosen temperature, 30 °. The system performed a quick wash of the empty pots and discharged the water to eliminate any possible residue from the previous experiments. When the pots had been filled with 1 L of city water, the lids were opened and the detergent and swatches loaded separately. Detergent and PBA were dissolved and mixed for 15 s, forming a homogeneous solution. After mixing the swatches were added with particular attention to spreading them in the pot and then the washing process started.

The tests for the different concentrations were carried out on three separate occasions, and three different washing processes were performed. With the lower concentration (0.5 mg/L), a washing process of 25 min was followed by a 5 min rinse. A slightly longer wash can be beneficial to allow the PBA to be adsorbed onto the swatches' surface. Furthermore, one experiment set was performed without any detergent, to investigate the PBA-alone performance. With 2.5 mg/L and 5 mg/L, the washing process was 20 min long followed by 5 min rinse. Detergent was added in all of these experiments. Each experiment was repeated twice to decrease the inevitable error due to the many variables present. After washing, all of the swatches were exposed to 1 h of 'solar' light and left in the dark until thoroughly dry.

## 4.4 Assessment

The stain analysis was carried out with DigiEye equipment (see Section 2.5). A high-resolution picture of the swatches was taken before and after the washing. Each swatch was tracked and compare **L**,**a**,**b** values compared after the treatment. The performance was assessed with the stain removal index (SRI), a method based on the **L**,**a**,**b** values extrapolated before and after the washing (Figure 87).

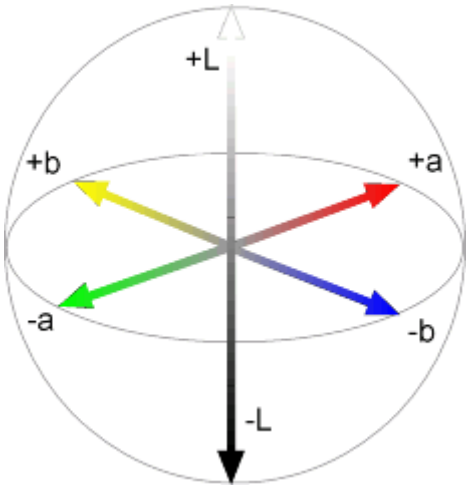


***Figure 87 L,a,b*** *colour space*

**L** is the lightness parameter, and a high positive value corresponds to a 'whiter' material and a negative value a darker material. A positive **a** value corresponds to an increase in redness and a negative value to a green colour. The **b** parameter evaluates the yellowness, which corresponds to a positive value, a negative **b** indicates blueness. Thus the colour of the stain used can be codified with a set of unique **L**, **a**,**b** parameters.

The stain removal index (SRI) equation correlated the **L**, **a**,**b** values of clean and unclean swatches and provided a valuation of the overall performance of detergents or, in this case, PBA[91]

$$SRI = 100 * \frac{[(L_W - L_U)^2 + (a_W - a_U)^2 + (b_W - b_U)^2]^{1/2}}{[(L_C - L_U)^2 + (a_C - a_U)^2 + (b_U - b_U)^2]^{1/2}}$$

where W refers to the washed, U to the unclean swatch, and C to a standard clean **L**, **a**,**b** value of 95,0,0. An item with a final SRI with a value higher than 80 was considered to be acceptably clean (Figure 88).

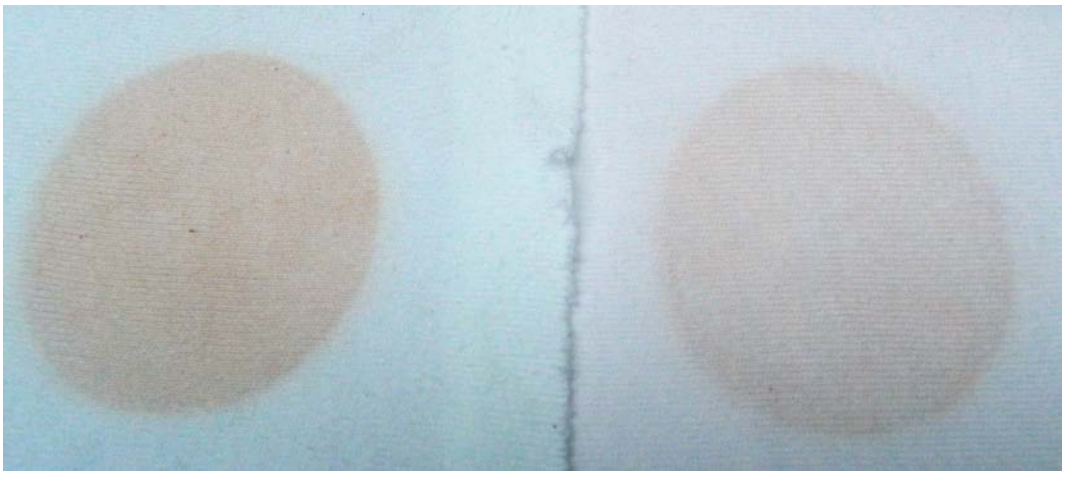

***Figure 88*** *Example of swatches with SRI higher than 80*

The **L**, **a**,**b**, values were obtained with specific software from DigiEye tools which allowed definition of both the shape and area to be analysed. In this case, a circular area with a diameter of 1.2 cm was selected. The **L**, **a**,**b** values were measured three times in three

different positions, always within the 5 cm stain diameter to reduce the standard deviation of the SRI value. Each experiment set was replicated twice, and each stain analysed three times before and after the washing. All three SRI values, calculated from six **L**, **a**,**b** numbers collected from one set, were compared with the SRI of the second set to further improve the statistics.

## 4.5 Results and Discussion

The first tests carried out were with the lowest concentration of PBA equal to 0.5 mg/L. The aim of this set of experiments was twofold; first, to understand if at this low concentration the new TX PBAs had a better performance than those currently used commercially (BH), and second if, without any detergent, it is possible to obtain an improvement in the swatches' SRI value.

All the data collected will be presented in appendix A, in this chapter a summary will be presented to simplify the reading of the chapter.

The following tables show the SRI values and standard deviations of the various stains, treated with different PBAs. Furthermore, the tables compare the SRI values with and without the presence of detergent. The control SRI value gives an understanding of how well the stain can be removed just with water (Table 13,14).

| PBA \ Stain | Baby food no detergent | Baby food detergent | Bolognese no detergent | Bolognese detergent | Vindaloo no detergent | Vindaloo detergent | Hot pepper sauce no detergent | Hot pepper sauce detergent |
|---|---|---|---|---|---|---|---|---|
| CONTROL | 83.3 (0.8) | 89.3 (0.5) | 75.3 (1.8) | 84.8 (2.0) | 56.8 (1.9) | 70.9 (2.7) | 91.8 (0.7) | 93.3 (1.0) |
| BH | 82.1 (1.0) | 91.7 (0.8) | 75.2 (1.5) | 83.0 (0.8) | 58.7 (1.8) | 68.0 (1.9) | 92.6 (0.5) | 93.5 (0.5) |
| TX | 81.8 (0.8) | 89.4 (0.5) | 77.2 (0.6) | 87.5 (0.7) | 62.9 (1.2) | 76.9 (1.3) | 92.3 (0.6) | 93.7 (0.6) |
| TXCOOH | 81.1 (0.7) | 88.9 (0.5) | 78.0 (0.4) | 85.6 (1.1) | 48.5 (0.7) | 67.1 (2.3) | 90.6 (0.8) | 92.9 (0.5) |
| TERTTX | 81.1 (0.8) | 88.6 (0.3) | 78.0 (1.6) | 84.5 (1.4) | 53.0 (1.9) | 63.6 (1.8) | 90.7 (1.1) | 94.6 (0.5) |
| $TXCONET_2$ | 80.4 (0.5) | 89.0 (0.6) | 76.2 (1.4) | 84.5 (1.1) | 56.7 (2.7) | 71.0 (1.5) | 90.5 (1.1) | 92.0 (0.9) |
| TXCOGLY | 81.8 (0.9) | 89.7 (0.5) | 77.2 (1.9) | 85.9 (1.3) | 49.5 (2.3) | 71.0 (3.0) | 89.9 (1.5) | 92.7 (0.5) |
| TXCOMORPH | 81.0 (1.6) | 89.2 (0.6) | 76.4 (0.8) | 83.6 (1.1) | 56.5 (1.9) | 66.0 (2.8) | 91.4 (0.9) | 94.2 (0.4) |
| TERTTXGLY | 81.0 (0.6) | 90.0 (0.2) | 79.4 (1.4) | 86.6 (0.5) | 60.8 (1.3) | 71.4 (32.9) | 92.6 (0.5) | 94.0 (0.5) |
| TERTTXMORPHO | 82.7 (0.8) | 90.7 (0.6) | 76.5 (1.5) | 86.1 (0.8) | 55.9 (2.0) | 68.3 (0.2) | 91.4 (0.8) | 93.8 (0.7) |

***Table 13*** *SRI values of the different stains used with a PBA concentration of 0.5 mg/L with and without detergent*

| PBA \ Stain | Paprika no detergent | Paprika detergent | Ragu no detergent | Ragu detergent | Sundried tomato no detergent | Sundried tomato detergent | Tomato puree no detergent | Tomato puree detergent |
|---|---|---|---|---|---|---|---|---|
| CONTROL | 61.0 (3.4) | 67.6 (1.1) | 69.6 (0.6) | 79.8 (0.6) | 87.8 (0.5) | 92.6 (0.5) | 78.0 (0.7) | 89.0 (0.9) |
| BH | 63.2 (1.4) | 65.7 (2.1) | 73.5 (1.0) | 83.3 (1.2) | 87.8 (1.8) | 94.7 (0.3) | 78.8 (1.0) | 91.0 (0.8) |
| TX | 74.2 (0.7) | 77.6 (1.8) | 72.5 (1.2) | 82.2 (0.9) | 89.0 (0.4) | 93.8 (0.2) | 76.3 (1.4) | 89.7 (0.9) |
| TXCOOH | 63.3 (1.3) | 71.2 (1.1) | 73.4 (0.9) | 82.5 (0.9) | 88.2 (0.7) | 93.8 (0.4) | 76.8 (0.9) | 88.4 (0.6) |
| TERTTX | 66.2 (2.9) | 65.2 (2.7) | 71.0 (1.0) | 80.9 (0.8) | 88.6 (0.6) | 92.6 (0.4) | 77.3 (0.3) | 89.2 (0.9) |
| $TXCONET_2$ | 63.5 (1.7) | 62.9 (1.9) | 70.6 (1.0) | 81.0 (1.2) | 88.5 (0.5) | 92.4 (0.5) | 77.5 (0.8) | 87.4 (1.4) |
| TXCOGLY | 64.3 (1.5) | 63.5 (1.1) | 73.4 (0.9) | 81.7 (0.9) | 90.1 (0.6) | 93.0 (0.3) | 80.1 (1.2) | 89.6 (0.8) |
| TXCOMORPH | 64.8 (2.0) | 70.8 (2.6) | 71.1 (1.0) | 80.4 (1.2) | 89.9 (0.7) | 93.7 (0.3) | 76.8 (1.2) | 90.0 (2.1) |
| TERTTXGLY | 66.9 (0.5) | 70.8 (3.3) | 72.5 (1.2) | 83.4 (0.7) | 88.9 (0.7) | 93.3 (0.6) | 78.9 (0.6) | 90.2 (0.7) |
| TERTTXMORPHO | 67.4 (2.1) | 61.1 (1.5) | 71.7 (1.3) | 81.7 (1.1) | 88.0 (0.8) | 93.2 (0.5) | 78.5 (0.5) | 90.8 (0.9) |

***Table 14*** *SRI values of the various stains used with a PBA concentration of 0.5 mg/L with and without detergent*

The SRI values of the controls of bolognese, vindaloo, paprika, ragu, and tomato puree stains, without detergent, were below 80, meaning the swatches have not been cleaned. The rest of the stains could be washed easily even with just water. Baby food, with an SRI of 83.3 and sundried tomato of 87.8 could still benefit from the PBA. Hot pepper sauce, in this experiment set, has been thoroughly washed out with and without detergent (Table 15).

| % Changing in SRI without detergent | Baby food | Bolognese | Vindaloo | Hot pepper sauce | Paprika | Ragu | Sundried tomato | Tomato puree |
|---|---|---|---|---|---|---|---|---|
| BH | -1.2 (1.8) | -0.1 (3.3) | 1.9 (3.7) | 0.8 (1.2) | 2.2 (4.8) | 3.9 (1.6) | 0.0 (2.3) | 0.8 (1.7) |
| TX | -1.5 (1.6) | 1.9 (2.4) | 6.1 (3.1) | 0.5 (1.3) | 13.2 (4.1) | 2.9 (1.8) | 1.2 (0.9) | -1.7 (2.1) |
| TXCOOH | -2.2 (1.5) | 2.7 (2.2) | -8.3 (2.6) | -1.2 (1.5) | 2.3 (4.7) | 3.8 (1.5) | 0.4 (1.2) | -1.2 (1.6) |
| TERTTX | -2.2 (1.6) | 2.7 (3.4) | -3.8 (3.8) | -1.1 (1.8) | 5.2 (6.3) | 1.4 (1.6) | 0.8 (1.1) | -0.7 (1.0) |
| $TXCONET_2$ | -2.9 (1.3) | 0.9 (3.2) | -0.1 (4.6) | -1.3 (1.8) | 2.5 (5.1) | 1.0 (1.6) | 0.7 (1.0) | -0.5 (1.5) |
| TXCOGLY | -1.5 (1.7) | 1.9 (3.7) | -7.3 (4.2) | -1.9 (2.2) | 3.3 (4.9) | 3.8 (1.5) | 2.3 (1.1) | 2.1 (1.9) |
| TXCOMORPH | -2.3 (2.4) | 1.1 (2.6) | -0.3 (3.8) | -0.4 (136) | 3.8 (5.4) | 1.5 (1.6) | 2.1 (1.2) | -1.2 (1.9) |
| TERTTXGLY | -2.3 (1.4) | 4.1 (3.2) | 4 .0 (3.2) | 0.8 (1.2) | 5.9 (3.9) | 2.9 (1.8) | 1.1 (1.2) | 0.9 (1.3) |
| TERTTXMORPHO | -0.6 (1.6) | 1.2 (3.3) | -0.9 (3.9) | -0.4 (1.5) | 6.4 (5.5) | 2.1 (1.9) | 0.2 (1.3) | 0.5 (1.2) |

***Table 15*** *Percentage change of the PBAs' SRI compared with control without detergent, in yellow the positive changes*

In the absence of detergent, PBAs improved the washing performances 20.8% of the time compared with the control. Although the low concentrations used the PBA has a positive action within the stains with a poorer SRI. Paprika stain, which had a poorer control SRI, showed the greatest improvement, with a peak of 13.2% with TX, 5.9 % with TERTTXGLY and 6.4% with TERTTXMORPHO. Even with the ragu stain, there was an improved apparent cleanness with the majority of PBAs.

As expected the available commercial BH showed a very weak effect on cleanness. All of the TX derivatives, except $TXCONET_2$, have a more consistence performance compare to BH. The most consistent molecules were TERTTXGLY and TX, which showed improvements across half the stains. An enhancement of the overall washing performance is expected by adding detergent.

More importantly, it will give an understanding of the interaction between the TX-based PBAs and the commercially used surfactant. It could be possible that the proposed PBAs will be highly solubilized and do not adsorb on the swatches.

From Tables 13 and 14, it is feasible to see the positive influence on the detergent, which improves the washing performance across all of the stains. Bolognese control increased its SRI from 75 to 85, crossing the threshold for the 'clean' value, the same behaviour as for tomato puree. Vindaloo and paprika showed a significant improvement, but without passing the goal SRI value (Table 16).

| % changing in SRI with detergent | Baby food | Bolognese | Vindaloo | Hot pepper sauce | Paprika | Ragu | Sundried tomato | Tomato puree |
|---|---|---|---|---|---|---|---|---|
| BH | 2.4 (1.3) | -1.8 (2.8) | -2.9 (4.6) | 0.2 (1.5) | -1.9 (3.2) | 3.5 (1.8) | 2.1 (0.8) | 2.0 (1.7) |
| TX | 0.1 (1.0) | 2.7 (2.7) | 6.0 (4.0) | 0.4 (1.6) | 10.0 (2.9) | 2.4 (1.5) | 1.2 (0.7) | 0.7 (1.8) |
| TXCOOH | -0.4 (1.0) | 0.8 (3.1) | -3.8 (5.0) | -0.4 (1.5) | 3.6 (2.2) | 2.7 (1.5) | 1.2 (0.9) | -0.6 (1.5) |
| TERTTX | -0.7 (0.8) | -0.3 (3.4) | -7.3 (4.5) | 1.3 (1.5) | -2.4 (3.8) | 1.1 (1.4) | 0.0 (0.9) | 0.2 (1.8) |
| $TXCONET_2$ | -0.3 (1.1) | -0.3 (3.1) | 0.1 (4.2) | -1.3 (1.9) | -4.7 (3.0) | 1.2 (1.8) | -0.2 (1.0) | -1.6 (2.3) |
| TXCOGLY | 0.4 (1.0) | 1.1 (3.3) | 0.1 (5.7) | -0.6 (1.5) | -4.1 (2.2) | 1.9 (1.5) | 0.4 (0.8) | 0.6 (1.7) |
| TXCOMORPH | -0.1 (1.1) | -1.2 (3.1) | -4.9 (5.5) | 0.9 (1.4) | 3.2 (3.7) | 0.6 (1.8) | 1.1 (0.8) | 1.0 (3.0) |
| TERTTXGLY | 0.7 (0.7) | 1.8 (2.5) | 0.5 (5.7) | 0.7 (1.5) | 3.2 (4.4) | 3.6 (1.3) | 0.7 (1.1) | 1.2 (1.6) |
| TERTTXMORPHO | 1.4 (1.1) | 1.3 (2.8) | -2.6 (2.9) | 0.5 (1.7) | -6.5 (2.6) | 1.9 (1.7) | 0.6 (1.0) | 1.8 (1.8) |

***Table 16*** *Percentage change of the PBAs' SRI compared with control with detergent, in yellow the positive changes*

Although the presence of detergent increases the washing performance, it does not improve the PBA adsorption. In fact, only 20.8% of the experiments have improved cleaning performance due to PBAs. Even in this case, the improvement is marginal due to the low concentration of additive used. Ragu stain has the best interaction with PBAs and increases

the SRI in two-thirds of the experiments. The most consistency PBA, in this case, are BH and TX, which improves the SRI for half of the stains.

Despite the equipment having been used by other researchers between experiments, the data collected seem to be consistent and reliable. This first set of tests showed encouraging results on the new PBAs. It might be possible to deliver better results by increasing the PBAs' concentration.

It is already known that using 2.5 mg/L and 5 mg/L of BH causes a colour deposition on clothes (Figure 89). This disadvantage was already noticed during sample loading where the BH solutions present an intense blue colour but are entirely soluble. On the other hand, TX PBAs were perfectly transparent but did not solubilize efficiently. To create a homogenous washing solution, 15 s of mixing were applied prior the washing cycle.

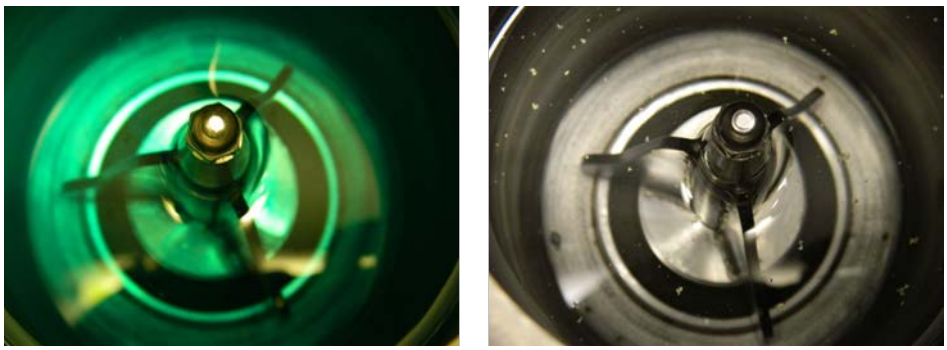

***Figure 89*** *Pots solution of 2.5 mg/L of BH (left) and 2.5 mg/L of TX before detergent addition*

After washing, all BH swatches showed a blue cover, as expected, proving BH's limitation (Figure 90). Despite the obvious and unwanted disadvantage, the tests were carried out as scheduled and SRIs were calculated only on the stained part (Table 17).

***Figure 90*** *Swatches after the washing process, BH on the left and TX on the right*

| PBA 2.5 mg/L \ Stain | baby food detrgent | bolognese detrgent | vindaloo detrgent | hot pepper sauce detrgent | paprika detrgent | ragu detrgent | sundried tomato detrgent | tomato puree detrgent |
|---|---|---|---|---|---|---|---|---|
| CONTROL | 86.4 (0.6) | 63.7 (1.6) | 63.4 (1.1) | 69.2 (2.4) | 53.6 (1.0) | 82.5 (0.5) | 92.0 (0.3) | 92.0 (0.3) |
| BH | 89.6 (0.4) | 67.4 (0.7) | 25.7 (3.9) | 71.4 (1.2) | 46.6 (1.0) | 86.4 (0.4) | 92.8 (0.6) | 92.8 (0.6) |
| TX | 89.0 (0.2) | 79.6 (1.7) | 60.5 (1.7) | 88.4 (0.8) | 72.6 (2.5) | 83.4 (0.7) | 92.5 (0.4) | 92.5 (0.4) |
| TXCOOH | 84.9 (0.8) | 63.0 (2.2) | 16.4 (1.9) | 75.2 (1.4) | 54.2 (1.6) | 83.0 (0.4) | 91.2 (0.2) | 91.2 (0.2) |
| TERTTX | 87.4 (0.9) | 66.7 (1.6) | 77.7 (1.0) | 75.2 (1.1) | 54.2 (1.5) | 82.8 (0.6) | 90.8 (0.5) | 90.8 (0.5) |
| $TXCONET_2$ | 85.8 (0.7) | 67.8 (1.9) | 22.8 (2.5) | 78.7 (1.7) | 55.9 (1.4) | 84.7 (1.0) | 92.3 (0.5) | 92.3 (0.5) |
| TXCOGLY | 86.1 (1.0) | 72.9 (1.5) | 82.2 (0.6) | 73.4 (1.4) | 56.3 (1.5) | 83.7 (0.9) | 92.2 (0.3) | 91.8 (0.5) |
| TXCOMORPH | 83.9 (0.3) | 71.2 (2.1) | 51.9 (1.9) | 74.0 (1.1) | 50.6 (1.2) | 82.1 (0.8) | 89.5 (0.6) | 89.5 (0.6) |
| TERTTXGLY | 84.6 (0.8) | 68.9 (1.8) | 79.2 (1.3) | 71.6 (2.2) | 56.5 (2.4) | 83.5 (0.8) | 90.6 (0.4) | 90.6 (0.4) |
| TERTTXMORPHO | 90.6 (1.1) | 71.1 (0.7) | 51.9 (1.3) | 70.2 (1.0) | 57.4 (2.0) | 84.8 (1.1) | 92.6 (0.7) | 92.1 (0.7) |

***Table 17*** *SRI values of the different stains used with a PBA concentration of 2.5 mg/L*

For a few control SRI values, it is possible to see differences compared with the one obtained from 0.5 mg/L. These changes will be explained later in this chapter where a direct comparison of different stains will be given.

Bolognese, hot pepper sauce, paprika, and vindaloo have a control SRI below 80, and they should be the stains showing more benefit of PBAs' action (Table 18).

| % changing in SRI 2.5 mg/L | Baby food | Bolognese | Vindaloo | Hot pepper sauce | Paprika | Ragu | Sundried tomato | Tomato puree |
|---|---|---|---|---|---|---|---|---|
| BH | 3.2 (1.0) | 3.7 (2.3) | -37.7 (5.0) | 2.2 (3.6) | -7.0 (2.0) | 3.9 (0.9) | 0.8 (0.9) | 0.8 (0.9) |
| TX | 2.6 (0.8) | 15.9 (3.3) | -2.9 (2.8) | 19.2 (3.2) | 19.0 (3.5) | 0.9 (1.2) | 0.5 (0.7) | 0.5 (0.7) |
| TXCOOH | -1.5 (1.4) | -0.7 (3.8) | -47.0 (3.0) | 6.0 (3.8) | 0.6 (2.6) | 0.5 (0.9) | -0.8 (0.5) | -0.8 (0.5) |
| TERTTX | 1.0 (1.5) | 3.0 (3.2) | 14.3 (2.1) | 6.0 (3.5) | 0.6 (2.5) | 0.3 (1.1) | -1.2 (0.8) | -1.2 (0.8) |
| $TXCONET_2$ | -0.6 (1.3) | 4.1 (3.5) | -40.6 (3.6) | 9.5 (4.1) | 2.3 (2.4) | 2.2 (1.5) | 0.3 (0.8) | 0.3 (0.8) |
| TXCOGLY | -0.3 (1.6) | 9.2 (3.1) | 18.8 (1.7) | 4.2 (3.8) | 2.7 (2.5) | 1.2 (1.4) | 0.2 (0.6) | -0.2 (0.8) |
| TXCOMORPH | -2.5 (0.9) | 7.5 (3.7) | -11.5 (3.0) | 4.8 (3.5) | -3.0 (2.2) | -0.4 (1.3) | -2.5 (0.9) | -2.5 (0.9) |
| TERTTXGLY | -1.8 (1.4) | 5.2 (3.4) | 15.8 (2.4) | 2.4 (3.6) | 2.9 (3.4) | 1.0 (1.3) | -1.4 (0.7) | -1.4 (0.7) |
| TERTTXMORPHO | 4.2 (1.7) | 7.4 (2.3) | -11.5 (2.4) | 1.0 (3.4) | 3.8 (3.0) | 2.3 (1.6) | 0.6 (1.0) | 0.1 (1.0) |

***Table 18*** *Percentage change of the PBAs' SRI compared with control with detergent, in yellow the positive change and in red the BH improvements*

Despite the intense coloration of the BH swatches and the consequently failed action as an additive, SRI revealed improvements in 37.5% of the cases. Such result could be due to the mixing of colours of the blue BH and yellow stains leading to a false positive SRI.

Ragu stain cleanness improved in only three cases; best performance was found with BH, which represents a false positive result. This could be due to the mixing colour rather than a real improvement, as explained earlier. The other two best increments are $TXCONET_2$ and TERTTXMORPHO, which have SRIs of 84.7 and 84.8, respectively.

The SRIs of bolognese, hot pepper sauce and paprika improved compared to control in most of the cases. TX action gave the highest SRI value increase for those stains, 15.9% for bolognese, 19.2% for hot pepper sauce and 19.0% with paprika. Five derivatives showed an SRI improvement for bolognese sauces; TXCOGLY present the most significant increase with 9.2%.

The majority of PBAs had a decisive action on hot pepper sauce; TX improved significantly to pass the clear point and resulted in 88. Vindaloo stain presents an inconsistency in the SRI values, due to the chemical nature of the spices in the curry sauces. TERTTX, TXCOGLY, and TERTGLY have a decisive action on the cleanness of this stain with an SRI improvement of 14.3%, 18.8%, 15.8% respectively.

The PBAs with the more consistence performance are TX, TXCOGLY, and TERTTXMORPHO which improve the SRI of half of the stains.

Overall, PBAs enhanced the cleanness in 35% of the cases, improving the performance of 15% compare to 0.5 mg/L experiment with greater differences. Those results show the significant potential of TX and derivatives. Furthermore by using 2.5 mg/L PBA the difference in SRI results are higher in most of the cases compare to 0.5 mg/L. Such result indicates a positive trend of PBA upon increasing of concentration (Table 19).

| % changing in SRI with detergent | Baby food | | Bolognese | | Vindaloo | | Hot pepper sauce | | Paprika | | Ragu | | Sundried tomato | | Tomato puree | |
|---|---|---|---|---|---|---|---|---|---|---|---|---|---|---|---|---|
| | 0.5 mg/L | 2.5 mg/L | 0.5 mg/L | 2.5 mg/L | 0.5 mg/L | 2.5 mg/L | 0.5 mg/L | 2.5 mg/L | 0.5 mg/L | 2.5 mg/L | 0.5 mg/L | 2.5 mg/L | 0.5 mg/L | 2.5 mg/L | 0.5 mg/L | 2.5 mg/L |
| BH | 2.4 | 3.2 | -1.8 | 3.7 | -2.9 | -37.7 | 0.2 | 2.2 | -1.9 | -7.0 | 3.5 | 3.9 | 2.1 | 0.8 | 2.0 | 0.8 |
| TX | 0.1 | 2.6 | 2.7 | 15.9 | 6.0 | -2.9 | 0.4 | 19.2 | 10.0 | 19.0 | 2.4 | 0.9 | 1.2 | 0.5 | 0.7 | 0.5 |
| TXCOOH | -0.4 | -1.5 | 0.8 | -0.7 | -3.8 | -47.0 | -0.4 | 6.0 | 3.6 | 0.6 | 2.7 | 0.5 | 1.2 | -0.8 | -0.6 | -0.8 |
| TERTTX | -0.7 | 1.0 | -0.3 | 3.0 | -7.3 | 14.3 | 1.3 | 6.0 | -2.4 | 0.6 | 1.1 | 0.3 | 0.0 | -1.2 | 0.2 | -1.2 |
| $TXCONET_2$ | -0.3 | -0.6 | -0.3 | 4.1 | 0.1 | -40.6 | -1.3 | 9.5 | -4.7 | 2.3 | 1.2 | 2.2 | -0.2 | 0.3 | -1.6 | 0.3 |
| TXCOGLY | 0.4 | -0.3 | 1.1 | 9.2 | 0.1 | 18.8 | -0.6 | 4.2 | -4.1 | 2.7 | 1.9 | 1.2 | 0.4 | 0.2 | 0.6 | -0.2 |
| TXCOMORPH | -0.1 | -2.5 | -1.2 | 7.5 | -4.9 | -11.5 | 0.9 | 4.8 | 3.2 | -3.0 | 0.6 | -0.4 | 1.1 | -2.5 | 1.0 | -2.5 |
| TERTTXGLY | 0.7 | -1.8 | 1.8 | 5.2 | 0.5 | 15.8 | 0.7 | 2.4 | 3.2 | 2.9 | 3.6 | 1.0 | 0.7 | -1.4 | 1.2 | -1.4 |
| TERTTXMORPHO | 1.4 | 4.2 | 1.3 | 7.4 | -2.6 | -11.5 | 0.5 | 1.0 | -6.5 | 3.8 | 1.9 | 2.3 | 0.6 | 0.6 | 1.8 | 0.1 |

***Table 19*** *Comparison of percentage change of the PBAs' SRI compared with control with detergent with 0.5 mg/L and 2.5 mg/L, in yellow the increasing change with 2.5 mg/L compared with 0.5 mg/L*

By doubling the PBA concentration, it might be possible to improve the overall positive effect of this additive. Even in this case, all BH swatches presented the blue cover as shown previously.

| Stain / PBA 5 mg/L | Baby food | Bolognese | Vindaloo | Hot pepper sauce | Paprika | Ragu | Sundried tomato | Tomato puree |
|---|---|---|---|---|---|---|---|---|
| CONTROL | 87.8 (0.1) | 59.3 (1.6) | 67.5 (2.7) | 70.4 (1.2) | 53.0 (2.2) | 83.4 (0.7) | 91.8 (0.3) | 88.7 (0.7) |
| BH | 87.8 (1.0) | 61.9 (1.1) | 60.4 (2.3) | 76.5 (2.5) | 53.6 (1.7) | 85.2 (1.0) | 91.7 (0.2) | 88.2 (0.6) |
| TX | 89.5 (0.8) | 79.9 (0.7) | 79.6 (1.4) | 87.1 (0.5) | 76.7 (0.5) | 65.6 (0.8) | 92.4 (0.4) | 88.9 (0.7) |
| TXCOOH | 87.1 (0.7) | 66.2 (1.5) | 65.1 (1.9) | 69.8 (1.2) | 54.2 (0.9) | 81.8 (0.8) | 89.2 (0.8) | 86.4 (0.6) |
| TERTTX | 86.3 (1.0) | 61.6 (1.0) | 67.6 (1.4) | 87.1 (2.0) | 76.7 (1.2) | 81.1 (0.8) | 89.5 (0.6) | 87.1 (0.6) |
| $TXCONET_2$ | 87.8 (0.6) | 72.9 (1.3) | 75.3 (0.8) | 79.4 (0.7) | 59.1 (2.1) | 82.0 (0.5) | 90.3 (0.4) | 86.9 (0.6) |
| TXCOGLY | 84.1 (0.8) | 68.0 (0.8) | 59.8 (1.6) | 71.8 (2.0) | 51.8 (1.7) | 84.0 (0.9) | 91.3 (0.6) | 88.4 (0.7) |
| TXCOMORPH | 86.3 (0.8) | 66.0 (1.4) | 68.9 (1.6) | 74.3 (1.0) | 53.5 (0.5) | 80.1 (1.0) | 88.9 (0.4) | 84.7 (1.2) |
| TERTTXGLY | 86.3 (0.9) | 74.9 (0.9) | 62.8 (0.7) | 67.3 (3.6) | 51.0 (0.9) | 82.3 (0.7) | 89.7 (0.3) | 86.0 (0.7) |
| TERTTXMORPHO | 87.2 (0.6) | 71.1 (1.0) | 69.2 (1.1) | 71.6 (1.2) | 56.0 (1.0) | 84.1 (0.8) | 90.6 (0.6) | 88.0 (0.8) |

***Table 20*** *SRI values of the different stains used with a PBA concentration of 5 mg/L*

Even in this experiment, bolognese, vindaloo, hot pepper sauce, and paprika stain had SRI results below 80 and ragu, with SRI of 83.41, can be improved by PBAs (Table 20).

| % changing in SRI 5 mg/L | Baby food | Bolognese | Vindaloo | Hot pepper sauce | Paprika | Ragu | Sundried tomato | Tomato puree |
|---|---|---|---|---|---|---|---|---|
| BH | 0.0 (1.1) | 2.6 (2.7) | -7.1 (5.0) | 6.1 (3.7) | 0.6 (3.9) | 1.8 (1.7) | -0.1 (0.5) | -0.5 (1.3) |
| TX | 1.7 (0.9) | 20.6 (2.3) | 12.1 (4.1) | 16.7 (1.7) | 23.7 (2.7) | -17.8 (1.5) | 0.6 (0.7) | 0.2 (1.4) |
| TXCOOH | -0.7 (0.8) | 6.9 (3.1) | -2.4 (4.6) | -0.6 (2.4) | 1.2 (3.1) | -1.6 (1.5) | -2.6 (1.1) | -2.3 (1.3) |
| TERTTX | -1.5 (1.1) | 2.3 (2.6) | 0.1 (4.1) | 16.7 (3.2) | 23.7 (3.4) | -2.3 (1.5) | -2.3 (0.9) | -1.6 (1.3) |
| $TXCONET_2$ | 0.0 (0.7) | 13.6 (2.9) | 7.8 (3.5) | 9.0 (1.9) | 6.1 (4.3) | -1.4 (1.2) | -1.5 (0.7) | -1.8 (1.3) |
| TXCOGLY | -3.7 (0.9) | 8.7 (2.4) | -7.7 (4.3) | 1.4 (3.2) | -1.2 (3.9) | 0.6 (1.6) | -0.5 (0.9) | -0.3 (1.4) |
| TXCOMORPH | -1.5 (0.9) | 6.7 (3.0) | 1.4 (4.3) | 3.9 (2.2) | 0.5 (2.7) | -3.3 (1.7) | -2.9 (0.7) | -4.0 (1.9) |
| TERTTXGLY | -1.5 (1.0) | 15.6 (2.5) | -4.7 (3.4) | -3.1 (4.8) | -2.0 (3.1) | -1.1 (1.4) | -2.1 (0.6) | -2.7 (1.4) |
| TERTTXMORPHO | -0.6 (0.7) | 11.8 (2.6) | 1.7 (3.8) | 1.2 (2.4) | 3.0 (3.2) | 0.7 (1.5) | -1.2 (0.9) | -0.7 (1.5) |

***Table 21*** *Percentage change of the PBAs' SRI compared with control with 5 mg/L, in yellow the positive change and in red the BH improvements*

Overall the TX based PBAs improved results in 25% of cases, which is lower than the experiment performed with 2.5 mg/L of the additive but higher compared to 0.5 mg/L (Table 21). This result can be due to the insufficient solubility of TX derivatives and a sequential deposition of yellow particles on the swatches' surfaces, which increased the yellow appearance of the stains. Pre-mixing with detergent does not help, in this case, to dissolve the particles better and achieve a homogeneous solution. It is possible that this unwanted effect occurs even at a lower concentration, but the deposit does not interfere with the overall swatches' appearance and SRI.

A way to overcome this problem in the future could be an encapsulation to help in the delivery of these materials onto the surface and possibly of longer stability for storage, as happened for commercial PBA.

Despite the lower overall improvement, the bolognese stain has a good response across all PBAs with a peak of 20.6% with TX and 15.6% with TERTTXGLY.

In this set of tests, TX showed the most consistent PBA (62.5%) followed by $TXCONET_2$ (50%) and TERTTXMORPHO, which improved the cleanness of 25% of the stains.

All of the data sets collected for the individual tests showed consistent control and PBA SRI values. Unfortunately, there is an inconsistency between different data sets, as can be seen in the following table reporting SRI control values (Table 22).

| | Baby food | Bolognese | Vindaloo | Hot pepper sauce | Paprika | Ragu | Sundried tomato | Tomato puree |
|---|---|---|---|---|---|---|---|---|
| 0.5 mg/L no detergent | 83.3 | 75.3 | 56.8 | 91.8 | 61.0 | 69.6 | 87.8 | 78.0 |
| 0.5 mg/L detergent | 89.3 | 84.8 | 70.9 | 93.3 | 67.6 | 79.8 | 92.6 | 88.9 |
| 2.5 mg/L | 86.4 | 63.7 | 63.4 | 69.2 | 53.6 | 82.5 | 92.0 | 92 |
| 5 mg/L | 87.8 | 59.3 | 67.5 | 70.4 | 53.0 | 83.4 | 91.8 | 88.7 |

***Table 22*** *Control SRI values of the different stains across all the performed tests*

Hot pepper sauce seemed to be completely washable in the first two experiments with 0.5 mg/L with and without detergent, but showed SRI values below 80 for the two following tests. Even vindaloo, bolognese, and paprika stains show the same behaviour, although not as strongly as hot pepper sauce. This anomalous trend could be due to the stain itself. In fact, the tests were carried out on two different occasions more than 10 days apart.

Swatches were collected directly from the supplier and used immediately for the 0.5 mg/L experiments. The same swatches were used for the 2.5 mg/L and 5 mg/L tests more than a week later. During this time, although the fact swatches were kept in the dark at a safe location, stains can dry on the fabric and, consequently, be harder to remove. All of the stains showing this unwanted behaviour are paste based; this means oil has been used to create the stain. In a week's time, this ingredient can penetrate deeply into the textile and fix more of the stain onto the swatch. Another factor influencing the cleanness between the first two experiments and the third is the different duration of the washing programme. To improve the possibility of PBA to be absorbed, a length of 25 min has been chosen for 0.5 mg/L sets, with higher concentration the duration had been shortened to 5 min.

Other anomalous results have been found with vindaloo curry paste, which could be explained by investigating in more detail the chemical nature of this paste (Table 23).

| Vindaloo | NO DET 0.5 mg SRI | DET 0.5mg SRI | 2.5mg SRI | 5mg SRI |
|---|---|---|---|---|
| CONTROL | 56.8 | 70.9 | 63.4 | 67.5 |
| BH | 58.7 | 68.0 | 25.7 | 60.4 |
| TX | 62.9 | 76.9 | 60.5 | 79.6 |
| TXCOOH | 48.5 | 67.1 | 16.4 | 65.1 |
| TERTTX | 53.0 | 63.6 | 77.7 | 67.6 |
| $TXCONET_2$ | 56.7 | 71.0 | 22.8 | 75.3 |
| TXCOGLY | 49.5 | 71.0 | 82.2 | 59.8 |
| TXCOMORPH | 56.5 | 66.0 | 51.9 | 68.9 |
| TERTTXGLY | 60.8 | 71.4 | 79.2 | 62.8 |
| TERTTXMORPHO | 55.9 | 68.2 | 51.9 | 69.2 |

***Table 23*** *Vindaloo SRI values across all of the tests, the most drastic differences from control in yellow*

As with many curries, vindaloo stain contains turmeric as the main spice, which is responsible for the bright yellow paste colour. Turmeric is a well-known natural pH indicator that presents an intense yellow colour below pH 7.4 and turns red in alkaline solution (pH 8.6)[92,93]. The main chemical responsible for the change in colour is curcumin, which presents two different deprotonation sites responsible for the different behaviour in basic solution (Figure 91)[94].

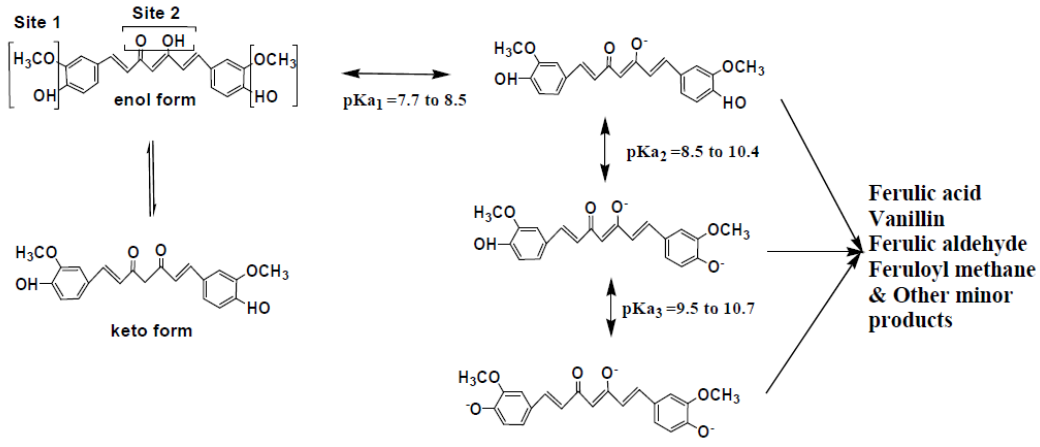


***Figure 91*** *Keto–enol tautomerism, prototropic equilibria and degradation products of curcumin. Figure is taken from*[94]

A standard detergent solution has pH around 8–9 and, inevitably, changes the curcumin colour and, consequently, the appearance of vindaloo stain from yellow to red. This has a high impact on **L**, **a,b**, and SRI values.

## 4.6 Conclusions

The new TX derivatives showed encouraging results across all of the simulated washing trials. The possibility of increasing the concentration without any dramatic inconvenience, as with BH, is clearly a significant advantage for the new proposed PBAs.

In the first set of experiments with 0.5 mg/L without any detergent, TX derivatives improved the cleanness of 19.4% of swatches, which shows the significant impact of this type of additive. The addition of detergent improved the overall stain removal but decrease the TX-PBA performance (15%).

The greatest overall improvement, with TX-based PBA, was reached with 2.5 mg/L with 35% more clean swatches and much more significant differences compared to control. In particular TX, TERTTXGLY, TERTTXMORPHO showed an excellent performance across half of the stains.

By considering all the experiments, the most consistent PBA has been revealed to be the commercially available TX (50%) follow by $TXCONET_2$, which increases the cleanness in 29% of the swatches in the presence of detergent. In general, four of the TX-based PBAs improved the cleanness of 20% or more of the swatches as showed in Table 24. This is clearly an extremely encouraging result, which can lead to new technology in PBA additives (Table 24).

| PBA | % of improvement |
|---|---|
| BH | 17 |
| TX | 50 |
| TXCOOH | 17 |
| TERTTX | 17 |
| $TXCONET_2$ | 29 |
| TXCOGLY | 21 |
| TXCOMORPH | 21 |
| TERTTXGLY | 17 |
| TERTTXMORPHO | 25 |

***Table 24*** *Overall percentage of improvement of all PBAs*

Another relevant comparison is considering the impact of PBA onto the different stains. By monitoring the change in SRI across all the experiments, it is possible to see which stain has greater improvements with PBA. Bolognese has the most beneficial results with all TX PBAs, which improve the cleanness in 52% of the cases (Table 25). It needs to be noted that the greater improvements are with stains with a lower SRI score and PBAs play an active role and help the weak detergent action.

| Stain | % of improvement |
|---|---|
| Baby food | 22 |
| Bolognese | 52 |
| Vindaloo | 22 |
| Hot pepper sauce | 41 |
| Paprika | 15 |
| Ragu | 33 |
| Sundried tomato | 15 |
| Tomato puree | 4 |

***Table 25*** *Overall percentage of improvement of all the stains*

# Chapter 5
# The behaviour of thioxanthone upon acidification

The aim of this chapter is to characterise the photophysical properties of thioxanthone (TX) in acidic media. Such changing in behaviour was observed during the synthesis of thioxanthone derivatives. The glassware containing residual of TXCOOH were washed with sulfuric acid, and the solution turned from colourless to bright yellow. Such dramatic change initiates the investigation of TX in acid media.

Two different acidified solvents are compared; dichloromethane (DCM) with trifluoroacetic acid (TFA) and methanol:water (MeOH:$H_2O$) mixture with sulfuric acid ($H_2SO_4$). The formation of the protonated species ($TXH^+$) occurs in both systems and has been identified using NMR spectroscopy, and shifts in the absorption and fluorescence spectra ($\lambda_{absTX}$= 380 nm, $\lambda_{absTXH+}$= 445, 470 nm, $\lambda_{emTX}$= 430 nm, $\lambda_{emTXH+}$= 500 nm). TX shows a significant difference in fluorescence lifetimes in protic and aprotic solvents ($\tau_{DCM}$=1.2 ns, $\tau_{MeOH: H2O}$=7.4 ns) and a common fluorescence lifetime of 18 ns is observed upon acidifying these solutions, ascribed to $TXH^+$. Furthermore, as described in the introduction, thioxanthone is a well-known singlet oxygen sensitiser, and the singlet oxygen phosphorescence lifetime produced by TX in neat TFA (13 M) has been determined to be $\tau$ = 57 μs. The data reported in this chapter demonstrates that despite the different solvent environments thioxanthone will be protonated in the same position.

## 5.1 Introduction

Thioxanthone is well known for its unusual solvatochromic behaviour that affects the fluorescence emission, quantum yield and lifetime, resulting in higher emission yields and longer lifetimes in protic solvents compared to aprotic[68,71,74,95,96].

It is well-established that the photophysical behaviour of a simple molecule is modified by changing the state of protonation[97–99], for example, deprotonation of phenol to yield the phenolate anion brings about a change in the emission spectrum[100]. Mizutani and co-workers have investigated the ultraviolet absorption, fluorescence, and excitation spectra of xanthone and derivatives in the presence of increasing concentrations of $H_2SO_4$. From the basicities of the compounds, it was proposed that protonation occur at the carbonyl oxygen atom[101].

The aim of this work is to investigate the formation of protonated TX via the characterisation of its spectroscopic properties in acid solution. Two solvent environments were examined: i) $H_2SO_4$ in highly polar aqueous methanol and ii), trifluoroacetic acid (TFA) in dichloromethane. Upon increasing the concentration of acid in these solutions the absorption and fluorescence emission show a red shift, such behaviour is directly connected with increasing concentration of $TXH^+$ in solution. This shift in absorption causes a visible change, with the solution becoming yellow at high acid concentrations (3 M) in both solvent systems. Analysis of the spectral and kinetic changes for the two systems yields $pK_a$ values of $(S_1)_{DCM} = 5.1$ and $pK_a(S_1)_{MeOH:H2O} = 4$. Furthermore, NMR experiments have shown that protonation occurs at the carbonyl oxygen atom.

TX is well known for its efficient intersystem crossing (ISC) to a give the low energy triplet excited state which is an effective sensitiser of singlet oxygen. The formation and quenching of the triplet state of the protonated species have been investigated using a flash-photolysis experiment.

## 5.2 Materials and equipment

Thioxanthone (Sigma Aldrich 98%) was purified via recrystallization in ethanol. Both dichloromethane (DCM) and a 1:1 methanol:water (MeOH:$H_2O$) mixture were used as solvents. Various aliquots of TFA (16 M) were added to DCM to give a final range of acid concentrations between $1.9 \times 10^{-6}$ M and 13 M. To confirm the total protonation, 0.5 mg of solid TX was dissolved in 5 mL of TFA (13 M) and 5 mL of $H_2SO_4$ (16.5 M, 97%). The acid used in the MeOH:$H_2O$ (1:1) mixture was $H_2SO_4$ (16.5 M, 97%) to give a final range between $7.2 \times 10^{-5}$ M and 13.5 M. In both systems, the TX concentration remains constant across all of the experiments ($7.5 \times 10^{-5}$ M).

# Results and discussion

## 5.3 NMR studies

NMR spectroscopy was employed to monitor and clarify the TX protonation site (Figure 92).

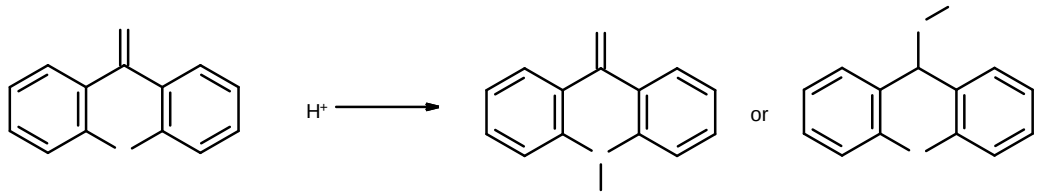


***Figure 92*** *Alternative protonation sites for thioxanthone.*

The {$^1$H}$^{13}$C carbon spectra of TX and its protonation product show the expected seven signals (Figure 77) which were assigned using HMBC and HMQC experiments (Figure 93).

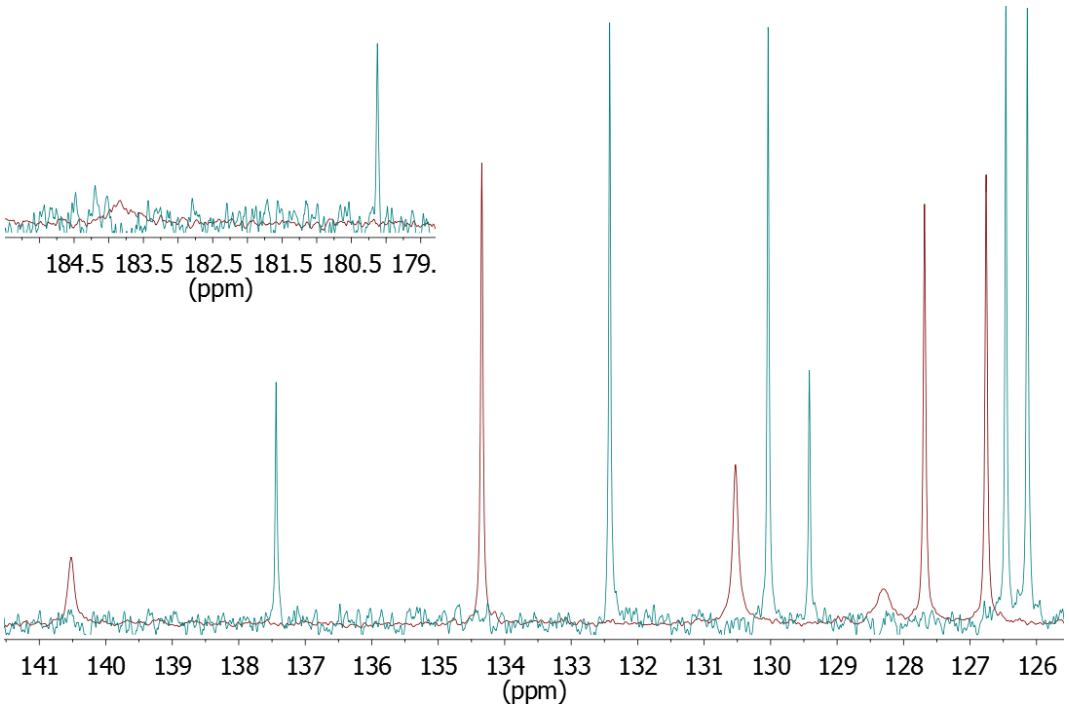


***Figure 93*** *C-NMR of protonated TX in $CDCl_3$ and TFA (red) and not protonated (blue).*

| Carbon | Not protonated TX (ppm) | Protonated TX (ppm) |
|---|---|---|
| 1 | 180.13 | 183.83 |
| 2 | 137.45 | 140.52 |
| 3 | 130.04 | 130.50 |
| 4 | 132.42 | 134.35 |
| 5 | 126.47 | 127.69 |
| 6 | 126.14 | 126.77 |
| 7 | 129.42 | 128.30 |

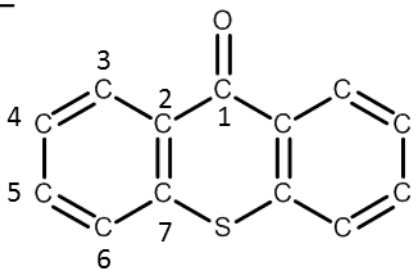


***Figure 94*** *TX carbon chemical shifts for neutral and protonated species.*

From the carbon NMR spectra, it is clear that the signal for the carbonyl group (carbon 1) is still present upon protonation but shifted by +3.70 ppm upon protonation, yet the signal is

significantly broader compared with the neutral compound. The broadening is attributed to the equilibrium between TX and $TXH^+$ in solution. The dynamic $TX + H^+ \leftrightarrow TXH^+$ is faster than the time resolution of the NMR response, results in a broadening of the peak and attenuation of the signal. Protonation at the sulphur atom would be expected to induce relatively large shifts in the C7 peak, however, comparing the difference of protonated C7 chemical shift with the ring C5 and C4 peaks the values are similar. It was possible to conclude that the C7, C5 and C6 shifts are simply small structural changes to the aromatic ring induced by protonation of at the C=O group, creating a distorted aromatic system, Figure 95.

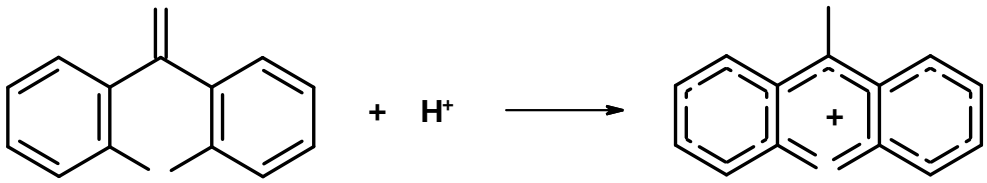


***Figure 95*** *Carbonyl protonation creates a positive charge that has resonance not only in one aromatic ring but, thanks to the presence of the sulphur atom, all of the systems became aromatic.*

## 5.4 UV–visible spectroscopy

When 8.4 M of TFA or $H_2SO_4$ was added to a TX solution, formation of the protonated product can be easily seen by the naked eye due to the yellow coloration caused by the extended conjugation of $TXH^+$ (Figure 96). Such reaction can be easily reverse by diluting the solution with the appropriate solvent.

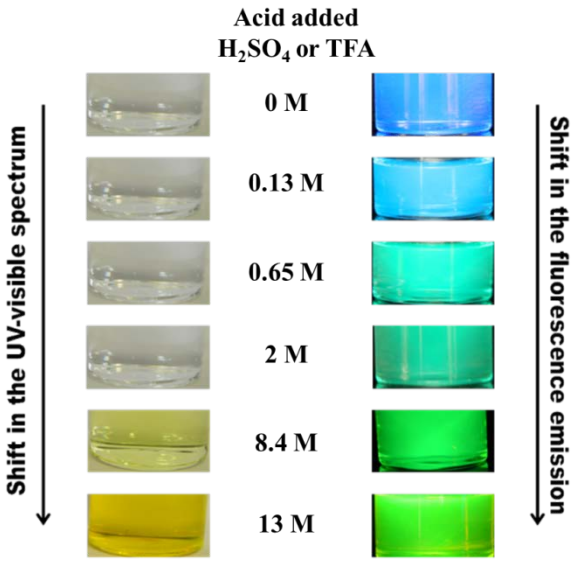


***Figure 96*** *Visual change of TX solution at a different acid concentration; on the left, TX and fluorescence emission under 365 nm irradiation.*

The absorption spectra were taken at a TX concentration of $7.5 \times 10^{-5}$ M in DCM and MeOH:water solutions with increasing concentrations of acid. The UV-visible spectra showed the appearance of two new peaks at 445 nm and 470 nm which occurs in both cases. In MeOH:$H_2O$ the absorption peaks remain unchanged in a wide concentration range, from 0 M to 3.2 M of $H_2SO_4$ where the absorbance of TX slowly decreases. At 8.4 M of added acid, the two new peaks at 445 nm and 470 nm rise in intensity and at 13 M of $H_2SO_4$ the peak at 380 nm disappears completely, and the two new peaks remain (Figure 97), indicating the complete formation of $TXH^+$. In a good approximation the $pK_a$ can extrapolated from the concentration of $H_2SO_4$ added when the two additional peaks appears, which is a sign of the formation of the protonated specie in solution. At a concentration of 8.4 M, when the two additional peaks appears, correspond to a $pK_a$ of $TXH^+$ in MeOH:$H_2O$/ $H_2SO_4$ of -0.9.

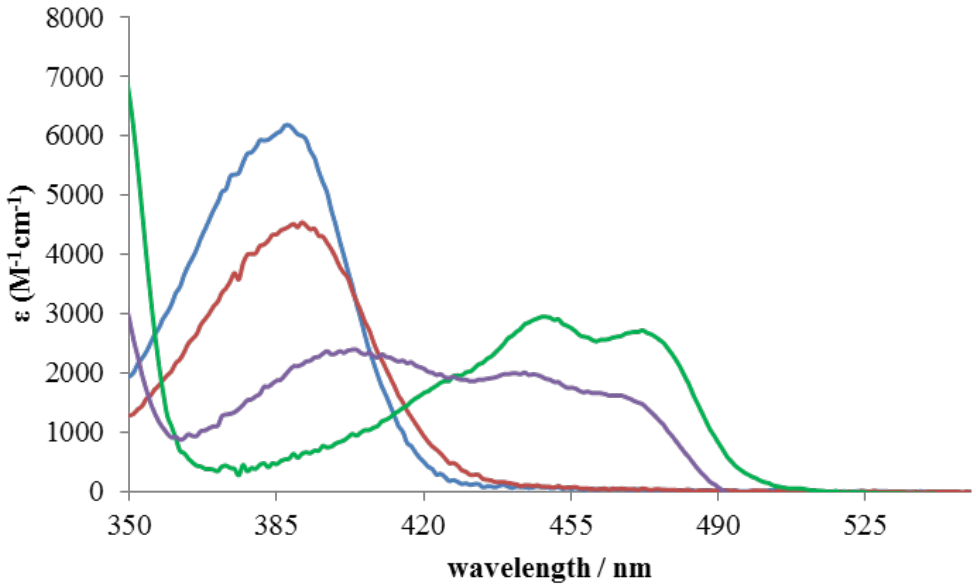


***Figure 97*** *Absorption spectra of TX in the presence of different $H_2SO_4$ concentrations. TX in: MeOH:water (blue), $H_2SO_4$ 5 M (red) , $H_2SO_4$ 8.4 M (purple), $H_2SO_4$ 13.5 M (green).*

The TFA solution showed a similar change in colour and, consequently, a shift in the main absorption peak from one peak $\lambda_{max.dep}$ = 380 nm to three $\lambda_{max.pro}$ = 400, 445, 470 nm. Despite the similarity to the spectra observed with MeOH:$H_2O$/ $H_2SO_4$ system, it was not possible to completely remove the peak at 400 nm (Figure 98). The three absorption peaks are remained even at the highest TFA concentrations (13 M). This behaviour can be explained by considering the $pK_a$ of TFA (-0.3). Because the $pK_a$ of TFA lower compared to that observed for $TXH^+$ pKa (-0.9), TFA acid ability id too week to enable the complete protonation of TX.

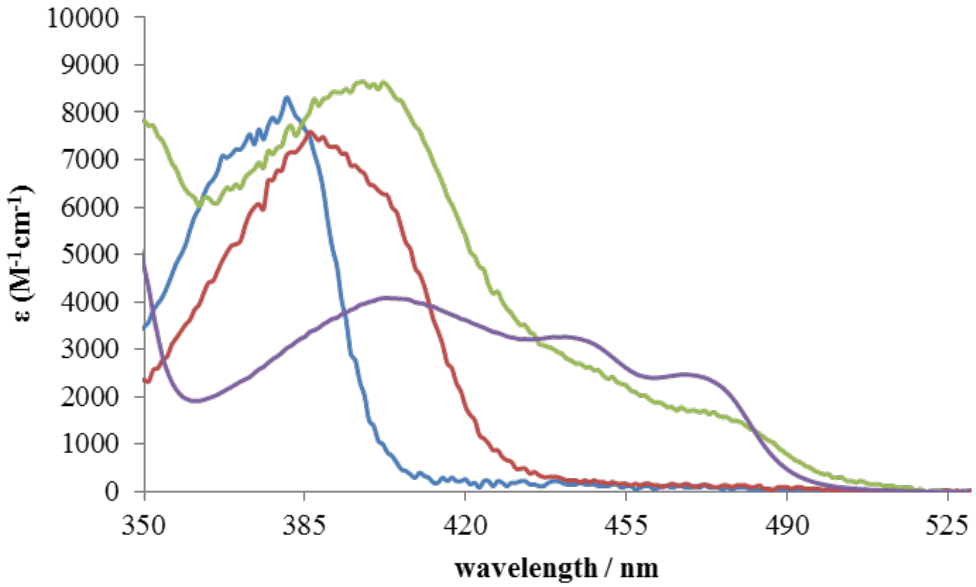


***Figure 98*** *Absorption spectra of TX in the presence of different TFA concentrations. Spectra in: DCM (blue), TFA 0.2 M (red), TFA 5.2 M (green), TFA 13 M (purple).*

Despite the different behaviour, via plotting the absorption of TX at the highest concentration of TFA (13 M) and $H_2SO_4$ (8.5 M), the two spectra show a good overlap indicating that the ground state, in the two cases, is affected in the same way (Figure 99).

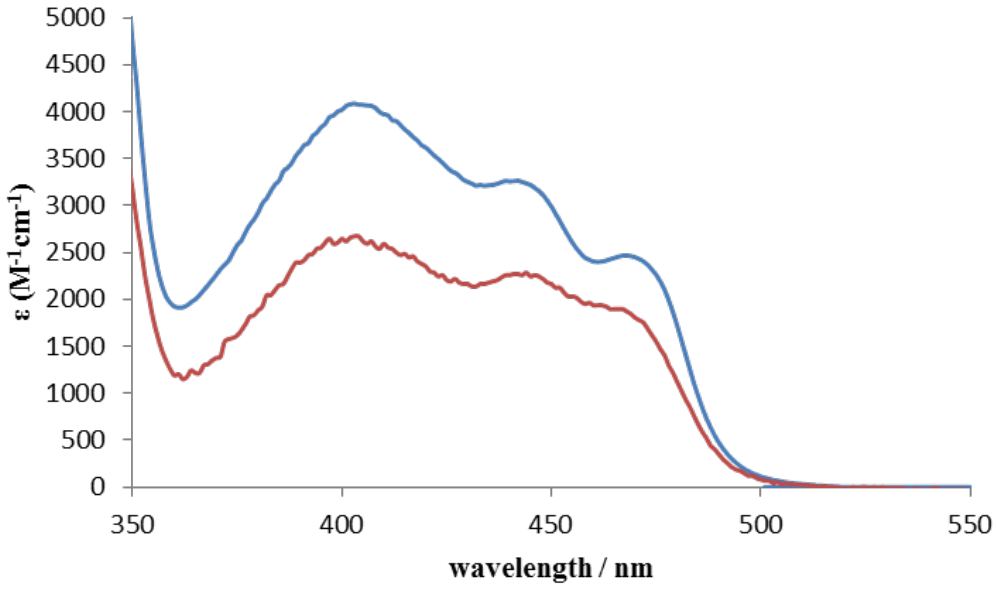


***Figure 99*** *Absorption spectra of TX in DCM/TFA (13 M) (blue), MeOH:water/$H_2SO_4$ (8.5 M) (red).*

## 5.6 Fluorescence emission, excitation, and lifetime measurements

The formation of $TXH^+$ influences the fluorescence emission and lifetime in both systems studied. All solutions were excited at 380 nm, where $TXH^+$ has a minimum absorption and TX a maximum in absorption.

The fluorescence emission of TX in MeOH:water solution showed a broad, intense peak at $\lambda_{em}$ 435 nm. The addition of $7.2 \times 10^{-5}$ M acid causes a decrease in the intensity of emission intensity at 435 nm and the appearance of a shoulder at 500 nm, the latter peak increasing in intensity at higher acid concentrations (Figure 100). This behaviour can be interpreted by assigning the emission peak at 500 nm to the protonated species $TXH^+$*.

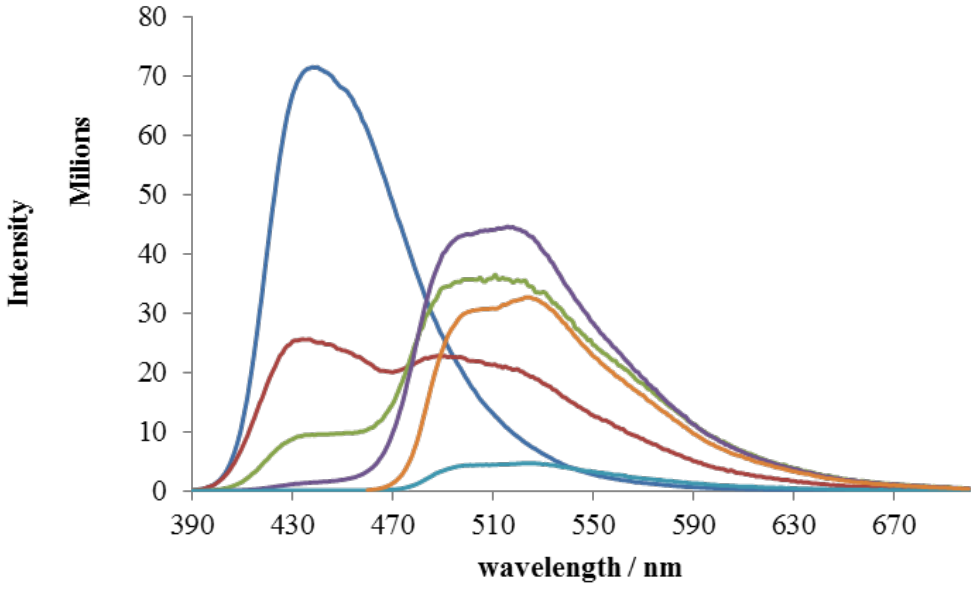


***Figure 100*** *Fluorescence emission of TX at different acid concentrations, $\lambda_{exc}$ 380 nm. Spectra in: MeOH:water (blue), $H_2SO_4$ 9 $\times 10^{-5}$ M (red), $H_2SO_4$ 5.8 $\times 10^{-4}$ M (green), $H_2SO_4$ 1.4 M (purple), $H_2SO_4$ 13.5 M (light blue), $H_2SO_4$ 13.5 M $\lambda_{exc}$ 450 nm (orange)*

At $7.2*10^{-5}$ M the absorption spectrum is identified as TX (Figure 81), with no evidence of $TXH^+$: from the calculated $pK_a$ the concentration of $TXH^+$ in solution is calculated to be less than $6.7*10^{-9}$ M and should yield a minimal change in the fluorescence spectrum. The appearance of such intense emission at 500 nm cannot, therefore, can't be due to the presence of the protonated species formed in solution. Instead, it must stem from a second process, and an additional route of formation of $TXH^+$ needs to be considered.

It is well known that the main electronic transition, between ground and excited state, in carbonyl compounds, is the nπ -> ππ* of the C=O group[77,79,80]. The TX* excited electronic state has obviously a different electron density. The electron density will be located in particular the O which will result more electronegative. Such behaviour will giving a higher basicity to TX and greater capability of O to be protonated in the excited state. It is plausible that after excitation, TX* is quenched by $H^+$ forming $TXH^+$* which emits at 500 nm.

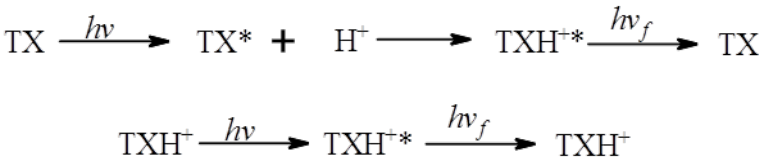

Further evidence for this hypothesis can be found by examining the excitation spectra at different acid concentrations. These spectra, recorded using emission wavelengths of 430 nm and 550 nm for the final solution, showed a significant overlap with the absorption spectra of TX (Figure 101). However, even for the emission assigned to the protonated species $TXH^+$ the excitation spectrum also matches that of the unprotonated form. The only possibility is that the $TXH^+$* arises due to quenching of the excited state of TX, TX*, by the acid.

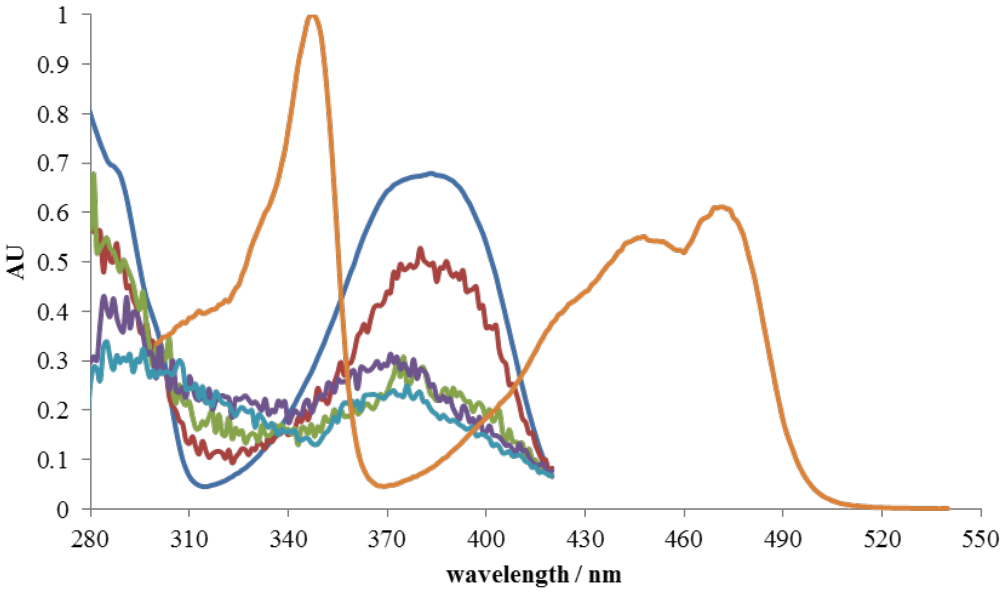


***Figure 101*** *Fluorescence excitation of TX at different acid concentrations, $\lambda_{exc}$ 430 nm. Spectra in: MeOH:water (blue), $H_2SO_4$ 3.6 M (red), $H_2SO_4$ 5 M (green), $H_2SO_4$ 8.4 M (purple), $H_2SO_4$ 13.5 M (light blue), $H_2SO_4$ 13.5 M $\lambda_{exc}$ 550 nm (orange).*

In a good approximation the $pK_a$ can extrapolated from the concentration of $H_2SO_4$ added when the emission at 500 nm appears, which is a sign of the formation of the protonated specie in solution. At a concentration of 9 $10^{-5}$ M, when the shift occurs, correspond to a $pK_a$ of $TXH^+$ in MeOH:$H_2O$/ $H_2SO_4$ of 4.

The quenching rate have be found $k_q$= 3.36*$10^9$ $dm^3mol^{-1}s^{-1}$, i.e. the diffusion limit. In DCM TX shows an maximum emission at 410 nm.

When a low concentration of TFA ($10^{-6}$ M) is added this peak shifts to 430 nm, the same wavelength observed for TX in protic solvents. The TFA acting, in this case, to affect the solvent polarity and hence causing a change in the vibronic overlap between $S_1$ and $S_2$ as occurs for protic solvents. Further increasing the acid concentration (2*$10^{-6}$ M), causes the 410 nm peak to disappear, and the 430 nm peak shows an increased intensity (Figure 102).

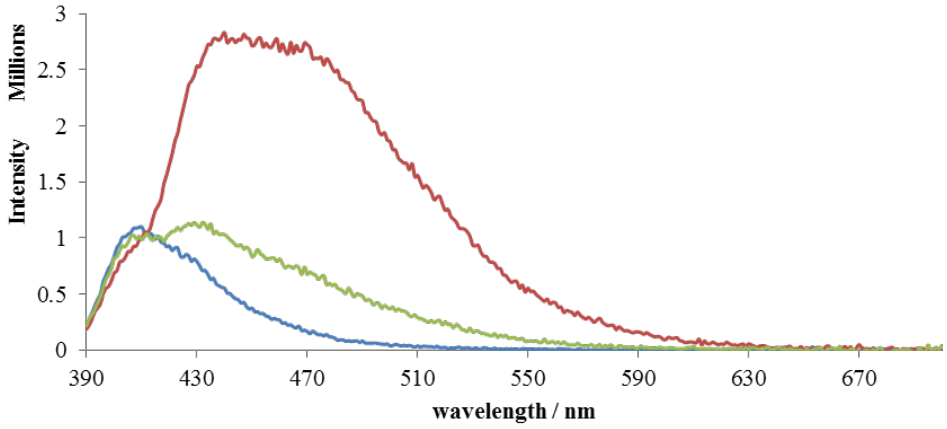


***Figure 102*** *Fluorescence emission of TX at different acid concentrations, $\lambda_{exc}$ 380 nm. Spectra in: DCM (blue), TFA 3.26 $\times 10^{-6}$ M (green), TFA 1.3 $\times 10^{-4}$ M (red).*

However, adding further amounts of TFA to the solution (2.08*$10^{-5}$ M) leads to the appearance of a new emission peak at 500 nm to (Figure 103). By assuming the $pK_a(S_0)$ calculated for MeOH:$H_2O$/$H_2SO_4$ is the same in the DCM solution, it is possible to estimate

the [$TXH^+$] present in this solution is 5 x$10^{-10}$ M. Once again such low concentration would not have such intense fluorescence emission. Therefore the emission observed is due to the protonated species formed in solution but again due to the quenching of TX* with $H^+$.

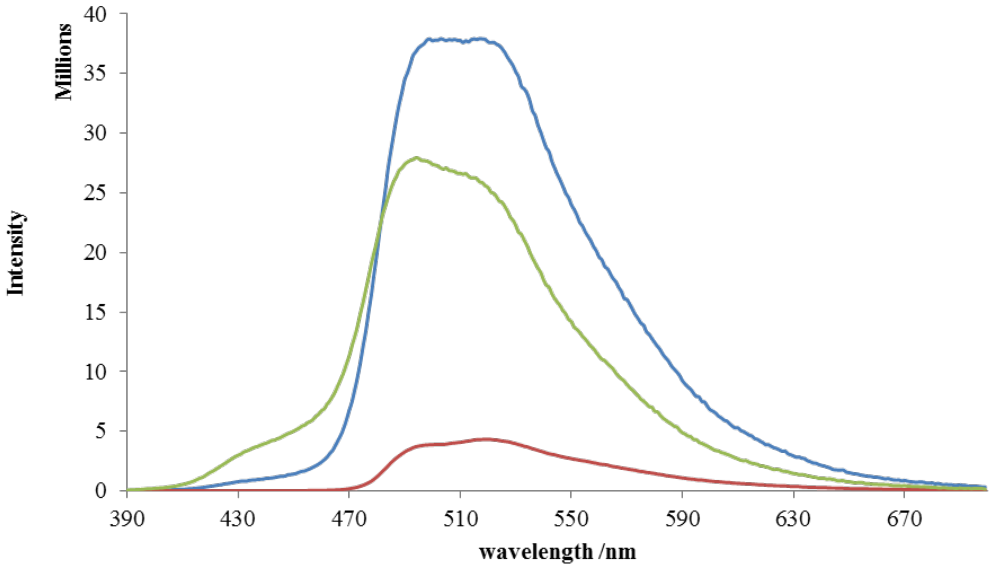


***Figure 103*** *Fluorescence emission of TX at different acid concentrations, $\lambda_{exc}$ 380 nm. Spectra in: TFA 0.13 M (green), TFA 0.5 M (blue), TFA 13 M (red).*

Like for the MeOH:$H_2O$/$H_2SO_4$ solutions even in the DCM/TFA system, the excitation spectra show an overlap with the absorption. Remarkably when absorption shift has been observed the excitation spectra shift too (Figure 104).

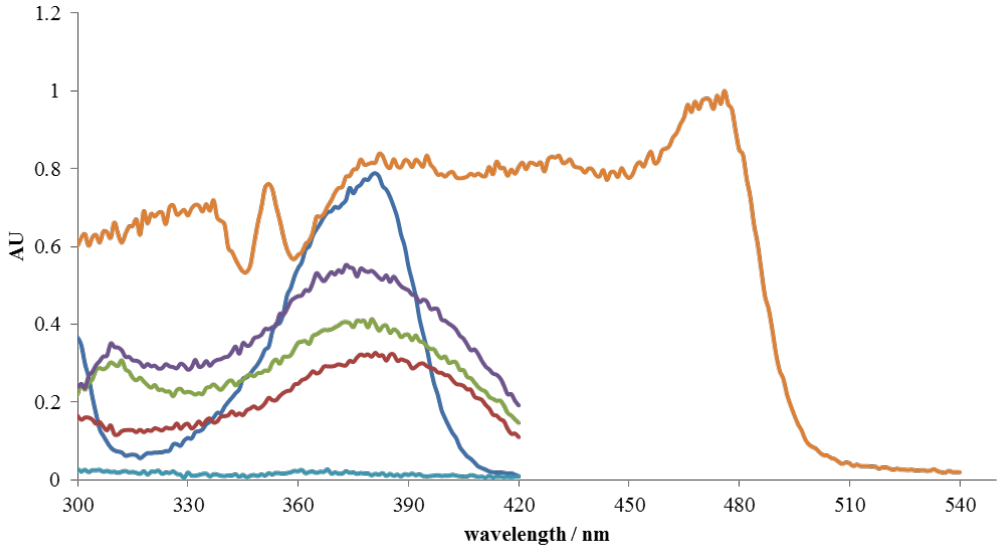


***Figure 104*** *Fluorescence excitation of TX at different acid concentrations, $\lambda_{exc}$ 430 nm. Spectra in: DCM (blue), TFA 1.95 M (red), TFA 3.26 M (green), TFA 5.21 M (purple), TFA 13.5 M (light blue), TFA 13.5 M $\lambda_{exc}$ 550 nm (orange).*

Despite the double shift, it is possible to extrapolate the quenching rate constant which gives $10^{10}$ $dm^3mol^{-1}s^{-1}$ and $pK_a(S_1)_{DCM}$ = 5.1. The difference between the two $pK_a(S_1)$ founded is tentatively ascribed to the differences in acid strengths and the ability of $TX^*$ to induce protonation in the two solvent systems. It needs to be noticed that fluorescence emission from the two solvent/acid systems considered is very similar, indicating the formation of the same protonated species in solution (Figure 105).

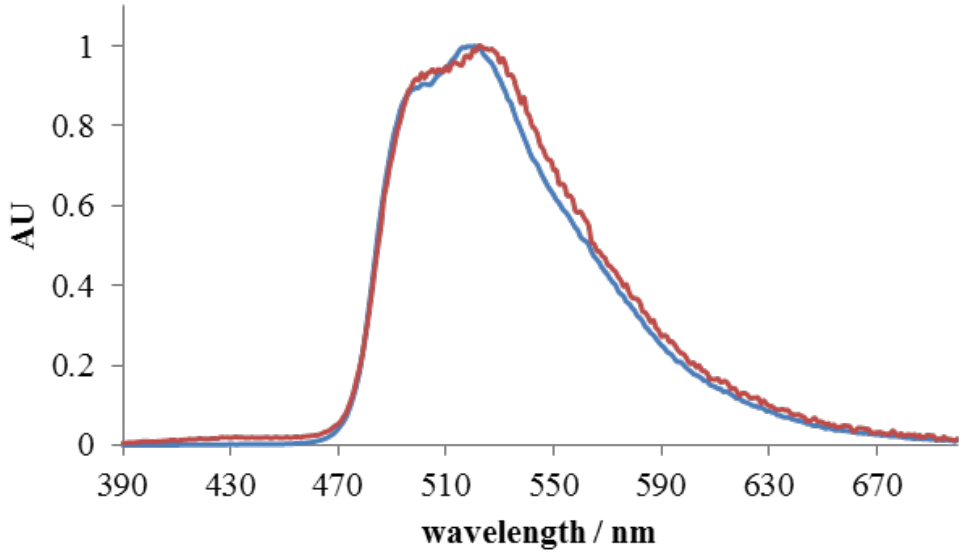


***Figure 105*** *Overlap of normalised fluorescence emission of TX in DCM/TFA (13 M) and MeOH:$H_2O$/$H_2SO_4$ (13.5 M).*

Fluorescence lifetime measurements of TX at 420 nm in MeOH:$H_2O$ and DCM are very different due to the solvent polarities and proximity effect ($\tau_{DCM}$=1.2 ns, $\tau_{MeOH:H2O}$=7.4 ns). However, upon acidification of both these solvents and monitoring at 550 nm, where only the protonated species emits, a monoexponential decay is observed, with a lifetime of $\tau$ = 18 ns.

The lifetime in MeOH:$H_2O$/$H_2SO_4$ was recorded at three different wavelengths 420 nm, 450 nm, and 550 nm.

The first wavelength corresponds to TX emission, the latter to $TXH^+$ emission. At 450 nm is an intermediate point which can clarify the hypothesis formulated previously on the second route of emission.

A double exponential equation was used to fit all the decays collected: $I(t)=A_1\ e^{-1/\tau\tau1} + A_2\ e^{-1/\tau\tau2}$. Most of the decay at 420 nm and 450 nm present two different components. At early

times the decay displays a fast component which disappears after 745 ps, after this point the decay display a long-lived tail (Figure 106).

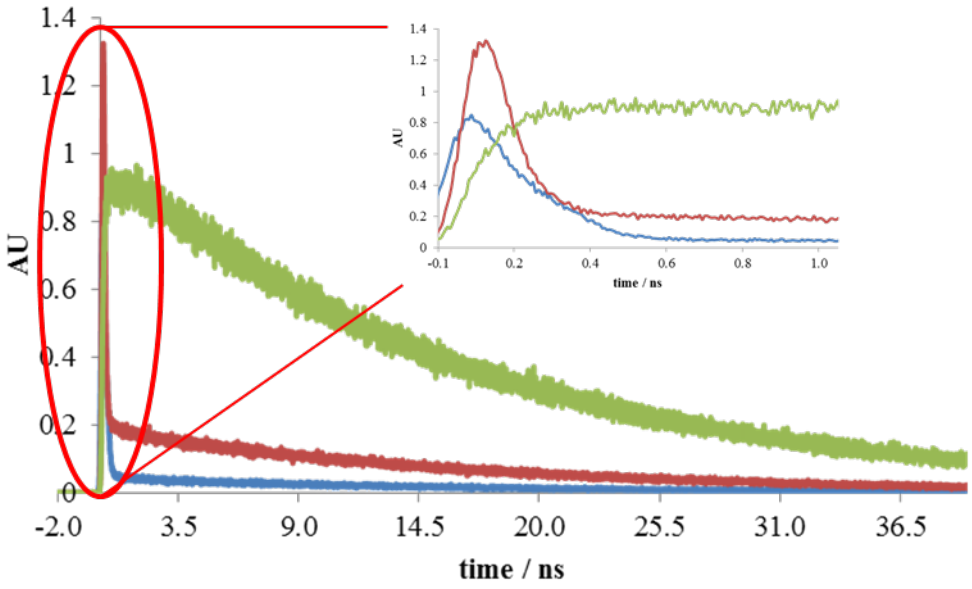


***Figure 106*** *Fluorescence lifetime decay of TX in MeOH:$H_2O$/$H_2SO_4$ (0.33 M) recorded at 420 nm (blue), 450 nm (red), 550 nm (green)*

The fast component is consistent with one species with a shorting of a lifetime of less than 0.20 ns and can be detected up to 0.7 M acid (Table 26). On the other hand, the tail can be fitted in a biexponential decay. The first specie is longer lived (circa 16 ns) and a short one (circa 1 ns). The coexistence of three different species can be explained by considering the second way of $TXH^{+*}$ formation suggested earlier. The faster components at early times can be referred to TX decay, and quick interactions with $H^+$, forming the long-lived protonated species which, appears after 7.45 x $10^{-10}$ s. The absence of the faster component in the early times at 550 nm is due to the TX weaker fluorescence emission of TX at this wavelength. This hypothesis is supported by the slow rise of the decay until $5*10^{-10}$ s and followed by a mono-exponential decay (16 ns).

| Concentration $H_2SO_4$ (M) | 420 nm | | 450 nm | | 550 nm |
|---|---|---|---|---|---|
| **0** | 7.4 ns (100%) | | 7.4 ns (100%) | | 7.4 ns (100%) |
| **0.34** | 0.19 ns (100%) | 16 ns (91%) 1.6 ns (9%) | 0.19 ns (100%) | 16 ns (94%) 0.4 ns (9%) | 16 ns (100%) |
| **0.67** | 0.15 ns (100%) | 16 ns (93%) 1.2 ns (9%) | 0.16 ns (100%) | 16 ns (94%) 1.09 ns (6%) | 16 ns (100%) |
| **1.01** | 17 ns (92%) 0.82 ns (8%) | | 17 ns (95%) 1.3 ns (5%) | | 17 ns (100%) |
| **1.68** | 17 ns (100%) | | 17 ns (96%) 1.09 ns (5%) | | 17 ns (100%) |
| **5.04** | 18 ns (100%) | | 18 ns (98%) 2.09 ns (2%) | | 18 ns (100%) |
| **13.5** | 18 ns (100%) | | 18 ns (100%) | | 18 ns (100%) |

***Table 26*** *MeOH:$H_2O$/$H_2SO_4$ lifetime*

The addition of acid leads to an increase in the fluorescence yield and lifetime of the protonated species at all wavelengths and a consequent decrease of [TX] which completely disappears at 8.4 M. This behaviour is consistent with the shift of absorption spectra, at 8.4 M $TXH^{+*}$ is the main species in solution with a final lifetime of 18 ns.

Thioxanthone presents the same behaviour in DCM and TFA as shown in Table 27.

| Concentration TFA (M) | 420 nm | | 450 nm | | 550 nm |
|---|---|---|---|---|---|
| **0** | 1.2 ns (100%) | | 1.2 ns (100%) | | 1.2 ns (100%) |
| **0.13** | 0.17 ns (100%) | 12 ns (80%) 7.1 ns (20%) | 0.16 ns (100%) | 12 ns (82%) 6.4 ns (18%) | 12 ns (100%) |
| **0.26** | 0.15 ns (100%) | 15 ns (85%) 6.5 ns (15%) | 0.13 ns (100%) | 15 ns (83%) 1.09 ns (6%) | 15 ns (100%) |
| **0.39** | 16 ns (85%) 5.15 ns (15%) | | 16 ns (82%) 5.1 ns (18%) | | 16 ns (100%) |
| **0.65** | 17 ns (100%) | | 17 ns (96%) 3.3 ns (5%) | | 17 ns (100%) |
| **5.21** | 18 ns (100%) | | 18 ns (98%) 1.2 ns (2%) | | 18 ns (100%) |
| **13.5** | 18 ns (100%) | | 18 ns (98%) 1 ns (2%) | | 18 ns (100%) |

***Table 27*** *DCM/TFA lifetime*

The presence of a faster component at 450 nm even in neat TFA can be amenable to the lower $pK_a$ of the acid and the partial shift of absorption spectra. Despite the high acid concentration, in solution will be in the presence of TX and the protonation specie. The coexistence of both species affect the fluorescence emission and consequently their lifetime.

## 5.7Triplet–Triplet absorption and lifetime

Another characteristic of TX is the ability to undergo intersystem crossing to form the triplet excited state, $^3$TX, and this species has been extensively investigated in chapter one because of its long lifetime in solution and solvent dependent T-T absorption spectra.

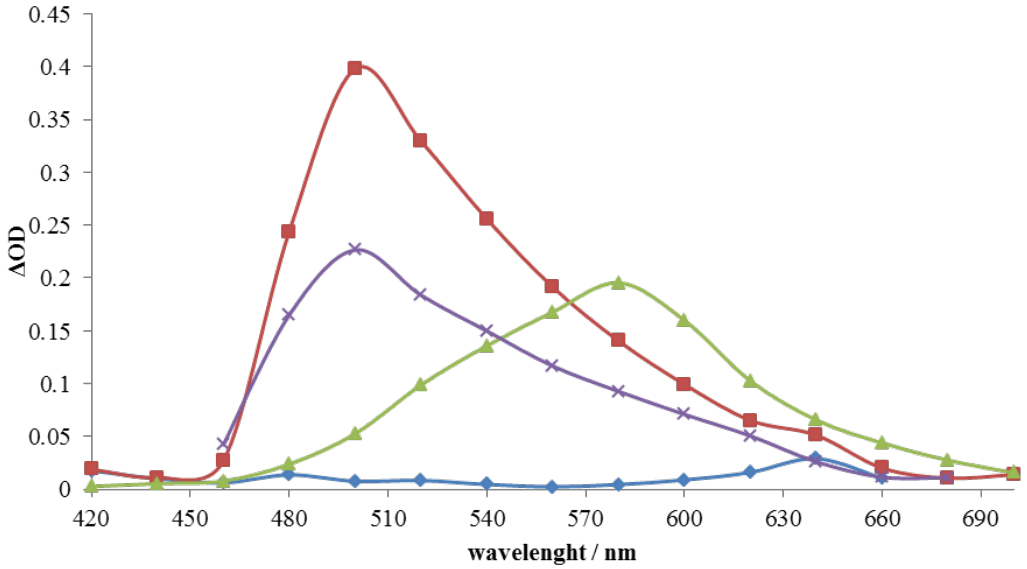


***Figure 107*** *Triplet–triplet absorption spectra of TX: DCM (blue), MeOH:$H_2O$ (green), $H_2SO_4$ (13 M) (purple), TFA (13 M) (red).*

The triplet absorption spectrum of TX in four different solvents is shown in Figure 107. In the absence of any acid, TX display a definite difference in DCM and MeOH:$H_2O$ not only regarding intensity but also$\lambda_{max}$, $\lambda_{T\text{-}TMeOH:H2O}$= 580 nm and $\lambda_{T\text{-}TDCM}$= 640 nm. This confirms the well-established solvatochromic behaviour of this excited state of the ketone. When TX is dissolved in $H_2SO_4$ or TFA, the spectra recorded have a common maximum peak at 500 nm, indicative of the TXH+ triplet-triplet absorption in a polar solvent environment.

Upon acidification, the transient absorption at 500 nm quickly increases in intensity in both systems (Figure 107). Furthermore, the transient decay shows the opposite behaviour compared to absorption, in fact, the neutral species has a lifetime of 8.24 μs in DCM and 6.6 μs in methanol:water and decreases to 5.3 μs when TFA or $H_2SO_4$ were added (Figure 109).

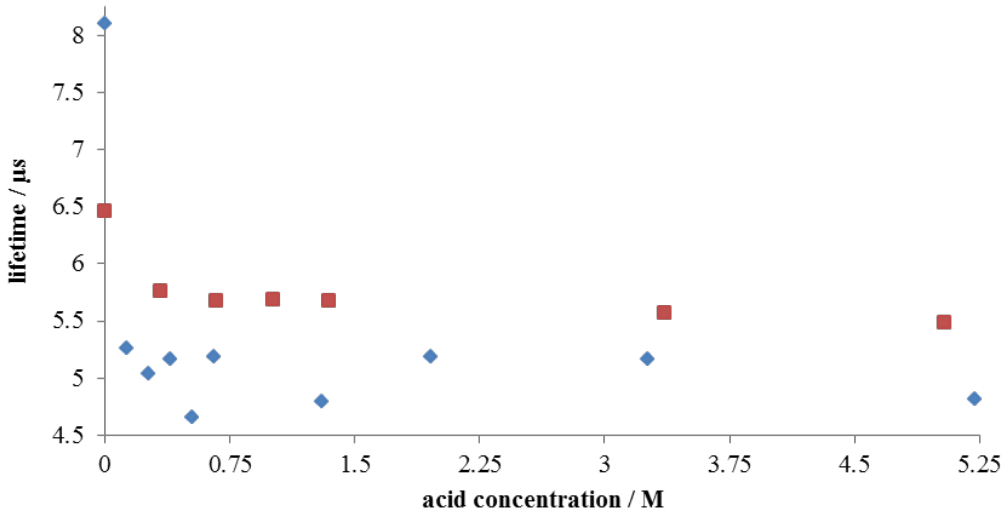


***Figure 108*** *TX transient lifetime at 500 nm upon acidification ( TFA: blue, $H_2SO_4$: red)*

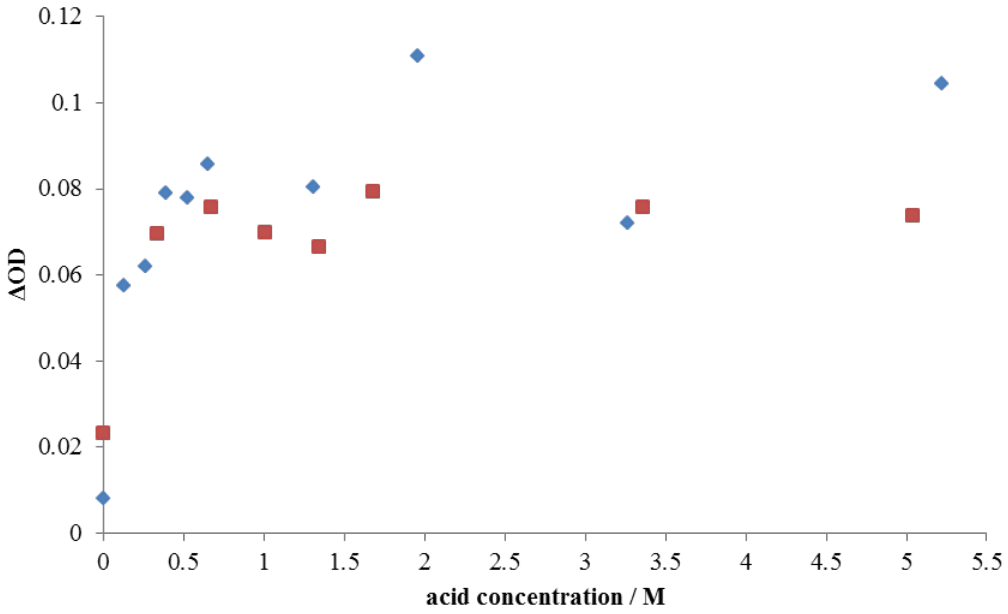


***Figure 109*** *Increasing of optical density of TX transient upon acidification ( TFA: blue, $H_2SO_4$: red)*

From the data collected it is evident that the triplet excited state is influenced by the presence of acid in solution and the T-T transition shifts to 500 nm. As for the fluorescence emission, the $^{3}TXH^{+}$ transient absorption increases in intensity even when the presence of the ground state protonated species concentration in the solution is negligible. Such behaviour shows how $TXH^{+*}$, formed by $TX^{*}/H^{+}$ quenching, can populate $^{3}TXH^{+}$ via ISC and make the absorption transition possible.

## 5.8 Singlet Oxygen generation

A characteristic property of TX is the efficient quenching of the triplet excited state by $^{3}O_2$ leading to the production of singlet oxygen. The phosphoresce lifetime of $^{1}O_2$ has been recorded only in DCM/TFA in which singlet oxygen has a strong intensity and long a lifetime.

In such systems, the lifetime remained constant (95 μs) for an extensive of acid concentrations range (0–1.5 M). At higher acid concentrations (1.9- 5 M), the $^{1}O_2$ phosphorescence lifetime became shorter but still detectable. The $^{1}O_2$ phosphorescence lifetime was detectable even a high concentration of TFA (5 M, 57.3 μs) (Figure 110).

The decrease in the lifetime decay is due to the solvent dependence of the radiation decay of $^{1}O_2$. ,

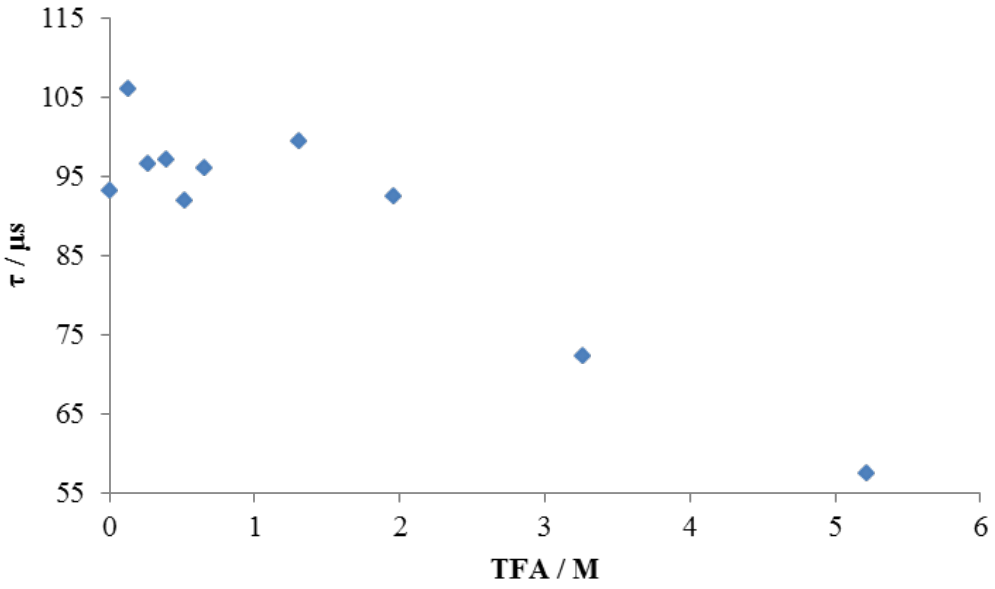


***Figure 110*** *Singlet oxygen lifetimes of TX in DCM at different TFA concentrations.*

## 5.9 Conclusions

It is possible study and defines the change of a different aspect of thioxanthone photophysical property in acid media. The two solvent systems studied, DCM/TFA and MeOH:$H_2O$/$H_2SO_4$, gave an overview of the different behaviour of this compound in protic and aprotic solvents. The absorption spectra display a shift from 380 nm to the visible region (470 nm) upon acidification of both solvents by strong acids. The shift observed with TFA was only partial with the coexistence of the two TX species in solution. This scenario is due to the lower pKa of TFA compared to the protonated species it was not observed a formation of $TXH^+$ in solution. In MeOH:$H_2O$/$H_2SO_4$ a shift was observed in the fluorescence emission from 430 nm to 500 nm, and this occurs even at low concentrations of acid where there is a low concentration of the ground state protonated species in solution. It is shown that the observed $TXH^+$ emission arises from quenching of the highly basic TX*. This has been

confirmed by lifetime measurements with the appearance of a long-lived tail 745 ps even at a lower acid concentration (0.36 M).

This hypothesis is confirmed by pump-probe experiments. The transient absorption of TX in MeOH:$H_2O$/$H_2SO_4$ and DCM/TFA shifts from 580 nm and 640 nm respectively to 500 nm at a lower acid concentration (0.36 M). Finally, singlet oxygen phosphorescence decay has been measured across all the concentration range of acid.

# Chapter 6
# Conclusions and future steps

The main goal of this project was the synthesis, characterisation and testing of novel thioxanthone derivatives as a potential new photobleaching agent in laundry detergents. In the three most important chapters of this thesis, enough evidence has been given to prove the full achievement of the project.

The synthesis was aimed to create a library of thioxanthone derivatives with a simple, cheap and highly reproducible route.

Furthermore, the full photophysical characterisation carried out in Chapter 4, proved all derivatives has a similar photophysical behaviour compare to TX as wanted.

The experiments performed in P&G (Chapter 5) were aimed to test a selection of derivatives in a real customer situation. Thioxanthone and its derivatives performed better than the commercial used PBA. Although TX has the best overall performance, the majority of derivatives improve the cleanness of the stains used.

In the last chapter (Chapter 6) focused on the protonation of thioxanthone in two different solvent and the changing of its property upon acidification.

A series a photophysical characterisation should be consider to have a further understanding of the property of the derivatives proposed here.

It is possible have a better idea of the actual solubility by calculation the LogP of the derivatives. The partition coefficient or Log P is a measure of differential solubility of a

compound in a 1-octanol and water. The logarithm of these two values enables compounds to be ranked in terms of hydrophilicity (or hydrophobicity). The quantity in the different phase can be found by recording the absorption spectra.

Another step could be the addition of other laundry component in solution like optical brighteners or bleachers. By slowly complicating the chemical environment it will be possible understand the photophysical property PBA in the consumer situation.

Another useful technique could be the Evanescent Wave Induced Fluorescence Spectroscopy (EWIFS) (for more detail on the setup please view[102–106]). This technique, based on total internal reflection of a laser beam, allow to investigate only the first few hundreds of nm of the surface after the prism. It will be possible reveal how the derivatives behave close to a surface. Furthermore it is possible to modify the surface to mimic the cotton fabric and understand how the derivatives interact with simile-cotton.

All derivatives have been given to P&G which can test further the performance of this novel and promising compounds.

In P&G it will be possible to extend the investigation not only to carotenoids and have a better understanding of the potential of this new type of PBA with other stains.

# Appendix A

In this section it will present the data collected in chapter 5 in a graphic manner.

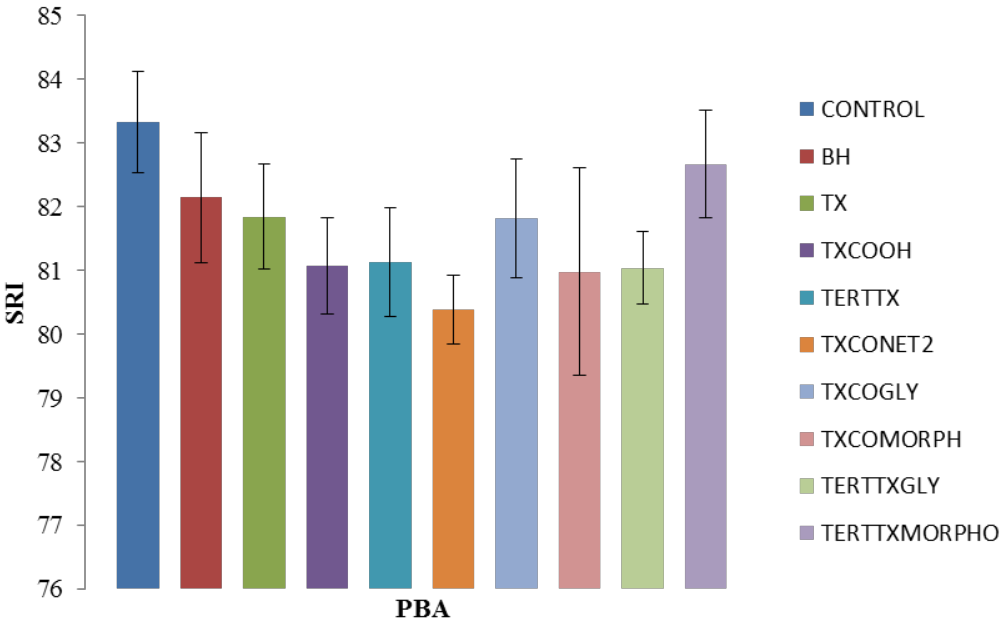


***Figure 111*** *SRI values of baby food with a PBA concentration of 0.5 mg/L without detergent*

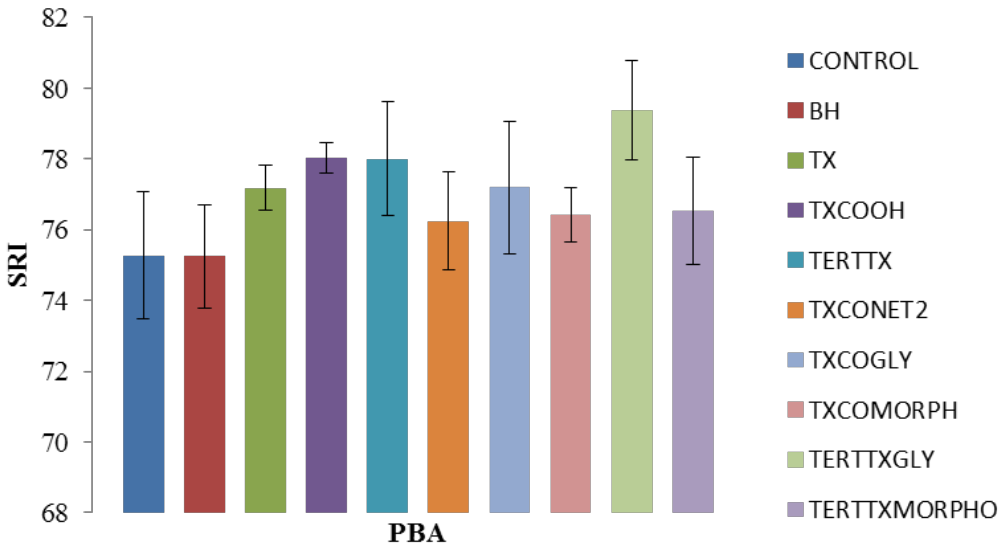


***Figure 112*** *SRI values of bolognese with a PBA concentration of 0.5 mg/L without detergent*

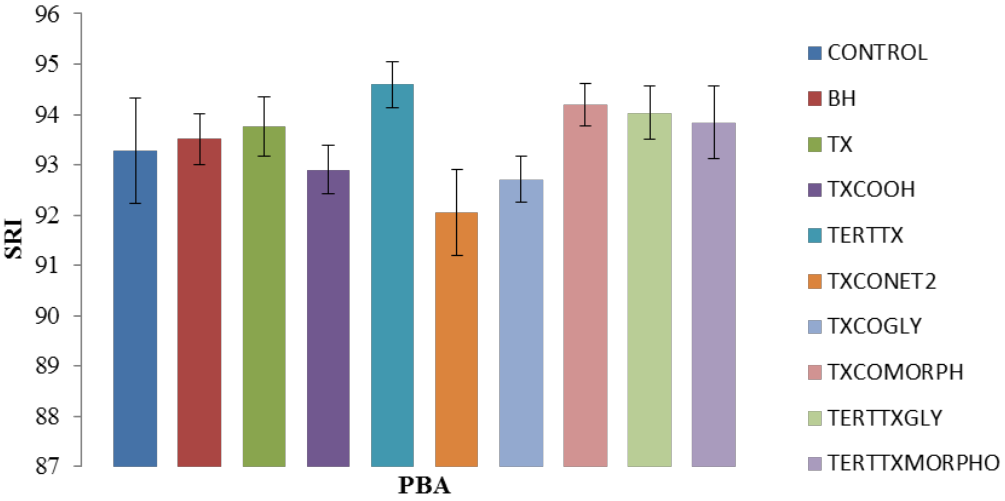


***Figure 113*** *SRI values of hot pepper sauce with a PBA concentration of 0.5 mg/L without detergent*

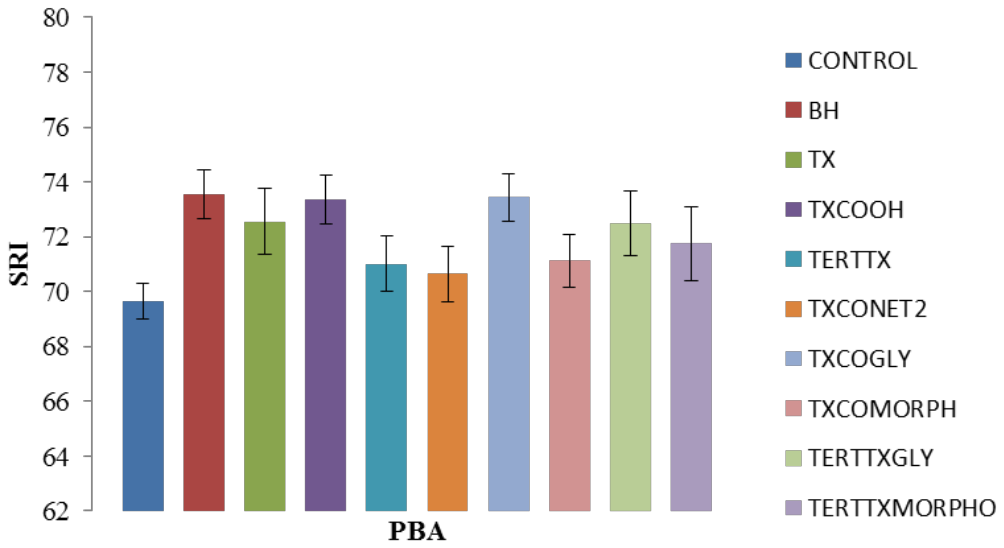


***Figure 114*** *SRI values of ragu with a PBA concentration of 0.5 mg/L without detergent*

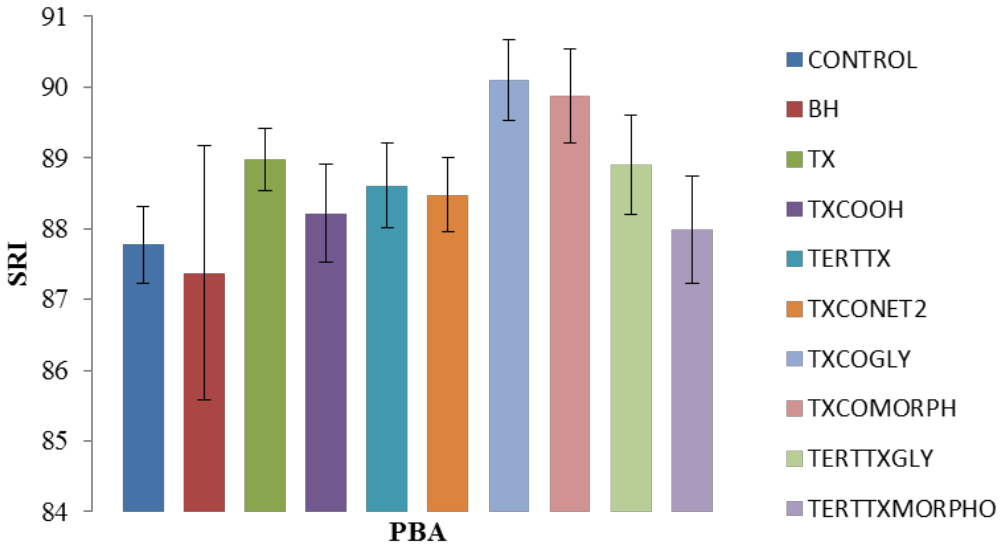


***Figure 115*** *SRI values of sundried tomato with a PBA concentration of 0.5 mg/L without detergent*

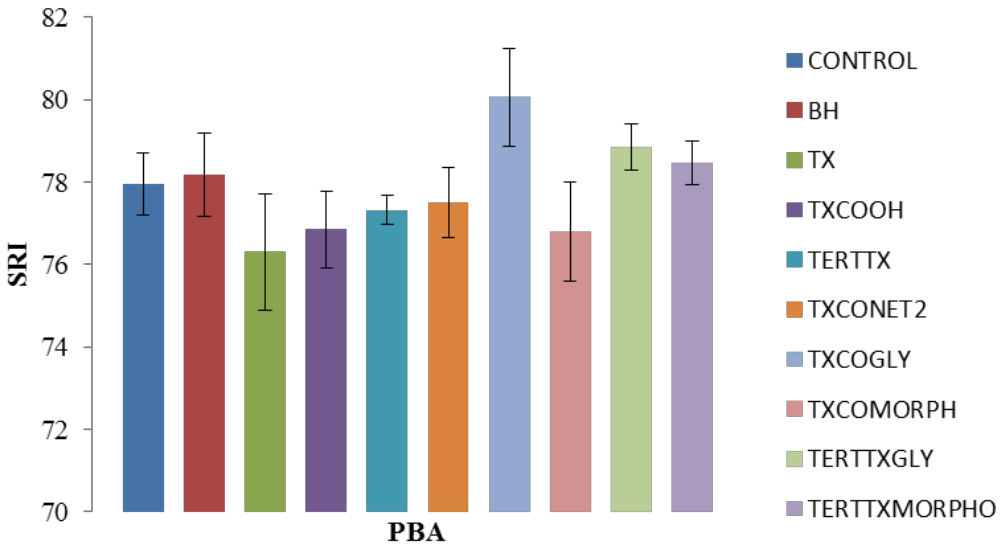


***Figure 116*** *SRI values of tomato puree with a PBA concentration of 0.5 mg/L without detergent*

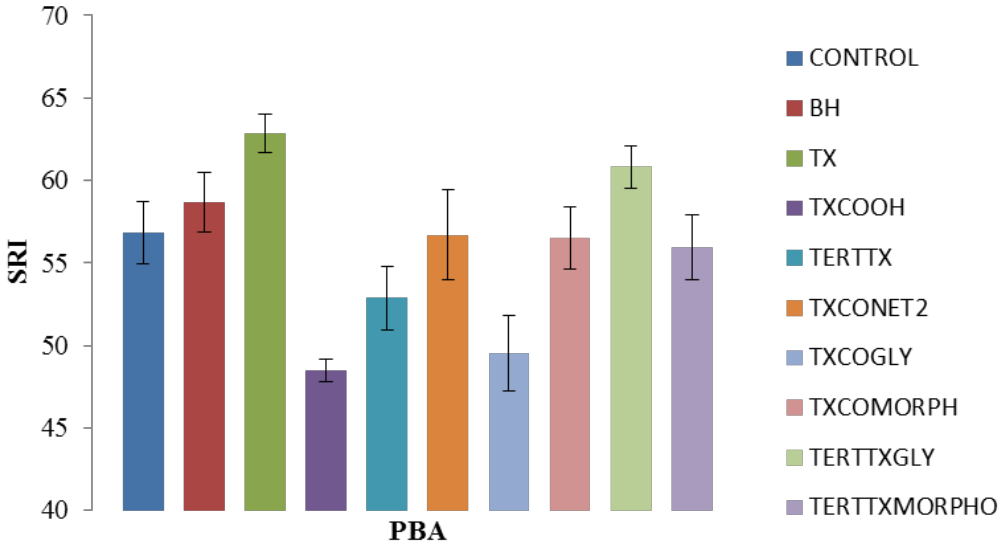


***Figure 117*** *SRI values of vindaloo with a PBA concentration of 0.5 mg/L without detergent*

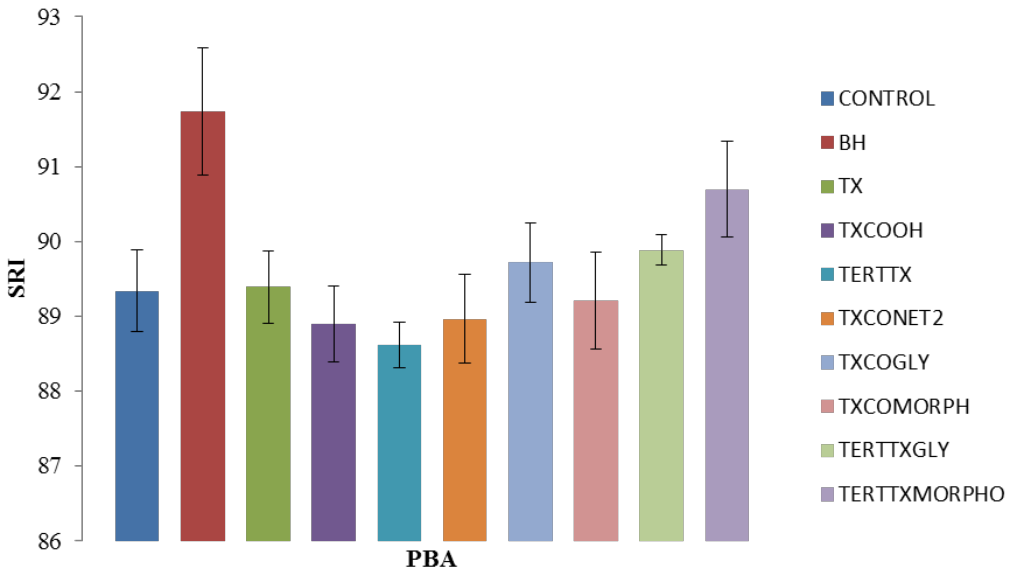


***Figure 118*** *SRI values of baby food with a PBA concentration of 0.5 mg/L with detergent*

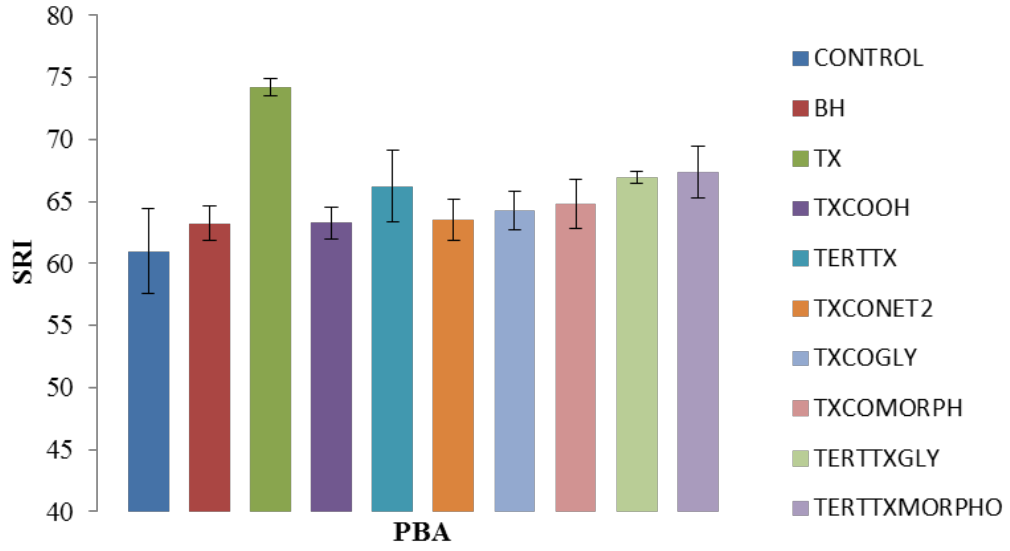


***Figure 119*** *SRI values of paprika with a PBA concentration of 0.5 mg/L without detergent*

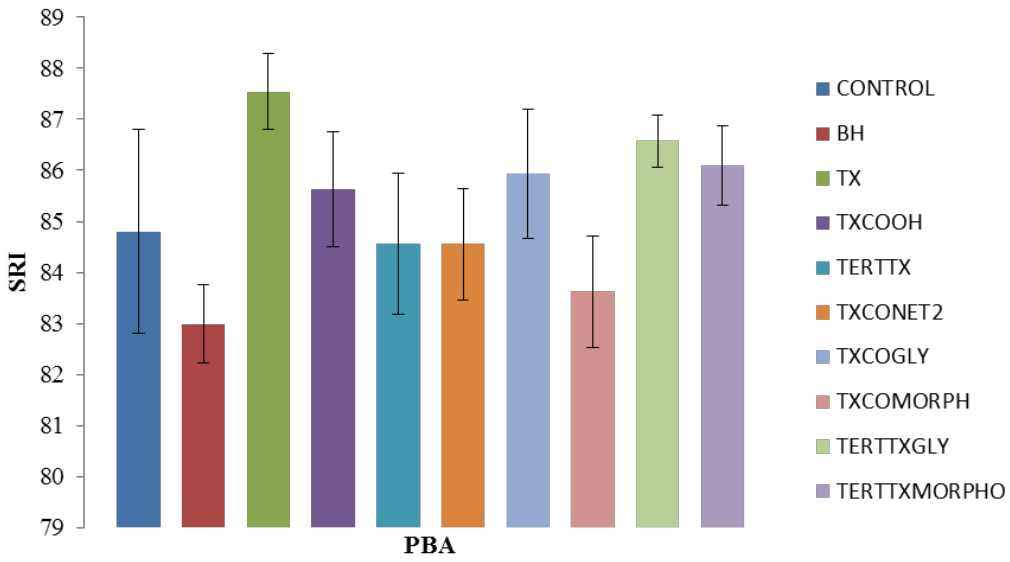


***Figure 120*** *SRI values of bolognese with a PBA concentration of 0.5 mg/L with detergent*

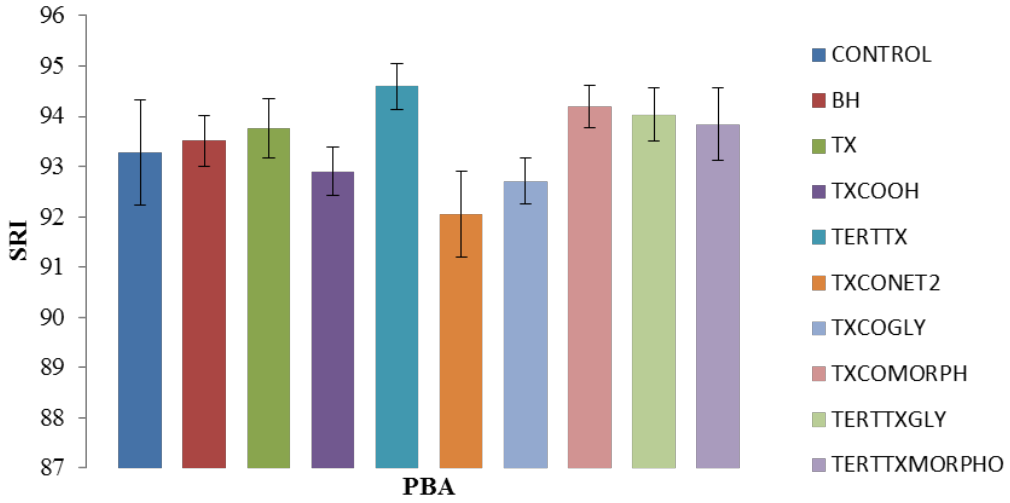


***Figure 121*** *SRI values of hot pepper sauce with a PBA concentration of 0.5 mg/L with detergent*

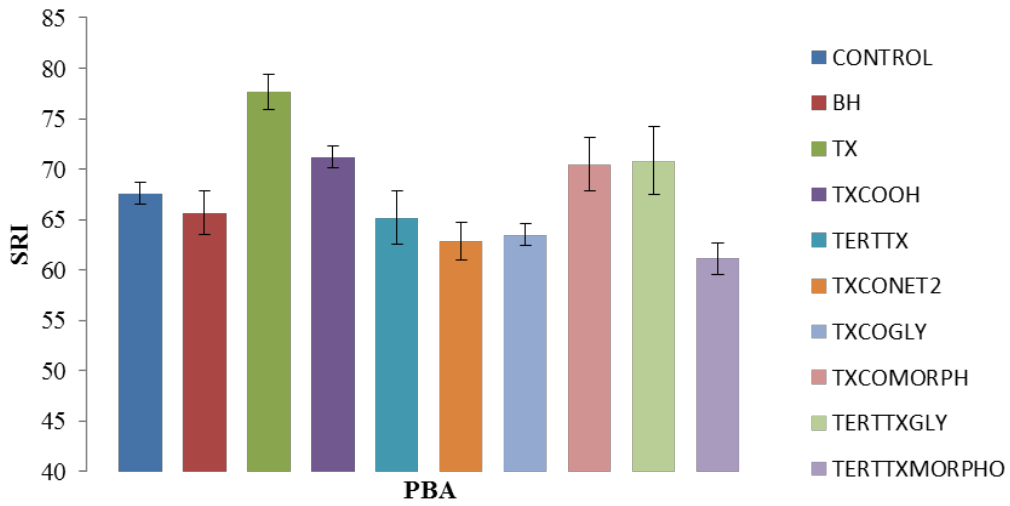


***Figure 122*** *SRI values of paprika with a PBA concentration of 0.5 mg/L with detergent*

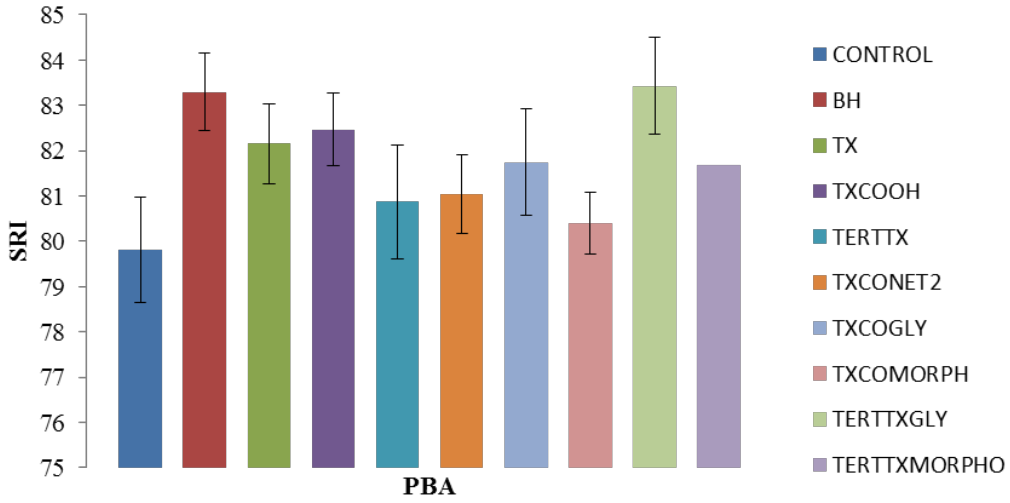


***Figure 123*** *SRI values of ragu with a PBA concentration of 0.5 mg/L with detergent*

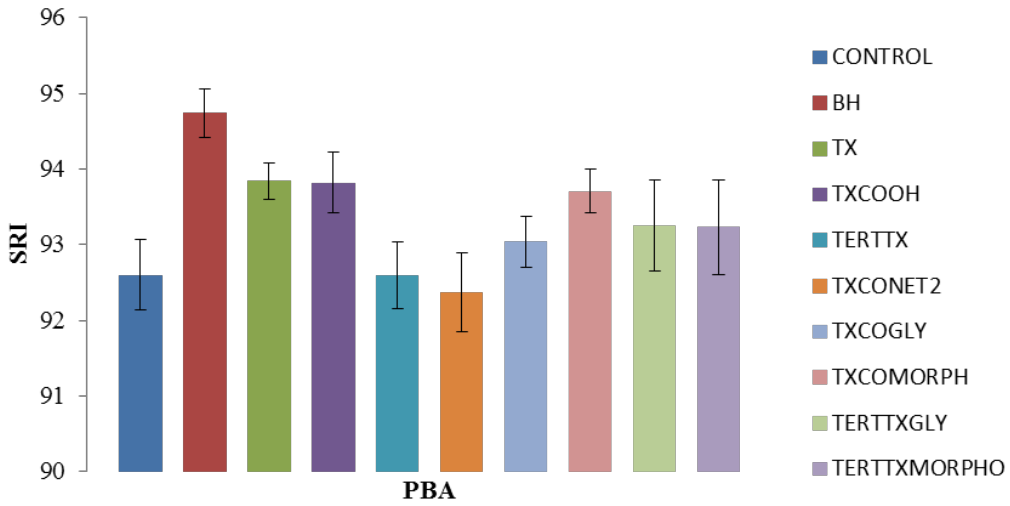


***Figure 124*** *SRI values of sundried tomato with a PBA concentration of 0.5 mg/L with detergent*

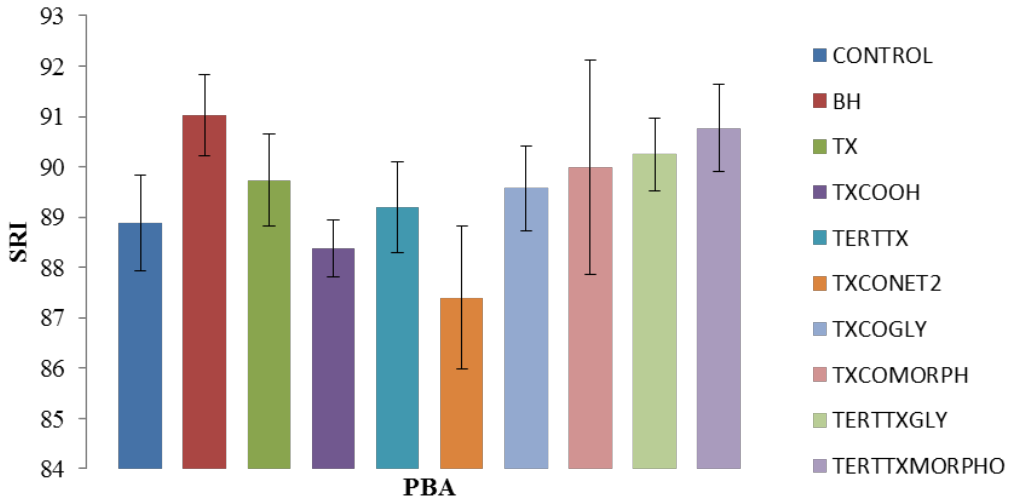


***Figure 125*** *SRI values of tomato puree with a PBA concentration of 0.5 mg/L with detergent*

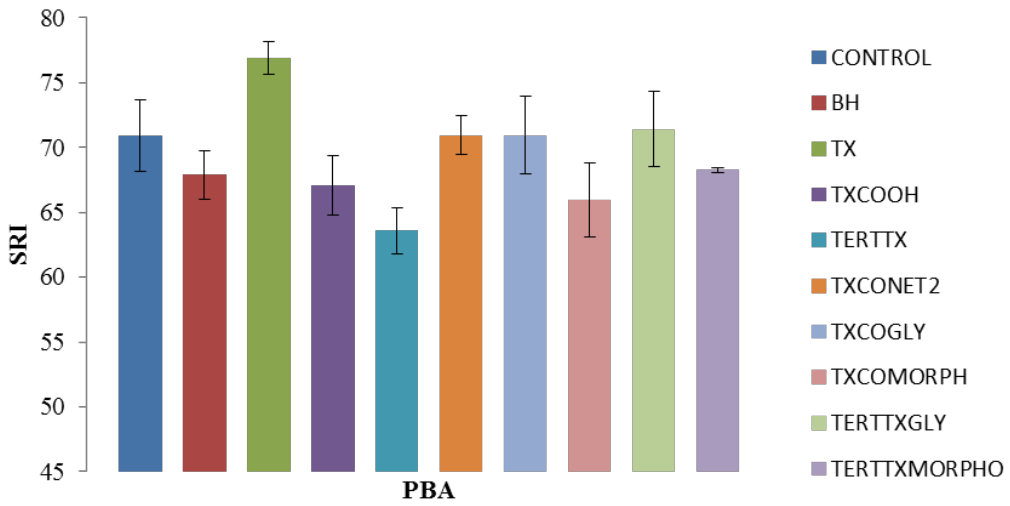


***Figure 126*** *SRI values of vindaloo with a PBA concentration of 0.5 mg/L with detergent*

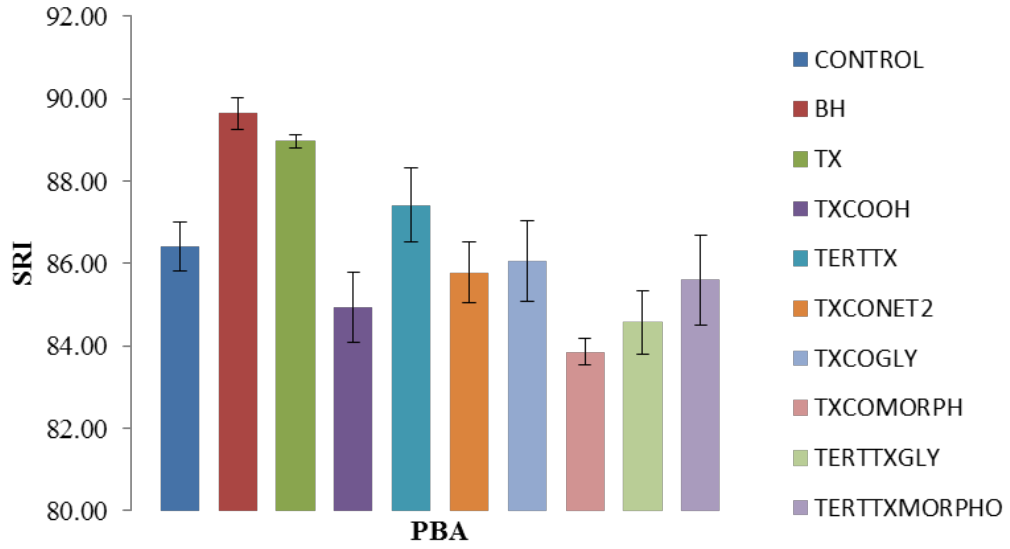


***Figure 127*** *SRI values of baby food with a PBA concentration of 2.5 mg/L with detergent*

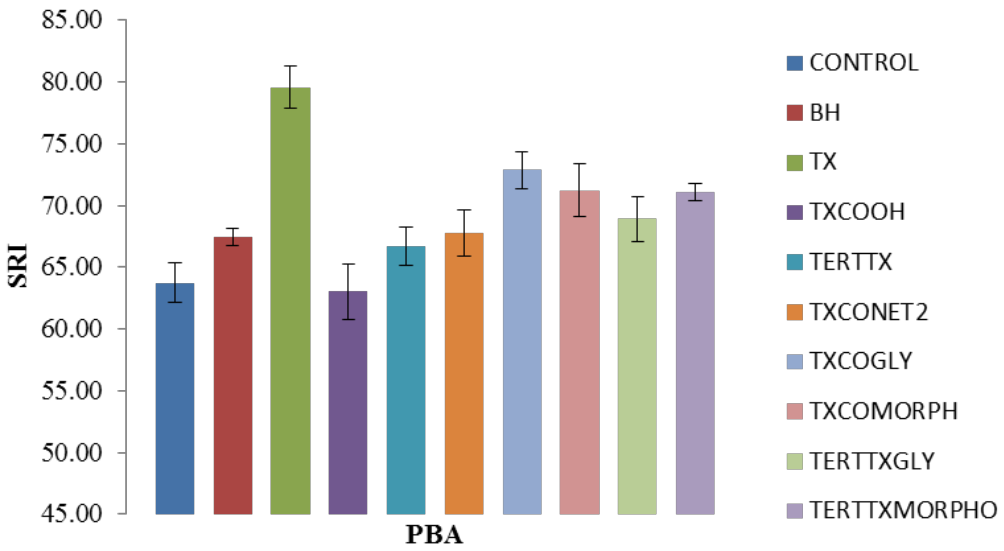


***Figure 128*** *SRI values of bolognese with a PBA concentration of 2.5 mg/L with detergent*

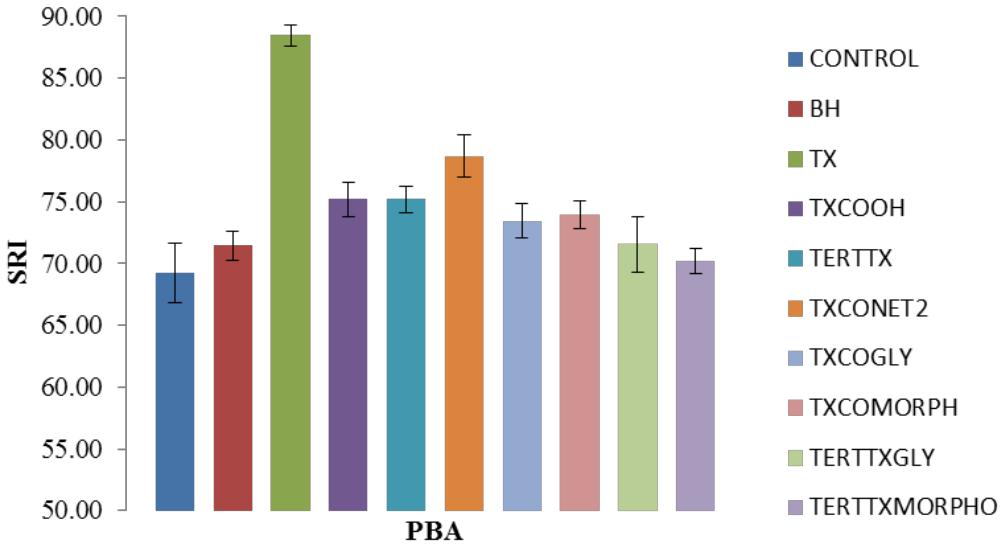


***Figure 129*** *SRI values of hot pepper sauce with a PBA concentration of 2.5 mg/L with detergent*

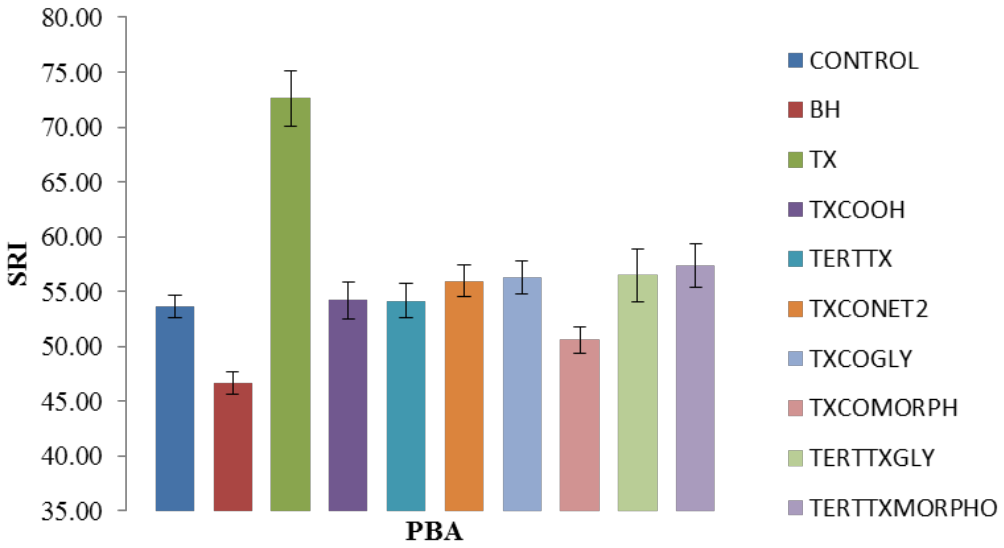


***Figure 130*** *SRI values of paprika with a PBA concentration of 2.5 mg/L with detergent*

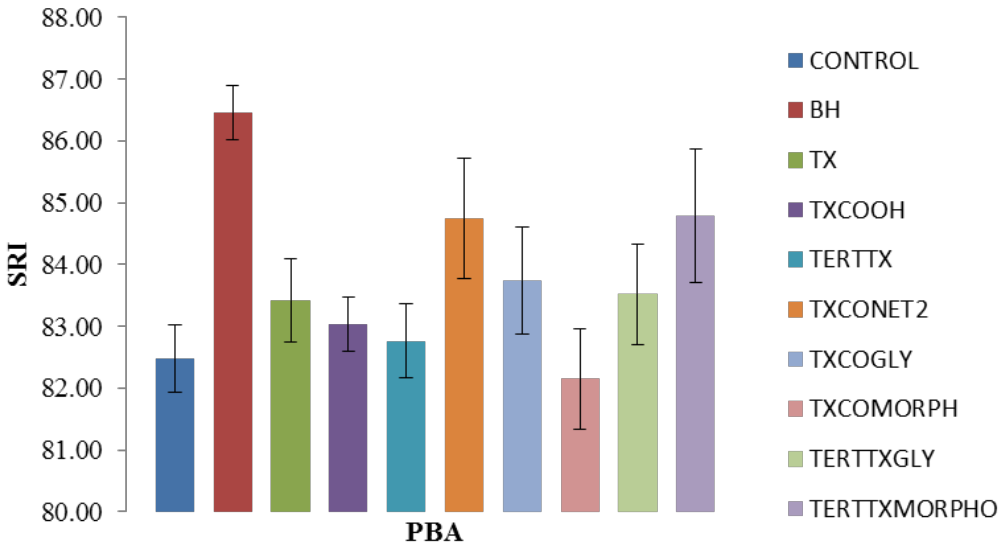


***Figure 131*** *SRI values of ragu with a PBA concentration of 2.5 mg/L with detergent*

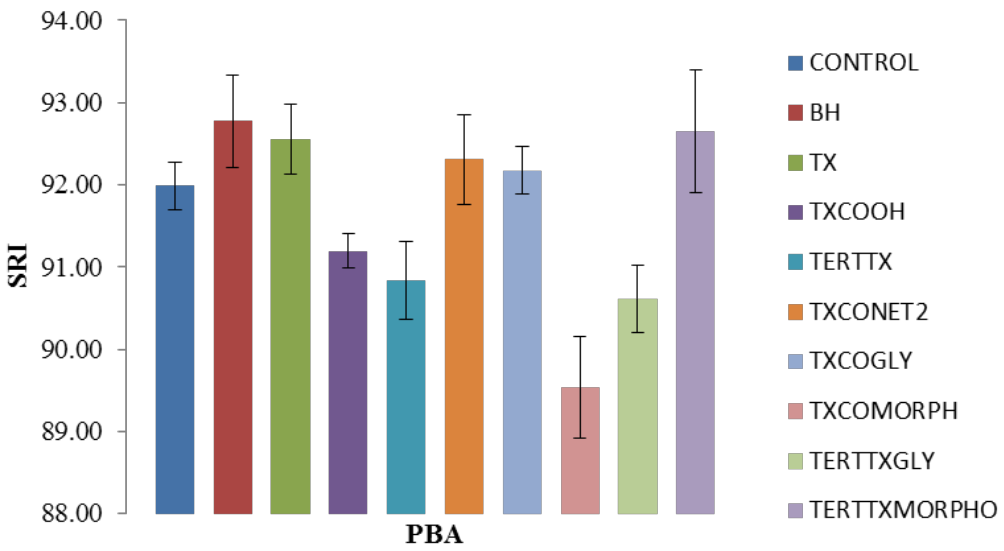


***Figure 132*** *SRI values of sundried tomato with a PBA concentration of 2.5 mg/L with detergent*

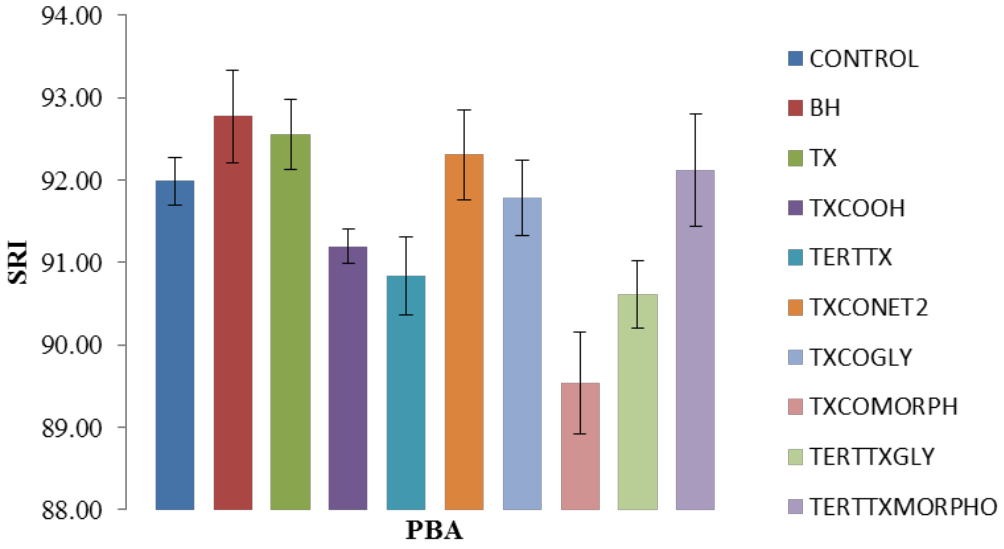


***Figure 133*** *SRI values of tomato puree with a PBA concentration of 2.5 mg/L with detergent*

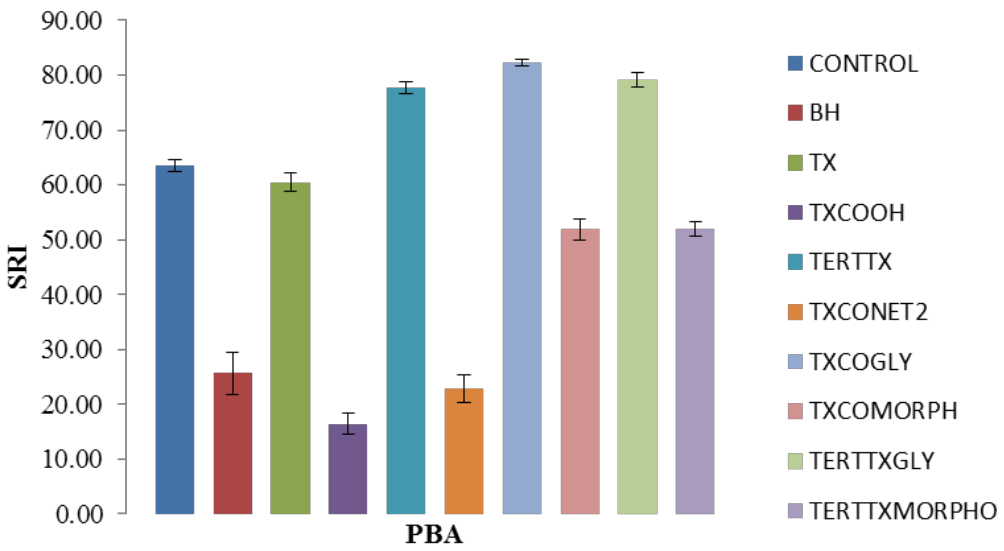


***Figure 134*** *SRI values of vindaloo with a PBA concentration of 2.5 mg/L with detergent*

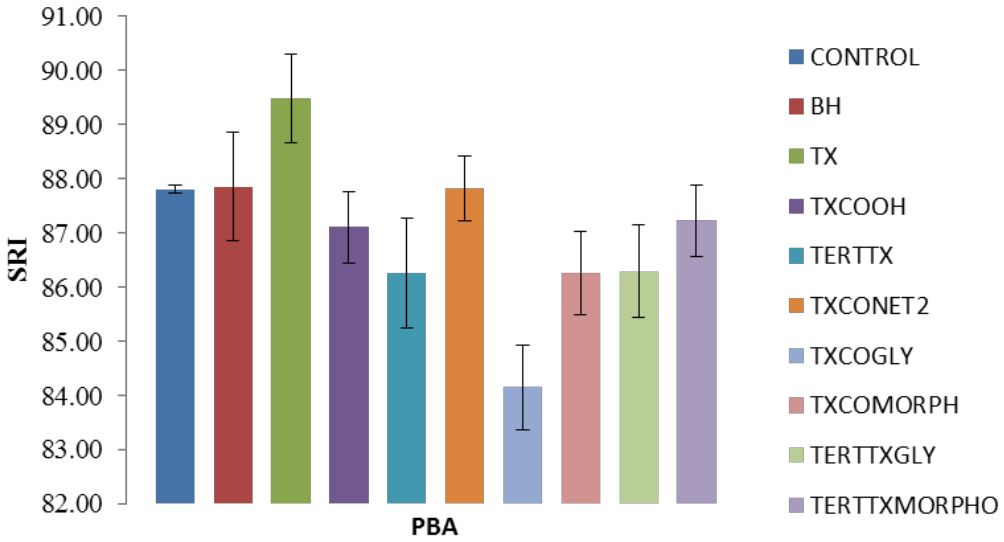


***Figure 135*** *SRI values of baby food with a PBA concentration of 5 mg/L with detergent*

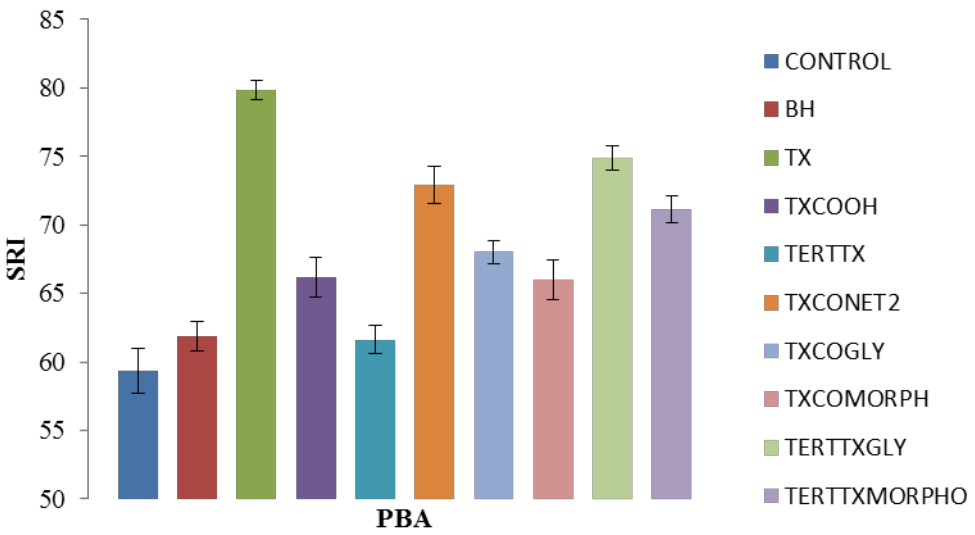


***Figure 136*** *SRI values of bolognese with a PBA concentration of 5 mg/L with detergent*

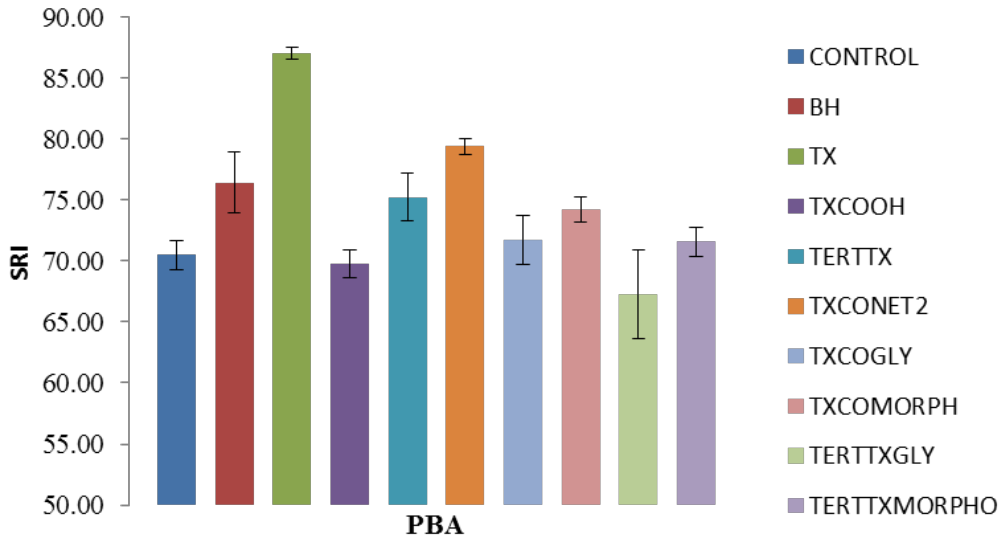


***Figure 137*** *SRI values of hot pepper sauce with a PBA concentration of 5 mg/L with detergent*

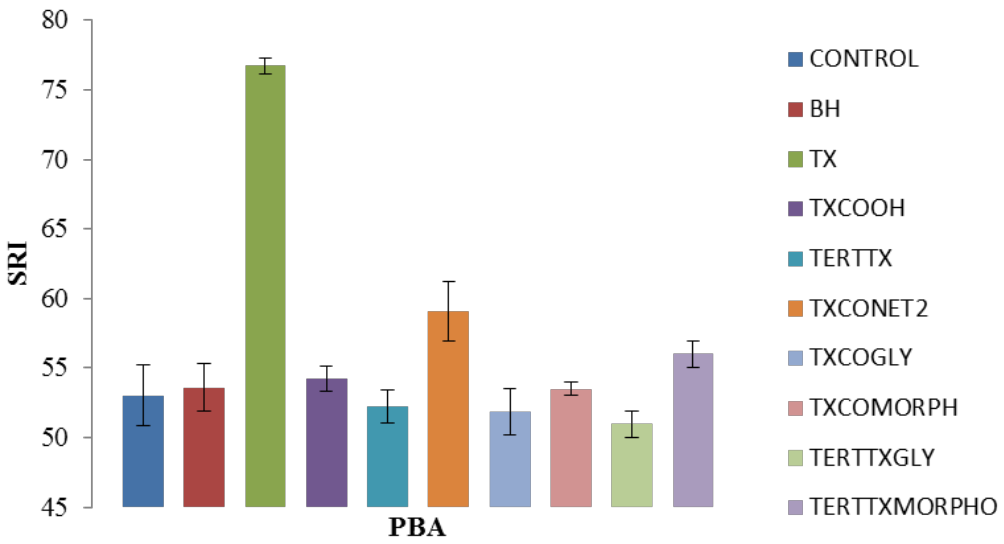


***Figure 138*** *SRI values of paprika with a PBA concentration of 5 mg/L with detergent*

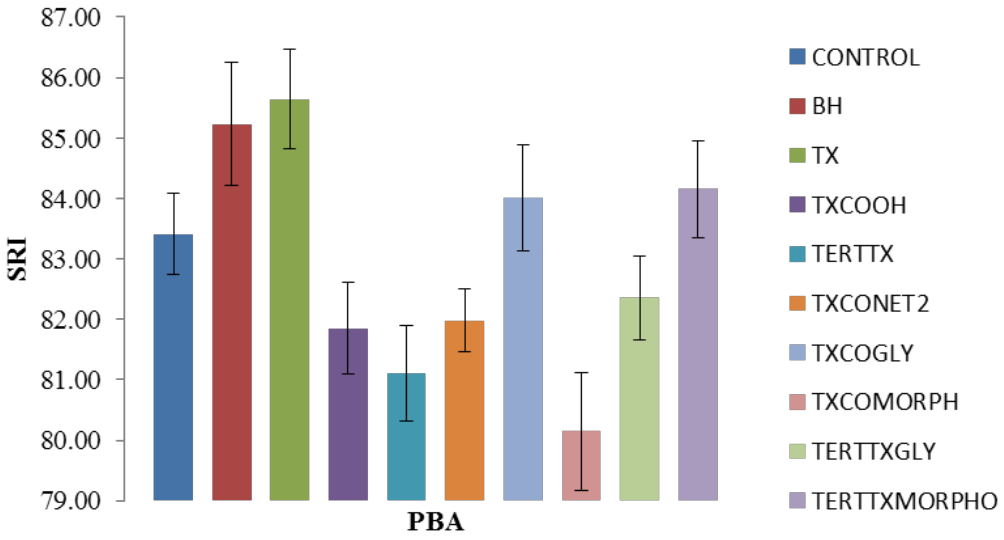


***Figure 139*** *SRI values of ragu with a PBA concentration of 5 mg/L with detergent*

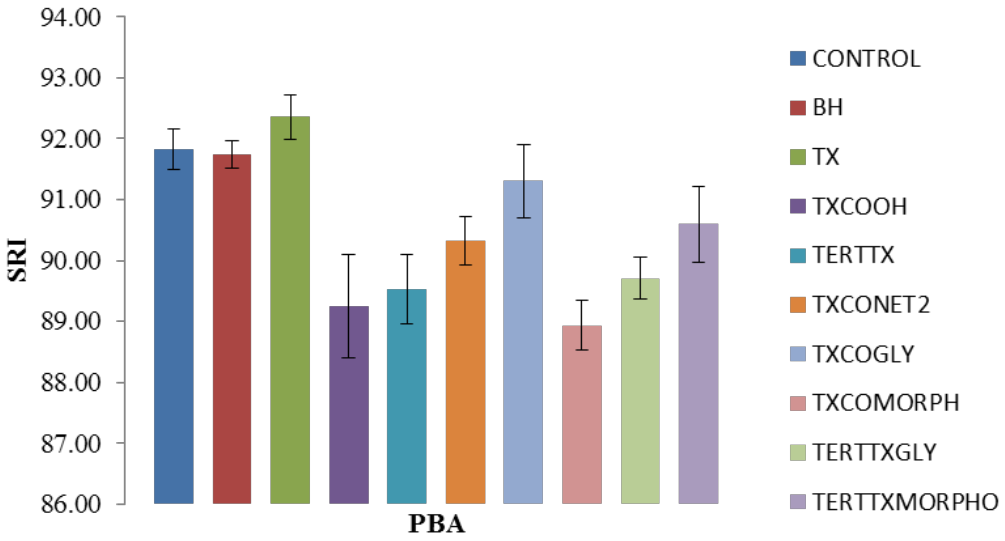


***Figure 140*** *SRI values of sundried tomato with a PBA concentration of 5 mg/L with detergent*

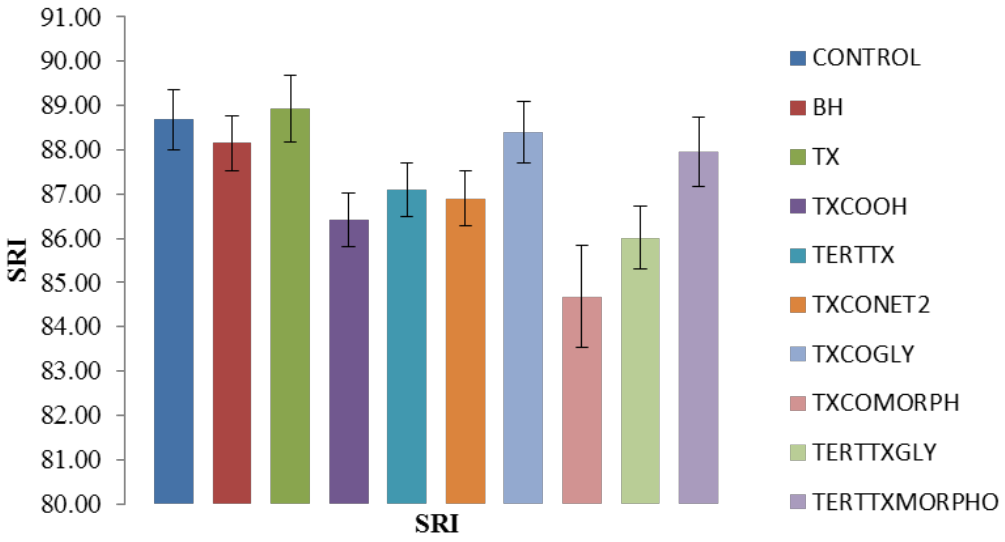


***Figure 141*** *SRI values of tomato puree with a PBA concentration of 5 mg/L with detergent*

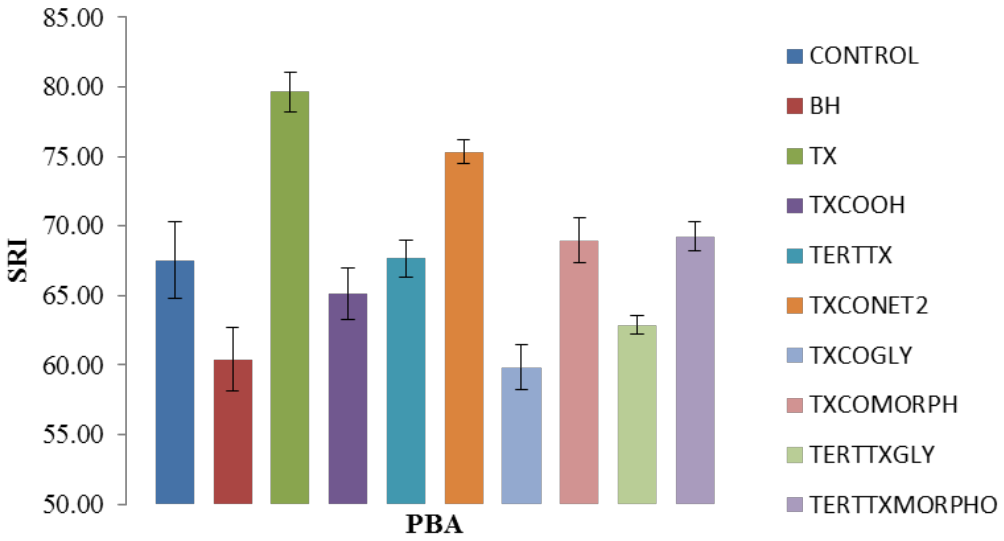


***Figure 142*** *SRI values of vindaloo with a PBA concentration of 5 mg/L with detergent*

# Bibliography


(1) Smulders, E.; Rähse, W.; Jakobi, G. *Laundry Detergents*; 2002.

(2) Harriman. *P&G PBA Agents*; 1993; Vol. HR93-47.

(3) GEORGE PORTER. Flash Photolysis and Some of Its Applications. In *Noble Lecture*; 1967.

(4) NORRISH, R. G. W.; PORTER, G. Chemical Reactions Produced by Very High Light Intensities. *Nature* **1949**, *164* (4172), 658–658.

(5) Dent, C. E.; Linstead, R. P.; Lowe, A. R. 217. Phthalocyanines. Part VI. The Structure of the Phthalocyanines. *J. Chem. Soc.* **1934**, No. 0, 1033.

(6) Linstead, R. P.; Lowe, A. R. 216. Phthalocyanines. Part V. The Molecular Weight of Magnesium Phthalocyanine. *J. Chem. Soc.* **1934**, No. 0, 1031.

(7) Dent, C. E.; Linstead, R. P. 215. Phthalocyanines. Part IV. Copper Phthalocyanines. *J. Chem. Soc.* **1934**, No. 0, 1027.

(8) Linstead, R. P.; Lowe, A. R. 214. Phthalocyanines. Part III. Preliminary Experiments on the Preparation of Phthalocyanines from Phthalonitrile. *J. Chem. Soc.* **1934**, 1022.

(9) Ethan; D.; Sternberg; David; Dolphin, C.; Brickner. Porphyrin-Based Photosensitizers for Use in Photodynamic Therapy. *Tetrahedron* **1998**, *54*, 4151–4202.

(10) Sakamoto, K.; Ohno-Okumura, E. Syntheses and Functional Properties of Phthalocyanines. *Materials (Basel).* **2009**, *2* (3), 1127–1180.

(11) de la Torre, G.; Vázquez, P.; Agulló-López, F.; Torres, T. Role of Structural Factors in the Nonlinear Optical Properties of Phthalocyanines and Related Compounds. *Chem. Rev.* **2004**, *104* (9), 3723–3750.

(12) Sakamoto, K.; Kato, T.; Ohno-Okumura, E.; Watanabe, M.; Cook, M. J. Synthesis of Novel Cationic Amphiphilic Phthalocyanine Derivatives for next Generation Photosensitizer Using Photodynamic Therapy of Cancer. *Dye. Pigment.* **2005**, *64* (1), 63–71.

(13) Sakamoto, K.; Ohno-Okumura, E. Syntheses and Functional Properties of Phthalocyanines. *Materials (Basel).* **2009**, *2* (3), 1127–1180.

(14) McKendrick, K. G. *Principles and Applications of Photochemistry*; 1989; Vol. 36.

(15) Moan J. Properties for Optimal PDT Sensitizers. *J Photochem Photobiol B.* **1990**, *5*, 521–524.

(16) Dougherty, T. J. Photodynamic Therapy. *Photochem. Photobiol.* **1993**, *58* (6), 895–900.

(17) Swavey, S.; Tr, M. Porphyrin and Phthalocyanine Photosensitizers as PDT Agents: A New Modality for the Treatment of Melanoma. In *Recent Advances in the Biology, Therapy and Management of Melanoma*; InTech, 2013.

(18) Ethirajan, M.; Chen, Y.; Joshi, P.; Pandey, R. K.; Pandey, R. K.; Goswami, L. N.; Chen, Y.; Gryshuk, A.; Missert, J. R.; Oseroff, A.; et al. The Role of Porphyrin Chemistry in Tumor Imaging and Photodynamic Therapy. *Chem. Soc. Rev.* **2011**, *40* (1), 340–362.

(19) Jurow, M.; Schuckman, A. E.; Batteas, J. D.; Drain, C. M. Porphyrins as Molecular Electronic Components of Functional Devices. *Coord. Chem. Rev.* **2010**, *254* (19–20), 2297–2310.

(20) Dayong Sun*, Fook S. Tham*, C. A. R.; †; and Peter D. W. Boyd. Extending Supramolecular Fullerene-Porphyrin Chemistry to Pillared Metal-Organic Frameworks. *PNAS* **2002**, *99*, 5088–5092.

(21) Auwärter, W.; Écija, D.; Klappenberger, F.; Barth, J. V. Porphyrins at Interfaces. *Nat. Chem.* **2015**, *7* (2), 105–120.

(22) Barona-Castaño, J.; Carmona-Vargas, C.; Brocksom, T.; de Oliveira, K. Porphyrins as Catalysts in Scalable Organic Reactions. *Molecules* **2016**, *21* (3), 310.

(23) Wardle, B. *Principles and Applications of Photochemistry*; Wiley, 2009.

(24) Balta, D. K.; Cetiner, N.; Temel, G.; Turgut, Z.; Arsu, N. An Annelated Thioxanthone as a New Type II Initiator. *J. Photochem. Photobiol. A Chem.* **2008**, *199* (2), 316–321.

(25) Aydin, M.; Arsu, N.; Yagci, Y.; Jockusch, S.; Turro, N. J. Mechanistic Study of Photoinitiated Free Radical Polymerization Using Thioxanthone Thioacetic Acid as One-Component Type II Photoinitiator. *Macromolecules* **2005**, *38* (10), 4133–4138.

(26) Belal, F.; Hefnawy, M. M.; Aly, F. A. Analysis of Pharmaceutically-Important Thioxanthene Derivatives. *J. Pharm. Biomed. Anal.* **1997**, *16* (3), 369–376.

(27) Corrales, T.; Catalina, F.; Peinado, C.; Allen, N. .; Rufs, A. .; Bueno, C.; Encinas, M. . Photochemical Study and Photoinitiation Activity of Macroinitiators Based on Thioxanthone. *Polymer (Guildf).* **2002**, *43* (17), 4591–4597.

(28) Jiang, X.; Yin, J. Water-Soluble Polymeric Thioxanthone Photoinitiator Containing Glucamine as Coinitiator. *Macromol. Chem. Phys.* **2008**, *209* (15), 1593–1600.

(29) Malval, J.-P.; Jin, M.; Balan, L.; Schneider, R.; Versace, D.-L.; Chaumeil, H.; Defoin, A.; Soppera, O. Photoinduced Size-Controlled Generation of Silver Nanoparticles Coated with Carboxylate-Derivatized Thioxanthones. *J. Phys. Chem. C* **2010**, *114* (23), 10396–10402.

(30) Nehlig, E.; Schneider, R.; Vidal, L.; Clavier, G.; Balan, L. Silver Nanoparticles Coated with Thioxanthone Derivative as Hybrid Photoinitiating Systems for Free Radical Polymerization. *Langmuir* **2012**, *28* (51), 17795–17802.

(31) Yagci, Y.; Jockusch, S.; Turro, N. J. Photoinitiated Polymerization: Advances, Challenges, and Opportunities. *Macromolecules* **2010**, *43* (15), 6245–6260.

(32) Wöll, D.; Smirnova, J.; Pfleiderer, W.; Steiner, U. E. Highly Efficient Photolabile Protecting Groups with Intramolecular Energy Transfer. *Angew. Chem. Int. Ed. Engl.* **2006**, *45* (18), 2975–2978.

(33) Brener, Z.; Pellegrino, J. Chemotherapy of Experimental Schistosomiasis. I. Drug Activity and Mode of Action of a New Thioxanthone Derivative. *J. Parasitol.* **1958**, *44* (6), 659.

(34) Palmeira, A.; Vasconcelos, M. H.; Paiva, A.; Fernandes, M. X.; Pinto, M.; Sousa, E. Dual Inhibitors of P-Glycoprotein and Tumor Cell Growth: (Re)discovering Thioxanthones. *Biochem. Pharmacol.* **2012**, *83* (1), 57–68.

(35) Paiva, A. M.; Pinto, M. M.; Sousa, E. A Century of Thioxanthones: Through Synthesis and Biological Applications. *Curr. Med. Chem.* **2013**, *20* (19), 2438–2457.

(36) Chemotherapy of Experimental Schistosomiasis. I. Drug Activity and Mode of Action of a New Thioxanthone Derivative on JSTOR.

(37) Stevenson, J. P.; DeMaria, D.; Reilly, D.; Purvis, J. D.; Graham, M. A.; Lockwood, G.; Drozd, M.; O'Dwyer, P. J. Phase I/pharmacokinetic Trial of the Novel Thioxanthone SR233377 (WIN33377) on a 5-Day Schedule. *Cancer Chemother. Pharmacol.* **1999**, *44* (3), 228–234.

(38) Yilmaz, G.; Aydogan, B.; Temel, G.; Arsu, N.; Moszner, N.; Yagci, Y. Thioxanthone−Fluorenes as Visible Light Photoinitiators for Free Radical Polymerization. *Macromolecules* **2010**, *43* (10), 4520–4526.

(39) Balta, D. K.; Temel, G.; Aydin, M.; Arsu, N. Thioxanthone Based Water-Soluble Photoinitiators for Acrylamide Photopolymerization. *Eur. Polym. J.* **2010**, *46* (6), 1374–1379.

(40) Shao, J.; Huang, Y.; Fan, Q. Visible Light Initiating Systems for Photopolymerization: Status, Development and Challenges. *Polym. Chem.* **2014**, *5* (14), 4195.

(41) Karaca, N.; Karaca Balta, D.; Ocal, N.; Arsu, N. Mechanistic Studies of Thioxanthone–carbazole as a One-Component Type II Photoinitiator. *J. Lumin.* **2014**, *146*, 424–429.

(42) Esen, D. S.; Temel, G.; Balta, D. K.; Allonas, X.; Arsu, N. One-Component Thioxanthone Acetic Acid Derivative Photoinitiator for Free Radical Polymerization. *Photochem. Photobiol.* **2014**, *90* (2), 463–469.

(43) Qiu, J.; Wei, J. Water-Soluble and Polymerizable Thioxanthone Photoinitiator Containing Imidazole. *J. Appl. Polym. Sci.* **2014**, *131* (16), n/a-n/a.

(44) Qiu, J.; Wei, J. Thioxanthone Photoinitiator Containing Polymerizable N-Aromatic Maleimide for Photopolymerization. *J. Polym. Res.* **2014**, *21* (9), 559.

(45) Dadashi-Silab, S.; Aydogan, C.; Yagci, Y. Shining a Light on an Adaptable Photoinitiator: Advances in Photopolymerizations Initiated by Thioxanthones. *Polym. Chem.* **2015**, *6* (37), 6595–6615.

(46) Kork, S.; Yilmaz, G.; Yagci, Y. Poly(vinyl Alcohol)-Thioxanthone as One-Component Type II Photoinitiator for Free Radical Polymerization in Organic and Aqueous Media. *Macromol. Rapid Commun.* **2015**, *36* (10), 923–928.

(47) Neumann, M. G.; Gehlen, M. H.; Encinas, M. V.; Allen, N. S.; Corrales, T.; Peinado, C.; Catalina, F. Photophysics and Photoreactivity of Substituted Thioxanthones. *J. Chem. Soc. Faraday Trans.* **1997**, *93* (8), 1517–1521.

(48) Lougnot, D. J.; Turck, C.; Fouassier, J. P. Water-Soluble Polymerization Initiators Based on the Thioxanthone Structure: A Spectroscopic and Laser Photolysis Study. *Macromolecules* **1989**, *22* (1), 108–116.

(49) Zhao, J.; Larock, R. C. Synthesis of Xanthones, Thioxanthones, and Acridones by the Coupling of Arynes and Substituted Benzoates. *J. Org. Chem.* **2007**, *72* (2), 583–588.

(50) Yates, S. F.; Schuster, G. B. Photoreduction of Triplet Thioxanthone by Amines: Charge Transfer Generates Radicals That Initiate Polymerization of Olefins. *J. Org. Chem.* **1984**, *49* (18), 3349–3356.

(51) Hafez, H. N.; Hegab, M. I.; Ahmed-Farag, I. S.; el-Gazzar, A. B. A. A Facile Regioselective Synthesis of Novel Spiro-Thioxanthene and Spiro-Xanthene-9',2-[1,3,4]thiadiazole Derivatives as Potential Analgesic and Anti-Inflammatory Agents. *Bioorg. Med. Chem. Lett.* **2008**, *18* (16), 4538–4543.

(52) Corrales, T.; Catalina, F.; Peinado, C.; Allen, N. S. Free Radical Macrophotoinitiators: An Overview on Recent Advances. *J. Photochem. Photobiol. A Chem.* **2003**, *159* (2), 103–114.

(53) Lalevée, J.; Blanchard, N.; Tehfe, M. A.; Fries, C.; Morlet-Savary, F.; Gigmes, D.; Fouassier, J. P.; Encinas, M. V.; Rufs, A. M.; Corrales, T.; et al. New Thioxanthone and Xanthone Photoinitiators Based on Silyl Radical Chemistry. *Polym. Chem.* **2011**, *2* (5), 1077.

(54) Malval, J.-P.; Jin, M.; Morlet-Savary, F.; Chaumeil, H.; Defoin, A.; Soppera, O.; Scheul, T.; Bouriau, M.; Baldeck, P. L. Enhancement of the Two-Photon Initiating Efficiency of a Thioxanthone Derivative through a Chevron-Shaped Architecture. *Chem. Mater.* **2011**, *23* (15), 3411–3420.

(55) Malval, J.-P.; Jin, M.; Morlet-Savary, F.; Chaumeil, H.; Defoin, A.; Soppera, O.; Scheul, T.; Bouriau, M.; Baldeck, P. L. Enhancement of the Two-Photon Initiating Efficiency of a Thioxanthone Derivative through a Chevron-Shaped Architecture. *Chem. Mater.* **2011**, *23* (15), 3411–3420.

(56) Wutzel, H.; Jarvid, M.; Bjuggren, J. M.; Johansson, A.; Englund, V.; Gubanski, S.; Andersson, M. R. Thioxanthone Derivatives as Stabilizers against Electrical Breakdown in Cross-Linked Polyethylene for High Voltage Cable Applications. *Polym. Degrad. Stab.* **2015**, *112*, 63–69.

(57) Chapman, O. L.; Wampfler, G. Photochemical Transformations. XXXIV. Concentration Dependence of the Efficiency of Energy Transfer from 3(.pi.,.pi.*) Aromatic Ketones. *J. Am. Chem. Soc.* **1969**, *91* (19), 5390–5392.

(58) DeBoer, C. D.; Schlessinger, R. H. Rate of the Self-Quenching Reaction for Thioxanthone Triplets. *J. Am. Chem. Soc.* **1972**, *94* (2), 655–656.

(59) Yip, R. W.; Szabo, A. G.; Tolg, P. K. Triplet State of Ketones in Solutions. Quenching Rate Studies of Thioxanthenone Triplets by Flash Absorption. *J. Am. Chem. Soc.* **1973**, *95* (13), 4471–4472.

(60) Abdullah, K. A.; Kemp, T. J. Quenching of Excited-State Xanthone and Thioxanthone by Inorganic Anions. *J. Chem. Soc. Perkin Trans. 2* **1985**, No. 8, 1279.

(61) Rehm, D.; Weller, A. Kinetics of Fluorescence Quenching by Electron and H-Atom Transfer. *Isr. J. Chem.* **1970**, *8* (2), 259–271.

(62) Dalton, J. C.; Montgomery, F. C. Solvent Effects on Thioxanthone Fluorescence. *J. Am. Chem. Soc.* **1974**, *96* (19), 6230–6232.

(63) Lai, T.; Lim, E. C. Photophysical Behavior of Aromatic Carbonyl Compounds Related to Proximity Effect: Thioxanthone. *Chem. Phys. Lett.* **1980**, *73* (2), 244–248.

(64) Lai, T.; Lim, E. C. Time-Resolved Fluorescence Spectra and Energy-Resolved Decays of Vibronically Coupled Electronic States: Effects of Solvent Relaxation on the Excited-State Dynamics of Thioxanthone. *Chem. Phys. Lett.* **1981**, *84* (2), 303–307.

(65) Burget, D.; Jacques, P. Dramatic Solvent Effects on Thioxanthone Fluorescence Lifetime. *J. Lumin.* **1992**, *54* (3), 177–181.

(66) BURGET, D.; JACQUES, P. SOLVENT EFFECTS ON THE FLUORESCENCE OF THIOXANTHONE - INTERPRETATION BY SOLVATOCHROMIC PARAMETERS PI, ALPHA AND BETA. *J. Chim. Phys. PHYSICO-CHIMIE Biol.* **1991**, *88* (5), 675–688.

(67) Neumann, M. G.; Gehlen, M. H.; Encinas, M. V.; Allen, N. S.; Corrales, T.; Peinado, C.; Catalina, F. Photophysics and Photoreactivity of Substituted Thioxanthones. *J. Chem. Soc. Faraday Trans.* **1997**, *93* (8), 1517–1521.

(68) Ley, C.; Morlet-Savary, F.; Jacques, P.; Fouassier, J. P. Solvent Dependence of the Intersystem Crossing Kinetics of Thioxanthone. *Chem. Phys.* **2000**, *255* (2–3), 335–346.

(69) Cavaleri, J. J.; Prater, K.; Bowman, R. M. An Investigation of the Solvent Dependence on the Ultrafast Intersystem Crossing Kinetics of Xanthone. *Chem. Phys. Lett.* **1996**, *259* (5–6), 495–502.

(70) Ley, C.; Morlet-Savary, F.; Jacques, P.; Fouassier, J. P. Solvent Dependence of the Intersystem Crossing Kinetics of Thioxanthone. *Chem. Phys.* **2000**, *255* (2–3), 335–346.

(71) Abdullah, K. A.; Kemp, T. J. Solvatochromic Effects in the Fluorescence and Triplet—triplet Absorption Spectra of Xanthone, Thioxanthone and N-Methylacridone. *J. Photochem.* **1986**, *32* (1), 49–57.

(72) Kamlet, M. J.; Abboud, J. L.; Taft, R. W. The Solvatochromic Comparison Method. 6. The .pi.* Scale of Solvent Polarities. *J. Am. Chem. Soc.* **1977**, *99* (18), 6027–6038.

(73) Kamlet, M. J.; Taft, R. W. Linear Solvation Energy Relationships. Part 3. Some Reinterpretations of Solvent Effects Based on Correlations with Solvent Π* and α Values. *J. Chem. Soc., Perkin Trans. 2* **1979**, No. 3, 349–356.

(74) Morlet-Savary, F.; Ley, C.; Jacques, P.; Wieder, F.; Fouassier, J. P. Time Dependent Solvent Effects on the T1–Tn Absorption Spectra of Thioxanthone: A Picosecond Investigation. *J. Photochem. Photobiol. A Chem.* **1999**, *126* (1–3), 7–14.

(75) Allonas, X.; Ley, C.; Bibaut, C.; Jacques, P.; Fouassier, J. P. Investigation of the Triplet Quantum Yield of Thioxanthone by Time-Resolved Thermal Lens Spectroscopy: Solvent and Population Lens Effects. *Chem. Phys. Lett.* **2000**, *322* (6), 483–490.

(76) Krystkowiak, E.; Maciejewski, A.; Kubicki, J. Spectral and Photophysical Properties of Thioxanthone in Protic and Aprotic Solvents: The Role of Hydrogen Bonds in S1-Thioxanthone Deactivation. *Chemphyschem* **2006**, *7* (3), 597–606.

(77) Rubio-Pons, Ò.; Serrano-Andrés, L.; Burget, D.; Jacques, P. A Butterfly like Motion as a Clue to the Photophysics of Thioxanthone. *J. Photochem. Photobiol. A Chem.* **2006**, *179* (3), 298–304.

(78) Rai-Constapel, V.; Salzmann, S.; Marian, C. M. Isolated and Solvated Thioxanthone: A Photophysical Study. *J. Phys. Chem. A* **2011**, *115* (31), 8589–8596.

(79) Rai-Constapel, V.; Kleinschmidt, M.; Salzmann, S.; Serrano-Andrés, L.; Marian, C. M. Thioxanthone: On the Shape of the First Absorption Band. *Phys. Chem. Chem. Phys.* **2010**, *12* (32), 9320–9327.

(80) Angulo, G.; Grilj, J.; Vauthey, E.; Serrano-Andrés, L.; Rubio-Pons, O.; Jacques, P. Ultrafast Decay of the Excited Singlet States of Thioxanthone by Internal Conversion and Intersystem Crossing. *Chemphyschem* **2010**, *11* (2), 480–488.

(81) Landrum, J. T. *Carotenoids : Physical, Chemical, and Biological Functions and Properties*; CRC Press, 2010.

(82) Williams, A. T. R.; Winfield, S. A.; Miller, J. N. Relative Fluorescence Quantum Yields Using a Computer-Controlled Luminescence Spectrometer. *Analyst* **1983**, *108* (1290), 1067.

(83) Desmond V O'Connor, D. P. *Time-Correlated Single Photon Counting - Desmond O'Connor - Google Books*; 1984.

(84) W. Becker. *Advanced Time-Correlated Single Photon Counting Techniques - Wolfgang Becker - Google Books*, Springer.; Castleman, Ed.; New York.

(85) Grinvald, A.; Steinberg, I. Z. On the Analysis of Fluorescence Decay Kinetics by the Method of Least-Squares. *Anal. Biochem.* **1974**, *59* (2), 583–598.

(86) O'Connor, D. V.; Ware, W. R.; Andre, J. C. Deconvolution of Fluorescence Decay Curves. A Critical Comparison of Techniques. *J. Phys. Chem.* **1979**, *83* (10), 1333–1343.

(87) DigiEye Systems | VeriVide https://www.verivide.com/category-list/digieye-system.

(88) Identifying Color Differences Using L*a*b* or L*C*H* Coordinates http://sensing.konicaminolta.us/2014/04/identifying-color-differences-using-l-a-b-or-l-c-h-coordinates/.

(89) Geertsema, E. M.; Schoevaars, A. M.; Meetsma, A.; Feringa, B. L.; Pedersen, C. J.; Izatt, R. M.; Bradshaw, J. S.; Nielsen, S. A.; Lamb, J. D.; Christensen, J. J.; et al. Bisthioxanthylidene Biscrown Ethers as Potential Stereodivergent Chiral Ligands. *Org. Biomol. Chem.* **2006**, *4* (22), 4101.

(90) Nonell, S.; Braslavsky, S. E. Time-Resolved Singlet Oxygen Detection. *Methods Enzymol.* **2000**, *319*, 37–49.

(91) Neiditch, O. W.; Mills, K. L.; Gladstone, G. The Stain Removal Index (SRI): A New Reflectometer Method for Measuring and Reporting Stain Removal Effectiveness. *J. Am. Oil Chem. Soc.* **1980**, *57* (12), 426–429.

(92) Self made acid/base indicators, PH indicators, homemade litmus paper http://www.tuxgraphics.org/npa/litmus-redcabbage-tumeric-radish-ph-indicator/.

(93) Breedlove, C. H. Turmeric as an Acid-Base Indicator. *J. Chem. Educ.* **1995**, *72* (6), 540.

(94) Priyadarsini, K.; Indira, K. The Chemistry of Curcumin: From Extraction to Therapeutic Agent. *Molecules* **2014**, *19* (12), 20091–20112.

(95) BURGET, D.; JACQUES, P. SOLVENT EFFECTS ON THE FLUORESCENCE OF THIOXANTHONE - INTERPRETATION BY SOLVATOCHROMIC PARAMETERS PI, ALPHA AND BETA. *J. Chim. Phys. PHYSICO-CHIMIE Biol.* **1991**, *88* (5), 675–688.

(96) Villnow, T.; Ryseck, G.; Rai-Constapel, V.; Marian, C. M.; Gilch, P. Chimeric Behavior of Excited Thioxanthone in Protic Solvents: I. Experiments. *J. Phys. Chem. A* **2014**, *118* (50), 11696–11707.

(97) Shine, H. J.; Hughes, L. Ion Radicals. XI. The Reactions of Thioxanthene and Thioxanthene 10-Oxide in Sulfuric Acid 1. *J. Org. Chem.* **1966**, *31* (10), 3142–3146.

(98) Ternay, A. L.; Chasar, D. W. Behavior of Thioxanthenol Sulfoxides in Trifluoroacetic Acid and Its Anhydride. *J. Org. Chem.* **1968**, *33* (9), 3641–3642.

(99) Wolfbeis, O. S.; Fuerlinger, E. pH-Dependent Fluorescence Spectroscopy. 15. Detection of an Unusual Excited-State Species of 3-Hydroxyxanthone. *J. Am. Chem. Soc.* **1982**, *104* (15), 4069–4072.

(100) Rappoport, Z. *The Chemistry of Phenols*; Wiley, 2003.

(101) Mizutani, K.; Miyazaki, K.; Ishigaki, K. Spectroscopic and Theoretical Studies on the Protonation to Xanthone Derivatives. *Bull. Chem.* **1974**.

(102) McCain, K. S.; Harris, J. M. Total Internal Reflection Fluorescence-Correlation Spectroscopy Study of Molecular Transport in Thin Sol−Gel Films. *Anal. Chem.* **2003**, *75* (14), 3616–3624.

(103) Rumbles, G.; Brown, A. J.; Phillips, D. Time-Resolved Evanescent Wave Induced Fluorescence Spectroscopy. Part 1.—Deviations in the Fluorescence Lifetime of Tetrasulphonated Aluminium Phthalocyanine at a Fused Silica/methanol Interface. *J. Chem. Soc., Faraday Trans.* **1991**, *87* (6), 825–830.

(104) Rapson, A. C.; Gee, M. L.; Clayton, A. H. A.; Smith, T. A. Interactions of a Lytic Peptide with Supported Lipid Bilayers Investigated by Time-Resolved Evanescent Wave-Induced Fluorescence Spectroscopy. *Methods Appl. Fluoresc.* **2016**, *4* (4), 44001.

(105) de Mello, A. J.; Elliott, J. A.; Rumbles, G. Evanescent Wave-Induced Fluorescence Study of Rhodamine 101 at Dielectric Interfaces. *J. Chem. Soc. Faraday Trans.* **1996**, *92* (23), 4723.

(106) Mello, A. De; Crystall, B.; Rumbles, G. Evanescent Wave Spectroscopic Studies of Surface Enhanced Fluorescence Quantum Efficiencies. *J. colloid interface …* **1995**, *169* (1), 161–167.